IMPACT FACTOR
10.057

#1 NUCLEAR MEDICINE, MOLECULAR IMAGING AND MOLECULAR RADIOTHERAPY JOURNAL

Vol. 63 ▪ Suppl. 1 ▪ June 2022

# JNM

The Journal of Nuclear Medicine

## Molecular Imaging of Neurodegeneration: The Way to New Horizons

Guest Editors: Victor L. Villemagne, MD, and Henryk Barthel, MD, PhD

SNMMI Value Initiative
SOCIETY OF NUCLEAR MEDICINE & MOLECULAR IMAGING

**PETNET Solutions**

# Imaging Alzheimer's Disease with PET/CT

With the broadest portfolio of PET radiopharmaceuticals for Alzheimer's Disease

## Now expanding access to PET radiopharmaceuticals for imaging neurodegenerative diseases like Alzheimer's

PETNET Solutions, Inc., a Siemens Healthineers company, reliably delivers PET radiopharmaceuticals via the largest network of cyclotron-equipped radiopharmacies in the United States. Supported by experts averaging more than 20 years of industry experience, PETNET customers unlock access to a wide array of biomarkers, customized data analytics, and educational resources to drive growth.

**PETNET distribution in the USA**

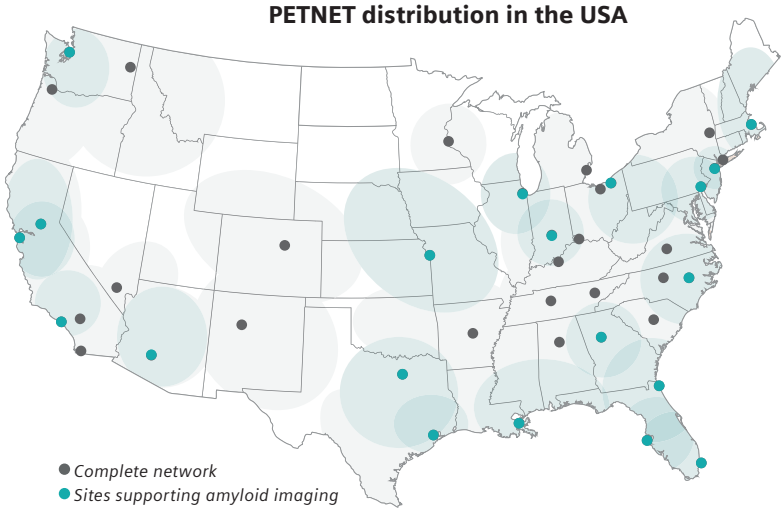


**1,280,000**
**PET doses delived annually**[1]

**Delivering to 92% of imaging centers in the United States**[2]

**43 cyclotron-equipped radiopharmacies nationwide**

[1] *Data for all products on file; CNJ Market Orders (Q1FY22)*

[2] *Based on commercially available IMV 2020 study results compared with internal data on file*

## Ask us today about PET radiopharmaceuticals for Alzheimer's Disease imaging

**Customer Care Team | +1 (877) 473-8638**
**customercare@petnetsolutions.com**

**Partnership delivering outcomes**
**PETNETsolutions.com**

SIEMENS Healthineers

JNM

Volume 63 • Supplement 1 • June 2022

JNM The Journal of NUCLEAR MEDICINE

The Official Publication of **SNMMI**



**MISSION STATEMENT:** *The Journal of Nuclear Medicine* advances the knowledge and practice of molecular imaging and therapy and nuclear medicine to improve patient care through publication of original basic science and clinical research.

*JNM* (ISSN 0161-5505 [print]; ISSN 2159-662X [online]) is published monthly by SNMMI, 1850 Samuel Morse Drive, Reston, VA 20190-5316. Periodicals postage is paid at Herndon, VA, and additional mailing offices. Postmaster, send address changes to *The Journal of Nuclear Medicine,* 1850 Samuel Morse Drive, Reston, VA 20190-5316. The costs of publication of all nonsolicited articles in *JNM* were defrayed in part by the payment of page charges. Therefore, and solely to indicate this fact, these articles are hereby designated "advertisements" in accordance with 18 USC section 1734.

**DISCLOSURE OF COMMERCIAL INTEREST:** Johannes Czernin, MD, editor-in-chief of *The Journal of Nuclear Medicine,* has indicated that he is a founder of Sofie Biosciences and holds equity in the company and in intellectual property invented by him, patented by the University of California, and licensed to Sofie Biosciences. He is also a founder and board member of Trethera Therapeutics and holds equity in the company and in intellectual property invented by him, patented by the University of California, and licensed to Triangle. He also serves on the medical advisory board of Actinium Pharmaceuticals and on the scientific advisory boards of POINT Biopharma, RayzeBio, and Jubilant Pharma and is a consultant for Amgen. No other potential conflicts of interest were reported. Manuscripts submitted to *JNM* with potential conflicts are handled by a guest editor.

**EDITORIAL COMMUNICATIONS** should be sent to: Editor-in-Chief, Johannes Czernin, MD, *JNM* Office, SNMMI, 1850 Samuel Morse Drive, Reston, VA 20190-5316. Phone: (703) 326-1185; Fax: (703) 708-9018. To submit a manuscript, go to https://submit-jnm.snmjournals.org.

**BUSINESS COMMUNICATIONS** concerning permission requests should be sent to the publisher, SNMMI, 1850 Samuel Morse Drive, Reston, VA 20190-5316; (703) 708-9000; home page address: jnm.snmjournals.org. Subscription requests and address changes should be sent to Membership Department, SNMMI at the address above. Notify the Society of change of address and telephone number at least 30 days before date of issue by sending both the old and new addresses. Claims for copies lost in the mail are allowed within 90 days of the date of issue. Claims are not allowed for issues lost as a result of insufficient notice of change of address. For information on advertising, contact Team SNMMI (Kevin Dunn, Rich Devanna, and Charlie Meitner; (201) 767-4170; fax: (201) 767-8065; TeamSNMMI@cunnasso.com). Advertisements are subject to editorial approval and are restricted to products or services pertinent to nuclear medicine. Closing date is the first of the month preceding the date of issue.

**INDIVIDUAL SUBSCRIPTION RATES** for the 2022 calendar year are $603 within the United States and Canada; $648 elsewhere. Make checks payable to the SNMMI. CPC IPM Sales Agreement No. 1415158. Sales of individual back copies from 1999 through the current issue are available for $60 at http://www.snmmi.org/subscribe (subscriptions@snmmi.org; fax: (703) 667-5134). Individual articles are available for sale online at http://jnm.snmjournals.org.

## LILLY FOR BETTER

It begins with a purpose to create medicines that make life better. To find a way to come through, no matter the odds. To be stronger than we thought we could be and to share our strength with the world around us. Our purpose makes us who we are. And every day, we work to share our purpose with those we touch. And to help them fulfill theirs.

**lilly.com**



Lilly

JNM The Journal of NUCLEAR MEDICINE

# CREATING HOPE THROUGH INNOVATION

At Eisai, everything we do is guided by a simple principle: patients and their families come first. We spend time with them. We listen and we learn about their lives, their desires and their greatest needs. We call this *human health care* or *hhc*, giving first thoughts to patients and their families and helping increase the benefits health care provides.

Our *hhc* mission is what drives us to discover innovative solutions and therapies that help address unmet needs within the communities that we seek to serve.

*hhc*
*human health care*

TO LEARN MORE, PLEASE VISIT WWW.EISAI.COM/US

# Molecular Imaging of Neurodegeneration: The Way to New Horizons

Victor L. Villemagne[1] and Henryk Barthel[2]

*[1]Department of Psychiatry, University of Pittsburgh, Pittsburgh, Pennsylvania; and [2]Department of Nuclear Medicine, University Medical Center, University of Leipzig, Leipzig, Germany*

Neurodegenerative disorders are chronic and progressive conditions characterized by tissue loss in certain brain systems. They encompass most dementias, movement disorders, amyotrophic lateral sclerosis, Creutzfeldt–Jakob disease, and other diseases. Because the incidence of most of these disorders increases with age, they are of enormous socioeconomic relevance in our aging societies. Among other similarities, the disease-specific trigger events in these disorders are still mainly unknown, and consequently, no preventive or curative treatment is currently available. Optimism for progress in this regard, however, grows as our understanding of underlying molecular pathologies in these disorders steadily increases.

Different molecular imaging techniques are available in clinical care to support a biomarker-based diagnosis of neurodegenerative disorders and in research to support basic research and drug testing. Excitingly, many new tracer classes and molecular imaging concepts are currently entering the neurodegeneration imaging field. They come at the right time, because a paradigm shift is currently under way in which the traditional concept of defining or diagnosing neurodegenerative disorders as a syndromal construct will likely be replaced by a biologic definition or diagnosis of these disorders.

This supplement to *The Journal of Nuclear Medicine* aims to provide an up-to-date overview on the different aspects of molecular imaging in neurodegeneration and a discussion on what the future will bring to the field. For that purpose, we managed to acquire respective top experts. Minoshima et al. discuss the still-relevant role of $^{18}$F-FDG PET in the imaging of neurodegeneration (*1*). Chapleau et al. review the current state of amyloid PET imaging as a technology on the edge of entering clinical praxis (*2*), whereas Groot et al. provide an overview on the most driving developments in tau PET imaging (*3*). This is followed by reviews by Wallert et al. and Tiepolt et al. on current opportunities to image dopaminergic and cholinergic neurotransmission in neurodegenerative disorders (*4*,*5*). Masdeu et al. discuss the great potential of imaging neuroinflammation (*6*), and Kenou et al. focus on imaging cyclooxygenases as neuroinflammation targets in neurodegeneration (*7*). Carson et al. review the current state of the recently emerging field of synaptic density imaging in neurodegenerative disorders (*8*). Finally, our group discusses future directions in this most exciting field of molecular imaging of neurodegeneration (*9*). We hope you enjoy reading this supplement.

## DISCLOSURE

Victor Villemagne received consulting fees from Eli-Lilly, Life Molecular Imaging, Hospicom, and IXICO and speaker honoraria from ACE Barcelona and IXICO. Henryk Barthel received speaker honoraria from Novartis/AAA and reader honoraria from Life Molecular Imaging. No other potential conflict of interest relevant to this article was reported.

## REFERENCES

1. Minoshima S, Cross D, Thientunyakit T, Foster N, Drzezga A. $^{18}$F-FDG PET imaging in neurodegenerative dementing disorders: insights into subtype classification, emerging disease categories, and mixed dementia with copathologies. *J Nucl Med.* 2022;63:2S–12S.
2. Chapleau M, Iaccarino L, Soleimani-Meigooni D, Rabinovici GD. The role of amyloid PET in imaging neurodegenerative disorders: a review. *J Nucl Med.* 2022; 63:13S–19S.
3. Groot C, Villeneuve S, Smith R, Hansson O, Ossenkoppele R. Tau PET imaging in neurodegenerative disorders. *J Nucl Med.* 2022;63:20S–26S.
4. Wallert ED, van de Giessen E, Knol RJJ, Beudel M, de Bie RMA, Booij J. Imaging dopaminergic neurotransmission in neurodegenerative disorders. *J Nucl Med.* 2022; 63:27S–32S.
5. Tiepolt S, Meyer PM, Patt M, et al. PET imaging of cholinergic neurotransmission in neurodegenerative disorders. *J Nucl Med.* 2022;63:33S–44S.
6. Masdeu JC, Pascual B, Fujita M. Imaging neuroinflammation in neurodegenerative disorders. *J Nucl Med.* 2022;63:45S–52S.
7. Kenou BV, Manly LS, Rubovits SB, et al. Cyclooxygenases as potential PET imaging biomarkers to explore neuroinflammation in dementia. *J Nucl Med.* 2022; 63:53S–59S.
8. Carson RE, Naganawa M, Toyonaga T, et al. Imaging of synaptic density in neurodegenerative disorders. *J Nucl Med.* 2022;63:60S–67S.
9. Barthel H, Villemagne VL, Drzezga A. Future directions in molecular imaging of neurodegenerative disorders. *J Nucl Med.* 2022;63:68S–74S.

Received and accepted Apr. 6, 2022.
For correspondence or reprints, contact Henryk Barthel (henryk.barthel@medizin.uni-leipzig.de).

DOI: 10.2967/jnumed.121.264237

# $^{18}$F-FDG PET Imaging in Neurodegenerative Dementing Disorders: Insights into Subtype Classification, Emerging Disease Categories, and Mixed Dementia with Copathologies

Satoshi Minoshima[1], Donna Cross[1], Tanyaluck Thientunyakit[2], Norman L. Foster[3], and Alexander Drzezga[4–6]

*[1]Department of Radiology and Imaging Sciences, Spencer Fox Eccles School of Medicine, University of Utah, Salt Lake City, Utah; [2]Division of Nuclear Medicine, Department of Radiology, Faculty of Medicine, Siriraj Hospital, Bangkok, Thailand; [3]Department of Neurology, Spencer Fox Eccles School of Medicine, University of Utah, Salt Lake City, Utah; [4]Department of Nuclear Medicine, Faculty of Medicine and University Hospital Cologne, University of Cologne, Cologne, Germany; [5]German Center for Neurodegenerative Diseases (DZNE), Bonn-Cologne, Bonn, Germany; and [6]Institute of Neuroscience and Medicine (INM-2), Molecular Organization of the Brain, Forschungszentrum Jülich, Jülich, Germany*

Since the invention of $^{18}$F-FDG as a neurochemical tracer in the 1970s, $^{18}$F-FDG PET has been used extensively for dementia research and clinical applications. FDG, a glucose analog, is transported into the brain via glucose transporters and metabolized in a concerted process involving astrocytes and neurons. Although the exact cellular mechanisms of glucose consumption are still under investigation, $^{18}$F-FDG PET can sensitively detect altered neuronal activity due to neurodegeneration. Various neurodegenerative disorders affect different areas of the brain, which can be depicted as altered $^{18}$F-FDG uptake by PET. The spatial patterns and severity of such changes can be reproducibly visualized by statistical mapping technology, which has become widely available in the clinic. The differentiation of 3 major neurodegenerative disorders by $^{18}$F-FDG PET, Alzheimer disease (AD), frontotemporal dementia (FTD), and dementia with Lewy bodies (DLB), has become standard practice. As the nosology of FTD evolves, frontotemporal lobar degeneration, the umbrella term for pathology affecting the frontal and temporal lobes, has been subclassified clinically into behavioral variant FTD; primary progressive aphasia with 3 subtypes, semantic, nonfluent, and logopenic variants; and movement disorders including progressive supranuclear palsy and corticobasal degeneration. Each of these subtypes is associated with differential $^{18}$F-FDG PET findings. The discovery of new pathologic markers and clinicopathologic correlations via larger autopsy series have led to newly recognized or redefined disease categories, such as limbic-predominant age-related TDP-43 encephalopathy, hippocampus sclerosis, primary age-related tauopathy, and argyrophilic grain disease, which have become a focus of investigations by molecular imaging. These findings need to be integrated into the modern interpretation of $^{18}$F-FDG PET. Recent pathologic investigations also have revealed a high prevalence, particularly in the elderly, of mixed dementia with overlapping and coexisting pathologies. The interpretation of $^{18}$F-FDG PET is evolving from a traditional dichotomous diagnosis of AD versus FTD (or DLB) to a determination of the most predominant underlying pathology that would best explain the patient's symptoms, for the purpose of care guidance. $^{18}$F-FDG PET is a relatively low cost and widely available imaging modality that can help assess various neurodegenerative disorders in a single test and remains the workhorse in clinical dementia evaluation.

Received Feb. 1, 2022; revision accepted Apr. 22, 2022.

For correspondence or reprints, contact Satoshi Minoshima (sminoshima@hsc.utah.edu).



**Key Words**: FDG; PET; dementing disorders; neurodegeneration; differential diagnosis

**J Nucl Med 2022; 63:2S–12S**
DOI: 10.2967/jnumed.121.263194

Since the development of FDG (2-deoxy-2-[F-18]fluoro-D-glucose [$^{18}$F-FDG]) as a radiopharmaceutical to measure brain metabolism with PET imaging in the 1970s, both research and clinical applications in neurodegeneration continue to grow. Although the number of research publications concerning $^{18}$F-FDG PET and dementia has been surpassed recently by proteomic-specific imaging such as amyloid and tau PET, $^{18}$F-FDG PET remains a major workhorse for the clinical evaluation of cognitive disorders.

## $^{18}$F-FDG AS A NEUROCHEMICAL TRACER

Glucose is the principal source of energy for the mammalian brain. In adult humans, the brain represents approximately 2% of the total body mass, yet it uses approximately 20%–25% of the glucose consumed daily (*1*). Regional changes in neuronal activity due to neurodegeneration can be sensitively reflected by regional brain glucose consumption. A structural analog of glucose, 2-deoxy-D-glucose, was labeled with $^{14}$C, $^{11}$C, and $^{18}$F and used as a tool to investigate energy metabolism in the brain in both preclinical and clinical studies in the 1970s (*2,3*). Applications of the tracer were quickly extended to the investigations of myocardial and cancer glucose metabolism, and the tracer is now widely available and used in clinical nuclear medicine practices worldwide.

Glucose is transported from plasma to the brain via glucose transporters (GLUTs), primarily GLUT1 expressed in the blood–brain barrier/astrocytes and GLUT3 expressed in neurons (*4*). Glucose is then phosphorylated by hexokinase to glucose-6-phosphate in cells and metabolized in the glycolytic pathway to produce adenosine triphosphate (*2*). However, unlike glucose-6-phosphate, deoxyglucose-6-phosphate cannot be used as a substrate for further glycolysis and subsequently accumulates in cells because glucose-6-phosphatase (the reverse enzyme) activity in the brain is low (*5*).

## CELLULAR MECHANISMS OF $^{18}$F-FDG UPTAKE IN THE BRAIN

$^{18}$F-FDG uptake in the brain is considered to represent general neuronal activity. The cellular mechanisms of brain glucose metabolism and $^{18}$F-FDG uptake have been further elucidated over the past several decades. Although energy consumption in neurons occurs for various signaling and neurotransmitter processes, synaptic currents and action potentials seem to comprise the greater part of the consumption (*6*). This observation coincides with deoxyglucose uptake in the axonal terminals when neurons are stimulated electrophysiologically (*7*). Excitatory synapses, in particular glutamatergic, predominate among cortical synapses and thus consume a large portion of the $^{18}$F-FDG uptake in the human brain (*6*). Recent studies indicate that glucose is transported from the capillaries to the astrocytes and metabolized into lactate, which subsequently serves as an energy source for neurons ("astrocyte-neuron lactate shuttle") (*8*). For simplicity, the terms *hypometabolism* and *decreased $^{18}$F-FDG uptake* on $^{18}$F-FDG PET are used interchangeably hereafter.

## REMOTE EFFECTS ON $^{18}$F-FDG UPTAKE (DIASCHISIS)

$^{18}$F-FDG uptake not only represents local neuronal/synaptic activity, but also can reflect remote effects via deactivation of projection neurons without local neuronal injury. One classic example of such phenomena is crossed cerebellar diaschisis (CCD) (Fig. 1A) initially discovered in stroke patients (*9*). Decreased $^{18}$F-FDG uptake/perfusion in the contralateral cerebellar hemisphere is caused by deactivated ponto–cerebellar neurons secondary to the primary injury in corticopontine neurons from the supratentorial lesion. Such remote effects (diaschisis) can also be seen in neurodegeneration such as Alzheimer disease (AD) (*10*), frontotemporal dementia (FTD) (*11*), corticobasal syndrome, and semantic and logopenic variants of primary progressive aphasia (PPA) (*12*). In AD, decreased $^{18}$F-FDG uptake due to diaschisis can be seen in the cerebellar hemisphere contralateral to the predominant cortical involvement as well as in the ipsilateral thalamus and basal ganglia (*13*). Similarly, decreased $^{18}$F-FDG uptake in the caudate nucleus is often seen in FTD. Although the imaging modalities of $^{18}$F-FDG PET and MRI are combined under the term *Neurodegeneration* (N) as a category in the recent National Institute on Aging and Alzheimer's Association (NIA-AA) Research Framework (*14*), careful translation of $^{18}$F-FDG PET findings to a pathophysiologic interpretation is needed for a better understanding of such disease processes. When interpreting $^{18}$F-FDG PET scans, it is crucial to understand the underlying anatomy of white matter tracts and fiber projections so that the primary and remote pathologies can be inferred correctly.

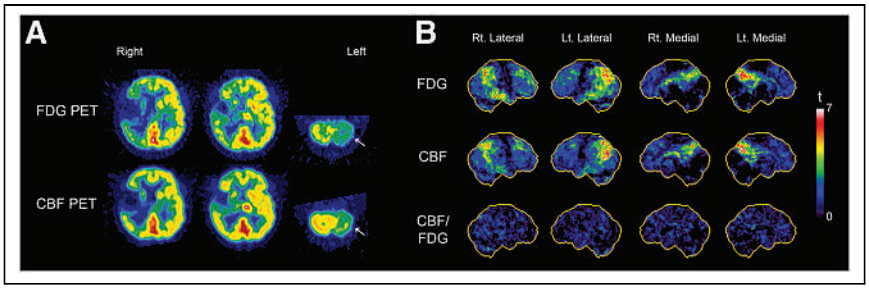


**FIGURE 1.** $^{18}$F-FDG and cerebral blood flow (CBF) PET. Crossed cerebellar diaschisis (CCD) (A) seen in a right (Rt.) middle cerebral artery (MCA) stroke. Decreased glucose metabolism ($^{18}$F-FDG) and perfusion (CBF) in contralateral left (Lt.) cerebellar hemisphere (white arrow) where no ischemic injury is present. Decreased $^{18}$F-FDG uptake and CBF are secondary to deactivation of cortico–ponto–cerebellar tract ("remote effect"). Such remote effects are known to occur in neurodegenerative disorders. $^{18}$F-FDG uptake not only reflects local pathology, but also could reflect remote pathology. Knowledge of cortical pathways is crucial for scan interpretation. (B) Coupling between glucose metabolism ($^{18}$F-FDG) and CBF in AD measured by PET and 3D-SSP analysis. Statistical t maps (top 2 rows) represent regional hypometabolism and hypoperfusion seen in a group of AD patients. Both $^{18}$F-FDG and CBF PET show similar regional changes, though CBF PET appears slightly less sensitive. Ratio maps between CBF and $^{18}$F-FDG (bottom row) indicate that metabolic-flow coupling is relatively preserved in areas both affected and not affected by AD. This observation supports use of various flow-related measurements such as perfusion SPECT, early flow images obtained as a part of amyloid PET or tau PET, or MRI-based perfusion imaging for dementia evaluation.

## IMAGE INTERPRETATION USING STATISTICAL MAPPING TECHNIQUES

One significant advancement for $^{18}$F-FDG PET interpretation in neurodegeneration is the widespread use of statical mapping for image interpretation and analysis. Various neurodegenerative dementias are known to affect specific regions of the brain. PET scans can demonstrate altered $^{18}$F-FDG uptake corresponding to the regions affected directly or indirectly. For the differential diagnosis of dementing disorders, interpreters must recognize the spatial distribution of the changes in $^{18}$F-FDG uptake, and the magnitude of such regional changes. This interpretational task may not be straightforward due to several factors, including: the anatomic information on PET is tracer-specific and relatively limited as compared with that on structural imaging such as MRI; the image presentation (e.g., image orientation, color scale) can be variable in clinical settings; the metabolic changes associated with neurodegeneration can be subtle and diffuse; and it is difficult to consistently assess the extent and severity of metabolic alterations by visual inspection of the reconstructed images. To overcome these challenges, a quantitative statistical mapping approach for scan interpretation was developed (*15*).

In statistical mapping, the original reconstructed images are realigned in the stereotactic coordinate system (*16*), and individual anatomic differences across subjects are minimized by anatomic standardization (*17,18*). The anatomically standardized image set from an individual subject is compared with a normal database composed of similarly processed image sets from multiple age-similar cognitively normal subjects, and the differences between the individual scan compared with the normal database are visualized as a *z* score map (*15*). To further reduce the residual anatomic differences across subjects and to minimize effects of cortical atrophy on this comparison, a 3-dimensional stereotactic surface projection (3D-SSP) algorithm can be applied as a data extraction/reduction method (Fig. 2) (*15*). *z* score maps demonstrate the pattern of altered $^{18}$F-FDG uptake in a standardized format, which can be used for scan interpretation in conjunction with the original reconstructed images. This approach not only improves overall diagnostic accuracy (Fig. 3), but also offers quantitative information on the significance level of detected abnormalities, helps to standardize interpretation, allows cross-institutional comparisons, and helps support consistent scan interpretation by physicians with

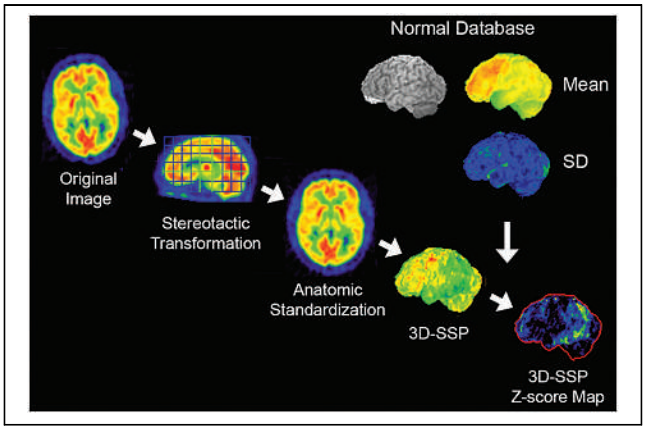


**FIGURE 2.** 3D-SSP. Original transaxial images are anatomically standardized in the stereotactic coordinate system, and gray matter activity is extracted on a pixel-by-pixel basis by the 3D-SSP algorithm. Extracted data are then compared with a normal database (mean and SD), which is composed of similarly processed PET scans from multiple normal subjects. Differences between individual data and normal database are expressed as *z* score maps.

different levels of experience (*19*). Statistical mapping relies on the consistency of image quality that can be improved by standardized imaging protocols and image reconstruction.

Statistical mapping with $^{18}$F-FDG PET was also used to discover metabolic signatures unique to different types of dementing disorders. Hypometabolism in the posterior cingulate cortex was found in an early stage of AD (*20,21*) and in APOE4 homozygote subjects (*22*). Hypometabolism in the primary visual cortex and the occipital lobe was found in Parkinson disease with dementia (*23*) as well as autopsy-proven DLB (*24*). These findings are now hallmarks in the clinical interpretation of $^{18}$F-FDG PET scans.

When applying imaging biomarkers to better understand the pathologic changes occurring in AD (*25*), differences in the detection threshold of each imaging modality or biomarker need to be carefully incorporated into the interpretation. The detection threshold is also significantly affected by the method used for the analysis of the imaging data. According to a metaanalysis based on the imaging biomarker framework of "Metrics" and "Submarkers" (*26*), the diagnostic positive likelihood ratio of $^{18}$F-FDG PET analyzed by 3D-SSP was equivalent to that of an amyloid PET distribution volume ratio (DVR) analysis. However, when $^{18}$F-FDG PET was interpreted visually, the diagnostic positive likelihood ratio decreased precipitously. Different statistical mapping methods can also yield different outcomes (*27*). If biomarker findings are used to infer the pathogenesis of the disease and the time course for progression, such differences in the detection threshold simply due to the analytic method can cause a significant bias in research.

## CLINICAL IMAGING ALTERNATIVES TO $^{18}$F-FDG PET FOR DEMENTIA EVALUATION

Regional energy metabolism and cerebral blood flow are tightly coupled in physiologic or nonacute pathologic conditions (*28*), and such coupling may be generally preserved in aging (*29*) and neurodegeneration (Fig. 1B). These observations serve as the physiologic basis to use cerebral blood flow as measured by perfusion SPECT (or PET) as an alternative to $^{18}$F-FDG PET for dementia evaluation. However, perfusion SPECT suffers from technical factors, such as a lower spatial resolution and sensitivity, inaccuracy in the attenuation correction, and difficulties in standardizing image quality and quantification. Recent efforts to translate perfusion SPECT/PET techniques to MRI-based perfusion measurements, such as arterial spine labeling MRI, are ongoing (*30,31*). Perfusion-equivalent information can also be obtained from early-phase dynamic PET imaging of amyloid (*32,33*) or tau (*34*) PET. The diagnostic accuracy of these alternative techniques needs to be established prospectively among dementia patients seen in clinical settings.

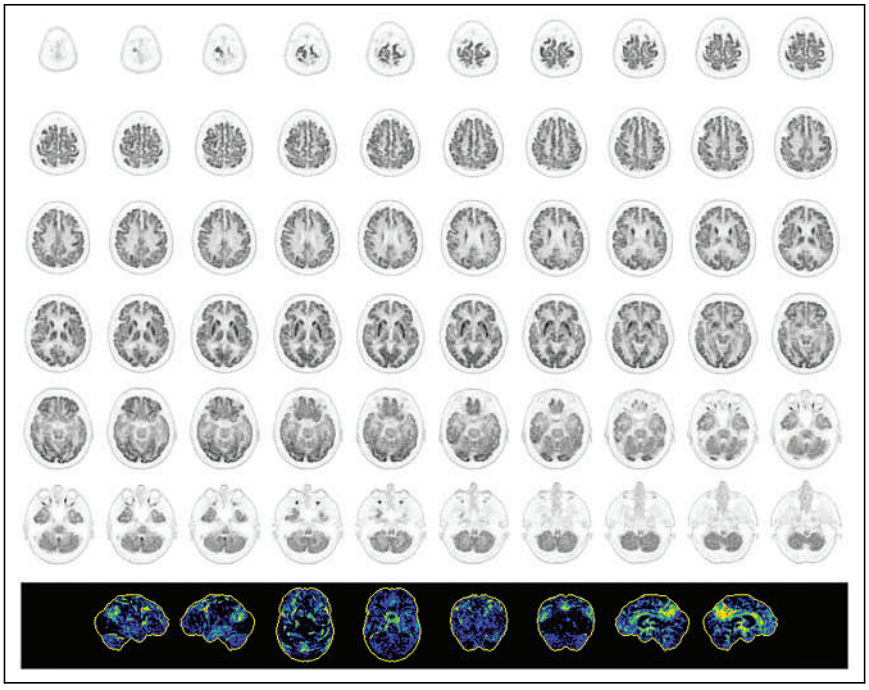

**FIGURE 3.** $^{18}$F-FDG PET scan of patient with progressive mild cognitive decline. Original transaxial images (top 6 rows, black and white) demonstrate very mild metabolic reductions in parietal association cortex and posterior cingulate cortex/precuneus. However, such mild changes cannot be appreciated consistently. 3D-SSP *z* score maps (bottom row, from left to right: right lateral, left lateral, superior, inferior, anterior, posterior, right medial, and left medial views) from same patient demonstrate apparent metabolic reductions in posterior cingulate cortex/precuneus as well as parietal association cortex bilaterally seen on lateral, superior, and posterior views. Statistical mapping, if used appropriately, improves diagnostic accuracy and consistency.

## DIFFERENTIAL DIAGNOSIS OF AD, FTD, AND DLB: STANDARD OF CARE

The most common use of $^{18}$F-FDG PET in the context of a dementia evaluation is to differentiate AD, FTD, and DLB (Table 1). The clinical course, complications, and clinical management of these conditions differ. An accurate and specific diagnosis guides both clinicians and family care partners, permitting early interventions and proactive

**TABLE 1**
Differential Diagnosis of Neurodegenerative Dementing Disorders by $^{18}$F-FDG PET

| |
|---|
| Major differential diagnosis: standard of care |
| Alzheimer disease (AD) |
| Frontotemporal dementia (FTD) |
| Dementia with Lewy bodies (DLB) |
| Subtype Classification of FTLD/FTD |
| Behavioral variant FTD (bvFTD) and Pick's disease (PiD) |
| Primary progressive aphasia (PPA) |
| Semantic variant PPA (svPPA) or semantic dementia (SD) |
| Nonfluent variant PPA (nfvPPA) or progressive nonfluent aphasia (PNFA) |
| Logopenic variant PPA (lvPPA) or logopenic progressive aphasia (LPA) |
| Movement disorders |
| Progressive supranuclear palsy (PSP) |
| Corticobasal degeneration (CBD) |
| Recently recognized neurodegenerative disorders |
| Limbic-predominant age-related TDP-43 encephalopathy (LATE) |
| Hippocampus sclerosis (HS) |
| Primary age-related tauopathy (PART) |
| Argyrophilic grain disease (AGD) |
| Fused in sarcoma (FUS) |
| Mixed dementia with copathologies and overlapping disorders |
| AD and vascular dementia (VaD) |
| Dementia with multiple neurodegenerative copathologies +/− VaD |

planning. Cholinesterase inhibitors and memantine are effective in AD, but not in FTD (*35*). Amyloid targeting immunotherapy has the potential to be disease modifying only in AD. $^{18}$F-FDG PET offers improved diagnosis of DLB, sometimes not initially considered by the clinician. Adverse events are more frequently associated with neuroleptics in DLB and Parkinson disease with dementia (*36*). Therefore, the clinical differential diagnosis of major neurodegenerative disease categories, AD, FTD, and DLB, becomes critical in terms of appropriate medication and patient management. In the United States, the clinical use of $^{18}$F-FDG PET for the differential diagnosis of AD versus FTD can be covered by the Centers for Medicare & Medicaid Services.

$^{18}$F-FDG PET imaging features associated with AD, FTD, and DLB have been characterized by numerous investigators over the last 4 decades. Different types of neurodegenerative disorders tend to affect specific brain regions (selective vulnerability) while relatively sparing other regions. The spatial patterns of decreased versus relatively preserved $^{18}$F-FDG uptake in the brain give differential clues to the specific neurodegenerative substrate (Fig. 4).

In AD, the parietotemporal association cortices as well as the posterior cingulate cortex and precuneus are commonly involved. However, the metabolic activity in the primary sensorimotor and primary visual cortices as well as the basal ganglia, thalamus, pons, and cerebellum is relatively preserved (*15*). The areas of relatively preserved activity, such as the pons, can be used as a reference region for pixel normalization in quantitative image analysis (*37*). As the disease progresses, the frontal association cortex becomes involved. However, in a fraction of AD patients with prominent behavioral symptoms (behavioral variant of AD [bvAD]), the frontal lobe involvement can be distinguished at an early stage of the disease, and it is difficult to differentiate from the behavioral variant of FTD (bvFTD) on $^{18}$F-FDG PET imaging (*38*).

FTD or classic Pick's disease generally affects the frontal association cortex and the anterior temporal lobe. Additional decreased uptake can be seen progressively in the caudate nucleus and thalamus (*39*). The frontal involvement in bvFTD is often sharply demarcated, and was initially described as "lobar atrophy" on CT or MRI (*40*). Asymmetric involvement of the hemispheres appears to be quite common (*41*).

DLB shows $^{18}$F-FDG PET findings similar to those of AD, but additional hypometabolism is seen in the primary visual cortex in the medial occipital lobe where activity is relatively preserved in AD (*24*). Such metabolic reductions in the occipital lobe make the differential diagnosis between DLB and posterior cortical atrophy somewhat challenging (*42*). Metabolic activity in the posterior cingulate cortex seems less affected in DLB than AD ("cingulate island sign") (*43*). Both occipital hypometabolism and cingulate island sign on $^{18}$F-FDG PET are considered as supportive features in the consensus diagnostic criteria for DLB (*36*).

## PREDICTIVE VALUE OF $^{18}$F-FDG PET IN EVALUATION OF COGNITIVE DECLINE

One significant value of $^{18}$F-FDG PET has been attributed to the short-term prediction of impending dementia in subjects with mild cognitive impairment (MCI). Particularly, metabolic reductions in the posterior cingulate cortex have been demonstrated to have high predictive value (*21,44*). Interestingly, the added predictive value of $^{18}$F-FDG PET over amyloid PET imaging has also been demonstrated, as it was shown that amyloid-positive MCI patients without hypometabolic abnormalities maintained clinical stability over years (*45*). It has been discussed frequently that $^{18}$F-FDG PET also represents an ideal tool for disease staging and follow-up due to its tight association with patient symptoms and clinical severity (*46*). $^{18}$F-FDG PET has found entrance into various expert recommendations within this context (*47,48*).

## CLINICAL SUBTYPES OF AD

Suspected AD patients may show atypical clinical features and $^{18}$F-FDG PET findings. Recent investigations using molecular imaging biomarkers have contributed to the consideration of AD subtypes, which are not as infrequent as previously assumed. AD subtypes are accompanied by characteristic patterns of hypometabolism on $^{18}$F-FDG PET, closely reflecting symptomatic features. Investigations demonstrated similar spatial variations of neuropathology in AD (*49*). These observations also indicate that, in later stages of the disease, different subtypes may converge to a common pattern of disease topography.

AD subtypes with visual symptoms (posterior cortical atrophy), a frontal executive or behavioral variant (bvAD, discussed earlier in the article), and a language-dominant variant (logopenic variant PPA, discussed later in the article) have been described. Clinically, posterior cortical atrophy is initially characterized by dominant visual-constructive deficits (*50*). On $^{18}$F-FDG PET, a distinct bilateral occipitoparietal hypometabolism has been described (*42*).

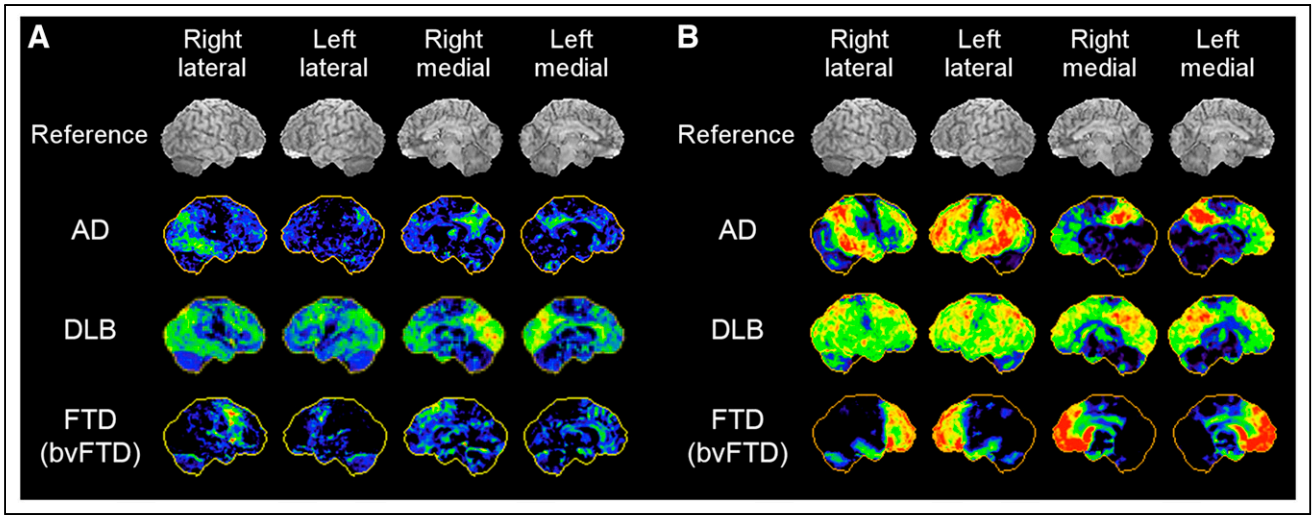


**FIGURE 4.** $^{18}$F-FDG PET 3D-SSP maps from representative cases of AD, DLB, versus bvFTD. Red indicates more severe hypometabolism. Mild cases (A) and severe cases (B) are shown.

In the fraction of AD patients with the frontal/executive subtype (bvAD), behavioral symptoms dominate the initial clinical appearance, and, also in $^{18}$F-FDG PET, the frontal lobe involvement can be prominent from an early stage of the disease. In a fraction of patients clinically diagnosed with a logopenic form of aphasia (lvPPA) and often assigned clinically to FTD (see below), amyloid pathology was confirmed as one of the underlying neuropathologies (*51*).

## CLINICAL SUBTYPES OF FRONTOTEMPORAL LOBAR DEGENERATION (FTLD)/FTD

Over the last few decades, there has been an evolving recognition of different clinical presentations and neuropathologies in frontotemporal dementia, as well as a better understanding of the clinicopathologic and imaging correlations. FTLD, an umbrella term used for several different neurodegenerative disorders, is characterized by neurodegeneration predominantly involving the frontal and temporal lobes (*52*). FTLD and FTD are sometimes used interchangeably. They present heterogeneous clinical features and underlying pathologies not in one-to-one correspondence, creating a complex clinicopathologic relationship. Generally, FTLD/FTD encompasses clinical presentations of bvFTD, often referred to as simply FTD or Pick's disease; PPA; and atypical parkinsonism/movement disorders such as progressive supranuclear palsy (PSP) and corticobasal degeneration (CBD) (Table 1). PPA is further subclassified based on clinical features of the language disturbance into semantic variant PPA (svPPA), also called semantic dementia (SD); nonfluent variant PPA (nfvPPA); and

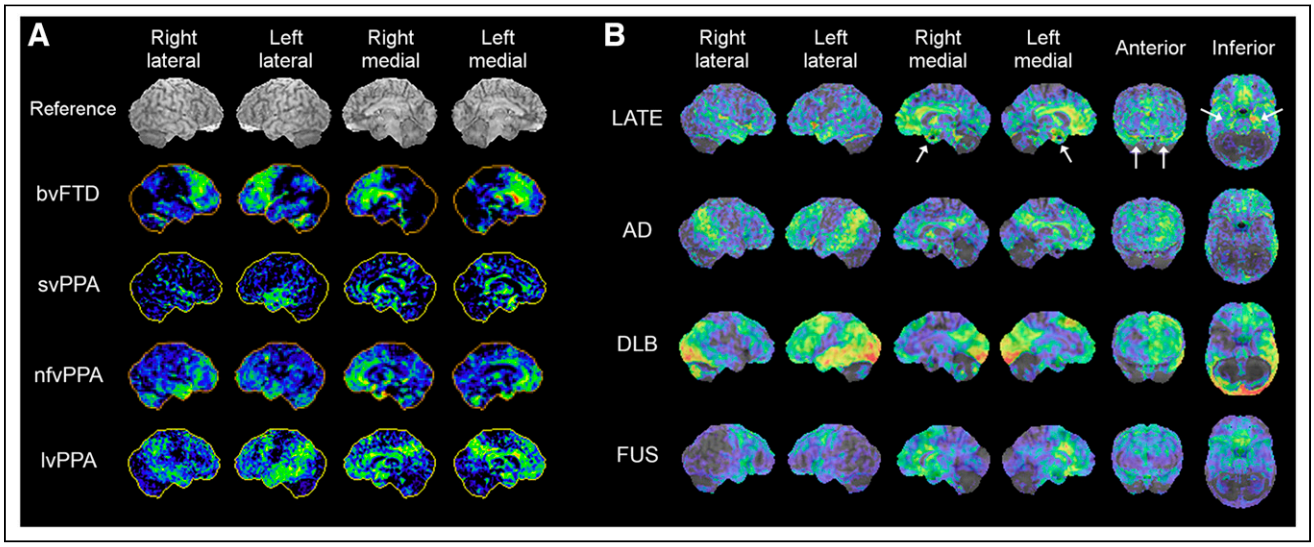


**FIGURE 5.** $^{18}$F-FDG PET 3D-SSP *z* score maps of representative cases of FTLD/FTD variants, bvFTD, svPPA, nfvPPA, lvPPA, and PSP (A) and LATE, AD, DLB, and FUS (B, *z* score maps superimposed on reference MR image). The case of nfvPPA presented here shows bilateral temporofrontal involvement with right side slightly more prominent than left. LATE demonstrates prominent involvement of medial temporal lobe and hippocampus (white arrows) and medial and orbital frontal cortices. $^{18}$F-FDG uptake in medial temporal lobe is relatively mild in AD and DLB. FUS demonstrates pattern involving frontal and anterior temporal lobes, resembling FTLD/FLD spectrum.

lvPPA. The underlying pathologic changes of the PPA subtypes are heterogeneous. Classification of PPA subtypes also provides information valuable to patient management. Although there are no disease pathology–modifying treatments yet available for PPA, an accurate diagnosis of PPA subtypes facilitates the appropriate patient management including speech therapy and planning of care, as each subtype presents with a different time course of disease progression and clinical complications (*53*). There has been increasing evidence of differential findings on $^{18}$F-FDG PET associated with FTLD/FTD subtypes (Fig. 5A) relevant to clinical interpretation (*54–56*). Consequently, a recent expert consensus recommends $^{18}$F-FDG PET as a first-line PET examination for workup of patients with suspected non–AD-type dementia (*48*).

## PPA: THREE SUBTYPES

Patients with svPPA or SD present with a loss of semantic memory in both verbal and nonverbal domains. $^{18}$F-FDG PET findings are fairly characteristic, involving the anterior temporal lobe bilaterally, but often the left temporal lobe is more severely hypometabolic than the right (Fig. 5A, svPPA). Hypometabolism in the anterior temporal lobe is distinct from the pattern of temporal lobe involvement seen in AD, in which the mid to posterior lateral temporal cortex is often affected. A similar pattern of decreased $^{18}$F-FDG uptake can be seen in the right anterior temporal lobe (right-sided SD) often presenting with a different language/behavioral profile than that of left-sided SD (*57*), and the differential diagnosis from bvFTD can become challenging (*58*).

Patients with nfvPPA or progressive nonfluent aphasia experience difficulty in speaking, apraxia of speech, agrammatism, and impaired comprehension of complex sentences, as well as difficulty in swallowing and other motor symptoms sometimes apparent in other types of FTD. Decreased $^{18}$F-FDG uptake is often seen in the left lateral posterior frontal and superior medial frontal cortices, as well as the insula (Fig. 5A, nfvPPA) (*55,59*), which is distinct from the anterior temporal lobe hypometabolism seen in svPPA/SD.

Patients with lvPPA or logopenic progressive aphasia often manifest impaired naming and sentence repetition and an inability to retain complex verbal information, as the disease progresses. They also tend to exhibit more cognitive and behavioral symptoms as compared with other types of PPA (*59*), likely reflecting a frequent underlying AD pathology (*59*), but other pathologies have also been identified in lvPPA (*60*). Decreased $^{18}$F-FDG uptake is typically seen in the posterior temporal cortex and inferior parietal lobule in lvPPA, with the left hemisphere often more severely affected than the right (Fig. 5A, lvPPA). These findings are somewhat similar to those of AD (*55,56*). reflecting the underlying pathology.

## ATYPICAL PARKINSONIAN MOVEMENT DISORDERS (PSP AND CBD)

Atypical parkinsonism caused by neurodegeneration including PSP and CBD can manifest with variable motor and cognitive disorders. PSP and CBD affect the frontal and temporal lobes and are often considered FTD variants. Both conditions are marked by tauopathy. PSP and CBD show diminished radiotracer uptake in the striatum on dopamine transporter SPECT imaging or presynaptic dopaminergic PET imaging, unlike AD and most FTD (*61*). Although dopamine transporter SPECT findings cannot differentiate PSP and CBD, patterns of decreased $^{18}$F-FDG uptake can provide a clue for the differential diagnosis among these Parkinson-plus syndromes.

The antemortem diagnosis of PSP versus other cognitive disorders can be challenging. $^{18}$F-FDG PET shows decreased cortical uptake in the medial frontal and anterior cingulate cortices as well as caudate nuclei and thalami (*62*). In addition, distinct focally decreased uptake is seen in the midbrain (*63*) before atrophy of the midbrain tegmentum detected by MRI, which is known as the Hummingbird sign (*64*). CBD is characterized by rigidity, apraxia, uncontrollable limb movement ("alien limb syndrome") and cognitive impairment. Recently, the term corticobasal syndrome has been used for the clinical classification of this entity because of a growing recognition that different neuropathologies including AD pathology can underlie this symptom-complex (*65*). $^{18}$F-FDG PET shows decreased uptake in the frontoparietal regions without sparing of the sensorimotor cortex, basal ganglia, and thalamus in CBD, and is often noticeably asymmetric, which is consistent with the pattern of clinical symptoms (*66*).

## RECENTLY RECOGNIZED NEURODEGENERATIVE DEMENTING DISORDERS

Recent efforts in the development and identification of new pathologic markers, investigations based on large series of clinicopathologic correlations, and consensus efforts have resulted in the recognition of new categories for neurodegenerative disorders. The prevalence of some of these disorders is greater than previously suspected. Molecular imaging plays a major role in the antemortem characterization of such disorders, and the differential findings from $^{18}$F-FDG PET need to be incorporated into the interpretation (Table 1).

## LIMBIC-PREDOMINANT AGE-RELATED TDP-43 ENCEPHALOPATHY (LATE) AND HIPPOCAMPUS SCLEROSIS (HS)

The recent identification of the transactive response DNA binding protein of 43 kDa (TDP-43) proteinopathy has led to a new category of neurodegenerative dementia occurring late in life, namely LATE. The anatomic manifestation of LATE can be a profound atrophy in the hippocampus, likely making up a significant proportion of cases previously classified as HS (*67*). Frequent occurrence of HS in dementia patients was later recognized in some large autopsy series (*68,69*). Phosphorylated TDP-43 was initially identified in FTLD and amyotrophic lateral sclerosis (*70*) and subsequently identified in patients with AD and HS (*71*), particularly among elderly patients above the age of 80 y. These observations have led to the recognition of TDP-43 proteinopathy, which is often associated with HS and cognitive impairment, as a distinct disease entity (*72*) despite significant overlap with other neurodegenerative disorders such as AD and FTLD. A consensus working group report describing LATE has been published recently (*73*).

LATE mainly affects people older than 80 y and manifests with cognitive impairment, which mimics amnestic dementia similar to AD. LATE neuropathologic changes exist in more than 20% (ranging from 5% to 50%) of subjects in an autopsy series, and the overall public health impact of LATE is considered to be the same order of magnitude as AD (*73*). LATE is often associated with hippocampal atrophy as seen by MRI. In elderly patients with Alzheimer dementia, hippocampal volume was more strongly associated with TDP-43/HS than AD (*74*).

The number of reports of $^{18}$F-FDG PET findings in autopsy-confirmed LATE is increasing, and findings are also extrapolated from observations in HS and amyloid-negative, tau-negative

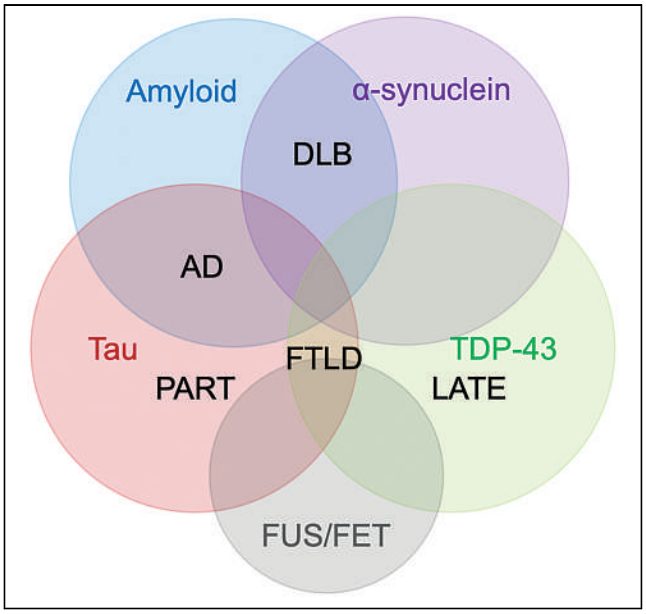


**FIGURE 6.** Cooccurrence of 4 major proteinopathies: amyloid, tau, α-synuclein, and TDP-43, and overlapping neurodegenerative disorders: AD, DLB, FTLD, PART, and LATE. Emerging proteinopathies such as fused in sarcoma (FUS), which belongs to the FET family of proteins (FUS, EWS, TAF15), have been identified in FTLD, comorbid with other proteinopathies, and awaiting further characterization. Pathologic diagnosis of neurodegenerative disorders involves new markers, and further investigations of clinicopathologic correlations including imaging will allow more precise antemortem diagnosis in the future.

dementia patients (suspected non-Alzheimer disease pathophysiology (*14*)). These investigations demonstrated significant hypometabolism in the medial temporal lobe including hippocampus, whereas in AD hippocampal $^{18}$F-FDG uptake is less affected (*75*); hypometabolism in the medial temporal lobe and the superior medial frontal and orbital frontal cortices (*76*); and decreased uptake in the medial and lateral temporal lobes as well as the prefrontal cortex (Fig. 5B) (*77*). The ratio of inferior temporal metabolism over medial temporal metabolism was significantly higher in HS patients (*75*). However, how specific these findings are to LATE is not currently known. As described in the next section, other neurodegenerative disorders affecting the medial temporal lobe also demonstrate decreased uptake, which can mimic LATE findings on $^{18}$F-FDG PET imaging.

When an amnestic patient has $^{18}$F-FDG PET findings not typical of AD, FTD, or DLB, LATE could be a differential diagnostic consideration particularly in elderly patients. Hippocampal atrophy detected by MRI suggests not only AD, but also LATE. Currently, there is no specific imaging biomarker or TDP-43 ligand, and TDP-43/LATE-neuropathologic changes pathology could be indirectly speculated by exclusion (negative amyloid PET and negative tau PET). Alternatively, $^{18}$F-FDG PET may provide supportive evidence of LATE by demonstrating medial temporal lobe abnormalities. Further investigations on the clinicopathologic and imaging correlations of LATE are clearly warranted.

### ARGYROPHILIC GRAIN DISEASE (AGD), PRIMARY AGE-RELATED TAUOPATHY (PART), AND FUSED IN SARCOMA (FUS)

Recent advances in tau PET are shedding new light on neurodegenerative disorders that have been described by neuropathologists in the past 2 decades. AGD is characterized by pathologic features of small argyrophilic inclusions in the hippocampus, which are largely composed of 4-repeat tau isoforms (*78*). Patients manifest a slowly progressive MCI, often accompanied by behavioral symptoms suggesting FTD. The prevalence was reported as high as 30% in an autopsy series of patients with dementia and also can be found in normal control individuals (*79*), and AGD often coexists with other neurodegenerative disorders such as AD and FTLD (*80*).

PART is characterized by neurofibrillary tangles without coexisting Alzheimer neuritic amyloid plaques and appears to be common in elderly patients (*81*). Previously described as "tangle-only dementia," the neurofibrillary tangles seen in PART are composed of 3-repeat and 4-repeat isoforms similar to AD, and the changes are typically seen in the temporal lobe (*80*). It has been debated if PART is a distinct disease entity or within the spectrum of AD. PART patients demonstrate slower decline in memory, language, and visuospatial functions than patients with AD (*82*).

The presence of tau deposition in PART can be depicted by tau PET (*83*). A recent investigation using both amyloid and tau PET revealed a significant fraction of patients with negative amyloid and positive tau PET findings (A−T+N+), which might be consistent with a high prevalence of PART (*84*). The diagnostic features of $^{18}$F-FDG PET are still under investigation but thus far demonstrated medial temporal hypometabolism with extension into the frontolimbic regions in amyloid-negative and very slowly progressing amnestic MCI patients with suspected PART, AGD, or LATE pathologies.

Abnormal deposition of FUS protein is found in amyotrophic lateral sclerosis as well as in FTLD and recognized relatively recently as a form of neurodegenerative dementia (*70*). Clinicopathologic characterization is still under investigation, and some

**TABLE 2**
Examples of Mixed/Comorbid Neurodegenerative Dementing Disorders

| Mixed/comorbid neurodegenerative dementing disorders | Reference |
|---|---|
| AD and TDP-43, cerebral amyloid angiopathy | (*91*) |
| AD and corticobasal syndrome, FTLD-TDP, Lewy body disease | (*92*) |
| AD and CBD | (*93*) |
| AD and tauopathy, TDP-43 | (*72*) |
| AD and DLB with TDP-43, tau, α-synuclein pathologies | (*94*) |
| DLB and AD pathology | (*95*) |
| FTLD-tau and AD and vascular copathologies | (*96*) |
| PSP and AD | (*97*) |
| PSP and AD and PD | (*98*) |
| PSP and AD, AGD, CBD, Lewy body disease | (*99*) |
| PiD and AD | (*100*) |
| PiD and AD, cerebral amyloid angiopathy, Lewy body disease | (*101*) |
| PiD and PSP | (*102*) |

PiD = Pick's disease.

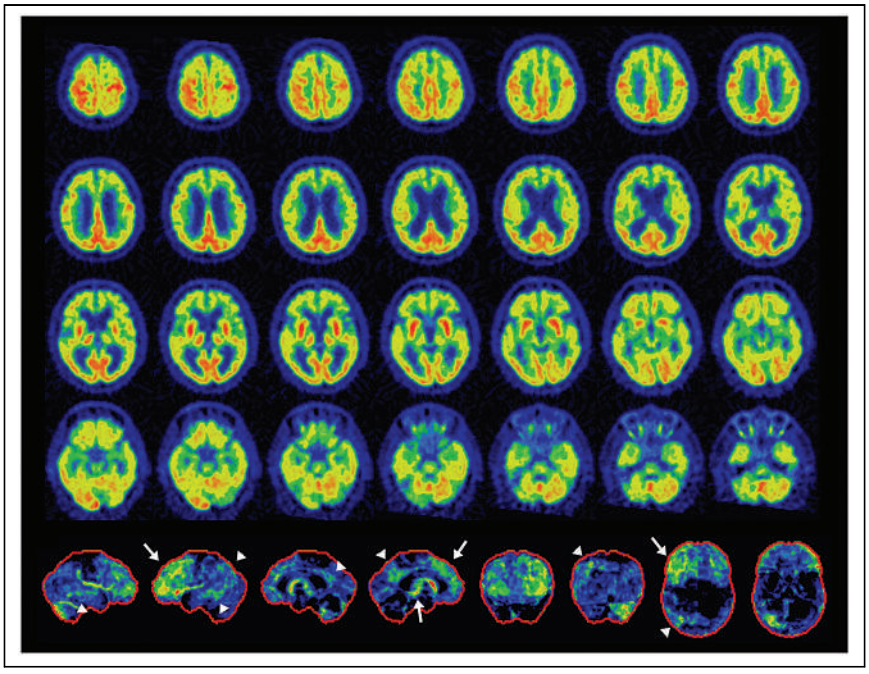

**FIGURE 7.** Example of mixed dementia, PSP+AD. Antemortem $^{18}$F-FDG PET: transaxial images (top 4 rows) and 3D-SSP *z* score maps (bottom row, from the left to right: right lateral, left lateral, right medial, and left medial, anterior, posterior, superior, inferior views). Findings are consistent with PSP (white arrows) and AD (arrowheads). Left-dominant pathologies associated with crossed-cerebellar diaschisis in right cerebellar hemisphere. It is important to note that these findings do not necessarily preclude other mixed pathologies. However, the frontal findings best explained the patient's clinical symptoms.

report indicated caudate atrophy as one of the features of FUS (*85*). $^{18}$F-FDG PET findings of FUS have not been characterized systematically, but the pattern of hypometabolism appears to conform to the FTLD spectrum (Fig. 5B).

## MIXED DEMENTIA AND COEXISTING PATHOLOGIES

There has been renewed enthusiasm to better characterize overlapping and coexisting neurodegenerative disorders because of the discovery of new pathologic markers, molecular imaging, and investigations of clinicopathologic correlations. It has been long appreciated that 2 or more pathologies can often coexist in dementia patients. For example, AD and vascular dementia (VaD), 2 common causes of dementia, often coexist (*86*) and this is referred to as "mixed dementia," for which the prevalence may be quite high. With the development of new pathologic markers, mixed dementia with coexisting multiple neurodegenerative disorders, in addition to vascular changes, is becoming recognized more frequently, particularly in elderly patients. A recent autopsy investigation showed 94% with one or more pathologies, 78% with 2 or more, 58% with 3 or more, and 35% with 4 or more pathologies, among elderly patients with cognitive impairment (*87*). The presence of major pathologic markers such as amyloid, tau, α-synuclein, and TDP-43 overlaps and coexists in such dementia patients (Fig. 6). Various mixed dementia with multiple comorbid neurodegenerative disorders as defined by pathologic markers have been reported (Table 2; Fig. 7).

When $^{18}$F-FDG PET does not demonstrate typical patterns of known neurodegenerative disorders or when multimodal imaging results are incongruent, mixed dementia with multiple copathologies should be a clinical consideration (*88,89*). Even in cases with characteristic patterns of $^{18}$F-FDG PET, it is important to recognize that the topography of neuronal dysfunction does not necessarily indicate specific or exclusive neuropathologies or proteomic abnormalities. However, $^{18}$F-FDG PET may be able to confirm the clinically congruent predominant cause of dementia, even in the presence of copathologies (*90*).

## THE EVOLVING ROLE OF $^{18}$F-FDG PET IN DEMENTIA EVALUATION

$^{18}$F-FDG PET has been used as a research tool as well as a clinical diagnostic tool in dementia evaluation. It can depict early metabolic changes associated with neurodegenerative disorders before the structural changes seen on CT or MRI. Early diagnosis of AD, FTD, and DLB has been, in part, complemented by the detection of specific pathologies on imaging biomarkers such as amyloid PET, tau PET, and dopamine transporter SPECT. However, access to amyloid and tau PET biomarkers is limited clinically, in part due to limited reimbursement. Currently, $^{18}$F-FDG PET is used primarily for the differential diagnosis of dementia and prediction of further cognitive decline among patients with MCI. It is relatively inexpensive, is widely available, and can differentiate multiple neurodegenerative disorders in a single test when images are interpreted accurately by trained clinicians using validated statistical mapping technology.

The dichotomous distinction of AD versus FTD by $^{18}$F-FDG PET is no longer sufficient or possible, given our increasing knowledge of disease subtypes and a recognition of the overlapping cooccurrence of multiple pathologies, particularly in elderly patients. It becomes less relevant to fit $^{18}$F-FDG PET findings into a single category of neurodegeneration. $^{18}$F-FDG PET findings supporting the cause of a patient's main clinical features and identifying possible copathologies are important for clinical management. Such an approach is often required when interpreting cases with complex or atypical clinical presentations, which tend to be referred for advanced imaging by dementia specialists.

Currently, extensive efforts are under way to demonstrate the clinical effectiveness of amyloid-targeting immunotherapy to treat AD. When such treatments become widely available, the evaluation of copathologies in patients with amyloid-positive PET may become critical since antiamyloid monotherapy in such situations is likely to have limited efficacy. The use of imaging and nonimaging biomarkers, if available, is one way to address this issue. However, $^{18}$F-FDG PET may be a less expensive and more direct way to provide insight into the cause of typical and atypical clinical presentations and identify concurrent neurodegenerative disorders, thus helping guide the use of disease specific therapeutics.

## SUMMARY

$^{18}$F-FDG PET has been used for dementia research and clinical applications for more than 4 decades. Although the detailed cellular

mechanisms of glucose metabolism are still under investigation, $^{18}$F-FDG PET can sensitively display the distinct patterns of neuronal and synaptic dysfunction associated with neurodegeneration, allowing early diagnosis and prediction of further cognitive decline. Differential patterns of altered $^{18}$F-FDG uptake can provide important differential diagnostic clues to clinicians, particularly when the interpretation of images is aided by statistical mapping technologies, which have become widely available in the clinic. The recognition by $^{18}$F-FDG PET of the 3 major neurodegenerative disorders, AD, FTD, and DLB, has become a standard of care. In addition, the subtypes of FTD/FTLD have been more widely recognized clinically, as well as pathologically, and are distinguishable by $^{18}$F-FDG PET and other molecular imaging techniques. New disease categories, such as LATE, PART, AGD, and FUS, have also been identified, and need to be incorporated into the differential diagnoses. Mixed dementia, not only AD and VaD but also multiple neurodegenerative disorders as defined by pathologic markers, is prevalent, particularly in elderly patients. By integrating recent insights into the modern interpretation of $^{18}$F-FDG PET, the potential of this diagnostic tool can be extended beyond established applications as a precise imaging biomarker of functional disease endophenotype and can contribute to care management. When $^{18}$F-FDG PET scans do not demonstrate typical features of known neurodegenerative disorders or typical features with atypical secondary findings, considerations for mixed dementia with copathologies or a newly recognized form of dementia such as LATE are needed in the clinical interpretation of $^{18}$F-FDG PET.

## DISCLOSURE

No potential conflict of interest relevant to this article was reported.

## REFERENCES


1. Bélanger M, Allaman I, Magistretti PJ. Brain energy metabolism: focus on astrocyte-neuron metabolic cooperation. *Cell Metab.* 2011;14:724–738.
2. Sokoloff L, Reivich M, Kennedy C, et al. The [$^{14}$C]deoxyglucose method for the measurement of local cerebral glucose utilization: theory, procedure, and normal values in the conscious and anesthetized albino rat. *J Neurochem.* 1977;28:897–916.
3. Reivich M, Kuhl D, Wolf A, et al. Measurement of local cerebral glucose metabolism in man with $^{18}$F-2-fluoro-2-deoxy-d-glucose. *Acta Neurol Scand Suppl.* 1977;64:190–191.
4. Vannucci SJ, Maher F, Simpson IA. Glucose transporter proteins in brain: delivery of glucose to neurons and glia. *Glia.* 1997;21:2–21.
5. Nelson T, Lucignani G, Atlas S, Crane AM, Dienel GA, Sokoloff L. Reexamination of glucose-6-phosphatase activity in the brain in vivo: no evidence for a futile cycle. *Science.* 1985;229:60–62.
6. Attwell D, Laughlin SB. An energy budget for signaling in the grey matter of the brain. *J Cereb Blood Flow Metab.* 2001;21:1133–1145.
7. Sokoloff L. Function-related changes in energy metabolism in the nervous system: localization and mechanisms. *Keio J Med.* 1993;42:95–103.
8. Magistretti PJ, Pellerin L. Cellular bases of brain energy metabolism and their relevance to functional brain imaging: evidence for a prominent role of astrocytes. *Cereb Cortex.* 1996;6:50–61.
9. Baron JC, Bousser MG, Comar D, Castaigne P. "Crossed cerebellar diaschisis" in human supratentorial brain infarction. *Trans Am Neurol Assoc.* 1981;105:459–461.
10. Reesink FE, García DV, Sánchez-Catasús CA, et al. Crossed cerebellar diaschisis in Alzheimer's disease. *Curr Alzheimer Res.* 2018;15:1267–1275.
11. Franceschi AM, Clifton MA, Naser-Tavakolian K, et al. FDG PET/MRI for Visual Detection of Crossed Cerebellar Diaschisis in Patients With Dementia. *AJR.* 2021;216:165–171.
12. Provost K, La Joie R, Strom A, et al. Crossed cerebellar diaschisis on $^{18}$F-FDG PET: frequency across neurodegenerative syndromes and association with $^{11}$C-PIB and $^{18}$F-flortaucipir. *J Cereb Blood Flow Metab.* 2021;41:2329–2343.
13. Akiyama H, Harrop R, McGeer PL, Peppard R, McGeer EG. Crossed cerebellar and uncrossed basal ganglia and thalamic diaschisis in Alzheimer's disease. *Neurology.* 1989;39:541–548.
14. Jack CR Jr, Bennett DA, Blennow K, et al. NIA-AA research framework: toward a biological definition of Alzheimer's disease. *Alzheimers Dement.* 2018;14:535–562.
15. Minoshima S, Frey KA, Koeppe RA, Foster NL, Kuhl DE. A diagnostic approach in Alzheimer's disease using three-dimensional stereotactic surface projections of fluorine-18-FDG PET. *J Nucl Med.* 1995;36:1238–1248.
16. Talairach J, Tournoux P. *Co-Planar Stereotaxic Atlas of the Human Brain.* New York: Thieme; 1988.
17. Minoshima S, Koeppe RA, Frey KA, Kuhl DE. Anatomic standardization: linear scaling and nonlinear warping of functional brain images. *J Nucl Med.* 1994;35:1528–1537.
18. Ishii K, Willoch F, Minoshima S, et al. Statistical brain mapping of $^{18}$F-FDG PET in Alzheimer's disease: validation of anatomic standardization for atrophied brains. *J Nucl Med.* 2001;42:548–557.
19. Burdette JH, Minoshima S, Vander Borght T, Tran DD, Kuhl DE. Alzheimer disease: improved visual interpretation of PET images by using three-dimensional stereotaxic surface projections. *Radiology.* 1996;198:837–843.
20. Minoshima S, Foster NL, Kuhl DE. Posterior cingulate cortex in Alzheimer's disease. *Lancet.* 1994;344:895.
21. Minoshima S, Giordani B, Berent S, Frey KA, Foster NL, Kuhl DE. Metabolic reduction in the posterior cingulate cortex in very early Alzheimer's disease. *Ann Neurol.* 1997;42:85–94.
22. Reiman EM, Caselli RJ, Yun LS, et al. Preclinical evidence of Alzheimer's disease in persons homozygous for the epsilon 4 allele for apolipoprotein E. *N Engl J Med.* 1996;334:752–758.
23. Vander Borght T, Minoshima S, Giordani B, et al. Cerebral metabolic differences in Parkinson's and Alzheimer's diseases matched for dementia severity. *J Nucl Med.* 1997;38:797–802.
24. Minoshima S, Foster NL, Sima AA, Frey KA, Albin RL, Kuhl DE. Alzheimer's disease versus dementia with Lewy bodies: cerebral metabolic distinction with autopsy confirmation. *Ann Neurol.* 2001;50:358–365.
25. Jack CR Jr, Knopman DS, Jagust WJ, et al. Tracking pathophysiological processes in Alzheimer's disease: an updated hypothetical model of dynamic biomarkers. *Lancet Neurol.* 2013;12:207–216.
26. Frisoni GB, Bocchetta M, Chételat G, et al; ISTAART's NeuroImaging Professional Interest Area. Imaging markers for Alzheimer disease: which vs how. *Neurology.* 2013;81:487–500.
27. Garibotto V, Trombella S, Antelmi L, et al. A comparison of two statistical mapping tools for automated brain FDG-PET analysis in predicting conversion to Alzheimer's disease in subjects with mild cognitive impairment. *Curr Alzheimer Res.* 2020;17:1186–1194.
28. Kuschinsky W. Coupling of blood flow and metabolism in the brain. *J Basic Clin Physiol Pharmacol.* 1990;1:191–201.
29. Noda A, Ohba H, Kakiuchi T, Futatsubashi M, Tsukada H, Nishimura S. Age-related changes in cerebral blood flow and glucose metabolism in conscious rhesus monkeys. *Brain Res.* 2002;936:76–81.
30. Ceccarini J, Bourgeois S, Van Weehaeghe D, et al. Direct prospective comparison of $^{18}$F-FDG PET and arterial spin labelling MR using simultaneous PET/MR in patients referred for diagnosis of dementia. *Eur J Nucl Med Mol Imaging.* 2020;47:2142–2154.
31. Fällmar D, Haller S, Lilja J, et al. Arterial spin labeling-based Z-maps have high specificity and positive predictive value for neurodegenerative dementia compared to FDG-PET. *Eur Radiol.* 2017;27:4237–4246.
32. Rostomian AH, Madison C, Rabinovici GD, Jagust WJ. Early $^{11}$C-PIB frames and $^{18}$F-FDG PET measures are comparable: a study validated in a cohort of AD and FTLD patients. *J Nucl Med.* 2011;52:173–179.
33. Asghar M, Hinz R, Herholz K, Carter SF. Dual-phase [$^{18}$F]florbetapir in frontotemporal dementia. *Eur J Nucl Med Mol Imaging.* 2019;46:304–311.
34. Beyer L, Nitschmann A, Barthel H, et al. Early-phase [$^{18}$F]PI-2620 tau-PET imaging as a surrogate marker of neuronal injury. *Eur J Nucl Med Mol Imaging.* 2020;47:2911–2922.
35. Noufi P, Khoury R, Jeyakumar S, Grossberg GT. Use of cholinesterase inhibitors in non-Alzheimer's dementias. *Drugs Aging.* 2019;36:719–731.
36. McKeith IG, Boeve BF, Dickson DW, et al. Diagnosis and management of dementia with Lewy bodies: fourth consensus report of the DLB consortium. *Neurology.* 2017;89:88–100.
37. Minoshima S, Frey KA, Foster NL, Kuhl DE. Preserved pontine glucose metabolism in Alzheimer disease: a reference region for functional brain image (PET) analysis. *J Comput Assist Tomogr.* 1995;19:541–547.
38. Ossenkoppele R, Singleton EH, Groot C, et al. Research criteria for the behavioral variant of Alzheimer disease: a systematic review and meta-analysis. *JAMA Neurol.* 2022;79:48–60.

39. Grimmer T, Diehl J, Drzezga A, Förstl H, Kurz A. Region-specific decline of cerebral glucose metabolism in patients with frontotemporal dementia: a prospective $^{18}$F-FDG-PET study. *Dement Geriatr Cogn Disord.* 2004;18:32–36.
40. Tobo M, Fujii I, Hoaki T. Computed tomography in Pick's disease. *Folia Psychiatr Neurol Jpn.* 1984;38:137–141.
41. Jeong Y, Cho SS, Park JM, et al. $^{18}$F-FDG PET findings in frontotemporal dementia: an SPM analysis of 29 patients. *J Nucl Med.* 2005;46:233–239.
42. Whitwell JL, Graff-Radford J, Singh TD, et al. $^{18}$F-FDG PET in posterior cortical atrophy and dementia with Lewy bodies. *J Nucl Med.* 2017;58:632–638.
43. Lim SM, Katsifis A, Villemagne VL, et al. The $^{18}$F-FDG PET cingulate island sign and comparison to $^{123}$I-beta-CIT SPECT for diagnosis of dementia with Lewy bodies. *J Nucl Med.* 2009;50:1638–1645.
44. Drzezga A, Grimmer T, Riemenschneider M, et al. Prediction of individual clinical outcome in MCI by means of genetic assessment and (18)F-FDG PET. *J Nucl Med.* 2005;46:1625–1632.
45. Iaccarino L, Sala A, Perani D; Alzheimer's Disease Neuroimaging Initiative. Predicting long-term clinical stability in amyloid-positive subjects by FDG-PET. *Ann Clin Transl Neurol.* 2019;6:1113–1120.
46. Herholz K. Use of FDG PET as an imaging biomarker in clinical trials of Alzheimer's disease. *Biomarkers Med.* 2012;6:431–439.
47. Arbizu J, Festari C, Altomare D, et al; EANM-EAN Task Force for the Prescription of FDG-PET for Dementing Neurodegenerative Disorders. Clinical utility of FDG-PET for the clinical diagnosis in MCI. *Eur J Nucl Med Mol Imaging.* 2018; 45:1497–1508.
48. Chételat G, Arbizu J, Barthel H, et al. Amyloid-PET and $^{18}$F-FDG-PET in the diagnostic investigation of Alzheimer's disease and other dementias. *Lancet Neurol.* 2020;19:951–962.
49. Vogel JW, Young AL, Oxtoby NP, et al; Alzheimer's Disease Neuroimaging Initiative. Four distinct trajectories of tau deposition identified in Alzheimer's disease. *Nat Med.* 2021;27:871–881.
50. Crutch SJ, Lehmann M, Schott JM, Rabinovici GD, Rossor MN, Fox NC. Posterior cortical atrophy. *Lancet Neurol.* 2012;11:170–178.
51. Rabinovici GD, Rosen HJ, Alkalay A, et al. Amyloid vs FDG-PET in the differential diagnosis of AD and FTLD. *Neurology.* 2011;77:2034–2042.
52. Cairns NJ, Bigio EH, Mackenzie IR, et al; Consortium for Frontotemporal Lobar Degeneration. Neuropathologic diagnostic and nosologic criteria for frontotemporal lobar degeneration: consensus of the Consortium for Frontotemporal Lobar Degeneration. *Acta Neuropathol (Berl).* 2007;114:5–22.
53. Tippett DC, Keser Z. Clinical and neuroimaging characteristics of primary progressive aphasia. *Handb Clin Neurol.* 2022;185:81–97.
54. Josephs KA, Duffy JR, Fossett TR, et al. Fluorodeoxyglucose F18 positron emission tomography in progressive apraxia of speech and primary progressive aphasia variants. *Arch Neurol.* 2010;67:596–605.
55. Taswell C, Villemagne VL, Yates P, et al. $^{18}$F-FDG PET improves diagnosis in patients with focal-onset dementias. *J Nucl Med.* 2015;56:1547–1553.
56. Rabinovici GD, Jagust WJ, Furst AJ, et al. Abeta amyloid and glucose metabolism in three variants of primary progressive aphasia. *Ann Neurol.* 2008;64:388–401.
57. Pozueta A, Lage C, García-Martínez M, et al. Cognitive and behavioral profiles of left and right semantic dementia: differential diagnosis with behavioral variant frontotemporal dementia and Alzheimer's disease. *J Alzheimers Dis.* 2019;72: 1129–1144.
58. Kamminga J, Kumfor F, Burrell JR, Piguet O, Hodges JR, Irish M. Differentiating between right-lateralised semantic dementia and behavioural-variant frontotemporal dementia: an examination of clinical characteristics and emotion processing. *J Neurol Neurosurg Psychiatry.* 2015;86:1082–1088.
59. Gorno-Tempini ML, Hillis AE, Weintraub S, et al. Classification of primary progressive aphasia and its variants. *Neurology.* 2011;76:1006–1014.
60. Josephs KA, Duffy JR, Strand EA, et al. Progranulin-associated PiB-negative logopenic primary progressive aphasia. *J Neurol.* 2014;261:604–614.
61. Kägi G, Bhatia KP, Tolosa E. The role of DAT-SPECT in movement disorders. *J Neurol Neurosurg Psychiatry.* 2010;81:5–12.
62. Meyer PT, Frings L, Rücker G, Hellwig S. $^{18}$F-FDG PET in parkinsonism: differential diagnosis and evaluation of cognitive impairment. *J Nucl Med.* 2017;58: 1888–1898.
63. Foster NL, Gilman S, Berent S, Morin EM, Brown MB, Koeppe RA. Cerebral hypometabolism in progressive supranuclear palsy studied with positron emission tomography. *Ann Neurol.* 1988;24:399–406.
64. Iwata M. Neuroimaging of motor disturbances [in Japanese]. *Rinsho Shinkeigaku.* 1998;38:1010–1012.
65. Lee SE, Rabinovici GD, Mayo MC, et al. Clinicopathological correlations in corticobasal degeneration. *Ann Neurol.* 2011;70:327–340.
66. Pardini M, Huey ED, Spina S, et al. FDG-PET patterns associated with underlying pathology in corticobasal syndrome. *Neurology.* 2019;92:e1121–e1135.
67. Dickson DW, Davies P, Bevona C, et al. Hippocampal sclerosis: a common pathological feature of dementia in very old (> or = 80 years of age) humans. *Acta Neuropathol (Berl).* 1994;88:212–221.
68. Crystal HA, Dickson D, Davies P, Masur D, Grober E, Lipton RB. The relative frequency of "dementia of unknown etiology" increases with age and is nearly 50% in nonagenarians. *Arch Neurol.* 2000;57:713–719.
69. Nelson PT, Smith CD, Abner EL, et al. Hippocampal sclerosis of aging, a prevalent and high-morbidity brain disease. *Acta Neuropathol (Berl).* 2013;126:161–177.
70. Mackenzie IR, Rademakers R, Neumann M. TDP-43 and FUS in amyotrophic lateral sclerosis and frontotemporal dementia. *Lancet Neurol.* 2010;9:995–1007.
71. Amador-Ortiz C, Lin WL, Ahmed Z, et al. TDP-43 immunoreactivity in hippocampal sclerosis and Alzheimer's disease. *Ann Neurol.* 2007;61:435–445.
72. Smith VD, Bachstetter AD, Ighodaro E, et al. Overlapping but distinct TDP-43 and tau pathologic patterns in aged hippocampi. *Brain Pathol.* 2018;28:264–273.
73. Nelson PT, Dickson DW, Trojanowski JQ, et al. Limbic-predominant age-related TDP-43 encephalopathy (LATE): consensus working group report. *Brain.* 2019; 142:1503–1527.
74. Yu L, Boyle PA, Dawe RJ, Bennett DA, Arfanakis K, Schneider JA. Contribution of TDP and hippocampal sclerosis to hippocampal volume loss in older-old persons. *Neurology.* 2020;94:e142–e152.
75. Botha H, Mantyh WG, Murray ME, et al. FDG-PET in tau-negative amnestic dementia resembles that of autopsy-proven hippocampal sclerosis. *Brain.* 2018; 141:1201–1217.
76. Buciuc M, Botha H, Murray ME, et al. Utility of FDG-PET in diagnosis of Alzheimer-related TDP-43 proteinopathy. *Neurology.* 2020;95:e23–e34.
77. Stage EC Jr, Svaldi D, Phillips M, et al; Alzheimer's Disease Neuroimaging Initiative. Neurodegenerative changes in early- and late-onset cognitive impairment with and without brain amyloidosis. *Alzheimers Res Ther.* 2020;12:93.
78. Tolnay M, Spillantini MG, Goedert M, Ulrich J, Langui D, Probst A. Argyrophilic grain disease: widespread hyperphosphorylation of tau protein in limbic neurons. *Acta Neuropathol (Berl).* 1997;93:477–484.
79. Rodriguez RD, Grinberg LT. Argyrophilic grain disease: an underestimated tauopathy. *Dement Neuropsychol.* 2015;9:2–8.
80. Jicha GA, Nelson PT. Hippocampal sclerosis, argyrophilic grain disease, and primary age-related tauopathy. *Continuum (Minneap Minn).* 2019;25:208–233.
81. Crary JF, Trojanowski JQ, Schneider JA, et al. Primary age-related tauopathy (PART): a common pathology associated with human aging. *Acta Neuropathol (Berl).* 2014;128:755–766.
82. Bell WR, An Y, Kageyama Y, et al. Neuropathologic, genetic, and longitudinal cognitive profiles in primary age-related tauopathy (PART) and Alzheimer's disease. *Alzheimers Dement.* 2019;15:8–16.
83. Das SR, Xie L, Wisse LEM, et al; Alzheimer's Disease Neuroimaging Initiative. In vivo measures of tau burden are associated with atrophy in early Braak stage medial temporal lobe regions in amyloid-negative individuals. *Alzheimers Dement.* 2019;15:1286–1295.
84. Weigand AJ, Bangen KJ, Thomas KR, et al; Alzheimer's Disease Neuroimaging Initiative. Is tau in the absence of amyloid on the Alzheimer's continuum? A study of discordant PET positivity. *Brain Commun.* 2020;2:fcz046.
85. Josephs KA, Whitwell JL, Parisi JE, et al. Caudate atrophy on MRI is a characteristic feature of FTLD-FUS. *Eur J Neurol.* 2010;17:969–975.
86. Zekry D, Hauw JJ, Gold G. Mixed dementia: epidemiology, diagnosis, and treatment. *J Am Geriatr Soc.* 2002;50:1431–1438.
87. Boyle PA, Yu L, Wilson RS, Leurgans SE, Schneider JA, Bennett DA. Person-specific contribution of neuropathologies to cognitive loss in old age. *Ann Neurol.* 2018;83:74–83.
88. Lesman-Segev OH, La Joie R, Iaccarino L, et al. Diagnostic accuracy of amyloid versus $^{18}$F-fluorodeoxyglucose positron emission tomography in autopsy-confirmed dementia. *Ann Neurol.* 2021; 89:389–401.
89. Minoshima S, Mosci K, Cross D, Thientunyakit T. Brain [F-18]FDG PET for clinical dementia workup: differential diagnosis of Alzheimer's disease and other types of dementing disorders. *Semin Nucl Med.* 2021;51:230–240.
90. Mesulam MM, Dickerson BC, Sherman JC, et al. Case 1-2017. A 70-year-old woman with gradually progressive loss of language. *N Engl J Med.* 2017;376: 158–167.
91. Thomas DX, Bajaj S, McRae-McKee K, Hadjichrysanthou C, Anderson RM, Collinge J. Association of TDP-43 proteinopathy, cerebral amyloid angiopathy, and Lewy bodies with cognitive impairment in individuals with or without Alzheimer's disease neuropathology. *Sci Rep.* 2020;10:14579.
92. Rojas JC, Stephens ML, Rabinovici GD, Kramer JH, Miller BL, Seeley WW. Multiproteinopathy, neurodegeneration and old age: a case study. *Neurocase.* 2018;24:1–6.

93. Zhang W, Zheng R, Wang Z, Yuan Y. The overlap of corticobasal degeneration and Alzheimer changes: an autopsy case. *Neuropathology.* 2009;29:720–726.
94. Higashi S, Iseki E, Yamamoto R, et al. Concurrence of TDP-43, tau and alpha-synuclein pathology in brains of Alzheimer's disease and dementia with Lewy bodies. *Brain Res.* 2007;1184:284–294.
95. Gomperts SN, Rentz DM, Moran E, et al. Imaging amyloid deposition in Lewy body diseases. *Neurology.* 2008;71:903–910.
96. Thal DR, von Arnim CA, Griffin WS, et al. Frontotemporal lobar degeneration FTLD-tau: preclinical lesions, vascular, and Alzheimer-related co-pathologies. *J Neural Transm.* 2015;122:1007–1018.
97. Sakamoto R, Tsuchiya K, Yoshida R, et al. Progressive supranuclear palsy combined with Alzheimer's disease: a clinicopathological study of two autopsy cases. *Neuropathology.* 2009;29:219–229.
98. Gearing M, Olson DA, Watts RL, Mirra SS. Progressive supranuclear palsy: neuropathologic and clinical heterogeneity. *Neurology.* 1994;44:1015–1024.
99. Keith-Rokosh J, Ang LC. Progressive supranuclear palsy: a review of co-existing neurodegeneration. *Can J Neurol Sci.* 2008;35:602–608.
100. Hof PR, Bouras C, Perl DP, Morrison JH. Quantitative neuropathologic analysis of Pick's disease cases: cortical distribution of Pick bodies and coexistence with Alzheimer's disease. *Acta Neuropathol (Berl).* 1994;87:115–124.
101. Choudhury P, Scharf EL, Paolini MA, 2nd, et al. Pick's disease: clinicopathologic characterization of 21 cases. *J Neurol.* 2020;267:2697–2704.
102. Wang LN, Zhu MW, Feng YQ, Wang JH. Pick's disease with Pick bodies combined with progressive supranuclear palsy without tuft-shaped astrocytes: a clinical, neuroradiologic and pathological study of an autopsied case. *Neuropathology.* 2006;26:222–230.

# The Role of Amyloid PET in Imaging Neurodegenerative Disorders: A Review

Marianne Chapleau[1], Leonardo Iaccarino[1], David Soleimani-Meigooni[1], and Gil D. Rabinovici[1–3]

*[1]Memory and Aging Center, Department of Neurology, University of California, San Francisco, San Francisco, California; [2]Weill Institute for Neurosciences, University of California, San Francisco, San Francisco, California; and [3]Department of Radiology and Biomedical Imaging, University of California, San Francisco, San Francisco, California*

Imaging of amyloid deposition using PET has been available in research studies for 2 decades and has been approved for clinical use by the U.S. Food and Drug Administration, the European Medicines Agency, and other regulatory agencies around the world. Amyloid PET is a crucial tool for the diagnosis of Alzheimer disease, as it allows the noninvasive detection of amyloid plaques, a core neuropathologic feature that defines the disease. The clinical use of amyloid PET is expected to increase with recent accelerated approval in the United States of aducanumab, an antiamyloid monoclonal antibody, for the treatment of mild cognitive impairment and mild dementia due to Alzheimer disease. However, amyloid pathology can also be found in cognitively unimpaired older adults and in patients with other neurodegenerative disorders. The aim of this review is to provide an up-to-date overview of the application of amyloid PET in neurodegenerative diseases. We provide an in-depth analysis of the clinical, pathologic, and imaging correlates; a comparison with other available biomarkers; and a review of the application of amyloid PET in clinical trials and clinical utility studies.

**Key Words:** neurology; PET; PET/MRI; Alzheimer disease; amyloid PET; neurodegenerative diseases

**J Nucl Med 2022; 63:13S–19S**
DOI: 10.2967/jnumed.121.263195

Alzheimer disease (AD) is defined by the pathologic accumulation of amyloid-β (Aβ) plaques and tau neurofibrillary tangles (*1*). The accumulation of plaques (and to a lesser extent tangles) begins 10–20 y before the onset of clinical impairment (*2*). Aβ polypeptides are formed by cleavage of the amyloid precursor protein into 38–43 amino acid polypeptide fragments. The 40–42 amino acid Aβ polypeptides tend to form soluble aggregates (also known as Aβ oligomers) that further aggregate into microscopically detectable extracellular diffuse deposits (diffuse plaques, composed primarily of $A\beta_{42}$) and finally more dense neuritic plaques (Fig. 1A), which also contain tau-positive neurites. $A\beta_{40}$ polypeptides aggregate in blood vessel walls to form cerebral amyloid angiopathy (CAA) (Fig. 1B). At autopsy, amyloid accumulation is staged using the Thal phase and CERAD score (Consortium to Establish a Registry for Alzheimer's Disease). Thal phase describes the topography of Aβ plaques (diffuse or neuritic) in 5 phases, beginning in the association neocortex and spreading progressively through the paralimbic and limbic cortex, diencephalon, brain stem, and cerebellum (Fig. 1C). The CERAD score is based on the maximal density of neuritic plaques observed in one or more standardly sampled brain regions (categorized as sparse, moderate, or frequent; Fig. 1D). The overall degree of AD neuropathologic change is determined by integrating Thal phase, CERAD score, and Braak stage, the latter being a measure of the spread of intraneuronal neurofibrillary tangles.

The abnormal accumulation of both amyloid and tau can be quantified in vivo using PET imaging (*3,4*). In 2004, Klunk et al. reported the first successful attempt to image amyloid plaques in AD, applying the radiotracer $^{11}$C-labeled Pittsburgh compound B ($^{11}$C-PiB) (*5*). $^{11}$C-PiB was developed as an analog of thioflavin-T, a dye used by pathologists to stain amyloid in brain tissue. At the nanomolar concentrations injected for human imaging, $^{11}$C-PiB binds with high sensitivity and specificity to fibrillar Aβ aggregates (neuritic more than diffuse plaques), as well as to vascular amyloid in CAA. A major limitation of $^{11}$C-PiB is the 20-min half-life of the $^{11}$C radioisotope, limiting the use of this tracer to research PET centers equipped with a cyclotron. Since the advent of $^{11}$C-PiB, several tracers labeled with $^{18}$F (110-min half-life) have been developed that can be distributed from commercial cyclotrons for more widespread applications. These include $^{18}$F-florbetapir (Amyvid; Eli Lilly and Company), $^{18}$F-florbetaben (Neuraceq; Life Molecular Imaging), $^{18}$F-flutemetamol (Vizamyl; GE Healthcare), and $^{18}$F-flutafuranol (also known as NAV4694) (*6*). $^{11}$C-PiB and $^{18}$F-flutemetamol belong to the chemical class of benzothiazoles, whereas $^{18}$F-florbetaben and $^{18}$F-florbetapir are derived from stilbene and $^{18}$F-flutafuranol from benzofuran (Fig. 2). These compounds, although different in their chemical composition, all share a high affinity for fibrillar amyloid aggregates (*7*), allowing the detection of amyloid pathology in AD (*8*) and other diseases that involve fibrillar Aβ deposition (*9*).

In 2018, a National Institute on Aging and Alzheimer's Association (NIA-AA) research framework was proposed to standardize the evaluation of AD with biomarkers in living individuals (*10*). Biomarkers were grouped into those that measure amyloid deposition (cerebrospinal fluid [CSF] or PET), pathologic tau (CSF or PET), and neurodegeneration (CSF, PET, or MRI). In this research framework, the definition of AD is based purely on biomarker abnormalities (irrespective of clinical symptoms or stage), with AD defined as abnormal amyloid and tau biomarkers (A-positive, T-positive) whereas the Alzheimer continuum is defined as amyloid without tau (A-positive, T-negative). Although the NIA-AA research framework was intended for use only in the research setting, the 2021 International Working Group recommendations describe how AD biomarkers can be used to

Received Jan. 24, 2022; revision accepted Mar. 22, 2022.
For correspondence or reprints, contact Marianne Chapleau (marianne.chapleau@ucsf.edu).

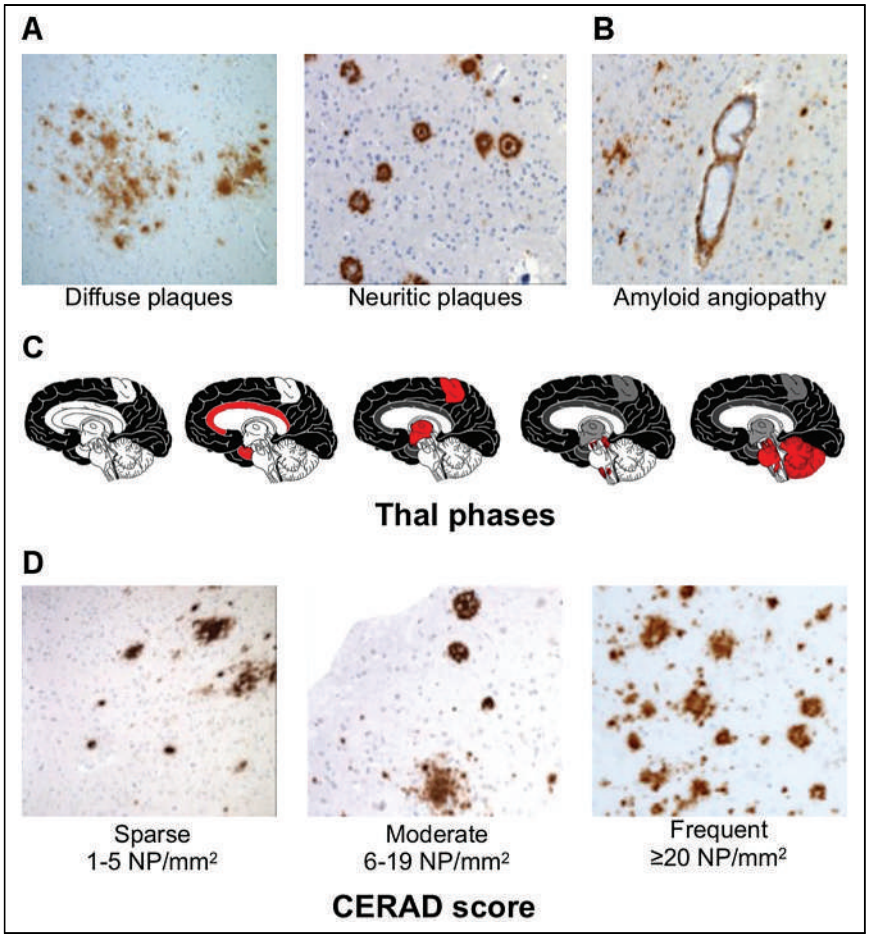


**FIGURE 1.** Postmortem measures of amyloid pathology. (A) Types of amyloid deposits. (B) Amyloid angiopathy. (C) Distribution of diffuse and neuritic plaques. (D) Neuritic plaque density (highest density score observed in brain). (A, B, and D are from UCSF Neurodegenerative Disease Brain Bank; C is reprinted with permission of (*53*).) NP = neuritic plaques.

supplement a clinical evaluation and support a diagnosis of AD in the clinic (*11*). In both contexts, assessing the utility of amyloid PET for diagnostic purposes is crucial, as in vivo biomarkers are increasingly playing a major role in research studies and the clinic. Furthermore, biomarkers such as amyloid PET will increasingly be used to assess the eligibility of patients for emerging anti-Aβ therapeutics such as aducanumab, an anti-Aβ monoclonal antibody recently granted accelerated approval in the United States for the treatment of mild cognitive impairment (MCI) or mild dementia due to AD (*12*). The aim of this review is to provide an overview of the application of amyloid PET in neurodegenerative diseases.

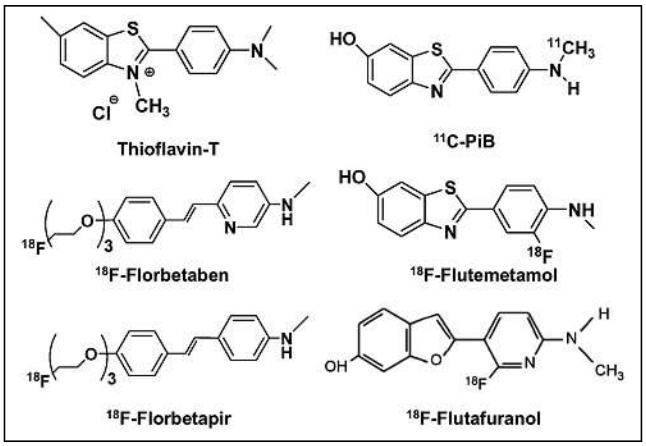


**FIGURE 2.** Structures of thioflavin-T, $^{11}$C-PiB, $^{18}$F-flutafuranol, and Food and Drug Administration–approved Aβ PET tracers. (Reprinted from (*54*).)

## VISUAL INTERPRETATION, QUANTIFICATION, AND THRESHOLDS

The typical distribution of amyloid PET uptake includes large portions of the neocortex and striatum, with relative sparing of the medial temporal lobes and primary unimodal cortices. This topography is consistent with the known postmortem distribution of amyloid pathology. The earliest and peak tracer uptake is usually observed in the posterior cingulate/precuneus and medial prefrontal regions (*13*). All Aβ tracers show nonspecific retention in the white matter, regardless of the presence of amyloid pathology. Tracer retention is more strongly linked to neuritic than diffuse plaques (*14*). Patients with CAA can present with occipital lobe–predominant retention (a common region in which CAA develops) (*15*), but the utility of amyloid PET for distinguishing between different types of Aβ deposits at the individual subject level is limited. Importantly, amyloid PET ligands do not bind to soluble Aβ oligomers, which have the highest neurotoxicity across Aβ aggregates.

Amyloid PET can be interpreted as positive or negative (or, alternatively, as elevated amyloid or nonelevated amyloid) on the basis of visual reads (Fig. 3; Table 1). In a negative scan, binding is restricted to white matter, showing a preserved gray matter–to–white matter contrast. Conversely, in a positive scan, cortical gray matter binding is equal to or greater than binding in the white matter, with subsequent loss of gray matter–to–white matter contrast. Despite slight differences in guidelines for visual interpretations among the clinically available amyloid PET tracers (Table 1), these positive and negative patterns tend to be consistent overall.

Cortical retention can also be quantified as a continuous measure, using a variety of PET modeling methods. The most common method involves calculation of tissue ratios between the target tissues (typically large regions of cortical gray matter) and a reference region known to be relatively devoid of amyloid until advanced stages (various combinations of cerebellum gray and white matter and brain stem), resulting in SUV ratios. The SUV ratio method is pragmatic in that reliable semiquantification can be accomplished with 10- to 20-min scans, but the method also has limitations compared with more rigorous quantification methods, including overestimation of the true concentration of pathology, and susceptibility to changes in blood flow. The centiloid method, which is derived from SUV ratio measurements, generates standardized units that can facilitate comparisons between tracers

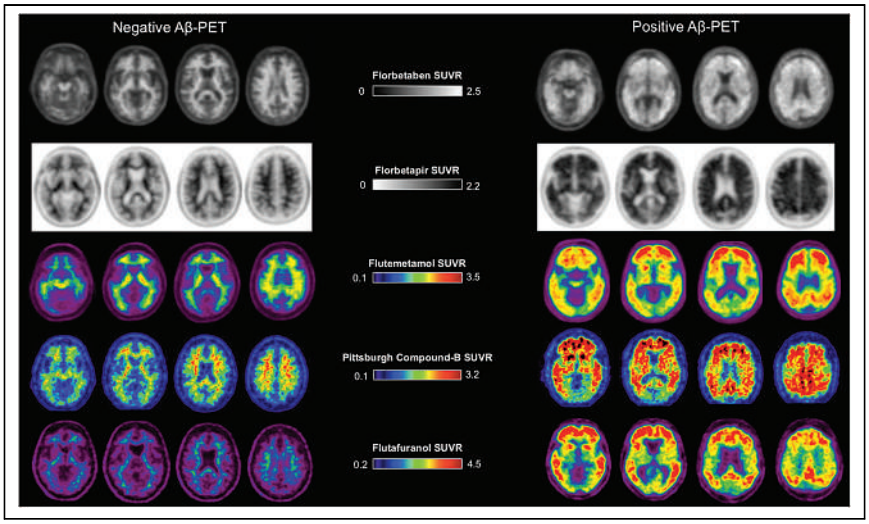


**FIGURE 3.** Examples of negative and positive Aβ PET findings using different tracers. ($^{18}$F-flutafuranol images are courtesy of Victor Villemagne and Christopher C. Rowe.)

and image processing methods. On this scale, 0 centiloid represents mean uptake in young adults devoid of amyloid, 12–25 centiloid represents a threshold for scan positivity, and 100 centiloid corresponds to the mean uptake in patients with mild AD dementia (*16,17*). Visual interpretations of amyloid PET are currently the standard in clinical practice, whereas SUV ratio and centiloid measurements are often used in research studies and drug trials.

The validation of amyloid PET as a reliable proxy for amyloid accumulation is based on PET-to-autopsy studies, in which individuals were imaged during life, and results were compared with the distribution and burden of amyloid after death (*17*). Visual reads of scans with $^{18}$F-labeled tracers as positive or negative, performed knowledge of any clinical information, showed 88%–98% sensitivity and 80%–95% specificity in distinguishing older adults with moderate to frequent neuritic plaques (according to the CERAD scale) from those with absent to sparse plaques (*18–20*). Quantification of $^{11}$C-PiB scans in patients with postmortem assessments show similar accuracy and reliably distinguish patients in Thal phases 3–5 from those in phases 0–2 (*17*). On the basis of these data, $^{18}$F-florbetapir, $^{18}$F-florbetaben, and $^{18}$F-flutemetamol were approved for clinical use by the U.S. Food and Drug Administration, the European Medicines Agency, and other regulatory agencies around the world.

## CLINICOIMAGING CORRELATES

Many studies have evaluated the prevalence of amyloid PET positivity in different clinical populations. In cognitively unimpaired older adults, amyloid PET scans are negative in 70%–90%, depending on age and apolipoprotein E (*APOE*) genotype (*21*). However, a considerable percentage of cognitively unimpaired older (>70 y old) subjects carry a significant amyloid burden (*21,22*), heightening the risk of false-positive findings (i.e., positive amyloid PET findings unrelated to the patient's symptoms) in older individuals. The prevalence of amyloid PET positivity in cognitively unimpaired adults increases linearly with age (~10% at age 50 y, ~15% at age 60 y, ~20% at age 70 y, ~30% at age 80 y, and ~40% at age 90 y). Additionally, the likelihood of amyloid positivity is strongly linked to *APOE* genotype, with people carrying at least 1 *APOE ε4* allele (the strongest genetic risk factor for sporadic AD) having a 2–3 times higher prevalence of amyloid pathology in any given age group (*21*).

As a group, cognitively unimpaired older adults who are amyloid PET–positive are at increased risk for developing MCI or dementia in subsequent years (*23*), though lifetime risk for any individual may be relatively low (*24*). The NIA-AA research framework considers cognitively unimpaired individuals to have preclinical AD if both amyloid and tau PET or CSF biomarkers are positive and to be on the AD continuum if their biomarker profile is A-positive, T-negative (*10*). The International Working Group recommendations take a slightly different approach, stratifying asymptomatic people into different risk levels depending on their genetic and biomarker profile (*11*).

The prevalence of amyloid PET positivity in patients with MCI is 27%–71% depending on the specific criteria used, increasing also with age and *APOE ε4* genotype (*21*). Amyloid PET is useful in identifying when MCI is due to underlying AD pathology and is included in the research diagnostic criteria for MCI due to AD (*25*) or prodromal AD (*11*) (Fig. 4). Amyloid PET positivity is associated with a 3–4 times increased risk of conversion to AD dementia over the next 3–5 y after adjusting for age, APOE genotype, and other covariates. However, the individual trajectories of amyloid-positive MCI patients are highly variable at the single-patient level (*26*). The combination of amyloid PET positivity, APOE4 genotype, and positive biomarkers of tau (CSF or PET) or neurodegeneration (MRI or $^{18}$F-FDG PET) increases the risk of conversion in the shorter term (*27–29*).

Approximately 70%–90% of patients meeting the clinical criteria for dementia due to AD have positive amyloid PET results (*30,31*). Interestingly, the prevalence of amyloid positivity decreases with age in patients clinically diagnosed with probable AD, probably because of an increase in the prevalence of non-Aβ brain pathologies that present with an amnestic dementia in older patients (e.g., limbic system–associated TDP-43 encephalopathy, vascular contributions to impairment and dementia, and primary age-related tauopathy) (*31*). The prevalence of amyloid pathology in cognitively unimpaired older adults is an important consideration in interpreting the clinical meaning of an amyloid PET scan. Although a negative amyloid PET result is useful for excluding AD at any age, the positive predictive value of amyloid PET decreases with increasing age, since at an older age it is more likely that the finding of amyloid is incidental, and the patient may have another condition that is primarily responsible for the symptoms. At the dementia stage, amyloid PET is useful for distinguishing AD from neurodegenerative conditions that are not associated with Aβ, such as frontotemporal dementia (*32,33*). Since amyloid and tau burden are positively correlated, a positive amyloid PET result is often associated with significant tau pathology and intermediate to high overall AD neuropathology (*33*), and amyloid PET has higher sensitivity than $^{18}$F-FDG PET for detecting clinically meaningful AD neuropathology. Amyloid PET is not useful at distinguishing AD from other disorders that involve Aβ deposits, such as dementia with Lewy bodies (50%–70% amyloid PET–positive) and CAA.

**TABLE 1**
Summary Guidelines for Interpretation of Amyloid PET Scans Using Different Tracers

| Tracer category | Tracer name | Dose and acquisition protocol (clinical) | Visualization | Interpretation criteria for positive scan |
|---|---|---|---|---|
| Food and Drug Administration–approved | $^{18}$F-florbetaben | ~300 MBq; 15- to 20-min acquisition beginning at 45–130 min (research use, 20-min acquisition beginning at 90–110 min) | Gray scale; window images to optimize GM/WM contrast in cerebellum | Increased GM uptake extending to cortical margin involving most slices in at least 1 of 4 target cortical regions: frontal, parietal, precuneus/posterior cingulate, lateral temporal; regional cortical tracer uptake/brain amyloid plaque load scores (*20*) |
| | $^{18}$F-florbetapir | ~370 MBq; 10- to 20-min acquisition beginning at 30–50 min (package insert guidelines) for clinical use or 50–70 min (optimized kinetics for quantification) for research use | Inverse gray scale; window images to optimize GM/WM contrast in cerebellum | Loss of GM/WM contrast due to increased cortical binding in, first, 2 or more brain areas (each larger than single gyrus) with reduced or absent GM/WM contrast or, second, 1 or more areas with intense signal where GM > WM |
| | $^{18}$F-flutemetamol | ~185 MBq; 10- to 20-min acquisition at 60–120 min (research use, 20-min acquisition at 90–110 min) | Color scale (NIH); normalize so that pons is at 90% of activity | Increased GM uptake (>50%–60% peak intensity) or loss of GM matter contrast in at least 1 of 4 cortical regions and 1 subcortical region: frontal, inferolateral parietal, precuneus/posterior cingulate, lateral temporal, striatum |
| Research | $^{11}$C-PiB | ~555 MBq; dynamic 60- to 90-min acquisition (distribution volume ratio) or 20-min acquisition at 50–70 min (SUV ratio) | Color scale (NIH); window images to optimize GM/WM contrast in cerebellum | No formal guidelines for reading (research use only) |
| | $^{18}$F-flutafuranol | ~185 MBq; 20- to 30-min acquisition beginning at 40–50 min | Color scale (NIH); window images to optimize GM/WM contrast in cerebellum | No formal guidelines for reading (research use only) |

GM = gray matter; NIH = National Institutes of Health; WM = white matter.

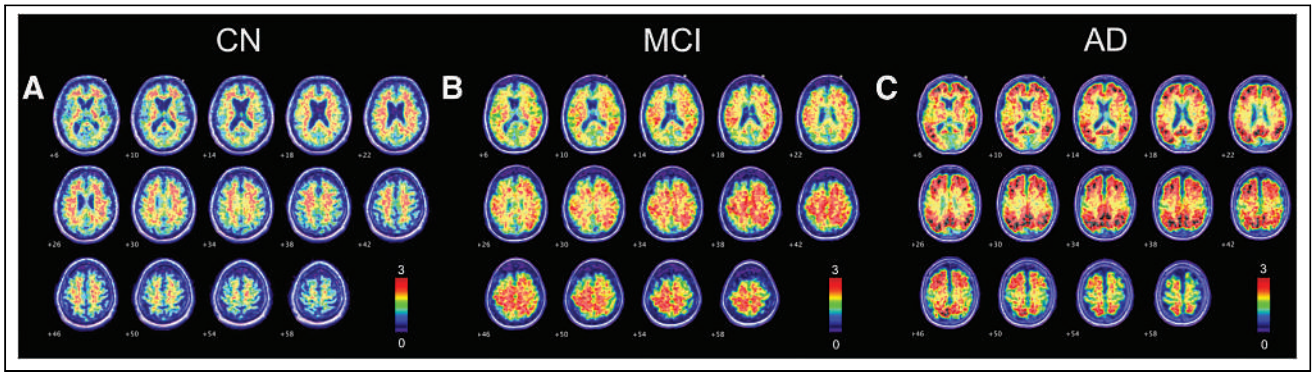


**FIGURE 4.** Evolution of amyloid PET positivity across AD spectrum. (A) Positive $^{11}$C-PiB scan of cognitively normal (CN) participant, in which significant binding is observed in precuneus, posterior cingulate cortex, and medial prefrontal areas. (B) Positive $^{11}$C-PiB scan of MCI patient, in which significant and moderate binding is observed throughout cortex. (C) Positive $^{11}$C-PiB scan of AD patient, in which significant and severe binding is observed throughout cortex.

## APPROPRIATE-USE CRITERIA (AUCS)

AUCs published in 2013 highlight appropriate and inappropriate clinical uses of amyloid PET. The AUCs state that clinical amyloid PET may be considered in patients with objectively confirmed cognitive impairment (i.e., MCI or dementia) but in whom the cause of impairment is uncertain after a comprehensive evaluation by a dementia specialist (including CT/MRI) and for whom knowledge of amyloid PET results is expected to increase diagnostic certainty and change patient management. The patients most likely to benefit include those with persistent or progressive unexplained MCI, those with possible AD but an atypical course or etiologically mixed presentation, and those with young-onset dementia (before age 65 y). Inappropriate scenarios include use for assessing dementia severity, use in unimpaired individuals (with or without subjective complaints), and nonmedical uses (e.g., legal, insurance coverage, or employment screening). An update to the AUCs is expected in 2022, incorporating tau PET and addressing the emerging availability of approved anti-Aβ therapeutics.

## CLINICAL UTILITY STUDIES

The clinical utility of amyloid PET has been reviewed (*34,35*) and assessed in various multisite cohort studies, including the Imaging Dementia–Evidence for Amyloid Scanning (IDEAS) study, the Amyloid Imaging to Prevent Alzheimer's Disease–Diagnostic and Patient Management Study (AMYPAD-DPMS) study, the Alzheimer Biomarkers in Daily Practice (ABIDE) study, and a randomized clinical trial (*36*). The IDEAS study was a United States–wide longitudinal study evaluating the impact of amyloid PET and health outcomes in over 18,000 patients with MCI or dementia who met the AUCs and were recruited at nearly 600 specialty clinics across the United States. The study was conducted in collaboration with the U.S. Centers for Medicare and Medicaid Services under Coverage with Evidence Development. Amyloid PET was associated with implemented changes in core elements of patient management 90 d after the scan in 60.2% of patients with MCI and 63.5% of patients with dementia, far exceeding the study's goal of a change in management in at least 30% of patients in each group. The most common change involved the use of approved medications (i.e., cholinesterase inhibitors or memantine) for AD (43.6% in MCI and 44.9% in dementia). The diagnosis changed after PET in about 35% of patients (25% switched from AD to non-AD, and 10% switched from non-AD to AD) (*30*). The impact of amyloid PET on health outcomes was more modest. Rates of 12-mo hospitalizations after PET were 23.98% in IDEAS participants, compared with 25.12% in a matched cohort of Medicare beneficiaries who had not undergone amyloid PET (4.5% relative reduction), falling short of the prespecified goal of no more than a 10% relative reduction (*37*). There was no significant difference in 12-mo rates of emergency department visits between IDEAS participants and controls. These results, in addition to the approval of novel amyloid-lowering treatments for AD, will inform future coverage policies for Centers for Medicare and Medicaid Services and other payers in the United States and globally.

The ABIDE project also assessed the association between amyloid PET and changes in diagnosis, diagnosis confidence, treatment, and patients' experiences in a memory clinic at the Vrije Universiteit Medical Center, The Netherlands (*38*). The authors found that the etiologic diagnosis changed for 25% of patients after amyloid PET, more often because of a negative than a positive scan. Also, diagnostic confidence increased, and for some patients, there was a change in the treatment received. The European AMYPAD-DPMS study has a similar goal of determining the value of amyloid imaging as a diagnostic and therapeutic marker for AD to supply physicians and health-care payers with data to plan management decisions (*39*). Results regarding this multisite project are pending. Another multicenter, randomized, and controlled study (*36*) showed that knowledge of the amyloid status affects diagnosis and patient management and involves mainly changes in AD medications.

## COMPARISON WITH FLUID BIOMARKERS

Concentrations of monomeric Aβ, total tau, and phosphorylated tau (at various epitopes) can also be measured in CSF and plasma. The ratio of CSF $A\beta_{42/40}$ concentrations is highly congruent with amyloid PET in classifying individuals as amyloid-positive or -negative (*40*), as is the ratio of $A\beta_{42}$ with total or phosphorylated tau (*41*). Changes in Aβ are likely detectable earlier in CSF than by amyloid PET (*42*). Similarly, novel plasma assays that measure $A\beta_{42/40}$ in plasma using mass spectrometry or highly sensitive immunoassays show high concordance with amyloid PET and CSF (*43–45*). Plasma measurements of phosphorylated tau also show promise in detecting brain amyloidosis (*46–48*). Compared with CSF, plasma Aβ and tau biomarkers are in earlier stages of standardization and require additional validation before clinical use. A future diagnostic algorithm for amyloid pathology may begin with plasma measurements, followed by more definitive CSF or amyloid PET testing. CSF and PET can be used interchangeably in the clinic, though amyloid PET would be the first-line test in patients in whom CSF is contraindicated (e.g., patient who are anticoagulated) or would be considered in patients with equivocal CSF results (*49*).

## CLINICAL TRIALS

Over the past decade, amyloid PET has been used in clinical trials to screen for treatment eligibility (i.e., to provide evidence of amyloid pathology) and assess target engagement for drugs designed to reduce amyloid plaques, most notably anti-Aβ monoclonal antibodies. The accelerated approval of aducanumab, an anti-Aβ monoclonal antibody that targets Aβ fibrils, in June 2021 by the U.S. Food and Drug Administration was based on the drug's dose-dependent ability to reduce amyloid PET signal (*12*). Although the drug reduced amyloid PET signal in 2 identically designed phase 3 randomized controlled trials, a significant (though modest) slowing of clinical decline was observed in only one study. Food and Drug Administration approval was based on lowering of amyloid on PET as a surrogate biomarker reasonably likely to predict clinical benefit, but a confirmatory trial evaluating clinical benefit was required as part of the accelerated approval pathway. Amyloid PET has also been a key outcome measure in trials of the potent anti-Aβ monoclonals donanemab (*50*), lecanemab (*51*), and gantenerumab (*52*). In early-phase studies, all antibodies convincingly lowered amyloid PET, and donanemab and lecanemab showed early evidence supportive of modest clinical benefit as well. Phase 3 randomized controlled trials of these antibodies are expected in the coming 1–2 years. In the donanemab phase 2 study, amyloid PET was used not only to select patients but also to titrate treatment. Drug dose was lowered on the basis of the amyloid PET response, and the drug was ultimately

switched to placebo when the scan findings were negative. This could represent an important future clinical algorithm for determining the duration of treatment with this class of drugs.

## CONCLUSION

Amyloid PET can detect cerebral Aβ deposition with precision, has good specificity for AD neuropathology, can inform on the presence of contributing amyloid copathology in other diseases, and will inform eligibility for emerging anti-Aβ therapeutics. Amyloid PET is a reliable diagnostic imaging tool, and its use should be encouraged to guide early differential diagnosis in clinical settings and, in the future, to select patients for disease-specific therapies.

## DISCLOSURE

Marianne Chapleau received research support from the Fonds de recherche du Québec - Santé (FRQS). Gil Rabinovici receives research support from NIH/NIA R35 AG072362, NIH/NIA, and P30 AG062422; has served on Scientific Advisory Boards for Eisai, Eli Lilly, Genentech, and Roche; serves on a Data Safety and Monitoring Board for Johnson & Johnson; and is an associate editor for *JAMA Neurology*. Other support includes NINDS, AA, American College of Radiology, Rainwater Charitable Foundation, Shanendoah Foundation, Avid Radiopharmaceuticals, GE Healthcare, Life Molecular Imaging, and Genentech. No other potential conflict of interest relevant to this article was reported.

## REFERENCES


1. DeTure MA, Dickson DW. The neuropathological diagnosis of Alzheimer's disease. *Mol Neurodegener.* 2019;14:32.
2. Sperling RA, Aisen PS, Beckett LA, et al. Toward defining the preclinical stages of Alzheimer's disease: recommendations from the National Institute on Aging-Alzheimer's Association workgroups on diagnostic guidelines for Alzheimer's disease. *Alzheimers Dement.* 2011;7:280–292.
3. Schöll M, Lockhart SN, Schonhaut DR, et al. PET imaging of tau deposition in the aging human brain. *Neuron.* 2016;89:971–982.
4. Ossenkoppele R, Schonhaut DR, Scholl M, et al. Tau PET patterns mirror clinical and neuroanatomical variability in Alzheimer's disease. *Brain.* 2016;139:1551–1567.
5. Klunk WE, Engler H, Nordberg A, et al. Imaging brain amyloid in Alzheimer's disease with Pittsburgh compound-B. *Ann Neurol.* 2004;55:306–319.
6. Villemagne VL, Dore V, Burnham SC, Masters CL, Rowe CC. Imaging tau and amyloid-beta proteinopathies in Alzheimer disease and other conditions. *Nat Rev Neurol.* 2018;14:225–236.
7. Querfurth HW, LaFerla FM. Alzheimer's disease. *N Engl J Med.* 2010;362:329–344.
8. Dickerson BC, McGinnis SM, Xia C, et al. Approach to atypical Alzheimer's disease and case studies of the major subtypes. *CNS Spectr.* 2017;22:439–449.
9. Rostagno A, Holton JL, Lashley T, Revesz T, Ghiso J. Cerebral amyloidosis: amyloid subunits, mutants and phenotypes. *Cell Mol Life Sci.* 2010;67:581–600.
10. Jack CR Jr, Bennett DA, Blennow K, et al. NIA-AA research framework: toward a biological definition of Alzheimer's disease. *Alzheimers Dement.* 2018;14:535–562.
11. Dubois B, Villain N, Frisoni GB, et al. Clinical diagnosis of Alzheimer's disease: recommendations of the international working group. *Lancet Neurol.* 2021;20:484–496.
12. Rabinovici GD. Controversy and progress in Alzheimer's disease: FDA approval of aducanumab. *N Engl J Med.* 2021;385:771–774.
13. Villeneuve S, Rabinovici GD, Cohn-Sheehy BI, et al. Existing Pittsburgh compound-B positron emission tomography thresholds are too high: statistical and pathological evaluation. *Brain.* 2015;138:2020–2033.
14. Seo SW, Ayakta N, Grinberg LT, et al. Regional correlations between [$^{11}$C]PIB PET and post-mortem burden of amyloid-beta pathology in a diverse neuropathological cohort. *Neuroimage Clin.* 2016;13:130–137.
15. Johnson KA, Gregas M, Becker JA, et al. Imaging of amyloid burden and distribution in cerebral amyloid angiopathy. *Ann Neurol.* 2007;62:229–234.
16. Klunk WE, Koeppe RA, Price JC, et al. The centiloid project: standardizing quantitative amyloid plaque estimation by PET. *Alzheimers Dement.* 2015;11:1–15.e4.
17. La Joie R, Ayakta N, Seeley WW, et al. Multisite study of the relationships between antemortem [$^{11}$C]PIB-PET centiloid values and postmortem measures of Alzheimer's disease neuropathology. *Alzheimers Dement.* 2019;15:205–216.
18. Clark CM, Pontecorvo MJ, Beach TG, et al. Cerebral PET with florbetapir compared with neuropathology at autopsy for detection of neuritic amyloid-beta plaques: a prospective cohort study. *Lancet Neurol.* 2012;11:669–678.
19. Curtis C, Gamez JE, Singh U, et al. Phase 3 trial of flutemetamol labeled with radioactive fluorine 18 imaging and neuritic plaque density. *JAMA Neurol.* 2015;72:287–294.
20. Sabri O, Sabbagh MN, Seibyl J, et al. Florbetaben PET imaging to detect amyloid beta plaques in Alzheimer's disease: phase 3 study. *Alzheimers Dement.* 2015;11:964–974.
21. Jansen WJ, Ossenkoppele R, Knol DL, et al. Prevalence of cerebral amyloid pathology in persons without dementia: a meta-analysis. *JAMA.* 2015;313:1924–1938.
22. Jansen WJ, Janssen O, Tijms BM, et al. Prevalence estimates of amyloid abnormality across the Alzheimer disease clinical spectrum. *JAMA Neurol.* 2022;79:228–243.
23. Donohue MC, Sperling RA, Petersen R, et al. Association between elevated brain amyloid and subsequent cognitive decline among cognitively normal persons. *JAMA.* 2017;317:2305–2316.
24. Brookmeyer R, Abdalla N. Estimation of lifetime risks of Alzheimer's disease dementia using biomarkers for preclinical disease. *Alzheimers Dement.* 2018;14:981–988.
25. Albert MS, DeKosky ST, Dickson D, et al. The diagnosis of mild cognitive impairment due to Alzheimer's disease: recommendations from the National Institute on Aging-Alzheimer's Association workgroups on diagnostic guidelines for Alzheimer's disease. *Alzheimers Dement.* 2011;7:270–279.
26. Jutten RJ, Sikkes SAM, Amariglio RE, et al. Identifying sensitive measures of cognitive decline at different clinical stages of Alzheimer's disease. *J Int Neuropsychol Soc.* 2021;27:426–438.
27. Wolk DA, Sadowsky C, Safirstein B, et al. Use of flutemetamol F 18-labeled positron emission tomography and other biomarkers to assess risk of clinical progression in patients with amnestic mild cognitive impairment. *JAMA Neurol.* 2018;75:1114–1123.
28. Mormino EC, Betensky RA, Hedden T, et al. Amyloid and APOE epsilon4 interact to influence short-term decline in preclinical Alzheimer disease. *Neurology.* 2014;82:1760–1767.
29. van der Kall LM, Truong T, Burnham SC, et al. Association of beta-amyloid level, clinical progression, and longitudinal cognitive change in normal older individuals. *Neurology.* 2021;96:e662–e670.
30. Rabinovici GD, Gatsonis C, Apgar C, et al. Association of amyloid positron emission tomography with subsequent change in clinical management among Medicare beneficiaries with mild cognitive impairment or dementia. *JAMA.* 2019;321:1286–1294.
31. Ossenkoppele R, Jansen WJ, Rabinovici GD, et al. Prevalence of amyloid PET positivity in dementia syndromes: a meta-analysis. *JAMA.* 2015;313:1939–1949.
32. Rabinovici GD, Rosen HJ, Alkalay A, et al. Amyloid vs FDG-PET in the differential diagnosis of AD and FTLD. *Neurology.* 2011;77:2034–2042.
33. Lesman-Segev OH, La Joie R, Iaccarino L, et al. Diagnostic accuracy of amyloid versus $^{18}$F-fluorodeoxyglucose positron emission tomography in autopsy-confirmed dementia. *Ann Neurol.* 2021;89:389–401.
34. Barthel H, Sabri O. Clinical use and utility of amyloid imaging. *J Nucl Med.* 2017;58:1711–1717.
35. Cotta Ramusino M, Perini G, Altomare D, et al. Outcomes of clinical utility in amyloid-PET studies: state of art and future perspectives. *Eur J Nucl Med Mol Imaging.* 2021;48:2157–2168.
36. Pontecorvo MJ, Siderowf A, Dubois B, et al. Effectiveness of florbetapir PET imaging in changing patient management. *Dement Geriatr Cogn Disord.* 2017;44:129–143.
37. Rabinovici G, Iaccarino L, La Joie R, et al. Amyloid and tau PET in sporadic early-onset Alzheimer's disease: preliminary results from LEADS: LEADS: sporadic early-onset Alzheimer's disease in the spotlight. *Alzheimers Dement.* 2020;16:1–4.
38. de Wilde A, van der Flier WM, Pelkmans W, et al. Association of amyloid positron emission tomography with changes in diagnosis and patient treatment in an unselected memory clinic cohort: the ABIDE project. *JAMA Neurol.* 2018;75:1062–1070.
39. Frisoni GB, Barkhof F, Altomare D, et al. AMYPAD diagnostic and patient management study: rationale and design. *Alzheimers Dement.* 2019;15:388–399.
40. Hansson O, Lehmann S, Otto M, Zetterberg H, Lewczuk P. Advantages and disadvantages of the use of the CSF amyloid beta (Abeta) 42/40 ratio in the diagnosis of Alzheimer's disease. *Alzheimers Res Ther.* 2019;11:34.
41. Campbell MR, Ashrafzadeh-Kian S, Petersen RC, et al. P-tau/Abeta42 and Abeta42/40 ratios in CSF are equally predictive of amyloid PET status. *Alzheimers Dement (Amst).* 2021;13:e12190.

42. Palmqvist S, Mattsson N, Hansson O; Alzheimer's Disease Neuroimaging Initiative. Cerebrospinal fluid analysis detects cerebral amyloid-beta accumulation earlier than positron emission tomography. *Brain.* 2016;139:1226–1236.
43. Schindler SE, Bollinger JG, Ovod V, et al. High-precision plasma beta-amyloid 42/40 predicts current and future brain amyloidosis. *Neurology.* 2019;93: e1647–e1659.
44. Jang H, Kim JS, Lee HJ, et al. Performance of the plasma Abeta42/Abeta40 ratio, measured with a novel HPLC-MS/MS method, as a biomarker of amyloid PET status in a DPUK-KOREAN cohort. *Alzheimers Res Ther.* 2021;13:179.
45. Pérez-Grijalba V, Romero J, Pesini P, et al. Plasma Abeta42/40 ratio detects early stages of Alzheimer's disease and correlates with CSF and neuroimaging biomarkers in the AB255 study. *J Prev Alzheimers Dis.* 2019;6:34–41.
46. Thijssen EH, La Joie R, Strom A, et al. Plasma phosphorylated tau 217 and phosphorylated tau 181 as biomarkers in Alzheimer's disease and frontotemporal lobar degeneration: a retrospective diagnostic performance study. *Lancet Neurol.* 2021; 20:739–752.
47. Thijssen EH, La Joie R, Wolf A, et al. Diagnostic value of plasma phosphorylated tau181 in Alzheimer's disease and frontotemporal lobar degeneration. *Nat Med.* 2020;26:387–397.
48. Ashton NJ, Pascoal TA, Karikari TK, et al. Plasma p-tau231: a new biomarker for incipient Alzheimer's disease pathology. *Acta Neuropathol (Berl).* 2021; 141:709–724.
49. Engelborghs S, Niemantsverdriet E, Struyfs H, et al. Consensus guidelines for lumbar puncture in patients with neurological diseases. *Alzheimers Dement (Amst).* 2017;8:111–126.
50. Mintun MA, Lo AC, Duggan Evans C, et al. Donanemab in early Alzheimer's disease. *N Engl J Med.* 2021;384:1691–1704.
51. Swanson CJ, Zhang Y, Dhadda S, et al. A randomized, double-blind, phase 2b proof-of-concept clinical trial in early Alzheimer's disease with lecanemab, an anti-Abeta protofibril antibody. *Alzheimers Res Ther.* 2021;13:80.
52. Salloway S, Farlow M, McDade E, et al. A trial of gantenerumab or solanezumab in dominantly inherited Alzheimer's disease. *Nat Med.* 2021;27:1187–1196.
53. Thal DR, Rub U, Orantes M, Braak H. Phases of A beta-deposition in the human brain and its relevance for the development of AD. *Neurology.* 2002; 58:1791–1800.
54. Uzuegbunam BC, Librizzi D, Hooshyar Yousefi B. PET radiopharmaceuticals for Alzheimer's disease and Parkinson's disease diagnosis, the current and future landscape. *Molecules.* 2020;25:977.

# Tau PET Imaging in Neurodegenerative Disorders

Colin Groot[1,2], Sylvia Villeneuve[3–5], Ruben Smith[1,6], Oskar Hansson[1,6], and Rik Ossenkoppele[1,2]

*[1]Clinical Memory Research Unit, Lund University, Lund, Sweden; [2]Alzheimer Center Amsterdam, Department of Neurology, Amsterdam Neuroscience, Amsterdam UMC, Location VUMC, Amsterdam, The Netherlands; [3]Department of Psychiatry, Faculty of Medicine, McGill University, Montreal, Canada; [4]Douglas Mental Health University Institute, Montreal, Canada; [5]McConnell Brain Imaging Centre, Montreal Neurological Institute, Montreal, Canada; and [6]Memory Clinic, Skåne University Hospital, Malmö, Sweden*

The advent of PET ligands that bind tau pathology has enabled the quantification and visualization of tau pathology in aging and in Alzheimer disease (AD). There is strong evidence from neuropathologic studies that the most widely used tau PET tracers (i.e., $^{18}$F-flortaucipir, $^{18}$F-MK6240, $^{18}$F-RO948, and $^{18}$F-PI2620) bind tau aggregates formed in AD in the more advanced (i.e., ≥IV) Braak stages. However, tracer binding in most non-AD tauopathies is weaker and overlaps to a large extent with known off-target binding regions, limiting the quantification and visualization of non-AD tau pathology in vivo. Off-target binding is generally present in the substantia nigra, basal ganglia, pituitary, choroid plexus, longitudinal sinuses, meninges, or skull in a tracer-specific manner. Most cross-sectional studies use the inferior aspect of the cerebellar gray matter as a reference region, whereas for longitudinal analyses, an eroded white matter reference region is sometimes selected. No consensus has yet been reached on whether to use partial-volume correction of tau PET data. Although an increased neocortical tau PET signal is rare in cognitively unimpaired individuals, even in amyloid-β–positive cases, such a signal holds important prognostic information because preliminary data suggest that an elevated tau PET signal predicts cognitive decline over time. Also, in symptomatic stages of AD (i.e., mild cognitive impairment or AD dementia), tau PET shows great potential as a prognostic marker because an elevated baseline tau PET retention forecasts future cognitive decline and brain atrophy. For differential diagnostic use, the primary utility of tau PET is to differentiate AD dementia from other neurodegenerative diseases, as is in line with the conditions for the approval of $^{18}$F-flortaucipir by the U.S. Food and Drug Administration for clinical use. The differential diagnostic performance drops substantially at the mild-cognitive-impairment stage of AD, and there is no sufficient evidence for detection of sporadic non-AD primary tauopathies at the individual level for any of the currently available tau PET tracers. In conclusion, while the field is currently addressing outstanding methodologic issues, tau PET is gradually moving toward clinical application as a diagnostic and possibly prognostic marker in dementia expert centers and as a tool for selecting participants, assessing target engagement, and monitoring treatment effects in clinical trials.

**Key Words**: molecular imaging; neurology; PET; Alzheimer; PET; tau; diagnosis; pathology

**J Nucl Med 2022; 63:20S–26S**
DOI: 10.2967/jnumed.121.263196

Tau is a phosphoprotein that is synthesized throughout the nervous system and is involved in the formation and stabilization of microtubules, which are, in turn, critical for cytoskeletal support and intracellular transport of organelles, secretory vesicles, and neurotransmitters. Tau physiology relies on phosphorylation, but when tau becomes hyperphosphorylated, its normal functionality is altered. Hyperphosphorylation also increases the aggregation of tau into straight filaments, twisted ribbons, or paired helical filaments (*1*). Collectively shared under the rubric of tauopathies, many of the most common neurodegenerative diseases are characterized by tau pathology, such as Alzheimer disease (AD), progressive supranuclear palsy, corticobasal degeneration and Pick disease (*2*). As of 2013, it has been possible to visualize and quantify tau pathology in the living human brain (*3*). Since then, studies using tau PET have shown an exponential rise within the field of neurodegenerative disorders (Fig. 1). To date, a wide array of tracers has been developed, which can roughly be categorized into first-generation and second-generation tau PET tracers. First-generation tau PET tracers include $^{18}$F-flortaucipir (also called $^{18}$F-T807, $^{18}$F-AV1451 and $^{18}$F-Tauvid [Eli Lilly and Co.], which is the most widely applied tracer to date), $^{11}$C-PBB3, and the $^{18}$F-THK family (*4,5*). Second-generation tracers include $^{18}$F-MK6240, $^{18}$F-RO948, $^{18}$F-PI2620, $^{18}$F-GTP1, and $^{18}$F-JNJ-64326067 (*6–11*) and were developed to minimize the off-target binding observed in the first-generation tau PET tracers.

Most neurodegenerative diseases (including the tauopathies) show a stereotypical distribution of pathology throughout the brain (*10,12*), and PET provides a unique opportunity to provide 3-dimensional topographic images of molecular physiology in the living brain. Therefore, tau PET can serve to detect the presence of a tauopathy in a diagnostic setting and additionally provide valuable information about the spatial patterns of tau pathology. Aside from the promising prospects for tau PET as a diagnostic tool, the strong association between spatial patterns of tau, neurodegeneration, and cognitive impairment (*13–15*) also highlights the potential of tau PET as a prognostic tool. Nearly a decade after the introduction of the first potent tau PET tracer, we will here summarize the current state of the art of the tau PET literature and highlight some of the opportunities and challenges of tau PET. We specifically focus on the neuropathologic correlates of tau PET; methodologic considerations, including on- and off-target binding, PVC, and reference region selection; and finally the potential clinical utility of tau PET in terms of early detection of tau pathology, differential diagnosis of dementia syndromes, and prediction of future rates of cognitive decline across the AD clinical spectrum.

## NEUROPATHOLOGIC CORRELATES OF TAU PET SIGNAL

For most established tau PET tracers, there is evidence of binding to the tau aggregates formed in AD (i.e., a mix of 3-repeat

Received Dec. 15, 2021; revision accepted Mar. 9, 2022.
For correspondence or reprints, contact Rik Ossenkoppele (r.ossenkoppele@amsterdamumc.nl).

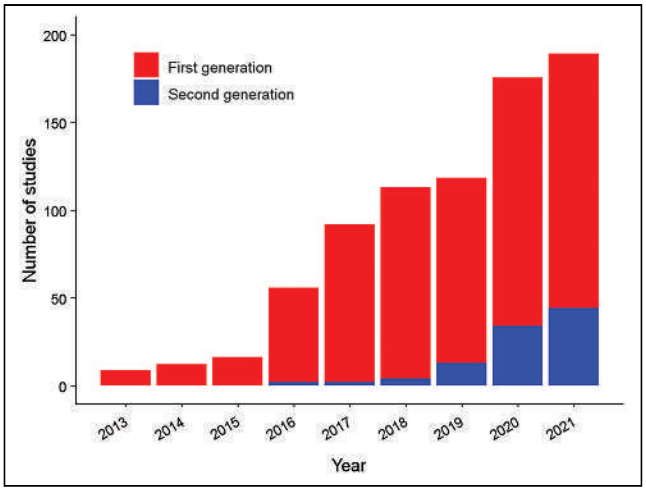


**FIGURE 1.** Rapid increase in tau PET publications since 2013. Records were obtained from database (https://pubmed.ncbi.nlm.nih.gov/) using search queries for first-generation tau tracers (THK* OR (T807 OR T808 OR AV1451 OR flortaucipir OR Tauvid) OR (PBB3 OR APN1607)) AND (PET OR "positron emission tomography") and for second-generation tau tracers (MK6240 OR (RO948 OR RO69558948) OR PI2620 OR GTP1 OR (JNJ64349311 OR JNJ311 OR JNJ067)) AND (PET OR "positron emission tomography"). Duplicates were not removed to ensure inclusion in both queries for studies that implemented multiple tau tracers.

[3R]/4-repeat [4R] tau isoforms) from autoradiography studies performed on postmortem brain tissue (*16–20*). However, most tracers have shown lower affinity for the 3R and 4R isoforms of tau that characterize many primary tauopathies, possibly related to the lower tau aggregate densities that hamper detection using PET. For $^{18}$F-flortaucipir and $^{18}$F-MK6240, binding to non-AD tau pathology has been limited according to autoradiography studies, whereas there is some autoradiographic evidence of $^{18}$F-PI2620 (*21*) and $^{18}$F-PM-PBB3 (a fluorinated version of $^{11}$C-PBB3) (*22*) binding to 4R tau inclusions observed in tissue of individuals with progressive supranuclear palsy. To fully validate the radiotracers, it is crucial to verify that the signal detected in vivo corresponds to tau pathology as assessed by postmortem neuropathologic examination of the brain. The most extensive neuropathologic correlations thus far have been performed for $^{18}$F-flortaucipir PET (Fig. 2). There is strong evidence, provided by a relatively large end-of-life study (*23*) and extended case series (*24,25*), that $^{18}$F-flortaucipir accurately detects AD-like tau neuropathology in individuals in more advanced Braak stages (i.e., Braak > IV; the accuracy for detecting tau load corresponding to Braak stages V and VI was 87.5% [95% CI, 77.2%–93.5%] (*23*)). These data are further supported by the strong correlations ($R^2$ range, 0.66–0.76) between tau PET levels and the quantitative neuropathologic tau burden in corresponding brain regions (*26,27*). Studies on non-AD tauopathies showed mixed results. In *MAPT*-mutation carriers with mixed 3R/4R tau pathology (akin to AD), there is a strong correspondence ($R^2$ = 0.86) between the antemortem tau PET scan and the postmortem neuropathologic tau burden (*28,29*). For 4R tauopathies such as progressive supranuclear palsy and corticobasal degeneration, however, the evidence is less clear. Some in vivo signal has been detected in individuals clinically diagnosed with a corticobasal syndrome (*29–31*). However, so far only 5 autopsy-confirmed cases have been published showing either moderate-to-high correlations ($R^2$ range, 0.59–0.79) of $^{18}$F-flortaucipir PET signal with tau pathology (*32,33*) or only minor increases in tracer uptake compared with controls with a limited correlation between the tau PET signal and neuropathology (*24*). There are multiple reports of group-level differences in vivo between controls and clinically diagnosed progressive supranuclear palsy patients using both $^{18}$F-flortaucipir (*29,34–36*) and $^{18}$F-PI2620 (*21*). Tracer retention is observed mostly in the basal ganglia and substantia nigra, complicating the interpretation because these regions also show off-target binding for several tau PET tracers ("Methodologic Considerations" section). The number of autopsy-confirmed cases is low (*24,37,38*) and demonstrated no correlation between cortical $^{18}$F-flortaucipir PET signal and neuropathologic 4R tau (*38*), with little binding outside the off-target regions (*24*). The binding profile of $^{18}$F-PI2620 in progressive supranuclear palsy seems more promising, potentially because of lower off-target binding in the basal ganglia. Autoradiography provided some evidence of binding to 4R tau pathology (*21*), but the only neuropathologic correlation study published to date showed limited binding of $^{18}$F-PI2620 PET to 4R tau pathology, suggesting that the in vivo tau PET signal only partially reflects postmortem 4R tau pathology (*39*).

In summary, the available neuropathologic data strongly indicate that the current tau PET tracers bind the tau aggregates formed in AD in the more advanced Braak stages (>IV). Tracer binding in most non-AD tauopathies is weaker and overlaps to a large extent with known off-target binding regions, hence limiting

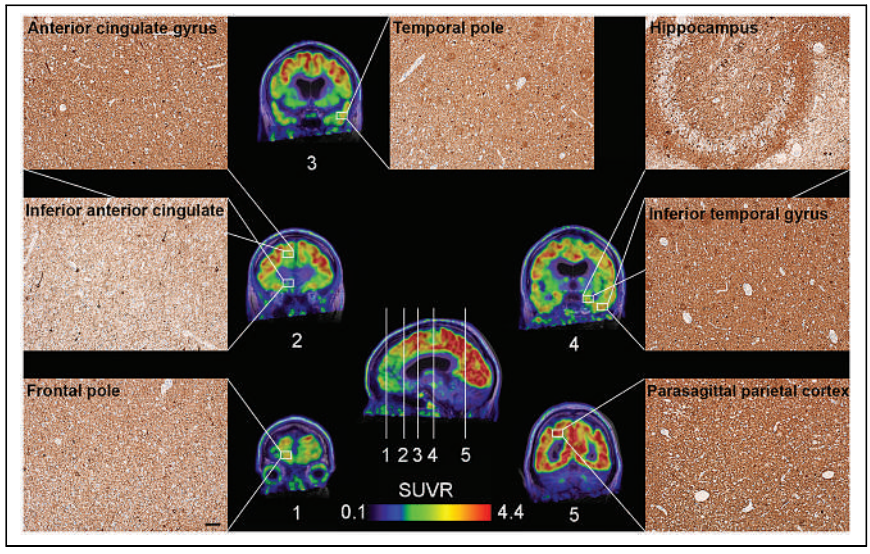


**FIGURE 2.** Correspondence between neuropathologic tau in comparison to antemortem $^{18}$F-flortaucipir PET retention in individual with AD dementia. Depicted are 5 coronal $^{18}$F-flortaucipir PET sections labeled as 1 to 5 in anteroposterior direction. Approximate locations of coronal sections are indicated in sagittal section. Corresponding AT8 (phospho-tau) immunohistochemistry images at ×10 magnification were captured from frontal pole, inferior anterior cingulate gyrus, anterior cingulate gyrus, temporal pole, hippocampus, inferior temporal gyrus, and parasagittal parietal cortex. Scale bar = 50 μm.

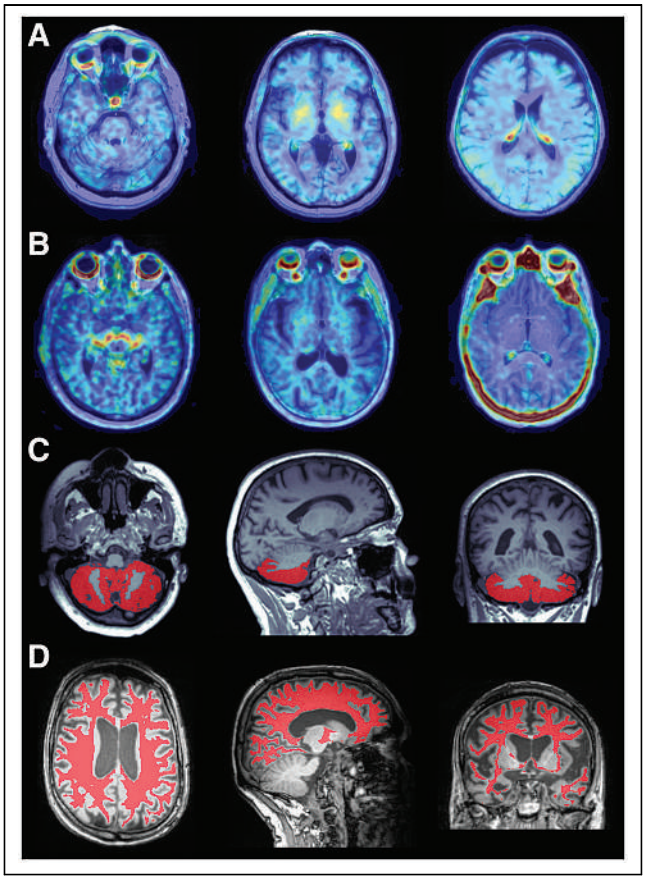


**FIGURE 3.** (A) $^{18}$F-Flortaucipir PET images showing, from left to right (all axial slices), off-target binding in retina and pituitary, basal ganglia, and choroid plexus. (B) $^{18}$F-RO948 images showing, from left to right (all axial slices), retinal, substantia nigra, and superior cerebellar off-target binding; retinal off-target binding and notable absence of basal ganglia off-target binding; and extreme case of skull/meningeal off-target binding. (C) Inferior cerebellar reference region. (D) White matter reference region.

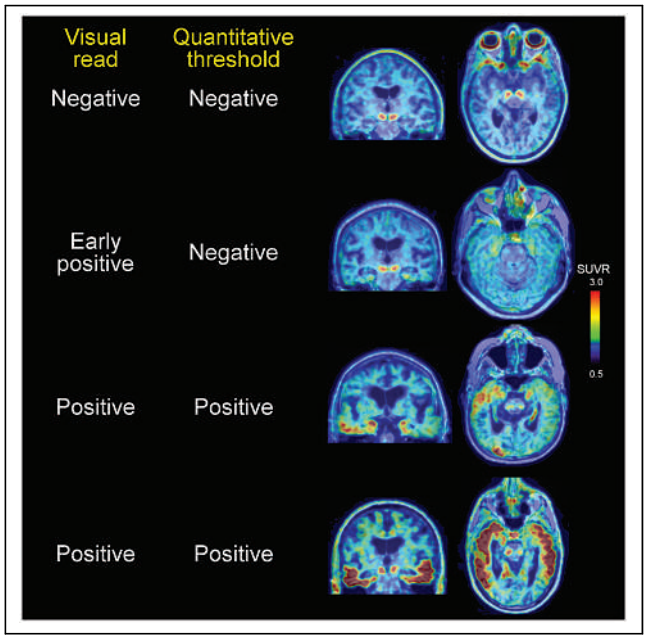


**FIGURE 4.** Four examples of $^{18}$F-RO9848 scans in ascending order of overall tau load, which were evaluated both visually and using quantitative threshold. Second case indicates that visual read can be positive (early) at subthreshold levels of tau PET signal.

the possibility of quantifying and visualizing non-AD tau pathology in vivo.

## METHODOLOGIC CONSIDERATIONS OF TAU PET

### Off-Target Binding

The off-target binding profile varies widely across tau PET tracers. Some of the first-generation tracers (e.g., $^{11}$C-PBB3 and the $^{18}$F-THK ligands) show off-target binding to amyloid deposits and monoamine oxidase B to such an extent that it hampers the specificity of these tracers to detect tau pathology (*5*). The most apparent off-target binding targets of $^{18}$F-flortaucipir, $^{18}$F-RO948, and $^{18}$F-MK6240 are neuromelanin in the substantia nigra and retinal pigment epithelium (*17,19,40*). In addition, $^{18}$F-flortaucipir shows substantial off-target binding in the basal ganglia, longitudinal sinuses, pituitary, and choroid plexus (Figs 3A–3C), as indicated by head-to-head studies against $^{18}$F-RO948 (*41*) and $^{18}$F-MK6240 (*42*). In contrast, $^{18}$F-RO948 and $^{18}$F-MK6240 show greater binding to the meninges and skull (Figs. 3D–3F), especially in women (*43,44*). Only a few reports are available on in vivo off-target binding of $^{18}$F-PI2620 to the meninges, skull, and venous sinuses, but published images of the tracer seem to indicate off-target binding to the meninges or skull as well (*39*). Potential sources of the off-target binding across tracers include monoamine oxidase, calcifications, iron, and microhemorrhages (*45*).

### PVC

No consensus has yet been reached on the use of partial-volume correction (PVC) in tau PET studies. A recent study assessed 5 different PVC methods and showed that PVC improved the discriminative accuracy between cognitively impaired and unimpaired individuals cross-sectionally but also resulted in less robust longitudinal changes in tau PET signal (*46*). PVC has also been used to reduce the impact of choroid plexus off-target binding on hippocampal signal when using $^{18}$F-flortaucipir PET (*47*), but standard (e.g., geometric transfer matrix) and more novel (e.g., Van Cittert iterative deconvolution with highly constrained backprojection denoising) PVC methods only modestly restore hippocampal signal and the correlation between hippocampal signal and clinical symptoms (*48,49*). In our personal experience, although numeric increases in tracer retention are observed in PVC data, the main effects (e.g., cognitive correlates or diagnostic performance) are generally highly similar with and without PVC. Still, in relevant scenarios (e.g., in longitudinal settings or in the presence of marked brain atrophy), we recommend reporting results both with and without PVC.

### Reference Region Selection

The most widely used reference region for tau PET studies is the cerebellar gray matter. This region is devoid of tau in neuropathologic studies (*27*) and shows low variance in amyloid-β–negative controls (*45*). Preferentially, the inferior cerebellar cortex or cerebellar crus, corresponding to the mid portion of the cerebellar gray matter, has been used to minimize spill-in from occipital lobe signal and to avoid off-target binding in the superior parts of the cerebellar vermis observed with some tracers (*47*). Recent studies indicate that an inferior cerebellar reference region provided the most sensitive measure for cross-sectional group differences (*50*), whereas an eroded white matter or an eroded white matter cerebellar composite reference region in conjunction with a dedicated longitudinal processing pipeline is most suitable for longitudinal

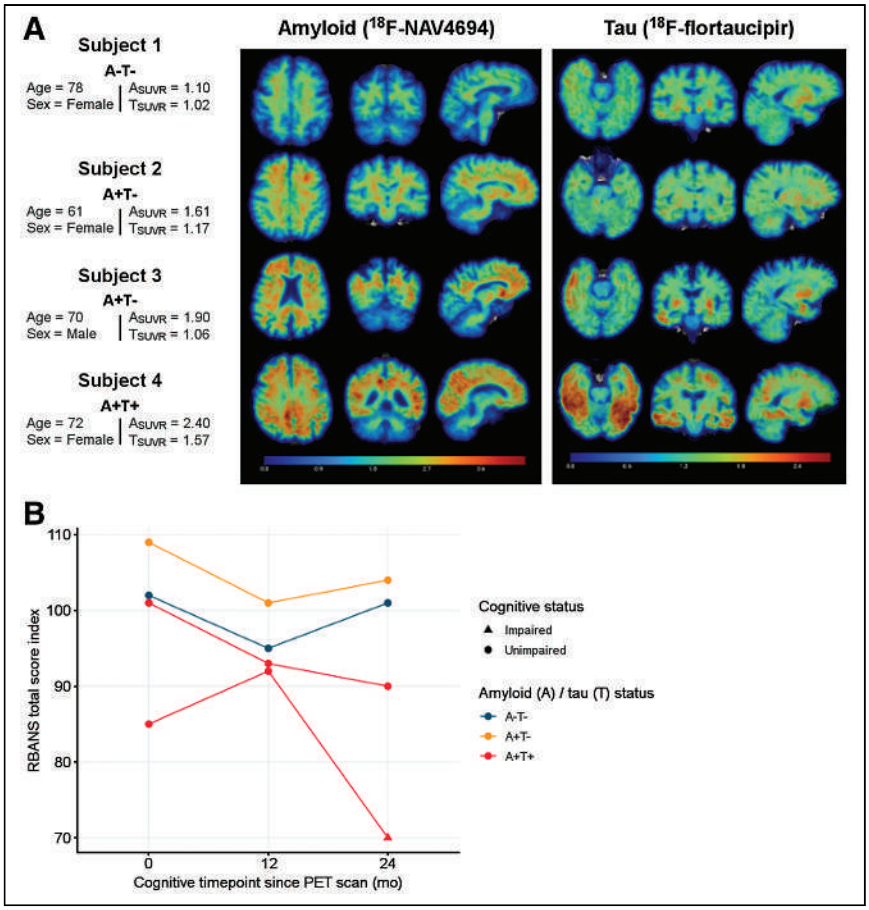


**FIGURE 5.** (A) Scans of 4 representative participants with different amyloid and tau profiles. One participant was negative on both biomarkers, 2 participants were positive on amyloid only, and 1 participant was positive on both amyloid and tau PET. Global amyloid level (NAV4694; global brain threshold of ≥1.29 SUVR; cerebellar cortex as reference region) and bilateral entorhinal cortex tau level (flortaucipir; bilateral entorhinal cortex of ≥1.23 SUVR; inferior cerebellum as reference region) were used to determine biomarker status. $A_{SUVR}$ and $T_{SUVR}$ represent values averaged across neocortical regions. (B) Prospective cognitive trajectories on RBANS total score index for each of the 4 participants. RBANS = Repeatable Battery for Assessment of Neuropsychological Status.

analyses (*46,50,51*). The latter will need to be verified in samples that contain more individuals with a high cortical tau burden, given the risk of spill-in due to the close proximity between a white matter reference region and the cortex.

### Determining Tau PET Positivity

There is currently no consensus on how to define tau PET positivity, thus hampering comparisons between studies. Positivity on a tau PET scan has been characterized by use of quantitative thresholds and visual assessment (*52*). Both require a selection of brain regions in which positivity will be determined. This selection of regions may differ between early stages (e.g., entorhinal cortex) and later stages (e.g., temporoparietal cortex) of AD. The binary classification of tau PET scans is further influenced by the methodologic approach to define a quantitative threshold (e.g., a gaussian mixture modeling or taking the 90th percentile in amyloid-β–negative cognitively unimpaired individuals) and the visual read procedures (53). This is particularly pertinent to early disease stages, when the signal-to-noise ratio is often low. Several regions of interest have been proposed as potential candidates to detect early tau accumulation. The entorhinal or transentorhinal cortex is usually considered the earliest region in which tau PET tracers can detect tau pathology and is therefore often used to define tau PET abnormality at the preclinical disease stage. However, tau pathology in the entorhinal cortex might not be specific to AD since autopsy studies have shown that entorhinal tau pathology commonly occurs in older individuals without amyloid-β pathology in a condition referred to as primary age-related tauopathy (*54*). An alternative approach is to use a temporal meta–region of interest (ROI) consisting of the entorhinal, fusiform, and inferior and middle temporal cortices; the amygdala; and the parahippocampus. This ROI has the advantage of being more specific to AD, although at the expense of its sensitivity in early stages because only a small proportion (5%–10%) of amyloid-β–positive cognitively unimpaired individuals is quantitatively classified as tau PET–positive in this ROI (*55,56*). Another advantage of the temporal meta-ROI (or temporoparietal cortex) is that it optimally captures the heterogeneous distribution of tau pathology across both typical presentations (i.e., ~70% conforms to the traditional Braak staging scheme of neurofibrillary tangle pathology) and atypical presentations (e.g., posterior cortical atrophy ["visual AD"] and logopenic variant primary progressive aphasia ["language AD"]) of AD (*57,58*). Importantly, visual assessment of mild temporal binding has been found to enhance sensitivity in detecting tau in early disease stages when compared with temporal meta-ROI quantification (Fig. 4) (*59*). When comparing visually versus quantitatively discordant tau PET status, visual assessment yielded the highest rate of tau PET positivity. Despite the fact that they did not reach the SUV ratio (SUVR) threshold for positivity, isolated visually positive individuals also showed elevated amyloid PET positivity, cerebrospinal fluid phosphorylated-tau 181 concentrations, and tau PET SUVRs.

## CLINICAL USE OF TAU PET

### Early Detection

In the past few decades, amyloid PET has been the imaging modality of choice for early detection of AD. Amyloid-β pathology, however, is highly prevalent among older adults, and although the presence of amyloid-β is necessary for a diagnosis of AD, it might not be sufficient to cause clinical AD (*60*). Furthermore, individuals with amyloidosis can remain cognitively normal for decades before they start experiencing cognitive symptoms, making amyloid-β a suboptimal predictor of clinical progression in cognitively unimpaired individuals. To improve the identification of individuals with early AD in a research setting, the amyloid-β (A), tau (T), and neurodegeneration (N) framework has been proposed (*61*). This biologic framework is especially useful for individuals that are not yet

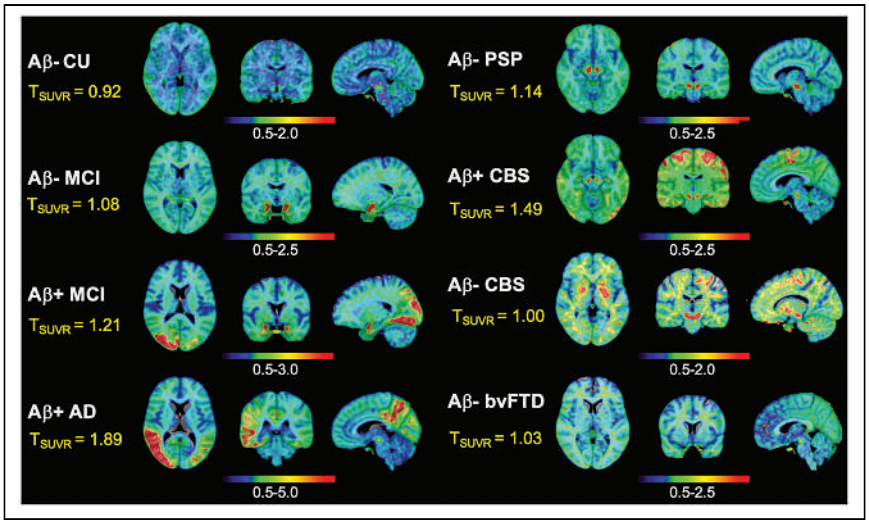


**FIGURE 6.** Examples of representative tau PET scans across different diagnostic groups. All PET scans were obtained 70–90 min after injection of 370 MBq of $^{18}$F-RO948 on GE Healthcare Discovery scanner, projected onto coregistered T1-weighted MRI scan, normalized to standard MNI space, and finally converted to SUVRs using inferior cerebellar cortex as reference tissue. Scans were obtained from BioFINDER-2 cohort. Color scales indicate SUVRs and are individually tailored to best visualize tau PET patterns across different diagnoses. $T_{SUVR}$ represents average uptake in late-stage (Braak V–VI) tau regions. All slices are depicted in radiologic convention. Aβ = amyloid β; bvFTD = behavioral variant of frontotemporal dementia; CBS = corticobasal syndrome; CU = cognitively unimpaired; MCI = mild cognitive impairment; PSP = progressive supranuclear palsy.

experiencing the clinical consequences of the disease. One challenge, however, is that it requires continuous biologic variables to be dichotomized into binary categoric classifications. Although a global measure can be used for defining amyloid PET positivity given the already widespread distribution of amyloid-β pathology in early stages, such is not the case for tau PET because tau pathology in the neocortex manifests closer to symptomatic stages of the disease and requires a more refined regional approach.

Given its high specificity, tau PET quantification has been found to be superior to amyloid PET and MRI in predicting preclinical and prodromal cognitive changes (*62*). In the PREVENT-AD study ("Presymptomatic Evaluation of Experimental or Novel Treatments for Alzheimer Disease"), 129 cognitively unimpaired participants (mean age, 67 y [SD, 5 y]) underwent amyloid and tau PET scans and were subsequently followed for a minimum of 2 y (*63*). Both increased amyloid and tau PET levels were associated with cognitive decline, but this relationship was predominantly driven by tau (i.e., when both amyloid and tau were included in the model, only tau remained significant). Figure 5A shows representative examples of amyloid and tau PET scans of 4 PREVENT-AD participants who were cognitively unimpaired at the time of these PET scans. Figure 5B shows the cognitive trajectory of these same individuals over the course of 2 y. Although both the A-negative, T-negative participant and the A-positive, T-negative participant remained cognitively unimpaired over the course of the follow-up, the A-positive, T-positive participants demonstrated cognitive decline, and one of them even met diagnostic criteria for mild cognitive impairment at the 2-y follow-up visit. Only one participant was classified as A-negative, T-positive; this participant was cognitively stable over time. In summary, T positivity, especially in combination with A positivity, seems to be a key driver of cognitive decline. Tau PET positivity could therefore be an excellent marker to predict short-term progression from cognitive nonimpairment to mild cognitive impairment in participants at risk of AD dementia.

### Prognosis in Symptomatic AD

In symptomatic stages of AD (i.e., mild cognitive impairment and AD dementia), elevated amyloid and tau PET levels at baseline are strongly associated with a more rapid cognitive decline (*62,64,65*) and outperformed amyloid PET and structural MRI measures in head-to-head comparisons (*62,66*). Furthermore, among participants with mild cognitive impairment and AD dementia, a visually determined positive $^{18}$F-flortaucipir PET scan was associated with an increased risk for future cognitive decline (Mini-Mental State Examination hazard ratio, 1.68 [95% CI, 1.22–2.32]) and functional decline (CDR sum of boxes hazard ratio, 1.40 [95% CI, 1.11–1.76]) after 18 mo of follow-up (*67*). Both the intensity and the extent of baseline tau PET levels were also strongly predictive for future rates of brain atrophy among participants with mild cognitive impairment and AD dementia (*68*). In summary, tau PET shows great potential as a prognostic marker in symptomatic stages of AD.

### Differential Diagnosis

Differentiating between neurodegenerative diseases is challenging because clinical presentations and patterns of neurodegeneration can substantially overlap across disorders. Given that most neurodegenerative dementias are characterized by tauopathy, it has been estimated that, when correctly implemented, tau PET imaging may be able to detect up to 70% of neurodegenerative dementias in a diagnostic setting (*69*). The most established tau PET tracers (i.e., $^{18}$F-flortaucipir, $^{18}$F-MK6240, and $^{18}$F-RO948) have demonstrated excellent diagnostic performance for distinguishing AD dementia from non-AD neurodegenerative disorders, with a sensitivity and specificity above 90% (*56,70,71*). Some exemplary BioFINDER-2 ("Biomarkers for Identifying Neurodegenerative Disorders Early and Reliably") cases with $^{18}$F-RO948 PET are shown in Figure 6. In this regard, tau PET is superior to other AD biomarkers, including structural MRI, amyloid-β PET, and most biofluid markers (*56,72–74*). Furthermore, tau PET can be helpful in accurately detecting atypical (nonamnestic) variants of AD, which show highly distinct patterns of tau pathology compared with typical (amnestic-predominant) AD cases (*75,76*). There are several remaining challenges for the use of tau PET in the clinic as a differential diagnostic tool. First, the discriminative accuracy of tau PET tracers drops substantially at the prodromal stage of AD, hence making it most suitable for use in more advanced (i.e., dementia) stages of AD (*56,77,78*). Second, although tau PET tracers are often capable of differentiating non-AD tauopathies such as progressive supranuclear palsy, corticobasal degeneration, and Pick disease from controls at a group level, their utility at an individual-patient level is limited ("Methodologic Considerations" section). Third, it will be important to understand why we commonly observe elevated tau PET signal in clinical syndromes

that are typically not associated with tau pathology, such as the semantic variant of primary progressive aphasia (*79,80*), which in most cases is caused by TDP-43 type C pathology. In summary, in line with the conditions of the approval of $^{18}$F-flortaucipir by the U.S. Food and Drug Administration, the current diagnostic utility of tau PET is mainly to differentiate AD dementia from other neurodegenerative diseases (*81*).

## CONCLUSIONS AND FUTURE DIRECTIONS

There is strong evidence from neuropathologic studies that the most widely used tau PET tracers (i.e., $^{18}$F-flortaucipir, $^{18}$F-MK6240, $^{18}$F-RO948, and $^{18}$F-PI2620) bind tau aggregates formed in AD in the more advanced Braak stages. However, tracer binding in most non-AD tauopathies is weaker and overlaps to a large extent with known off-target binding regions, hence limiting the possibility of quantifying and visualizing non-AD tau pathology in vivo. All tau PET tracers are characterized by off-target binding, and the application of PVC methods and selection of the optimal reference region for longitudinal studies are currently being refined. Tau PET has shown excellent diagnostic accuracy for distinguishing AD dementia from non-AD neurodegenerative disorders and has shown promise for early detection of AD among cognitively unimpaired individuals and for prognostic use in symptomatic stages of AD. Important next steps for the tau PET field include developing appropriate-use criteria akin to those for amyloid PET (*82*), investigating the diagnostic and prognostic value of tau PET in older and ethnically more diverse populations, performing head-to-head comparisons against cerebrospinal fluid and plasma biomarkers of AD pathology (e.g., p-tau and the $A\beta_{42-40}$ ratio) and neurodegeneration (e.g., neurofilament light chain and glial fibrillary acidic protein), determining the long-term cognitive consequences of being exposed to neocortical tau pathology in cognitively unimpaired individuals, and refining tau PET measures for participant selection, target engagement, and treatment monitoring in clinical trials.

## DISCLOSURE

Oskar Hansson has acquired research support (for the institution) from AVID Radiopharmaceuticals, Biogen, Eli Lilly, Eisai, GE Healthcare, Pfizer, and Roche. In the past 2 years, he has received consultancy or speaker fees from Roche, Genentech, Siemens, Biogen, Alzpath, and Cerveau. No other potential conflict of interest relevant to this article was reported.

## REFERENCES


1. Buée L, Bussière T, Buée-Scherrer V, Delacourte A, Hof PR. Tau protein isoforms, phosphorylation and role in neurodegenerative disorders. *Brain Res Brain Res Rev.* 2000;33:95–130.
2. Lee VMY, Goedert M, Trojanowski JQ. Neurodegenerative tauopathies. *Annu Rev Neurosci.* 2001;24:1121–1159.
3. Chien DT, Bahri S, Szardenings AK, et al. Early clinical PET imaging results with the novel PHF-tau radioligand [F-18]-T807. *J Alzheimers Dis.* 2013;34:457–468.
4. Wolters EE, Dodich A, Boccardi M, et al. Clinical validity of increased cortical uptake of [$^{18}$F]flortaucipir on PET as a biomarker for Alzheimer's disease in the context of a structured 5-phase biomarker development framework. *Eur J Nucl Med Mol Imaging.* 2021;48:2097–2109.
5. Chiotis K, Dodich A, Boccardi M, et al. Clinical validity of increased cortical binding of tau ligands of the THK family and PBB3 on PET as biomarkers for Alzheimer's disease in the context of a structured 5-phase development framework. *Eur J Nucl Med Mol Imaging.* 2021;48:2086–2096.
6. Maruyama M, Shimada H, Suhara T, et al. Imaging of tau pathology in a tauopathy mouse model and in Alzheimer patients compared to normal controls. *Neuron.* 2013;79:1094–1108.
7. Mattsson N, Schöll M, Strandberg O, et al. $^{18}$F-AV-1451 and CSF T-tau and P-tau as biomarkers in Alzheimer's disease. *EMBO Mol Med.* 2017;9:1212–1223.
8. Gobbi LC, Knust H, Körner M, et al. Identification of three novel radiotracers for imaging aggregated tau in Alzheimer's disease with positron emission tomography. *J Med Chem.* 2017;60:7350–7370.
9. Declercq L, Rombouts F, Koole M, et al. Preclinical Evaluation of $^{18}$F-JNJ64349311, a novel PET tracer for tau imaging. *J Nucl Med.* 2017;58:975–981.
10. Aguero C, Dhaynaut M, Normandin MD, et al. Autoradiography validation of novel tau PET tracer [F-18]-MK-6240 on human postmortem brain tissue. *Acta Neuropathol Commun.* 2019;7:37.
11. Bischof GN, Dodich A, Boccardi M, et al. Clinical validity of second-generation tau PET tracers as biomarkers for Alzheimer's disease in the context of a structured 5-phase development framework. *Eur J Nucl Med Mol Imaging.* 2021;48:2110–2120.
12. Williams DR, Holton JL, Strand C, et al. Pathological tau burden and distribution distinguishes progressive supranuclear palsy-parkinsonism from Richardson's syndrome. *Brain.* 2007;130:1566–1576.
13. Arriagada PV, Growdon JH, Hedley-Whyte ET, Hyman BT. Neurofibrillary tangles but not senile plaques parallel duration and severity of Alzheimer's disease. *Neurology.* 1992;42:631–639.
14. Nelson PT, Alafuzoff I, Bigio EH, et al. Correlation of Alzheimer disease neuropathologic changes with cognitive status: a review of the literature. *J Neuropathol Exp Neurol.* 2012;71:362–381.
15. Spires-Jones TL, Hyman BT. The intersection of amyloid beta and tau at synapses in Alzheimer's disease. *Neuron.* 2014;82:756–771.
16. Lowe VJ, Curran G, Fang P, et al. An autoradiographic evaluation of AV-1451 tau PET in dementia. *Acta Neuropathol Commun.* 2016;4:58.
17. Marquié M, Normandin MD, Vanderburg CR, et al. Validating novel tau positron emission tomography tracer [F-18]-AV-1451 (T807) on postmortem brain tissue. *Ann Neurol.* 2015;78:787–800.
18. Sander K, Lashley T, Gami P, et al. Characterization of tau positron emission tomography tracer [$^{18}$F]AV-1451 binding to postmortem tissue in Alzheimer's disease, primary tauopathies, and other dementias. *Alzheimers Dement.* 2016;12:1116–1124.
19. Aguero C, Dhaynaut M, Normandin MD, et al. Autoradiography validation of novel tau PET tracer [F-18]-MK-6240 on human postmortem brain tissue. *Acta Neuropathol Commun.* 2019;7:37.
20. Leuzy A, Chiotis K, Lemoine L, et al. Tau PET imaging in neurodegenerative tauopathies: still a challenge. *Mol Psychiatry.* 2019;24:1112–1134.
21. Brendel M, Barthel H, van Eimeren T, et al. Assessment of $^{18}$F-PI-2620 as a biomarker in progressive supranuclear palsy. *JAMA Neurol.* 2020;77:1408–1419.
22. Tagai K, Ono M, Kubota M, et al. High-contrast in vivo imaging of tau pathologies in Alzheimer's and non-Alzheimer's disease tauopathies. *Neuron.* 2021;109:42–58.e48.
23. Fleisher AS, Pontecorvo MJ, Devous MD Sr, et al. Positron emission tomography imaging with [$^{18}$F]flortaucipir and postmortem assessment of Alzheimer disease neuropathologic changes. *JAMA Neurol.* 2020;77:829–839.
24. Soleimani-Meigooni DN, Iaccarino L, La Joie R, et al. $^{18}$F-flortaucipir PET to autopsy comparisons in Alzheimer's disease and other neurodegenerative diseases. *Brain.* 2020;143:3477–3494.
25. Lowe VJ, Lundt ES, Albertson SM, et al. Tau-positron emission tomography correlates with neuropathology findings. *Alzheimers Dement.* 2020;16:561–571.
26. Pontecorvo MJ, Keene CD, Beach TG, et al. Comparison of regional flortaucipir PET with quantitative tau immunohistochemistry in three subjects with Alzheimer's disease pathology: a clinicopathological study. *EJNMMI Res.* 2020;10:65.
27. Smith R, Wibom M, Pawlik D, Englund E, Hansson O. Correlation of in vivo [$^{18}$F]flortaucipir with postmortem Alzheimer disease tau pathology. *JAMA Neurol.* 2019;76:310–317.
28. Smith R, Puschmann A, Scholl M, et al. $^{18}$F-AV-1451 tau PET imaging correlates strongly with tau neuropathology in MAPT mutation carriers. *Brain.* 2016;139:2372–2379.
29. Tsai RM, Bejanin A, Lesman-Segev O, et al. $^{18}$F-flortaucipir (AV-1451) tau PET in frontotemporal dementia syndromes. *Alzheimers Res Ther.* 2019;11:13.
30. Cho H, Baek MS, Choi JY, et al. $^{18}$F-AV-1451 binds to motor-related subcortical gray and white matter in corticobasal syndrome. *Neurology.* 2017;89:1170–1178.
31. Smith R, Scholl M, Widner H, et al. In vivo retention of $^{18}$F-AV-1451 in corticobasal syndrome. *Neurology.* 2017;89:845–853.
32. Josephs KA, Whitwell JL, Tacik P, et al. [$^{18}$F]AV-1451 tau-PET uptake does correlate with quantitatively measured 4R-tau burden in autopsy-confirmed corticobasal degeneration. *Acta Neuropathol (Berl).* 2016;132:931–933.
33. McMillan CT, Irwin DJ, Nasrallah I, et al. Multimodal evaluation demonstrates in vivo $^{18}$F-AV-1451 uptake in autopsy-confirmed corticobasal degeneration. *Acta Neuropathol (Berl).* 2016;132:935–937.
34. Cho H, Choi JY, Hwang MS, et al. Subcortical $^{18}$F-AV-1451 binding patterns in progressive supranuclear palsy. *Mov Disord.* 2017;32:134–140.

35. Smith R, Schain M, Nilsson C, et al. Increased basal ganglia binding of $^{18}$F-AV-1451 in patients with progressive supranuclear palsy. *Mov Disord.* 2017;32: 108–114.
36. Whitwell JL, Lowe VJ, Tosakulwong N, et al. [$^{18}$F]AV-1451 tau positron emission tomography in progressive supranuclear palsy. *Mov Disord.* 2017;32:124–133.
37. Smith R, Pawlik D, Nilsson CF, Englund E, Hansson O. [$^{18}$F]flortaucipir distinguishes Alzheimer's disease from progressive supranuclear palsy pathology in a mixed-pathology case. *Acta Neuropathol (Berl).* 2020;139:411–413.
38. Smith R, Scholl M, Honer M, Nilsson CF, Englund E, Hansson O. Tau neuropathology correlates with FDG-PET, but not AV-1451-PET, in progressive supranuclear palsy. *Acta Neuropathol (Berl).* 2017;133:149–151.
39. Tezuka T, Takahata K, Seki M, et al. Evaluation of [$^{18}$F]PI-2620, a second-generation selective tau tracer, for assessing four-repeat tauopathies. *Brain Commun.* 2021;3(4):fcab190.
40. Hansen AK, Damholdt MF, Fedorova TD, et al. In vivo cortical tau in Parkinson's disease using $^{18}$F-AV-1451 positron emission tomography. *Mov Disord.* 2017;32: 922–927.
41. Smith R, Scholl M, Leuzy A, et al. Head-to-head comparison of tau positron emission tomography tracers [$^{18}$F]flortaucipir and [$^{18}$F]RO948. *Eur J Nucl Med Mol Imaging.* 2020;47:342–354.
42. Gogola A, Minhas DS, Villemagne VL, et al. Direct comparison of the tau PET tracers [$^{18}$F]flortaucipir and [$^{18}$F]MK-6240 in human subjects. *J Nucl Med.* 2022; 63:108–116.
43. Betthauser TJ, Cody KA, Zammit MD, et al. In vivo characterization and quantification of neurofibrillary tau PET radioligand $^{18}$F-MK-6240 in humans from Alzheimer disease dementia to young controls. *J Nucl Med.* 2019;60:93–99.
44. Smith R, Strandberg O, Leuzy A, et al. Sex differences in off-target binding using tau positron emission tomography. *Neuroimage Clin.* 2021;31:102708.
45. Baker SL, Harrison TM, Maass A, La Joie R, Jagust WJ. Effect of off-target binding on $^{18}$F-flortaucipir variability in healthy controls across the life span. *J Nucl Med.* 2019;60:1444–1451.
46. Schwarz CG, Therneau TM, Weigand SD, et al. Selecting software pipelines for change in flortaucipir SUVR: balancing repeatability and group separation. *Neuroimage.* 2021;238:118259.
47. Baker SL, Maass A, Jagust WJ. Considerations and code for partial volume correcting [$^{18}$F]-AV-1451 tau PET data. *Data Brief.* 2017;15:648–657.
48. Pawlik D, Leuzy A, Strandberg O, Smith R. Compensating for choroid plexus based off-target signal in the hippocampus using $^{18}$F-flortaucipir PET. *Neuroimage.* 2020;221:117193.
49. Wolters EE, Ossenkoppele R, Golla SS, et al. Hippocampal [$^{18}$F]flortaucipir BPND corrected for possible spill-in of the choroid plexus retains strong clinicopathological relationships. *Neuroimage Clin.* 2020;25:102113.
50. Young CB, Landau SM, Harrison TM, Poston KL, Mormino EC; ADNI. Influence of common reference regions on regional tau patterns in cross-sectional and longitudinal [$^{18}$F]-AV-1451 PET data. *Neuroimage.* 2021;243:118553.
51. Southekal S, Devous MD Sr, Kennedy I, et al. Flortaucipir F18 quantitation using parametric estimation of reference signal intensity. *J Nucl Med.* 2018;59: 944–951.
52. Villemagne VL, Lopresti BJ, Dore V, et al. What is T+? A Gordian knot of tracers, thresholds, and topographies. *J Nucl Med.* 2021;62:614–619.
53. Maass A, Landau S, Baker SL, et al. Comparison of multiple tau-PET measures as biomarkers in aging and Alzheimer's disease. *Neuroimage.* 2017;157:448–463.
54. Crary JF, Trojanowski JQ, Schneider JA, et al. Primary age-related tauopathy (PART): a common pathology associated with human aging. *Acta Neuropathol (Berl).* 2014;128:755–766.
55. Ossenkoppele R, Jansen WJ, Rabinovici GD, et al. Prevalence of amyloid PET positivity in dementia syndromes: a meta-analysis. *JAMA.* 2015;313: 1939–1949.
56. Ossenkoppele R, Rabinovici GD, Smith R, et al. Discriminative accuracy of [$^{18}$F]flortaucipir positron emission tomography for Alzheimer disease vs other neurodegenerative disorders. *JAMA.* 2018;320:1151–1162.
57. Ossenkoppele R, Schonhaut DR, Scholl M, et al. Tau PET patterns mirror clinical and neuroanatomical variability in Alzheimer's disease. *Brain.* 2016;139:1551–1567.
58. Vogel JW, Young AL, Oxtoby NP, et al. Four distinct trajectories of tau deposition identified in Alzheimer's disease. *Nat Med.* 2021;27:871–881.
59. Provost K, Iaccarino L, Soleimani-Meigooni DN, et al. Comparing ATN-T designation by tau PET visual reads, tau PET quantification, and CSF PTau181 across three cohorts. *Eur J Nucl Med Mol Imaging.* 2021;48:2259–2271.
60. Small SA, Duff K. Linking Abeta and tau in late-onset Alzheimer's disease: a dual pathway hypothesis. *Neuron.* 2008;60:534–542.
61. Jack CR Jr, Bennett DA, Blennow K, et al. NIA-AA research framework: toward a biological definition of Alzheimer's disease. *Alzheimers Dement.* 2018; 14:535–562.
62. Ossenkoppele R, Smith R, Mattsson-Carlgren N, et al. Accuracy of tau positron emission tomography as a prognostic marker in preclinical and prodromal Alzheimer disease. *JAMA Neurol.* 2021;78:961–971.
63. Pichet Binette A, Vachon-Presseau E, Morris J, et al. Amyloid and tau pathology associations with personality traits, neuropsychiatric symptoms, and cognitive lifestyle in the preclinical phases of sporadic and autosomal dominant Alzheimer's disease. *Biol Psychiatry.* 2021;89:776–785.
64. Cho H, Choi JY, Lee HS, et al. Progressive tau accumulation in Alzheimer disease: 2-year follow-up study. *J Nucl Med.* 2019;60:1611–1621.
65. Pontecorvo MJ, Devous MD, Kennedy I, et al. A multicentre longitudinal study of ($^{18}$F)flortaucipir in normal ageing, mild cognitive impairment and Alzheimer's disease dementia. *Brain.* 2019;142:1723–1735.
66. Biel D, Brendel M, Rubinski A, et al. Tau-PET and in vivo Braak-staging as prognostic markers of future cognitive decline in cognitively normal to demented individuals. *Alzheimers Res Ther.* 2021;13:137.
67. Lu M, Pontecorvo MJ, Devous MD Sr, et al. Aggregated tau measured by visual interpretation of flortaucipir positron emission tomography and the associated risk of clinical progression of mild cognitive impairment and Alzheimer disease: results from 2 phase III clinical trials. *JAMA Neurol.* 2021;78:445–453.
68. La Joie R, Visani AV, Baker SL, et al. Prospective longitudinal atrophy in Alzheimer's disease correlates with the intensity and topography of baseline tau-PET. *Sci Transl Med.* 2020;12:eaau5732.
69. Higuchi M. Tau PET imaging. *Adv Exp Med Biol.* 2019;1184:217–230.
70. Jack CR, Wiste HJ, Botha H, et al. The bivariate distribution of amyloid-β and tau: relationship with established neurocognitive clinical syndromes. *Brain.* 2019;142: 3230–3242.
71. Leuzy A, Pascoal TA, Strandberg O, et al. A multicenter comparison of [$^{18}$F]flortaucipir, [$^{18}$F]RO948, and [$^{18}$F]MK6240 tau PET tracers to detect a common target ROI for differential diagnosis. *Eur J Nucl Med Mol Imaging.* 2021;48:2295–2305.
72. Mattsson N, Smith R, Strandberg O, et al. Comparing $^{18}$F-AV-1451 with CSF t-tau and p-tau for diagnosis of Alzheimer disease. *Neurology.* 2018;90:e388–e395.
73. Leuzy A, Smith R, Ossenkoppele R, et al. Diagnostic performance of F18-RO948 tau positron emission tomography in the differentiation of Alzheimer disease from other neurodegenerative disorders. *JAMA Neurol.* 2020;77:955–965.
74. Palmqvist S, Janelidze S, Quiroz YT, et al. Discriminative accuracy of plasma phospho-tau217 for Alzheimer disease vs other neurodegenerative disorders. *JAMA.* 2020;324:772–781.
75. Ossenkoppele R, Schonhaut DR, Schöll M, et al. Tau PET patterns mirror clinical and neuroanatomical variability in Alzheimer's disease. *Brain.* 2016;139:1551–1567.
76. Vogel JW, Young AL, Oxtoby NP, et al. Four distinct trajectories of tau deposition identified in Alzheimer's disease. *Nat Med.* 2021;27:871–881.
77. Leuzy A, Smith R, Ossenkoppele R, et al. Diagnostic performance of $^{18}$F-RO948 tau positron emission tomography in the differentiation of Alzheimer disease from other neurodegenerative disorders. *JAMA Neurol.* 2020;77:955–965.
78. Pascoal TA, Therriault J, Benedet AL, et al. $^{18}$F-MK-6240 PET for early and late detection of neurofibrillary tangles. *Brain.* 2020;143:2818–2830.
79. Smith R, Santillo AF, Waldö ML, et al. $^{18}$F-flortaucipir in TDP-43 associated frontotemporal dementia. *Sci Rep.* 2019;9:6082.
80. Mann DMA, Snowden JS. Frontotemporal lobar degeneration: pathogenesis, pathology and pathways to phenotype. *Brain Pathol.* 2017;27:723–736.
81. Ossenkoppele R, Hansson O. Towards clinical application of tau PET tracers for diagnosing dementia due to Alzheimer's disease. *Alzheimers Dement.* 2021;17: 1998–2008.
82. Johnson KA, Minoshima S, Bohnen NI, et al. Update on appropriate use criteria for amyloid PET imaging: dementia experts, mild cognitive impairment, and education. *Alzheimers Dement.* 2013;9:e106–e109.

# Imaging Dopaminergic Neurotransmission in Neurodegenerative Disorders

Elon D. Wallert[1], Elsmarieke van de Giessen[2], Remco J.J. Knol[3], Martijn Beudel[4], Rob M.A. de Bie[4], and Jan Booij[1]

*[1]Department of Radiology and Nuclear Medicine, Amsterdam UMC, University of Amsterdam, Amsterdam, The Netherlands; [2]Department of Radiology and Nuclear Medicine, Amsterdam UMC, Vrije Universiteit, Amsterdam, The Netherlands; [3]Department of Nuclear Medicine, Noordwest Ziekenhuisgroep, Alkmaar, The Netherlands; and [4]Department of Neurology, Amsterdam UMC, University of Amsterdam, Amsterdam, The Netherlands*

Imaging of dopaminergic transmission in neurodegenerative disorders such as Parkinson disease (PD) or dementia with Lewy bodies plays a major role in clinical practice and in clinical research. We here review the role of imaging of the nigrostriatal pathway, as well as of striatal receptors and dopamine release, in common neurodegenerative disorders in clinical practice and research. Imaging of the nigrostriatal pathway has a high diagnostic accuracy to detect nigrostriatal degeneration in disorders characterized by nigrostriatal degeneration, such as PD and dementia with Lewy bodies, and disorders of more clinical importance, namely in patients with clinically uncertain parkinsonism. Imaging of striatal dopamine $D_{2/3}$ receptors is not recommended for the differential diagnosis of parkinsonian disorders in clinical practice anymore. Regarding research, recently the European Medicines Agency has qualified dopamine transporter imaging as an enrichment biomarker for clinical trials in early PD, which underlines the high diagnostic accuracy of this imaging tool and will be implemented in future trials. Also, imaging of the presynaptic dopaminergic system plays a major role in, for example, examining the extent of nigrostriatal degeneration in preclinical and premotor phases of neurodegenerative disorders and to examine subtypes of PD. Also, imaging of postsynaptic dopamine $D_{2/3}$ receptors plays a role in studying, for example, the neuronal substrate of impulse control disorders in PD, as well as in measuring endogenous dopamine release to examine, for example, motor complications in the treatment of PD. Finally, novel MRI sequences as neuromelanin-sensitive MRI are promising new tools to study nigrostriatal degeneration in vivo.

**Key Words:** dopamine; neurodegeneration; PET, SPECT; Parkinson

**J Nucl Med 2022; 63:27S–32S**
DOI: 10.2967/jnumed.121.263197

Imaging of dopaminergic transmission in the brain is an important tool in neurodegenerative disorders such as Parkinson disease (PD) and dementia with Lewy bodies (DLB), not only as a research topic but also, frequently, for use in routine practice. In the first part of this review, we describe the role of dopaminergic imaging in routine practice. In the second part, we discuss its role in research.

## IMAGING BRAIN DOPAMINERGIC NEUROTRANSMISSION IN NEURODEGENERATIVE DISORDERS IN ROUTINE PRACTICE

### Imaging of Presynaptic Nigrostriatal Dopaminergic Pathway

In routine practice, imaging of the presynaptic nigrostriatal dopaminergic pathway is used to determine whether this is degenerated and, therefore, to differentiate patients with nigrostriatal degeneration from those without degeneration. The most common, and the relatively common, diseases characterized by nigrostriatal degeneration are PD, DLB, multiple-system atrophy (MSA), progressive supranuclear palsy (PSP), and corticobasal degeneration (*1–3*). PD, including PD dementia, and DLB are increasingly considered a disease continuum in view of their similar pathology (*4*). We will here focus on imaging of the dopaminergic system in these disorders.

The nigrostriatal dopaminergic pathway can be imaged using radiopharmaceuticals for the dopamine transporter (DAT), for the vesicular monoamine transporter-2 (VMAT-2), or for aromatic L-amino-acid decarboxylase (AADC) activity (mainly using $^{18}$F-6-fluoro-L-dopa [$^{18}$F-FDOPA]) (Fig. 1) (*5*). Regarding DAT imaging, many SPECT and PET tracers have been developed successfully (*6*). For VMAT-2 imaging, only PET tracers have been developed successfully (Fig. 1). Since the radiopharmaceutical $^{123}$I-labeled 2β-carbomethoxy-3β-(4-iodophenyl)-*N*-(3-fluoropropyl) nortropane ($^{123}$I-FP-CIT, or $^{123}$I-ioflupane, commercialized as DaTscan [in the United States; GE Healthcare], DaTSCAN [in Europe; GE Healthcare], or Striascan [Curium]) is the only licensed radiotracer to image the nigrostriatal dopaminergic pathway by the Food and Drug Administration and European Medicines Agency, most hospitals and institutes use this radiopharmaceutical to assess the integrity of the nigrostriatal pathway in routine clinical studies.

*DAT Imaging.* In PD, the loss of striatal DAT binding is typically more pronounced in the putamen than in the caudate nucleus (*6*). Characteristically, the loss of DAT binding starts in the posterior part of the putamen and is more pronounced in the dorsal than in the ventral part of the putamen (Fig. 2). Also, commonly, binding of the DAT tracer is lower at the contralateral than the ipsilateral striatum (i.e., contralateral to the clinically most affected body side) (Fig. 2). The loss of striatal DAT binding in PD can already be detected in the early motor phases of the disease and even at the premotor and preclinical stage (*7–10*). In line with this fact, systematic reviews and metaanalyses showed that DAT imaging is a sensitive and specific imaging tool to detect nigrostriatal degeneration in PD (*5,11*). The diagnostic accuracy of DAT imaging is also high in

Received Dec. 2, 2021; revision accepted Jan. 25, 2022.
For correspondence or reprints, contact Jan Booij (j.booij@amsterdamumc.nl).

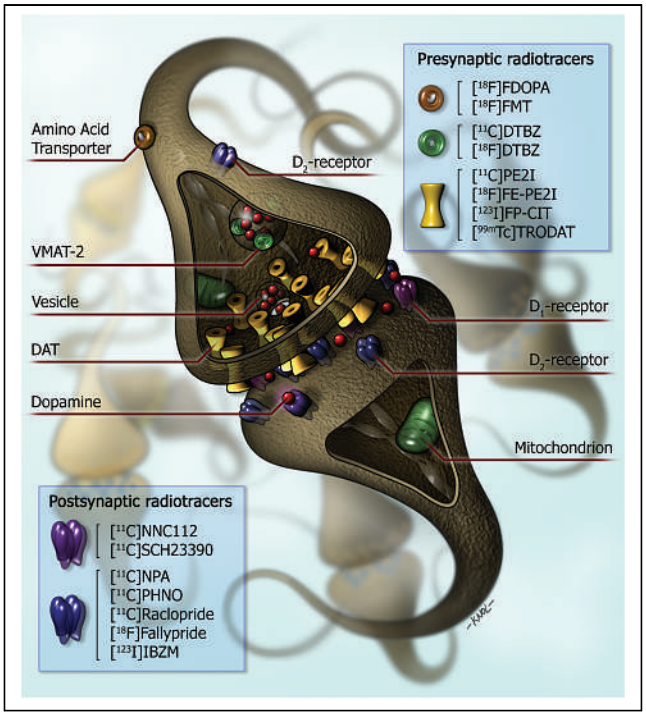


**FIGURE 1.** Simplified diagram of striatal dopaminergic synapse. On presynaptic side, markers for imaging of integrity of dopaminergic neurons in humans are shown. $^{18}$F-FDOPA and $^{18}$F-FMT PET provide measures of structural and biochemical integrity of dopaminergic neurons. $^{11}$C-DTBZ and $^{18}$F-DTBZ are radiopharmaceuticals for vesicular monoaminergic transporter. Substituted (nor)phenyltropanes ($^{11}$C-PE2I, $^{18}$F-FE-PE2I, $^{123}$I-FP-CIT, and $^{99m}$Tc-TRODAT) are frequently used PET and SPECT radioligands for imaging of DAT. On postsynaptic side, $^{11}$C-NNC112 and $^{11}$C-SCH23390 radiopharmaceuticals for dopamine $D_1$ receptor are shown. Dopamine $D_2$ receptors are expressed predominantly on postsynaptic side as compared with presynaptic side of dopaminergic synapse. $^{11}$C-NPA and $^{11}$C-PHNO are agonist radioligands for dopamine $D_{2/3}$ receptors. Commonly used antagonist radioligands for $D_{2/3}$ receptors are substituted benzamides ($^{11}$C-raclopride, $^{11}$C-FLB 457, $^{18}$F-fallypride, and $^{123}$I-IBZM). (Reprinted from (*6*).)

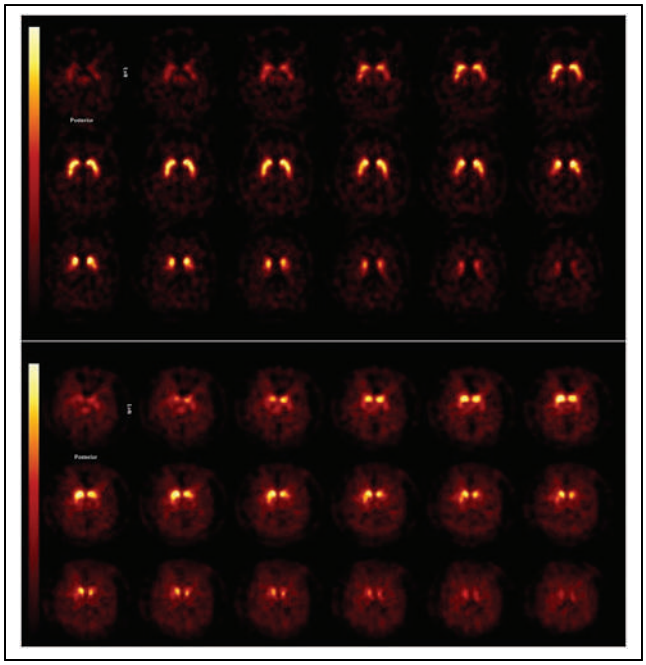

**FIGURE 2.** Transversal $^{123}$I-FP-CIT SPECT images obtained in patient with CUPS without striatal DAT loss (top) and in CUPS patient with striatal DAT loss (bottom). Asymmetric striatal binding can be seen, as well as severe loss of DAT binding, especially in putamen, in subject with dopaminergic deficit. This study was acquired on brain-dedicated SPECT system (InSPira; NeuroLogica).

patients with clinically uncertain parkinsonism (CUPS) and impacts clinical decision making, emphasizing its usefulness in clinical practice (*11–14*). This is of relevance since it can be challenging to diagnose PD clinically, especially in the early motor stage of disease (*15,16*). In addition to visual inspection, a quantitative or semiquantitative approach may increase reader confidence and create more reproducible reporting (*17,18*).

Clinically and neuropathologically, MSA can be divided into MSA with predominantly parkinsonian signs (MSA-P) or MSA with cerebellar features (MSA-C). As in PD, DAT binding is lower in the putamen than in the caudate nucleus (*19*). Some studies have demonstrated lower and more symmetric striatal DAT binding in MSA-P patients than in PD patients. However, the differences are relatively small, and findings consequently are inconsistent and cannot differentiate between these diagnoses at an individual level (*20,21*). Nevertheless, at the individual level there is a clear overlap in binding ratios between MSA-P and PD patients (*20,21*), thus precluding a role for DAT SPECT imaging in differentiating between degenerative parkinsonian diseases in daily clinical practice. DAT PET imaging offers the advantage of a better spatial resolution than DAT SPECT and, subsequently, a subregional analysis of striatal DAT binding. In this regard, Oh et al. showed that DAT PET imaging may indeed be able to differentiate PD from MSA-P at a group level (*22*). However, also in that study, MSA-P patients could not be differentiated completely from PD patients at an individual level.

In MSA-C, on average, striatal DAT binding is higher than in MSA-P and PD (*19*) and can even sometimes be normal (*21,23*). Fortunately, in routine practice, MSA-C patients can frequently be differentiated clinically from PD patients rather easily.

As in MSA-P and PD, DAT imaging is a sensitive means to detect loss of striatal DAT binding in PSP (*21*). Interestingly, a recent systematic review showed that striatal DAT binding in PSP is clearly lower than in PD and MSA-P (*5*). More specifically, DAT binding in PSP was on average approximately 34% and 18% lower than in PD in the caudate nucleus and putamen, respectively. Although studies on PSP, PD, and MSA-P do show an overlap in striatal DAT binding at an individual level, a very low DAT binding, particularly of the caudate nucleus, in an individual parkinsonian patient with a short disease duration (e.g., $<$2 y) might indicate the development of atypical parkinsonism. In corticobasal degeneration, the loss of striatal DAT binding can be very asymmetric, although it can also mimic the typical pattern of PD and can sometimes even be normal (*24*).

In Europe, $^{123}$I-FP-CIT SPECT is also frequently used to differentiate DLB from Alzheimer disease, since it is also approved by the European Medicines Agency for this indication. In Alzheimer disease, striatal DAT is typically not reduced, whereas DLB is characterized by loss of striatal DAT binding (*25,26*). Characteristically, in DLB, DAT binding is lower in the putamen than in the caudate nucleus; however, this posterior–anterior gradient may be more pronounced in PD than in DLB (*27*). Recent metaanalyses on the value of DAT imaging in DLB concluded that DAT imaging has a high diagnostic value for detecting DLB versus Alzheimer disease (sensitivity of 86.5% and specificity of 93%) and is more accurate than the

clinical diagnosis (*28,29*). However, some recent studies suggested that DAT imaging may initially be normal in a relatively rare DLB subtype (~10% of cases), with possibly a different severity or spread of α-synuclein pathology (neocortical predominant subtype) (*30–32*).

Among patients with clinically diagnosed PD who were enrolled in PD trials, around 10%–15% have been found to have normal DAT SPECT findings, also referred to as scans without evidence of dopaminergic deficit (*33*). Interestingly, in most patient with such scans, abnormal DAT SPECT scans do not develop on long-term follow up (*11*). In line with this observation, it is now well accepted that normal DAT SPECT findings exclude PD (*34*).

Although most institutes use $^{123}$I-FP-CIT SPECT to assess striatal DAT binding in routine practice, some institutes also use DAT PET tracers such as $^{18}$F-FE-PE2I (*6*).

*AADC Imaging.* Many studies have assessed striatal AADC activity in neurodegenerative disorders, particularly PD, using $^{18}$F-FDOPA PET (*5*). The pattern loss of striatal AADC mimics the loss of striatal DAT binding in diseases such as PD, MSA-P and PSP (Fig. 3) (*5,19*). Although $^{123}$I-FP-CIT SPECT is used in most hospitals as a diagnostic tool to support or exclude dopaminergic degeneration in routine practice, some institutes do use $^{18}$F-FDOPA PET for this purpose (*35*). Like DAT imaging, $^{18}$F-FDOPA PET is a sensitive technique, but a recent metaanalysis showed that the loss of striatal AADC activity is consistently smaller than that of striatal DAT activity in PD (*5*), possibly because of upregulation of AADC activity in surviving monoaminergic neurons. Consequently, especially in early stages of PD, $^{18}$F-FDOPA PET might be less sensitive to detect the dopaminergic deficit, but this postulate has not been proven yet (*36*).

*VMAT-2 Imaging.* Although the number of studies on VMAT-2 PET imaging in neurodegenerative disorders such as PD is much smaller than the number of studies on DAT imaging and $^{18}$F-FDOPA, the above-mentioned patterns of loss of striatal binding do—generally speaking—match the findings of DAT studies (*37–40*). Also, a 2018 study showed that the diagnostic accuracy of VMAT-2 imaging is high in patients with CUPS (*41*).

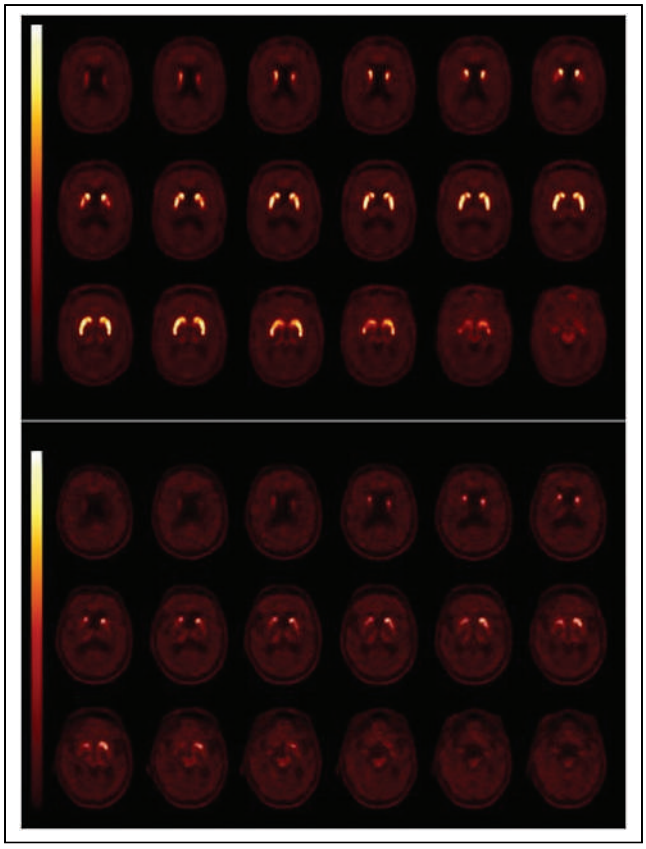

**FIGURE 3.** Transversal planes of $^{18}$F-FDOPA PET images obtained in patient with CUPS without nigrostriatal cell loss (top) and in CUPS patient with nigrostriatal degeneration (bottom). Asymmetric striatal uptake can be seen, as well as severe loss of $^{18}$F-FDOPA uptake, especially in putamen, of subject with nigrostriatal degeneration.

### Imaging of Postsynaptic Striatal Dopaminergic $D_{2/3}$ Receptors

Dopamine receptors can be differentiated in dopamine $D_1$- and $D_2$-like receptors. $D_1$ and $D_5$ receptors belong to the group of $D_1$-like receptors, whereas $D_2$, $D_3$, and $D_4$ receptors belong to the group of $D_2$-like receptors. Importantly, most radiopharmaceuticals used in PET/SPECT studies are nonselective tracers and bind to $D_{1/5}$ or $D_{2/3}$ receptors (Fig. 1) (*6,35*).

Dopamine $D_2$ receptors are expressed presynaptically in dopaminergic neurons. These receptors are called autoreceptors and play a role in the regulation of dopamine release (Fig. 1). Dopamine $D_{2/3}$ receptors, located in the striatum, are expressed predominantly postsynaptically (*6*).

MSA-P and PSP are characterized not only neuropathologically by degeneration of nigrostriatal dopaminergic neurons but also by loss of striatal $D_2$-like receptors (*42,43*). PET and SPECT studies showed loss of postsynaptic dopamine $D_{2/3}$ receptors in PSP and MSA-P (*44*). For many years, radiotracers such as $^{123}$I-IBZM or $^{11}$C-raclopride (Fig. 1) have been used in clinical practice to differentiate PSP/MSA-P from PD. Importantly, a recent metaanalysis of dopamine $D_{2/3}$ receptor studies in PD showed increased $D_{2/3}$ receptor binding (particularly on the contralateral side) in an early state of PD compared with control values (probably reflecting upregulation), but after a disease duration of approximately 4 y, PD patients had lower striatal $D_{2/3}$ receptor binding values than did controls (probably due to downregulation). This metaanalysis also showed that PSP and MSA-P patients indeed had lower striatal dopamine $D_{2/3}$ receptor binding than in PD, but this loss was only around 14% and 22%, respectively (*44*). This result indicates that imaging findings are in line with autopsy findings but also that the intraindividual values for striatal dopamine $D_{2/3}$ receptor binding do show a clear overlap between PD and MSA-P or PSP. Although striatal $D_{2/3}$ receptor binding has been used for many years in routine practice, in light of these diagnostic uncertainties, the diagnostic use of dopamine $D_{2/3}$ receptor imaging is not recommended anymore. Interestingly, the use of $^{18}$F-FDG PET is probably superior to dopamine $D_{2/3}$ receptor binding in differentiating PD from MSA-P or PSP and may be used in clinical practice for diagnostic support (*44–47*).

## IMAGING DOPAMINERGIC NEUROTRANSMISSION IN NEURODEGENERATIVE DISORDERS IN A RESEARCH SETTING

In the past 2 decades, an important research topic, related to imaging of the presynaptic pathway, has been the detection of nigrostriatal dopaminergic degeneration in the preclinical phase of neurodegenerative disorders. This topic is relevant, not only from a scientific point of view (e.g., to examine how many years before the motor signs of PD the nigrostriatal degeneration starts) but also to examine whether molecular imaging is able to detect subjects in

the preclinical phase of neurodegeneration and, if so, to determine the extent of degeneration. This ability is relevant, because when the motor signs of PD start, approximately half of DAT expression in the putamen is already lost (*5*), potentially hampering a potentially successful intervention aimed to slow disease progression. Fortunately, molecular imaging studies showed the ability to detect nigrostriatal degeneration in subjects with rapid-eye-movement sleep behavior disorder (RBD), hyposmia, and late-onset depression, all of which are related to an increased risk for developing a movement disorder characterized by a dopaminergic deficit (*7–10*).

There is consensus among PD researchers that disease-modifying drugs and neuroprotective drugs are likely to be most effective at an early stage of PD, when delaying disease progression will be most effective (*16*). At this stage, a large number of the nigrostriatal dopaminergic neurons are already lost (*5*). Also, at this stage it can be especially difficult to diagnose PD clinically (*15,16*). Since DAT imaging is a sensitive imaging tool to detect PD in an early disease stage (*11*) and there is consensus that subjects having scans without evidence of dopaminergic deficit show a much slower motor deterioration than subjects whose scans do show dopaminergic degeneration (*33,48*), the European Medicines Agency has qualified DAT imaging as an enrichment biomarker for clinical trials targeting early stages of PD (i.e., within 1–2 y of clinical diagnosis) (*16*). Data for the large Parkinson Research Examination of CEP-1347 study and the Parkinson Progression Markers Initiative study were essential to reach this important milestone (*33,49,50*). The first application of DAT imaging as an enrichment biomarker has been published recently (*51*). It is likely that DAT imaging will be increasingly used in clinical trials that evaluate the efficacy of potential drug-modifying drugs in early PD.

The Parkinson Progression Markers Initiative data are publicly available, offering the unique opportunity for all interested research groups to perform analyses on this large dataset. For example, studies using this dataset have been performed to test the relationship between striatal DAT binding and cognitive executive impairment in PD, as well as on the relationship between DAT binding and α-synuclein in the cerebral spinal fluid (*52,53*).

It is now well accepted that neurodegenerative diseases such as PD, MSA, and PSP are not single disease entities (*54,55*). In this regard, it is of interest that molecular imaging studies showed the loss of striatal DAT binding to be more pronounced in the akinetic-rigid subtype than in the tremor-dominant subtype (*56*). Also, striatal DAT binding may be higher in women than men with PD, at symptom onset and throughout the course of PD, as is in line with the observation that women more often present with tremor than do men (*57*). These findings suggest a more benign phenotype in women with PD (*57*). Interestingly, Horsager et al. recently proposed that PD may comprise 2 subtypes: brain-first versus body-first (*58*). They postulated that in the brain-first subtype, degeneration starts in a single hemisphere, leading to asymmetric nigrostriatal degeneration, whereas in the body-first form, the initial enteric pathology will spread through vagal innervation, leading to a more symmetric degeneration. Indeed, in line with their postulation, a recent combined study of $^{18}$F-FDOPA PET and $^{123}$I-FP-CIT SPECT on isolated RBD (which is suggested to be the prototype of the body-first subtype) and on de novo PD patients with and without RBD showed a more symmetric degeneration in isolated RBD subjects than in PD patients without RBD (*59*). Finally, DAT binding is lower in MSA-P than in MSA-C (*60*).

The SPECT tracer $^{123}$I-FP-CIT is not a selective DAT tracer, as this radiotracer also shows a modest affinity for the serotonin transporter. Studies on healthy controls showed that it is actually extrastriatal, but not striatal, $^{123}$I-FP-CIT binding that can be blocked by a selective serotonin reuptake inhibitor (*61,62*). Previous work has shown that analyses of extrastriatal $^{123}$I-FP-CIT binding may contribute to the differential diagnosis of parkinsonian syndromes, in that not only striatal DAT binding is lower in PSP and MSA-P than in PD but also extrastriatal binding may be lower in some brain areas such as the diencephalon (*21,63*). Also, DLB patients may show lower $^{123}$I-FP-CIT binding in the thalamus than do PD patients (*64*).

Selective DAT tracers have been developed successfully (*62,65*); one example is $^{18}$F-FE-PE2I (Fig. 1). As expected, $^{18}$F-FE-PE2I PET studies showed the ability to detect the loss of striatal DAT binding in PD (*66*), and small head-to-head studies with $^{123}$I-FP-CIT SPECT showed that $^{18}$F-FE-PE2I is not inferior to $^{123}$I-FP-CIT in detecting striatal DAT loss (*65,67*). However, it is still unclear whether this PET tracer will replace $^{123}$I-FP-CIT as a diagnostic tool in the future.

SPECT and PET tracers for dopamine $D_{2/3}$ receptors (Fig. 1) can be used not only to assess the baseline in vivo availability of these receptors but also to assess endogenous dopamine release (displacement experiments). Many studies have been performed to assess the baseline availability of these receptors in vivo in PD (*44,68*). Generally speaking, these studies showed an upregulation of striatal dopamine $D_{2/3}$ receptors in early PD, likely a compensating effect on the presynaptic dopaminergic deficit, that faded when the disease duration increased (*44*). Using the dopamine release paradigm, Piccini et al. showed that a methamphetamine challenge was able to induce a detectable dopamine release in the putamen of advanced PD cases, although this release was much lower than in healthy controls (*69*). Also, impulse control disorders are common in PD, and impulse control disorders in PD are associated with relatively increased dopamine in the ventral striatum (*70*). Interestingly, a $^{11}$C-raclopride PET study showed that although striatal dopamine $D_{2/3}$ binding is similar at baseline between PD patients with and those without impulse control disorders, dopamine release after presentation of reward-related visual cues (and after a levodopa challenge) was higher in PD patients with impulse control disorders (*71*). Finally, dopamine release is also assessed to better understand motor fluctuation in PD. Using $^{11}$C-raclopride PET, de la Fuente-Fernández et al. showed that 1 h after a levodopa challenge, the dopamine levels were increased in the putamen of PD patients with motor fluctuations as compared with those without such fluctuations (*72*). All in all, these findings highlight that disturbance of the dopaminergic system in neurodegenerative disorders is sometimes detectable only when the dopaminergic system is challenged.

The number of studies on dopamine $D_{1/5}$ receptors, using tracers such as $^{11}$C-SCH 23390 (Fig. 1), is much lower than the number on $D_{2/3}$ receptors. In general, these studies have not shown a significant difference in striatal $D_1$ receptor binding between PD and controls (*68*).

Different aspect of the dopaminergic system can be assessed directly only by imaging techniques such as PET or SPECT. However, novel MRI sequences are capable to indirectly assess the dopaminergic system in vivo. The so-called neuromelanin-sensitive MRI is capable of visualizing the loss of neuromelanin-containing dopaminergic cells in the substantia nigra (*73,74*). Recently, the correlation between signal intensity on neuromelanin-sensitive MRI and neuromelanin concentration in the substantia nigra was elegantly proven by an autopsy study by Cassidy et al. (*75*). Indeed, many studies have shown that the neuromelanin signal in the substantia nigra is lower in PD, MSA, and PSP than in controls (Fig. 4) (*76,77*). Although this new technique is promising, with potential advantages over DAT imaging (e.g., lower costs, faster acquisitions), large

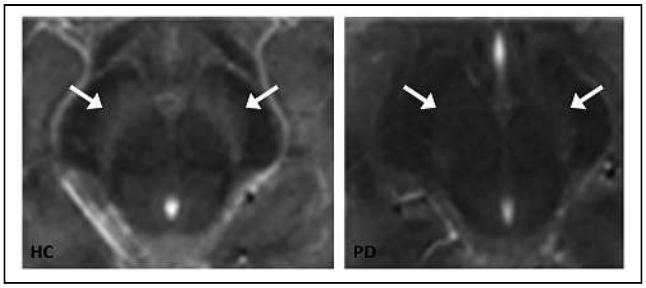


**FIGURE 4.** Transversal images of neuromelanin-sensitive MRI scans of mesencephalon. Substantia nigra is visible as hyperintense area next to cerebral peduncles. Left panel shows example of neuromelanin-sensitive MRI in healthy control, and right panel shows example of patient with PD. Loss of signal can be seen in substantia nigra in PD patient. Arrows point to substantia nigra. (Reprinted from (*74*).)

prospective clinical studies on patients with CUPS, and studies on CUPS patients with autopsy conformation, are needed to assess its diagnostic power in clinical practice.

## CONCLUSION

Imaging of the nigrostriatal pathway has high diagnostic accuracy in detecting nigrostriatal degeneration in common movement disorders characterized by a presynaptic dopaminergic deficit and in patients with CUPS. In clinical practice, imaging of striatal dopamine $D_{2/3}$ receptors no longer plays a major diagnostic role in the differential diagnosis of parkinsonian disorders. Regarding research, imaging of the dopaminergic system plays a major role in, for example, examining nigrostriatal degeneration in preclinical and premotor stages of neurodegenerative disorders or motor complications in the treatment of PD. Finally, neuromelanin-sensitive MRI is a promising new tool to study nigrostriatal degeneration in vivo.

## DISCLOSURE

Jan Booij is consultant at GE Healthcare and received research grants from GE Healthcare (all payments to the institution). Rob de Bie received research grants from GE Healthcare (paid to the institution). No other potential conflict of interest relevant to this article was reported.

## REFERENCES

1. Piggott MA, Marshall EF, Thomas N, et al. Striatal dopaminergic markers in dementia with Lewy bodies, Alzheimer's and Parkinson's diseases: rostrocaudal distribution. *Brain.* 1999;122:1449–1468.
2. Kish SJ, Shannak K, Hornykiewicz O. Uneven pattern of dopamine loss in the striatum of patients with idiopathic Parkinson's disease: pathophysiologic and clinical implications. *N Engl J Med.* 1988;318:876–880.
3. Kraemmer J, Kovacs GG, Perju-Dumbrava L, Pirker S, Traub-Weidinger T, Pirker W. Correlation of striatal dopamine transporter imaging with post mortem substantia nigra cell counts. *Mov Disord.* 2014;29:1767–1773.
4. Walker L, Stefanis L, Attems J. Clinical and neuropathological differences between Parkinson's disease, Parkinson's disease dementia and dementia with Lewy bodies: current issues and future directions. *J Neurochem.* 2019;150:467–474.
5. Kaasinen V, Vahlberg T. Striatal dopamine in Parkinson disease: a meta-analysis of imaging studies. *Ann Neurol.* 2017;82:873–882.
6. Booij J, van Wieringen J-P, van de Giessen E, Knol RJJ, Finnema SJ. PET and SPECT imaging of the central dopamine system in humans. In: Dierckx RAJO, Otte A, de Vries EFJ, van Waarde A, Lammertsma AA, eds. *PET and SPECT of Neurobiological Systems.* Springer; 2021:295–318.
7. Ponsen MM, Stoffers D, Booij J, van Eck-Smit BL, Wolters E, Berendse HW. Idiopathic hyposmia as a preclinical sign of Parkinson's disease. *Ann Neurol.* 2004; 56:173–181.
8. Iranzo A, Tolosa E, Gelpi E, et al. Neurodegenerative disease status and post-mortem pathology in idiopathic rapid-eye-movement sleep behaviour disorder: an observational cohort study. *Lancet Neurol.* 2013;12:443–453.
9. Kazmi H, Walker Z, Booij J, et al. Late onset depression: dopaminergic deficit and clinical features of prodromal Parkinson's disease: a cross-sectional study. *J Neurol Neurosurg Psychiatry.* 2021;92:158–164.
10. Doppler K, Jentschke HM, Schulmeyer L, et al. Dermal phospho-alpha-synuclein deposits confirm REM sleep behaviour disorder as prodromal Parkinson's disease. *Acta Neuropathol (Berl).* 2017;133:535–545.
11. Suwijn SR, van Boheemen CJ, de Haan RJ, Tissingh G, Booij J, de Bie RM. The diagnostic accuracy of dopamine transporter SPECT imaging to detect nigrostriatal cell loss in patients with Parkinson's disease or clinically uncertain parkinsonism: a systematic review. *EJNMMI Res.* 2015;5:12.
12. Marshall VL, Reininger CB, Marquardt M, et al. Parkinson's disease is overdiagnosed clinically at baseline in diagnostically uncertain cases: a 3-year European multicenter study with repeat [$^{123}$I]FP-CIT SPECT. *Mov Disord.* 2009;24:500–508.
13. Isaacson JR, Brillman S, Chhabria N, Isaacson SH. Impact of DaTscan imaging on clinical decision making in clinically uncertain Parkinson's disease. *J Parkinsons Dis.* 2021;11:885–889.
14. Bega D, Kuo PH, Chalkidou A, et al. Clinical utility of DaTscan in patients with suspected Parkinsonian syndrome: a systematic review and meta-analysis. *NPJ Parkinsons Dis.* 2021;7:43.
15. Adler CH, Beach TG, Hentz JG, et al. Low clinical diagnostic accuracy of early vs advanced Parkinson disease: clinicopathologic study. *Neurology.* 2014;83:406–412.
16. Stephenson D, Hill D, Cedarbaum JM, et al. The qualification of an enrichment biomarker for clinical trials targeting early stages of Parkinson's disease. *J Parkinsons Dis.* 2019;9:825.
17. Booij J, Dubroff J, Pryma D, et al. Diagnostic performance of the visual reading of $^{123}$I-ioflupane SPECT images with or without quantification in patients with movement disorders or dementia. *J Nucl Med.* 2017;58:1821–1826.
18. Söderlund TA, Dickson JC, Prvulovich E, et al. Value of semiquantitative analysis for clinical reporting of $^{123}$I-2-β-carbomethoxy-3β-(4-iodophenyl)-*N*-(3-fluoropropyl)nortropane SPECT studies. *J Nucl Med.* 2013;54:714–722.
19. Kaasinen V, Kankare T, Joutsa J, Vahlberg T. Presynaptic striatal dopaminergic function in atypical parkinsonism: a metaanalysis of imaging studies. *J Nucl Med.* 2019;60:1757–1763.
20. Varrone A, Marek KL, Jennings D, Innis RB, Seibyl JP. [$^{123}$I]beta-CIT SPECT imaging demonstrates reduced density of striatal dopamine transporters in Parkinson's disease and multiple system atrophy. *Mov Disord.* 2001;16:1023–1032.
21. Joling M, Vriend C, van den Heuvel OA, et al. Analysis of extrastriatal $^{123}$I-FP-CIT binding contributes to the differential diagnosis of parkinsonian diseases. *J Nucl Med.* 2017;58:1117–1123.
22. Oh M, Kim JS, Kim JY, et al. Subregional patterns of preferential striatal dopamine transporter loss differ in Parkinson disease, progressive supranuclear palsy, and multiple-system atrophy. *J Nucl Med.* 2012;53:399–406.
23. McKinley J, O'Connell M, Farrell M, Lynch T. Normal dopamine transporter imaging does not exclude multiple system atrophy. *Parkinsonism Relat Disord.* 2014;20:933–934.
24. Cilia R, Rossi C, Frosini D, et al. Dopamine transporter SPECT imaging in corticobasal syndrome. *PLoS One.* 2011;6:e18301.
25. McKeith I, O'Brien J, Walker Z, et al. Sensitivity and specificity of dopamine transporter imaging with $^{123}$I-FP-CIT SPECT in dementia with Lewy bodies: a phase III, multicentre study. *Lancet Neurol.* 2007;6:305–313.
26. Shirvan J, Clement N, Ye R, et al. Neuropathologic correlates of amyloid and dopamine transporter imaging in Lewy body disease. *Neurology.* 2019;93:e476–e484.
27. O'Brien JT, Colloby S, Fenwick J, et al. Dopamine transporter loss visualized with FP-CIT SPECT in the differential diagnosis of dementia with Lewy bodies. *Arch Neurol.* 2004;61:919–925.
28. McCleery J, Morgan S, Bradley KM, Noel-Storr AH, Ansorge O, Hyde C. Dopamine transporter imaging for the diagnosis of dementia with Lewy bodies. *Cochrane Database Syst Rev.* 2015;1:CD010633.
29. Papathanasiou ND, Boutsiadis A, Dickson J, Bomanji JB. Diagnostic accuracy of $^{123}$I-FP-CIT (DaTSCAN) in dementia with Lewy bodies: a meta-analysis of published studies. *Parkinsonism Relat Disord.* 2012;18:225–229.
30. van der Zande JJ, Booij J, Scheltens P, Raijmakers PG, Lemstra AW. [$^{123}$]FP-CIT SPECT scans initially rated as normal became abnormal over time in patients with probable dementia with Lewy bodies. *Eur J Nucl Med Mol Imaging.* 2016;43:1060–1066.
31. Colloby SJ, McParland S, O'Brien JT, Attems J. Neuropathological correlates of dopaminergic imaging in Alzheimer's disease and Lewy body dementias. *Brain.* 2012;135:2798–2808.
32. Thomas AJ, Attems J, Colloby SJ, et al. Autopsy validation of $^{123}$I-FP-CIT dopaminergic neuroimaging for the diagnosis of DLB. *Neurology.* 2017;88:276–283.
33. Marek K, Seibyl J, Eberly S, et al. Longitudinal follow-up of SWEDD subjects in the PRECEPT Study. *Neurology.* 2014;82:1791–1797.

34. Postuma RB, Berg D, Stern M, et al. MDS clinical diagnostic criteria for Parkinson's disease. *Mov Disord.* 2015;30:1591–1601.
35. Morbelli S, Esposito G, Arbizu J, et al. EANM practice guideline/SNMMI procedure standard for dopaminergic imaging in Parkinsonian syndromes 1.0. *Eur J Nucl Med Mol Imaging.* 2020;47:1885–1912.
36. Eshuis SA, Jager PL, Maguire RP, Jonkman S, Dierckx RA, Leenders KL. Direct comparison of FP-CIT SPECT and F-DOPA PET in patients with Parkinson's disease and healthy controls. *Eur J Nucl Med Mol Imaging.* 2009;36:454–462.
37. Hsiao IT, Weng YH, Hsieh CJ, et al. Correlation of Parkinson disease severity and $^{18}$F-DTBZ positron emission tomography. *JAMA Neurol.* 2014;71:758–766.
38. Okamura N, Villemagne VL, Drago J, et al. In vivo measurement of vesicular monoamine transporter type 2 density in Parkinson disease with $^{18}$F-AV-133. *J Nucl Med.* 2010;51:223–228.
39. Bohnen NI, Albin RL, Koeppe RA, et al. Positron emission tomography of monoaminergic vesicular binding in aging and Parkinson disease. *J Cereb Blood Flow Metab.* 2006;26:1198–1212.
40. Villemagne VL, Okamura N, Pejoska S, et al. Differential diagnosis in Alzheimer's disease and dementia with Lewy bodies via VMAT2 and amyloid imaging. *Neurodegener Dis.* 2012;10:161–165.
41. Xu SS, Alexander PK, Lie Y, et al. Diagnostic accuracy of imaging brain vesicular monoamine transporter type 2 (VMAT2) in clinically uncertain parkinsonian syndrome (CUPS): a 3-year follow-up study in community patients. *BMJ Open.* 2018; 8:e025533.
42. González AM, Berciano J, Figols J, Pazos A, Pascual J. Loss of dopamine uptake sites and dopamine $D_2$ receptors in striatonigral degeneration. *Brain Res.* 2000; 852:228–232.
43. Pascual J, Berciano J, Grijalba B, et al. Dopamine $D_1$ and $D_2$ receptors in progressive supranuclear palsy: an autoradiographic study. *Ann Neurol.* 1992;32:703–707.
44. Kaasinen V, Vahlberg T, Stoessl AJ, Strafella AP, Antonini A. Dopamine receptors in Parkinson's disease: a meta-analysis of imaging studies. *Mov Disord.* 2021;36: 1781–1791.
45. Hellwig S, Amtage F, Kreft A, et al. [$^{18}$F]FDG-PET is superior to [$^{123}$I]IBZM-SPECT for the differential diagnosis of parkinsonism. *Neurology.* 2012;79:1314–1322.
46. Tang CC, Poston KL, Eckert T, et al. Differential diagnosis of parkinsonism: a metabolic imaging study using pattern analysis. *Lancet Neurol.* 2010;9:149–158.
47. Schindlbeck KA, Gupta DK, Tang CC, et al. Neuropathological correlation supports automated image-based differential diagnosis in parkinsonism. *Eur J Nucl Med Mol Imaging.* 2021;48:3522–3529.
48. Marek K, Jennings D, Seibyl J. Single-photon emission tomography and dopamine transporter imaging in Parkinson's disease. *Adv Neurol.* 2003;91:183–191.
49. The Parkinson Progression Marker Initiative. The Parkinson progression marker initiative (PPMI). *Prog Neurobiol.* 2011;95:629–635.
50. Parkinson Study Group. Dopamine transporter brain imaging to assess the effects of pramipexole vs levodopa on Parkinson disease progression. *JAMA.* 2002;287: 1653–1661.
51. Hutchison RM, Evans KC, Fox T, et al. Evaluating dopamine transporter imaging as an enrichment biomarker in a phase 2 Parkinson's disease trial. *BMC Neurol.* 2021;21:459.
52. Siepel FJ, Brønnick KS, Booij J, et al. Cognitive executive impairment and dopaminergic deficits in de novo Parkinson's disease. *Mov Disord.* 2014;29:1802–1808.
53. Mollenhauer B, Zimmermann J, Sixel-Döring F, et al. Baseline predictors for progression 4 years after Parkinson's disease diagnosis in the De Novo Parkinson Cohort (DeNoPa). *Mov Disord.* 2019;34:67–77.
54. Thenganatt MA, Jankovic J. Parkinson disease subtypes. *JAMA Neurol.* 2014;71: 499–504.
55. Koga S, Dickson DW. Recent advances in neuropathology, biomarkers and therapeutic approach of multiple system atrophy. *J Neurol Neurosurg Psychiatry.* 2018; 89:175–184.
56. Kaasinen V, Kinos M, Joutsa J, Seppänen M, Noponen T. Differences in striatal dopamine transporter density between tremor dominant and non-tremor Parkinson's disease. *Eur J Nucl Med Mol Imaging.* 2014;41:1931–1937.
57. Haaxma CA, Bloem BR, Borm GF, et al. Gender differences in Parkinson's disease. *J Neurol Neurosurg Psychiatry.* 2007;78:819–824.
58. Horsager J, Andersen KB, Knudsen K, et al. Brain-first versus body-first Parkinson's disease: a multimodal imaging case-control study. *Brain.* 2020;143: 3077–3088.
59. Knudsen K, Fedorova TD, Horsager J, et al. Asymmetric dopaminergic dysfunction in brain-first versus body-first Parkinson's disease subtypes. *J Parkinsons Dis.* 2021;11:1677–1687.
60. Bu LL, Liu FT, Jiang CF, et al. Patterns of dopamine transporter imaging in subtypes of multiple system atrophy. *Acta Neurol Scand.* 2018;138:170–176.
61. Booij J, de Jong J, de Bruin K, Knol R, de Win MM, van Eck-Smit BL. Quantification of striatal dopamine transporters with $^{123}$I-FP-CIT SPECT is influenced by the selective serotonin reuptake inhibitor paroxetine: a double-blind, placebo-controlled, crossover study in healthy control subjects. *J Nucl Med.* 2007;48:359–366.
62. Ziebell M, Holm-Hansen S, Thomsen G, et al. Serotonin transporters in dopamine transporter imaging: a head-to-head comparison of dopamine transporter SPECT radioligands $^{123}$I-FP-CIT and $^{123}$I-PE2I. *J Nucl Med.* 2010;51:1885–1891.
63. Nicastro N, Fleury V, Broc N, Burkhard PR, Garibotto V. Extrastriatal $^{123}$I-FP-CIT SPECT impairment in degenerative parkinsonisms. *Parkinsonism Relat Disord.* 2020;78:38–43.
64. Pilotto A, Schiano di Cola F, Premi E, et al. Extrastriatal dopaminergic and serotonergic pathways in Parkinson's disease and in dementia with Lewy bodies: a $^{123}$I-FP-CIT SPECT study. *Eur J Nucl Med Mol Imaging.* 2019;46:1642–1651.
65. Delva A, Van Weehaeghe D, van Aalst J, et al. Quantification and discriminative power of $^{18}$F-FE-PE2I PET in patients with Parkinson's disease. *Eur J Nucl Med Mol Imaging.* 2020;47:1913–1926.
66. Fazio P, Svenningsson P, Forsberg A, et al. Quantitative analysis of $^{18}$F-(*E*)-*N*-(3-iodoprop-2-enyl)-2β-carbofluoroethoxy-3β-(4′-methyl-phenyl) nortropane binding to the dopamine transporter in Parkinson disease. *J Nucl Med.* 2015;56:714–720.
67. Jakobson Mo S, Axelsson J, Jonasson L, et al. Dopamine transporter imaging with [$^{18}$F]FE-PE2I PET and [$^{123}$I]FP-CIT SPECT: a clinical comparison. *EJNMMI Res.* 2018;8:100.
68. Niccolini F, Su P, Politis M. Dopamine receptor mapping with PET imaging in Parkinson's disease. *J Neurol.* 2014;261:2251–2263.
69. Piccini P, Pavese N, Brooks DJ. Endogenous dopamine release after pharmacological challenges in Parkinson's disease. *Ann Neurol.* 2003;53:647–653.
70. Vriend C, Pattij T, van der Werf YD, et al. Depression and impulse control disorders in Parkinson's disease: two sides of the same coin? *Neurosci Biobehav Rev.* 2014;38:60–71.
71. O'Sullivan SS, Wu K, Politis M, et al. Cue-induced striatal dopamine release in Parkinson's disease-associated impulsive-compulsive behaviours. *Brain.* 2011;134: 969–978.
72. de la Fuente-Fernández R, Ruth TJ, Sossi V, Schulzer M, Calne DB, Stoessl AJ. Expectation and dopamine release: mechanism of the placebo effect in Parkinson's disease. *Science.* 2001;293:1164–1166.
73. Sasaki M, Shibata E, Tohyama K, et al. Neuromelanin magnetic resonance imaging of locus ceruleus and substantia nigra in Parkinson's disease. *Neuroreport.* 2006; 17:1215–1218.
74. Reneman L, van der Pluijm M, Schrantee A, van de Giessen E. Imaging of the dopamine system with focus on pharmacological MRI and neuromelanin imaging. *Eur J Radiol.* 2021;140:109752.
75. Cassidy CM, Zucca FA, Girgis RR, et al. Neuromelanin-sensitive MRI as a noninvasive proxy measure of dopamine function in the human brain. *Proc Natl Acad Sci USA.* 2019;116:5108–5117.
76. Cho SJ, Bae YJ, Kim JM, et al. Diagnostic performance of neuromelanin-sensitive magnetic resonance imaging for patients with Parkinson's disease and factor analysis for its heterogeneity: a systematic review and meta-analysis. *Eur Radiol.* 2021; 31:1268–1280.
77. Matsuura K, Ii Y, Maeda M, et al. Neuromelanin-sensitive magnetic resonance imaging in disease differentiation for parkinsonism or neurodegenerative disease affecting the basal ganglia. *Parkinsonism Relat Disord.* 2021;87:75–81.

# PET Imaging of Cholinergic Neurotransmission in Neurodegenerative Disorders

Solveig Tiepolt*[1], Philipp M. Meyer*[1], Marianne Patt[1], Winnie Deuther-Conrad[2], Swen Hesse[1], Henryk Barthel[1], and Osama Sabri[1]

[1]*Department of Nuclear Medicine, University of Leipzig, Leipzig, Germany; and* [2]*Helmholtz-Zentrum Dresden-Rossendorf, Research Site Leipzig, Leipzig, Germany*

As a neuromodulator, the neurotransmitter acetylcholine plays an important role in cognitive, mood, locomotor, sleep/wake, and olfactory functions. In the pathophysiology of most neurodegenerative diseases, such as Alzheimer disease (AD) or Lewy body disorder (LBD), cholinergic receptors, transporters, or enzymes are involved and relevant as imaging targets. The aim of this review is to summarize current knowledge on PET imaging of cholinergic neurotransmission in neurodegenerative diseases. For PET imaging of presynaptic vesicular acetylcholine transporters (VAChT), (−)-$^{18}$F-fluoroethoxybenzovesamicol ($^{18}$F-FEOBV) was the first PET ligand that could be successfully translated to clinical application. Since then, the number of $^{18}$F-FEOBV PET investigations on patients with AD or LBD has grown rapidly and provided novel, important findings concerning the pathophysiology of AD and LBD. Regarding the α4β2 nicotinic acetylcholine receptors (nAChRs), various second-generation PET ligands, such as $^{18}$F-nifene, $^{18}$F-AZAN, $^{18}$F-XTRA, (−)-$^{18}$F-flubatine, and (+)-$^{18}$F-flubatine, were developed and successfully translated to human application. In neurodegenerative diseases such as AD and LBD, PET imaging of α4β2 nAChRs is of special value for monitoring disease progression and drugs directed to α4β2 nAChRs. For PET of α7 nAChR, $^{18}$F-ASEM and $^{11}$C-MeQAA were successfully applied in mild cognitive impairment and AD, respectively. The highest potential for α7 nAChR PET is seen in staging, in evaluating disease progression, and in therapy monitoring. PET of selective muscarinic acetylcholine receptors (mAChRs) is still in an early stage, as the development of subtype-selective radioligands is complicated. Promising radioligands to image mAChR subtypes M1 ($^{11}$C-LSN3172176), M2 ($^{18}$F-FP-TZTP), and M4 ($^{11}$C-MK-6884) were developed and successfully translated to humans. PET imaging of mAChRs is relevant for the assessment and monitoring of therapies in AD and LBD. PET of acetylcholine esterase activity has been investigated since the 1990s. Many PET studies with $^{11}$C-PMP and $^{11}$C-MP4A demonstrated cortical cholinergic dysfunction in dementia associated with AD and LBD. Recent studies indicated a solid relationship between subcortical and cortical cholinergic dysfunction and noncognitive dysfunctions such as balance and gait in LBD. Taken together, PET of distinct components of cholinergic neurotransmission is of great interest for diagnosis, disease monitoring, and therapy monitoring and to gain insight into the pathophysiology of different neurodegenerative disorders.

**Key Words:** neurology; PET; acetylcholine; Alzheimer disease; Lewy body disorder; neurodegenerative disorder; PET

**J Nucl Med 2022; 63:33S–44S**
DOI: 10.2967/jnumed.121.263198

Essential processes such as neuroplasticity, neuronal synchronization, and connectivity are modulated by the neurotransmitter acetylcholine, which is accordingly critically involved in and highly relevant to cognitive, mood, locomotor, sleep/wake, and olfactory functions (*1,2*). The cholinergic system in the central nervous system (CNS) consists of 2 major projections: the first is from the basal forebrain (Ch1 to Ch4 cholinergic groups) to the cortex, amygdala, hippocampus, and olfactory bulb, and the second is from the brain stem (Ch5 and Ch6 cholinergic groups) to the thalamus and other brain stem nuclei. There are also intrinsic striatal, cortical, and cerebellar cholinergic neurons (*1,3,4*).

In the synapse of the presynaptic cholinergic neuron, acetylcholine is synthetized by the choline acetyltransferase from choline and acetyl coenzyme A. Acetylcholine is transported via the vesicular acetylcholine transporter (VAChT) into the presynaptic vesicles of the cholinergic nerve terminals, where it is stored for future release. Released acetylcholine binds to and activates nicotinic and muscarinic acetylcholine receptors (nAChRs and mAChRs). Acetylcholine esterase (AChE) rapidly clears the synaptic cleft of acetylcholine by enzymatic hydrolysis to acetate and choline. Choline undergoes a recycling reuptake by the presynaptic high-affinity choline transporter (Fig. 1) (*2–4*).

In 1982, Bartus et al. published the cholinergic hypothesis of Alzheimer disease (AD), which described the loss of memory as a result of cortical and basal forebrain cholinergic dysfunction (*5*). This hypothesis was convincingly confirmed because anticholinergic drugs could be proved to induce cognitive impairment (*3,6*) whereas AChE inhibitors could be proved to induce the opposite (*3*).

The cholinergic pathophysiology of the 2 most prevalent neurodegenerative disorders—AD and LBD spectrum (the latter including Parkinson disease [PD], PD with dementia [PDD], and Lewy body dementia [DLB])—differs between each other. AD shows cholinergic dysfunction and loss of neurons in the basal forebrain, likely in close relationship to the relevant loss of cholinergic cortical axons from tau and amyloid proteinopathy. However, cholinergic striatal interneurons and cholinergic innervation of the thalamus receiving innervation from the brain stem are preserved (*4*). In contrast, LBD, likely in close association with α-synucleinopathy, shows cholinergic dysfunction and degeneration not only in the basal forebrain but also in the brain stem. In LBD, this more complex subcortical and cortical neuropathology and cholinergic

Received Mar. 23, 2022; revision accepted May 6, 2022.
For correspondence or reprints, contact Osama Sabri (osama.sabri@medizin.uni-leipzig.de).
*Contributed equally to this work.

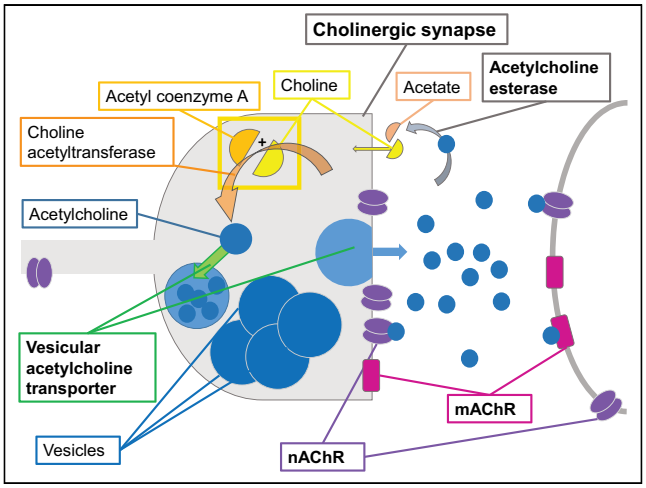


**FIGURE 1.** Cholinergic synapse: physiologic processes. In synapse of presynaptic cholinergic neuron, acetylcholine is synthetized by choline acetyltransferase from choline and acetyl coenzyme A. It is then stored in vesicles in very high concentrations. This storage process, as well as release of acetylcholine in synaptic cleft, is mediated by VAChT. Released acetylcholine binds to and activates nAChRs and mAChRs and, in case of postsynaptic receptors, transports signal to next neuron. AChE rapidly clears synaptic cleft of acetylcholine. This enzyme hydrolyzes acetylcholine to acetate and choline. The latter undergoes recycling reuptake into the presynaptic nerve terminal.

dysfunction are associated with and most likely explain the wide spectrum of motor and various nonmotor symptoms in LBD (*3,4*). Novel neuropathologic and cholinergic PET findings in the brain and body of LBD patients, especially the gut—present also in early or prodromal PD—led to a paradigm shift in our understanding of the pathophysiology of LBD and to the definition of body-first and brain-first LBD subtypes (*7,8*).

The possibility of obtaining in vivo information about the integrity of cholinergic transmission by means of PET imaging is of major interest in studying the pathophysiology of various neurodegenerative disorders such as AD and LBD and has major relevance in cholinergic drug development. This option refers to all the different compartments of this complex neurotransmitter system. The aim of this review is to summarize the current knowledge on PET imaging of cholinergic transmission, including imaging of VAChT, nAChRs, mAChRs, and AChE in neurodegenerative diseases.

## VAChT

### Structure and Distribution of VAChT

VAChT is an approximately 500-amino-acid polypeptide uniquely present in cholinergic nerve terminals of the central and peripheral nervous system and corresponding closely to choline acetyltransferase (*9*).

### Radioligands for Imaging VAChT

Many VAChT PET ligands have been generated (*9*). Vesamicol was used as the lead compound. The development of vesamicol derivatives showing high affinity to VAChT and high selectivity over off-targets such as σ-receptors was challenging. Several vesamicol-, trozamicol-, and benzovesamicol-based PET ligands, as well as morpholinovesamicols and other vesamicol analogs, were developed and tested preclinically (*9*). Only the PET ligand (−)-$^{18}$F-fluoroethoxybenzovesamicol ($^{18}$F-FEOBV) (Table 1; Fig. 2A) and the SPECT tracer (−)-5-$^{123}$I-iodobenzovesamicol ($^{123}$I-IBVM)

**TABLE 1**
Most Relevant VAChT PET (SPECT) Radioligands

| Tracer name | Formula |
|---|---|
| $^{123}$I-IBVM | (−)-5-$^{123}$I-iodobenzovesamicol |
| (−)-$^{18}$F-FEOBV | (2*R*,3*R*)-5-$^{18}$F-fluoroethoxy-benzovesamicol |
| $^{18}$F-VAT | (−)-(1-(8-(2-$^{18}$F-fluoroethoxy)-3-hydroxy-1,2,3,4-tetrahydronaphthalen-2-yl)-piperidin-4-yl)(4-fluorophenyl) methanone |

(Table 1; Fig. 2A) were successfully transferred to clinical application (*10,11*). According to validation in preclinical studies and human postmortem brain (*12–14*), $^{18}$F-FEOBV showed favorable characteristics for in vivo assessment of VAChT in healthy controls (HCs) (*15*). The pattern of distribution of the radioligand corresponded to the known heterogeneous organization of cholinergic projections in the human brain with the following rank order: striatum > thalamus > cerebellar vermis > amygdala–hippocampus complex > brain stem > cerebral cortex (*15,16*). Aging was associated with a decline in VAChT binding by 4% per decade within the striatum and approximately 3% per decade within the thalamus, anterior cingulate cortex, and premotor cortex (*16*). In addition to full kinetic modeling to calculate the distribution volume or binding potential of $^{18}$F-FEOBV, simplified approaches to VAChT quantification were validated using delayed static PET scans and reference regions such as the cerebellar cortex or white matter (*15,17,18*).

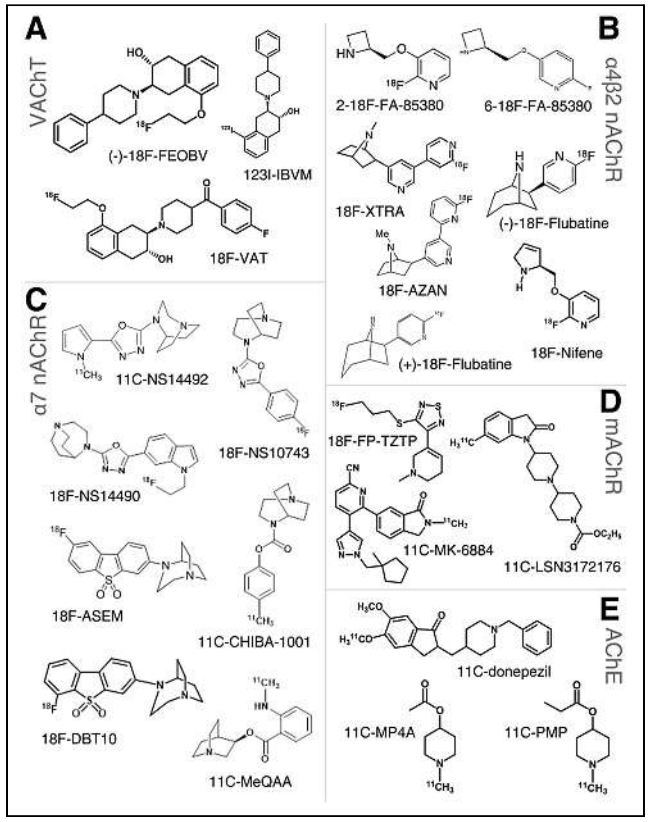


**FIGURE 2.** Names and structural chemical formulas of most relevant radioligands for distinct cholinergic targets.

$^{18}$F-VAT is a benzovesamicol-based VAChT PET ligand (Table 1; Fig. 2A). Recent in vitro, preclinical in vivo, and postmortem human brain findings were promising (*19,20*). A $^{18}$F-VAT PET trial in humans is under way.

### VAChT PET Imaging Results in Neurodegeneration

The first in vivo VAChT imaging study of the brain in AD, PD, PDD, and HC was performed by Kuhl et al. using $^{123}$I-IBVM SPECT. Compared with HCs, a widespread decrease in VAChT binding within the neocortex and hippocampus has been detected in PDD and early-onset AD (EOAD) (*21*). In contrast, in late-onset AD (LOAD), the VAChT decline was restricted to the temporal cortex and was less pronounced, indicating a distinct vulnerability of the basal forebrain in EOAD and LOAD (*21,22*). Of interest, in mild to moderate AD, as assessed by the clinical dementia rating scale, cortical VAChT binding was more declined in EOAD than in LOAD. In severe AD, VAChT binding was decreased to a similar degree in EOAD and LOAD. In Lewy body dementia (DLB), compared with HCs, $^{123}$I-IBVM SPECT showed a decrease in VAChT in Ch4 and pedunculopontine thalamic (Ch5) projections and within striatal interneurons. In contrast, septohippocampal cholinergic projections were spared (*23*). Thus, the pattern of cortical and subcortical cholinergic dysfunction in DLB differs from that in AD.

By $^{18}$F-FEOBV PET, lower VAChT binding in cholinergic terminals within the frontotemporoparietal and cingulate cortices has been detected in AD in comparison with HCs, as is presumed to reflect a characteristic caudorostral dysfunction of the nucleus basalis of Meynert (Ch4; Figs. 3A–3D) (*17,22*). Reduced cortical VAChT in AD was significantly associated with global cognitive dysfunction. In the same AD patients, $^{18}$F-FEOBV PET was more sensitive in detecting AD-related changes than was $^{18}$F-FDG PET or β-amyloid PET (*17*). In DLB, there was a widespread decrease in VAChT binding in the frontotemporoparietal and occipital cortices, hippocampus, amygdala, and thalamus (−17% to −21%; Fig. 3E) (*18*). In PD, the relationship between disturbances in VAChT binding and motor symptoms such as falls and freezing of gait as part of the postural instability gait disturbance subtype were investigated (*22*). Thalamic VAChT decrements, especially decrements in the right visual thalamus, were related to a history of falling. Freezing of gait correlated with lower VAChT in striatal interneurons and limbic cortices (*24*). In PD without dementia, dysfunction of memory, executive function, and attention correlated regionally with lower VAChT availability within the cingulate and insular cortices and thalamus (*25*). Sanchez-Catasus et al. determined striatal disbalance between acetylcholinergic and dopaminergic systems in mild to moderate PD using $^{18}$F-FEOBV PET and other techniques (*26*). In cognitively normal PD patients, higher VAChT binding in the hippocampus, associated with cognitive measures, and lower VAChT binding in the posterior cortical regions were reported. Higher hippocampal VAChT binding in cognitively normal PD patients suggests a novel compensatory role for VAChT in PD (*27*). However, another potential cause for higher VAChT binding could be inflammatory changes, as demonstrated by $^{18}$F-FEOBV PET in acute peripheral inflammation. More investigation, accounting for inflammatory changes, is required for VAChT PET studies of potential compensatory neuronal changes in neurodegenerative disorders (*28*).

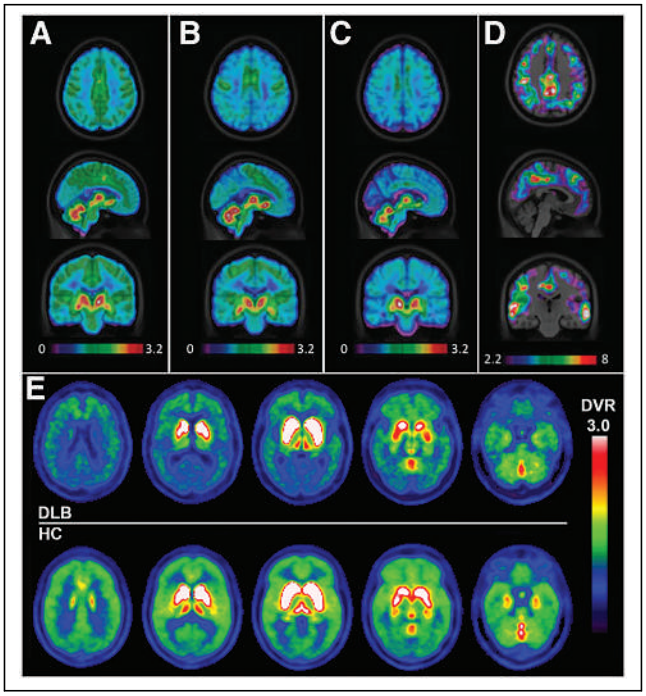


**FIGURE 3.** (A–D) $^{18}$F-FEOBV VAChT binding (SUV ratio) using PET in 1 representative HC (A), mild-AD patient (B), and severe-AD patient (C) showing lower cortical VAChT binding depending on severity of AD. Statistical parametric analysis indicates significant clusters of lower cortical VAChT binding in AD compared with HC (D). (Modified with permission of (*17*).) (E) Another $^{18}$F-FEOBV PET study demonstrating lower subcortical and cortical VAChT binding (SUV ratio) in 1 representative patient with LBD (top row) and 1 HC (bottom row). DVR = distribution volume ratio. (Reprinted with permission of (*18*).)

## α4β2 nAChR

### Structure, Distribution, and Function of α4β2 nAChRs

All nAChRs are pentameric. The heteromeric α4β2 subtype consists of α- and β-subunits, which form an ion channel (*29*). α4β2 nAChRs are ubiquitous in the human brain and are preferentially located at preterminal and presynaptic sites, acting as modulators of different neurotransmitters (*29*). The highest density of α4β2 nAChRs has been detected in the nucleus basalis of Meynert and the thalamus; density is moderate in the putamen and cerebellum and low in cortical regions (*30–32*). α4β2 nAChRs play an important role in higher cognitive processes such as learning and memory and are involved in addiction and depression (*31,33*). Postmortem studies reported a reduced α4β2 nAChR density in AD and LBD (*34–41*).

### PET Radioligands for Imaging α4β2 nAChRs

Because of space restrictions, we will focus on the radiotracers most often used in preclinical and clinical research. Their chemical structures are summarized in Table 2 and Figure 2B. $^{11}$C-nicotine was the first radiotracer used to image α4β2 nAChRs in vivo. Because the distribution of $^{11}$C-nicotine was influenced by blood flow and blood–brain barrier transport, the estimated receptor densities were not reliable. This problem was overcome by the 3-pyridylether derivatives 2-$^{18}$F-FA-85380 and 6-$^{18}$F-FA-85380. However, these PET tracers suffer from slow kinetics. Nonetheless, both radioligands have been applied to investigate α4β2 nAChRs in vivo for many years. The next generation of PET radiotracers targeting α4β2 nAChRs, developed after the turn of the millennium, showed faster brain kinetics. This next generation contains 3 chemical classes. There are the advanced 3-pyridylether derivatives, such as $^{18}$F-nifene; the derivatives of epibatidine,

**TABLE 2**
Most Relevant α4β2 nAChR PET Tracers

| Tracer name | Formula |
|---|---|
| 2-$^{18}$F-FA-85380 | 2-$^{18}$F-fluoro-3-(2(*S*)-azetidinylmethoxy)pyridine |
| 6-$^{18}$F-FA-85380 | 6-$^{18}$F-fluoro-3-(2(*S*)-azetidinylmethoxy)pyridine |
| $^{18}$F-AZAN | (1*R*,2*R*,4*S*)-2-[5-(6-$^{18}$F-fluoranylpyridin-2-yl)pyridin-3-yl]-7-methyl-7-azabicyclo[2.2.1]heptane |
| $^{18}$F-XTRA | 2-[5-[2-$^{18}$F-fluoropyridin-4-yl]pyridin-3-yl]-7-methyl-7-azabicyclo[2.2.1]heptane |
| (−)-$^{18}$F-flubatine | (−)-(1*R*,5*S*,6*S*)-6-(6-$^{18}$F-fluoropyridine-3-yl)-8-aza-bicyclo[3.2.1]octane |
| (+)-$^{18}$F-flubatine | (+)-(1*S*,5*R*,6*R*)-6-(6-$^{18}$F-fluoro-pyridine-3-yl)-8-aza-bicyclo[3.2.1]octane |
| $^{18}$F-nifene | 3-[[(2*S*)-2,5-dihydro-1*H*-pyrrol-2-yl]methoxy]-2-$^{18}$F-fluoranylpyridine |

such as $^{18}$F-AZAN and $^{18}$F-XTRA; and the derivatives of homoepibatidine, the enantiomers (−)-$^{18}$F-flubatine and (+)-$^{18}$F-flubatine. A scanning time of 40 min is sufficient for $^{18}$F-nifene (*42*), whereas the other 4 radioligands require scans of at least 90 min (*43–47*). All radiotracers demonstrated a high affinity to their target structure (*42–47*). However, a difference can be observed considering the metabolization of these PET radioligands. The homoepibatidine derivatives show only a low level of metabolization in the case of (−)-$^{18}$F-flubatine and a negligible level in the case of (+)-$^{18}$F-flubatine (*44,45,47*). In contrast, the epibatidine derivatives $^{18}$F-AZAN and $^{18}$F-XTRA suffer from severe metabolization (*43,46*). Whether and to what amount $^{18}$F-nifene is metabolized in humans has not been published, to the best of our knowledge.

For noninvasive quantitative modeling of α4β2 nAChR binding and to normalize for interindividual variability in α4β2 nAChR binding for between-group analyses, it is desired to have a receptor-free reference region. The human brain is most likely not fully free of α4β2 nAChRs. 2-$^{18}$F-FA-85380 PET studies revealed that α4β2 nAChR binding (distribution volume) in the corpus callosum is very low in nonsmokers but substantially higher in smokers (*48*). A 2-$^{18}$F-FA-85380 PET study was performed on smokers. Cigarette smoking to receptor satiety revealed that nicotinic receptor displacement in the corpus callosum was relatively low, at approximately 16% (*49*), and in a small (−)-$^{18}$F-flubatine PET study ($n$ = 3) it was approximately 21% (*50*). This led to the assumption that α4β2 nAChR in the corpus callosum is negligible in nonsmokers but not in smokers. It was proposed that the distribution volume in the corpus callosum of nonsmokers may be similar to nondisplaceable binding and that the corpus callosum would be appropriate for use as a reference region (*48*). Thus, in 2-$^{18}$F-FA85380 or $^{18}$F-flubatine PET studies, the corpus callosum was used as a reference region in nonsmoking patients with neurodegenerative disorders (*45,51,52*).

#### α4β2 nAChR Imaging Results in Neurodegeneration

Most PET imaging studies of α4β2 nAChRs in AD have been performed using 2-$^{18}$F-FA85380 PET. Clinical studies with the more recently developed second-generation α4β2 nAChR PET radioligands are limited to phase 0 and phase I data on (−)-$^{18}$F-flubatine and (+)-$^{18}$F-flubatine. Regarding AD, the conducted PET studies could confirm a reduction in cerebral α4β2 nAChRs in regions typically affected by AD, such as the temporal, mesiotemporal, frontal, prefrontal, and parietal cortices, as well as in subcortical areas such as the caudate nucleus and thalamus (*45,47,51–54*).

Different study groups also investigated the correlations between cognitive performance and availability of cerebral α4β2 nAChRs in AD. Two 2-$^{18}$F-FA-85380 studies showed significant correlations of the caudate nucleus and the frontal, temporal, anterior, and posterior cingulate cortices with global cognitive scores such as the mini mental state examination, DemTect, or clock-drawing test scores (*51,52*). Another 2-$^{18}$F-FA-85380 PET study reported a moderate to strong correlation between the frontal assessment battery and the mesiotemporal cortex and basal forebrain (*53*).

In the (−)-$^{18}$F-flubatine PET study on mild AD dementia, using volume-of-interest–based regression analysis, executive function showed an association with α4β2 nAChR availability in the frontal and parietal brain regions, and episodic memory showed an association with availability in the frontal, mesiotemporal, and parietal cortices. More interestingly, in AD, explorative voxel-based regression analysis revealed a highly significant association between memory and α4β2 nAChR availability in the basal forebrain (Fig. 4) (*45*).

In PD and DLB, in vivo examination and investigation of α4β2 nAChRs were performed mainly with 5-$^{123}$I-IA85380 SPECT and 2-$^{18}$F-FA-85380 PET. These studies consisted of small to moderately sized groups and showed reduced α4β2 nAChRs in the thalamus, caudate nucleus, substantia nigra, and different cortical regions in DLB and PD patients (*55–58*).

Using 2-$^{18}$F-FA-85380 PET in PD patients with an additional depressive syndrome or a mild cognitive impairment, the alterations were more pronounced (*58*). Using 5-$^{123}$I-IA85380 SPECT, the association between cognitive performance and α4β2 nAChR availability was confirmed by a further study on 25 nondemented patients with PD (*59*). Two 5-$^{123}$I-IA85380 SPECT studies reported that increased α4β2 nAChRs in the occipital cortex were observed in DLB with visual hallucinations (*56*) and in early PD in brain regions of the motor and limbic basal ganglia circuits (*60*).

### α7 α4β2 nAChR

#### Structure, Distribution, and Function of α7 nAChRs

α7 nAChRs represent the second most abundant nAChR subtype in the human brain. They are expressed by many brain cell types, such as neurons, astrocytes, microglia, oligodendrocyte precursor cells, and endothelial cells. As such, α7 nAChRs are widely distributed throughout the human brain, with density being highest in the thalamus, hippocampus, and basal forebrain (*61*). Regarding its nonneuronal expression, α7 nAChR acts as an essential regulator of inflammation (*62*).

The affinity of α7 nAChR to agonists such as nicotine or acetylcholine is low, whereas that to the antagonist α-bungarotoxin is high. A special feature of α7 nAChR is its high permeability for

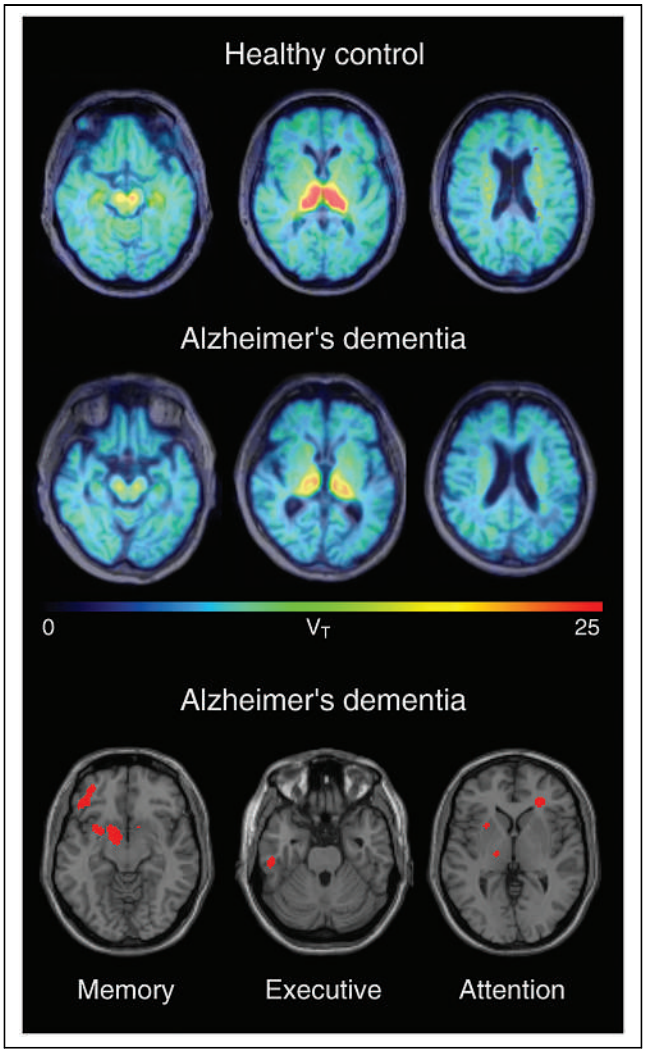


**FIGURE 4.** (−)-$^{18}$F-flubatine PET showed lower cortical α4β2 nAChR (α4β2 nAChR) availability (distribution volume [$V_T$] parametric images) in mild AD (middle row) than in HCs (top row). In AD, there were relevant associations between networks of disturbed subcortical and cortical α4β2 nAChR binding and dysfunction of episodic memory, executive/working memory, and attention (bottom row). (Modified from (*45*).)

$Ca^{2+}$ ions (*63*), rendering it a calcium channel. Via its influence on the $Ca^{2+}$ balance, α7 nAChRs influence different neurotransmitters, receptors, cell survival, brain plasticity and gene expression. Thus, under physiologic conditions, the action of α7 nAChRs influences memory, development, attention, and other processes.

### α7 nAChRs in Neurodegeneration

In several neurodegenerative diseases, this α7 nAChR action is altered. In the late-stage human AD brain, for instance, α7 nAChR protein levels are reduced in certain areas (*64*). In contrast, increased levels of α7 nAChR protein were reported in early AD stages (*65*). Of note, β-amyloid has picomolar—that is, very high—affinity to α7 nAChR (*66*). In advanced AD, the larger amyloid burden seems to block α7 nAChRs, possibly promoting, at least in part, cognitive breakdown (*67*). It is also known that binding of soluble β-amyloid to α7 nAChRs can promote intraneuronal amyloid accumulation and tau phosphorylation (*68*). Altogether, there is a direct, although complex, relationship between neurodegeneration, neuroinflammation, and α7 nAChR expression.

### PET Radioligands for Imaging α7 nAChRs

Here, we will give an overview of the most interesting α7 nAChR PET tracers that have been developed over the years. Details on these tracers are provided in Table 3 and Figure 2C.

The search for suitable α7 nAChR PET tracers faces some challenges: the density of these receptors in the human brain is lower than that of the abundant α4β2 nAChRs. Also, there is high structural similarity between α7 nAChR and another member of the ligand-gated ion channel superfamily, the 5-hydroxytryptamine-3 receptor.

Most α7 nAChR PET tracers of interest are diazabicyclononane derivatives. Of this group, $^{11}$C-CHIBA-1001 was the first entering human application (*69,70*). However, subsequent research reported limited binding affinity, limited binding selectivity, and inadequate brain distribution for this tracer (*71*). Also, a series of diazabicyclononane derivatives possessing sufficient brain uptake was developed ($^{11}$C-NS14492, $^{18}$F-NS10743, and $^{18}$F-NS14490). However, observation of specific brain binding in preclinical research was limited (*72*). Other candidates are the dibenzothiophene sulfone derivative $^{18}$F-ASEM and its paraisomer $^{18}$F-DBT10. Both tracers yielded satisfying and similar brain kinetics in nonhuman primates, as well as significant specific binding in the human brain (*71*). For $^{18}$F-ASEM applied to HCs of a considerable age range, regional $^{18}$F-ASEM binding correlated positively with age (*73*).

As an alternative α7 nAChR PET tracer, the azabicyclooctylester $^{11}$C-MeQAA was developed. Although specific in vitro binding was demonstrated for this tracer, in vivo selectivity was limited by

**TABLE 3**
Most Relevant α7 nAChR PET Tracers

| Tracer name | Formula |
|---|---|
| $^{11}$C-CHIBA-1001 | 4-$^{11}$C-methylphenyl)-1,4-diazabicyclo[3.2.2]nonane-4-carboxylate |
| $^{11}$C-NS14492 | (2-(1,4-diazabicyclo[3.2.2]nonan-4-yl)-5-(1-$^{11}$C-methyl-1*H*-pyrrol-2-yl)-1,3,4-oxadiazole) |
| $^{18}$F-NS10743 | 2-(1,4-diazabicyclo[3.2.2]nonan-4-yl)-5-(4-$^{18}$F-fluorophenyl)-1,3,4-oxadiazole |
| $^{18}$F-NS14490 | (1*R*,5*S*)-3-(6-(1-(2-$^{18}$F-fluoroethyl)indol-5-yl)pyridazin-3-yl)-9-methyl-3,9-diazabicyclo[3.3.1]nonane |
| $^{18}$F-DBT10 | 7-(1,4-diazabicyclo[3.2.2]nonan-4-yl)-2-$^{18}$F-fluorodibenzo[*b,d*]thiophene 5,5-dioxide |
| $^{18}$F-ASEM | 7-(1,4-diazabicyclo[3.2.2]nonan-4-yl)-4-$^{18}$F-fluorodibenzo[*b,d*]thiophene 5,5-dioxide |
| $^{11}$C-MeQAA | (1*S*,3*R*,4*S*)-quinuclidin-3-yl 3-($^{11}$C-methylamino)benzoate |

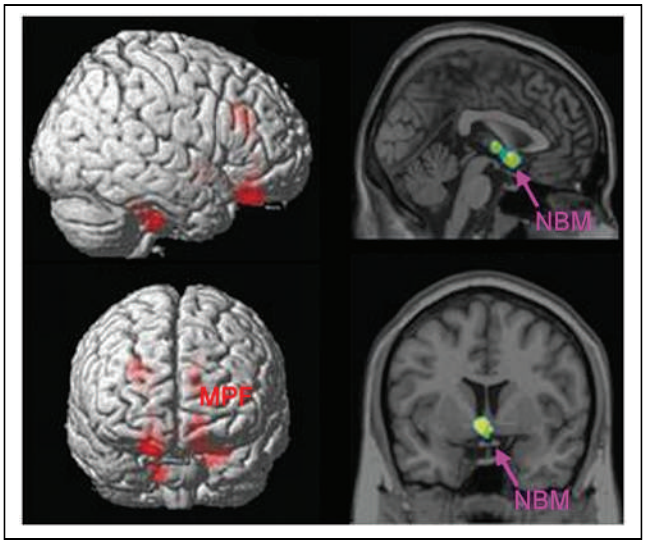


**FIGURE 5.** Statistical parametric mapping–based correlations between $^{11}$C-MeQAA α7 nAChR binding as assessed by PET imaging and frontal-assessment-battery scores in patients with AD. MPF = medial prefrontal cortex; NBM = nucleus basalis of Meynert. (Reprinted with permission of (*76*).)

concomitant off-target binding to 5-hydroxytryptamine-3 receptors (*74,75*).

#### α7 nAChR Imaging Results in Neurodegeneration

So far, 2 α7 nAChR PET imaging studies in human neurodegenerative disorders have been published: Nakaizumi et al. (2018) applied $^{11}$C-MeQAA α7 nAChR and $^{11}$C-Pittsburgh compound B amyloid PET imaging to 20 patients with clinically diagnosed AD and to 10 age-matched HCs (*76*). In this study, the specific $^{11}$C-MeQAA binding was significantly lower in AD than in HCs in the temporal and prefrontal brain areas. Further, there was a correlation between the $^{11}$C-MeQAA uptake in the basal cholinergic forebrain region and frontal cognition deficits in AD (Fig. 5) (*76*). In another study, Coughlin et al. (2020) compared the specific brain binding of $^{18}$F-ASEM in subjects with the potential prodromal AD stage of mild cognitive impairment with that in HCs. Higher uptake in the brain was observed for the mild cognitive impairment cohort (*77*). These initial human α7 nAChR PET data encourage expansion to other neurodegenerative disorders and other AD disease stages, thereby allowing gathering of more insight into potential future applications for this novel PET technology.

### mAChR

#### Structure, Distribution, and Function of mAChRs

The structure of mAChRs is completely different from that of nAChRs. They belong to the metabotropic G-protein–coupled receptors. Similar to nAChRs, the distribution of mAChRs is widespread in the human brain and mAChRs act as modulators of neuronal activity (*78*). The highest density of mAChRs is in the occipital and insular cortices and the basal ganglia. The thalamus and cerebellum possess only low and very low amounts of mAChRs, respectively (*79*). The 5 subtypes (M1–M5) divide into 2 classes. The M1 receptor class comprises the subtypes M1, M3, and M5, which are $G_{q/11}$ G-protein–coupled, whereas the M2 receptor class includes the M2 and M4 subtypes, which signal through $G_{i/o}$ G-proteins (*80,81*). In general, the subtypes M1, M3, and M5 are usually postsynaptically located and increase the excitatory effects of transmitters, whereas M2 and M4 display the main presynaptic mAChRs and have an inhibitory action by suppressing transmitter release (*81*).

In the human brain, M1, M2, and M4 mAChRs are the most frequent subtypes (*81*), whereas M1 and M4 are the most abundant, though M1 mAChRs are relatively higher in the cortex (35%–60%) and M4 mAChRs are relatively higher in the striatum, especially in the putamen (!50%) (*81*). The M2 mAChRs are the predominant subtype in the basal forebrain (!40%) and thalamus (*81*).

In consolidation of memory and in higher brain functions such as cortex-dependent processing and cortex–hippocampus interactions, the postsynaptic and predominantly cortically located M1 mAChR subtype plays an important role (*78,81*).

#### mAChRs in Neurodegeneration

Several histopathology studies using unselective mAChR radioligands showed lower mAChRs binding in the human brain in AD and PD (*79*).

In transgenic AD mouse models, the additional knockout of M1 mAChRs results in a severely increased AD pathology (*78*), supporting the assumption that M1 mAChRs seem to be an important regulator of amyloidogenesis and a therapeutic target for AD. Postmortem data from AD patients revealed a normal density of M1 mAChRs (*82,83*). A further recently published postmortem study hypothesized that the cholinergic dysfunction of M1 mAChRs might be associated with an activation of the glutamate receptor 5 (mGluR5) due to β-amyloid (*84*). Because both M1 mAChRs and mGluR5 use the same $G_{q/11}$ G-protein–coupled signal pathway, an increased activation of mGlu5R might result in a reduced availability of the G-proteins for the M1 mAChR (*84*). Another hypothesis is that β-amyloid itself destabilizes the M1/G-protein coupling (*84*). In the pathophysiologic process of PD, the M1 mAChRs seem to be of relevance, too. Two preclinical studies on rodents found an improvement in PD motor symptoms after blocking of M1 mAChRs on striatal neurons (*85,86*).

The knockout of M2 mAChR in mice resulted in an impairment of higher cognitive functions such as working memory, spatial learning, and behavioral flexibility (*78*). Overall, data on M2 mAChR in neurodegenerative diseases are limited. Two postmortem studies detected reduced presynaptic M2 mAChRs in cortical regions in AD patients (*87,88*). It is hypothesized that the loss of M2 mAChRs in AD begins in the late stage of mild cognitive impairment and progresses during the course of the disease (*81*).

M4 mAChRs are the predominant subtype in the striatum (*81*). M4 mAChR knockout mice showed unimpaired episodic memory and orientation but decreased anxiety (*78*). Moreover, in animal models, positive allosteric activators of M4 could decrease dopamine release and demonstrate antipsychotic effects (*89*). In contrast, blocking of postsynaptic M4 mAChRs on striatal medium spiny neurons seems to reduce motor symptoms in preclinical PD models (*85,86*). In a postmortem study of patients with moderate to severe PD, an upregulation of M2 and M4 mAChRs was demonstrated in the dorsolateral and mesioprefrontal cortices (*90*). The authors hypothesized a compensation for the loss of cholinergic innervation. In AD, 1 study showed an increase in immunoprecipitated M4 mAChRs in the frontal, temporal, and parietal cortices (*82*).

#### PET Radioligands for Imaging mAChRs

The development of PET radioligands to image mAChRs has a long history beginning in the late 1970s (*79,91*). As with the

**TABLE 4**
Most Relevant mAChR PET Tracers

| Tracer name | Formula | Selectivity |
|---|---|---|
| $^{18}$F-FP-TZTP | 3-(4-(3-$^{18}$F-fluoropropylthio)-1,2,5-thiadiazol-3-yl)-1-methyl-1,2,5,6-tetrahydropyridine | M2 (M1)* |
| $^{11}$C-LSN3172176 | Ethyl-4-(6-(methyl-$^{11}$C)-2-oxoindolin-1-yl)-[1,4′-bipiperidine]-1′-carboxylate | M1 |
| $^{11}$C-MK-6884 | 6-(2-methyl-3-oxoisoindolin-5-yl)-5-(1-((1-methylcyclopentyl)methyl)-1*H*-pyrazol-4-yl)picolinonitrile | M4 |

*Lower affinity as well reported for M1 (*91*).
Methodologic determination of selectivity was previously published (*91*).

nAChR-targeting radioligands, the first radiotracers developed to image mAChRs suffered from insufficient subtype selectivity and unfavorable tracer kinetics, resulting in complicated modeling analyses (*79,91*). The development of subtype-specific radiotracers is still a work in progress (*91*). There are promising candidates for imaging M1, M2, and M4 mAChRs (Table 4; Fig. 2D). $^{11}$C-LSN3172176 is a novel M1-selective mAChR PET radiotracer. In the first-in-humans study, a scan duration of 80 min was sufficient for quantification of M1 mAChR by 1-tissue-compartment modeling or by the noninvasive simplified reference tissue model 2, and the metabolization was classified as moderate (Fig. 6) (*92*). For imaging M2 mAChR, the PET radiotracer $^{18}$F-FP-TZTP showed encouraging results in preclinical and clinical studies (*93,94*). A scanning duration of 120 min is sufficient, and quantification is possible by using a 2-parameter multilinear reference tissue model (*95*). The M1-selective mAChR PET ligand $^{11}$C-GSK1034702 has recently been translated to clinical application using PET (*91*). Tracer development and clinical PET application of $^{11}$C-GSK1034702 was proposed to assess blood–brain barrier permeability and to lower the risk of the drug development process for GSK1034702. However, because of limited specific binding as a result of low affinity to the target, it was concluded that $^{11}$C-GSK1034702 is not a suitable PET ligand (*91*). A recently published study described the synthesis of, and preclinical data on, a novel $^{11}$C-labeled positive allosteric modulator of M4 mAChR named $^{11}$C-MK-6884 (*96*). In rhesus monkeys, the radioligand showed rapid penetration of the blood–brain barrier, a local distribution pattern in the CNS similar to the known pattern for M4 mAChR (i.e., highest in the striatum), and a high receptor occupancy of 87%. This PET ligand binds with high affinity and good selectivity to an allosteric site on M4 mAChR. It was shown that $^{11}$C-MK-6884 binds to activated M4 mAChR, a finding that agrees with its pharmacology as a highly cooperative positive allosteric modulator of M4 (*96,97*). $^{11}$C-MK-6884 was recently translated to clinical PET application (*96,97*). The first-in-humans application of the nonselective mAChR PET ligand 4-$^{18}$F-fluorodexetimide showed promising findings, including high brain uptake, high image quality, unspecific binding in the cerebellum (making it valid to be used as a reference region), low interindividual variability in healthy subjects, and irreversible kinetics of tracer distribution in brain regions high in mAChRs (*98*). The nonselective M1 and M4 SPECT ligand $^{123}$I-iodoquinuclidinylbenzilate, in combined use with $^{99m}$Tc-exametazime SPECT to account for cerebral blood flow, is successfully used for cholinergic receptor network investigations on neurodegenerative disorders (*99*).

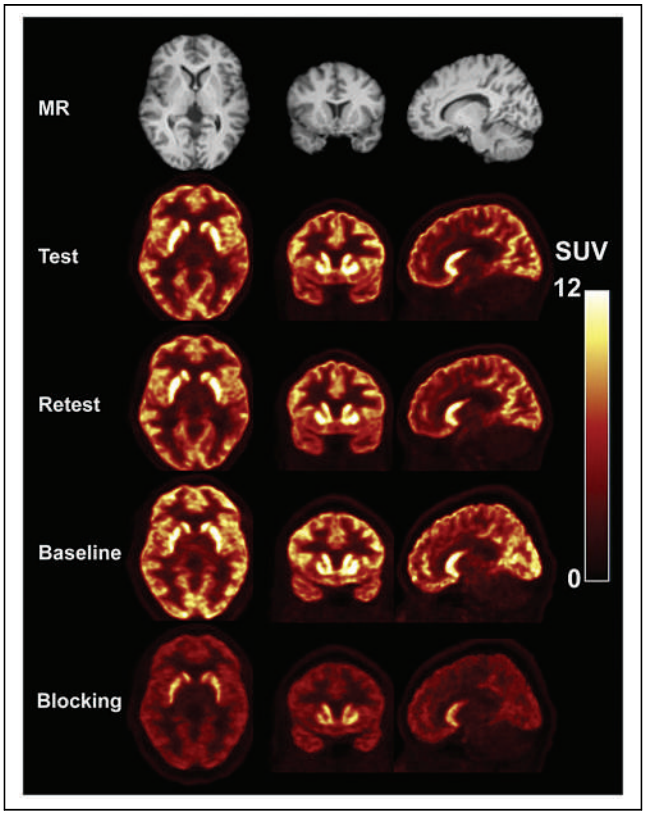


**FIGURE 6.** First-in-humans PET study on healthy subjects using M1 mAChR radioligand $^{11}$C-LSN3172176 showing high reproducibility under test–retest conditions and relevant blocking effects between baseline and blocking state using mAChR antagonist scopolamine. Cerebellum is potentially mAChR-free and can be used as reference region. (Reprinted from (*92*).)

### mAChR Imaging Results in Neurodegeneration

The nonselective SPECT ligand $^{123}$I-iodoquinuclidinylbenzilate targeting M1 and M4 mAChRs has been successfully used for novel important network analyses of mAChR modulatory contributions to large-scale alterations in brain-network function in AD and DLB (*99,100*).

M1- and M2-selective mAChR PET imaging studies on patients with neurodegenerative diseases are still pending, despite the promising first clinical data on the M1 mAChR–selective radioligand $^{11}$C-LSN3172176 and the availability of the M2 mAChR–selective radioligand $^{18}$F-FP-TZTP. The first-in-humans PET investigation of the M4 mAChR–selective PET ligand $^{11}$C-MK-6884 was performed in AD and HCs (*97*). In moderate to severe AD, compared with HCs, there was lower M4 mAChR binding in the

frontal and temporal cortices. In contrast, M4 mAChR binding in the striatum did not differ between groups. PET imaging of M1-, M2-, or M4-selective mAChRs is especially interesting to assess receptor occupancy by M1, M2, or M4 mAChR drugs or receptor activation by other cholinergic drugs such as AChE inhibitors, improving drug development in neurodegenerative disorders.

## ACETYLCHOLINESTERASE

### Local Distribution of AChE

In the human brain, AChE activity is highest in the striatum, followed by the basal forebrain, cerebellum, thalamus, brain stem, and cerebral cortex (*101–103*). The distribution of AChE in the CNS conforms widely to the distribution of choline acetyltransferase (*104*). AChE is located in presynaptic, intrasynaptic, and, to a lesser extent, postsynaptic neurons and in noncholinergic and cholinoceptive neurons. Although AChE is not so pure a preterminal cholinergic measure as choline acetyltransferase or VAChT, assessment of AChE activity is regarded as a reliable biomarker of the cholinergic system in the CNS (*102,103*).

### PET Radioligands for Imaging AChE Activity

Two different classes of PET tracers were developed to assess AChE activity in the brain: the first is AChE inhibitors, such as $^{11}$C-physostigmine or 5-$^{11}$C-methoxy-donepezil (*102,103*), and the second is substrates of ACh. The PET radioligands $^{11}$C-methylpiperidin-4-yl propionate ($^{11}$C-PMP) and *N*-$^{11}$C-methylpiperidinyl-4-acetate ($^{11}$C-MP4A) are analogs of acetylcholine (Table 5; Fig. 2E). They are hydrolyzed by AChE, and their hydrophilic metabolite *N*-$^{11}$C-methyl-piperidinol is irreversibly trapped within the brain. Compared with $^{11}$C-PMP, $^{11}$C-MP4A is slightly more selective for AChE (*105*) but possesses a higher relative hydrolysis rate ($k_3$) and is more flow-limited. Thus, $^{11}$C-PMP discriminates better between distinct AChE brain regions than does $^{11}$C-MP4A. $^{11}$C-PMP provides accurate measures of cortical and thalamic AChE, whereas $^{11}$C-MP4A gives precise measures of cortical AChE. Very high availability of striatal AChE and limitation of delivery restrict precise assessment of striatal AChE for both tracers (*102,103,105*). Both tracers were validated and sensitive enough to detect a 30%–50% decrease in AChE activity in an experimental AD model (*102,105,106*). Using AChE PET, there was no age-related decline of cerebral AChE activity in HCs (*107,108*). Using AChE PET in HCs, AChE activity was highest within the striatum, followed by the cerebellar cortex, thalamus, and cerebral cortex, paralleling the physiologic distribution of AChE activity in postmortem human brain (*101,108*). In HCs, AChE activity was sufficiently blocked by the AChE inhibitor physostigmine in the temporal cortex (49%) (*108*).

### AChE Imaging Results in Neurodegeneration

The first AChE PET investigations in AD, using $^{11}$C-MP4A or $^{11}$C-PMP PET, were performed in the late 1990s. Cholinergic dysfunction in neurodegenerative diseases using AChE PET has extensively been studied since then. Because of space restrictions, only a limited number of PET studies can be covered. Excellent recent reviews are recommended for further reading (*103,109,110*). As found by $^{11}$C-MP4A PET, cortical AChE activity was reduced by a maximum in the parietal (−38%) and temporal cortices (−31%), compared with HCs (*111*). Using $^{11}$C-PMP PET, cortical AChE activity, especially in the temporal cortex, was lower in AD than in HCs (−30%). The pattern of lower cortical AChE activity in AD was similar to the pattern of decreased VAChT binding but distinct from glucose metabolism (*108*). Shinotoh et al. demonstrated a progressive decline in cortical AChE activity in AD in a longitudinal study (2-y follow-up) and a relationship between lower cortical AChE activity and global cognitive dysfunction. Compared with HCs, EOAD showed lower cortical and hippocampal AChE activity than did LOAD (Fig. 7A and 7B) (*103,112*). Rinne et al. demonstrated a modest decline in hippocampal AChE activity in amnestic mild cognitive impairment (−17%) and early AD (−27%) (*113*). Similarly, in mild to moderate AD a modest decline in cortical AChE binding (−11%) was reported that correlated

**TABLE 5**
Most Relevant AChE PET Radioligands

| Tracer name | Formula |
|---|---|
| $^{11}$C-MP4A | *N*-$^{11}$C-methylpiperidyl acetate |
| $^{11}$C-PMP | *N*-$^{11}$C-methylpiperidyl propionate |
| $^{11}$C-donepezil | 5-$^{11}$C-methoxy-donepezil |

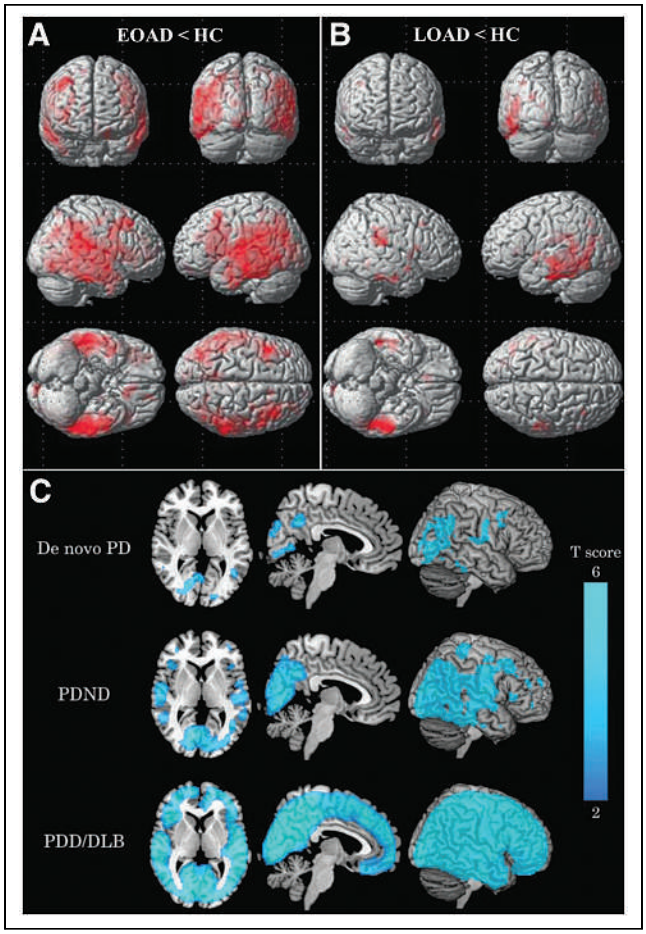


**FIGURE 7.** (A) As assessed by $^{11}$C-MP4A PET, compared with HCs there is lower AChE binding in temporoparietal cortices in EOAD. (B) However, in LOAD, decreased AChE binding is restricted to temporal cortices. (C) Using $^{11}$C-MP4A PET, various stages of LBD were investigated and compared with HCs. There is lower AChE binding in medial occipital cortex in de novo PD. There is reduced cortical AChE binding in PD without dementia (PDND). Most widespread cortical AChE decrease is in PDD or DLB, not differing from each other. (Reprinted with permission of (*103*).)

especially with disturbed attention and working memory but less with primary memory (*114*). Using $^{11}$C-PMP PET in AD, a clinical dose of the AChE inhibitor donepezil demonstrated minor inhibition of AChE activity (−27%) (*115*). This finding was supported by AChE PET studies using various AChE inhibitors reporting modest blocking of AChE activity by 20%–40% (*103*). Recently, an elegant placebo-controlled $^{11}$C-MP4A PET/functional MRI study using the AChE inhibitor rivastigmine was performed on patients with early AD and HCs. The authors demonstrated that lower cortical and rather preserved hippocampal AChE activity in early AD are prognostic for the memory response to rivastigmine (*116*).

Using $^{11}$C-PMP PET in atypical parkinsonian syndromes, such as multiple-system atrophy and progressive supranuclear palsy, subcortical AChE activity was more reduced than in PD. Lower AChE activity in the brain stem and cerebellum correlated with disturbances in gait and balance. The important findings potentially reflect greater dysfunction of the pontine cholinergic system, which is relevant for motor function, such as gait, in atypical parkinsonian syndromes (*117*).

An $^{11}$C-MP4A PET study performed by the Chiba group in 1999 investigated AChE activity in PD and progressive supranuclear palsy. Compared with HCs, PD patients showed the lowest cortical AChE activity (−17%) and progressive-supranuclear-palsy patients showed the lowest thalamic AChE activity (−38%). Different patterns of cholinergic dysfunction proposed a potential role for AChE PET in differential diagnosis between PD and progressive supranuclear palsy (*103*). In LBD patients, compared with HCs, there was lower cortical AChE activity, especially in the medial occipital cortex in early PD. Widespread, and the largest, reduction in AChE activity was found in PDD and DLB, not differing from each other (Fig. 6C) (*103*). Using $^{11}$C-PMP PET, compared with HCs, cortical AChE activity was lowest in PDD (−20%), followed by PD (−13%) and mild LOAD (−9%). Mild LOAD showed the lowest AChE activity within the temporal cortex (−15%) (*118*). In PD and PDD, there was the most significant relationship between lower cortical AChE activity and attentional and executive dysfunction (*119*).

More recently, there has been increasing interest in using AChE PET for investigation of associations between cholinergic dysfunction and noncognitive symptoms such as gait problems and falls, neuropsychiatric symptoms, olfactory dysfunction, and sleep problems in PD (*109,111*).

Bohnen et al. found that the decrease in brain stem–thalamic AChE activity was more related to the fall status in PD than to the decline in cortical AChE binding and was not related to nigrostriatal dopamine loss (*109*). Interestingly, most of these PD patients with lower thalamic AChE binding also had decreased cortical AChE activity. The Michigan group found that in PD with freezing of gait symptoms, the decline in cortical AChE activity was more pronounced than the decreased thalamic AChE binding. In PD, lower cortical AChE binding was related to a slower gait speed. In PD, lower thalamic AChE activity correlated with dysfunctional sensory processing while under postural control (*109*). Thus, gait and balance dysfunction in PD is possibly the result of a complex interrelationship between multiple dysfunctional systems and neurotransmitters, including degeneration of the cholinergic basal forebrain and the brain stem (*109,110*).

Importantly, higher AChE activity was reported in carriers of LRRK2 mutations in premanifest and manifest PD and may reflect compensatory changes (*120*). However, higher AChE activity may also be a result of inflammation, as shown in preclinical and clinical studies of peripheral inflammation using $^{11}$C-donepezil PET (*28*). More investigations, using both cholinergic and specific inflammation PET ligands in the same PD patients, are needed in future trials.

Importantly, recent reports of α-synucleinopathy in the body and brain in LBD and cholinergic dysfunction in the body in early or prodromal LBD, such as the gut, as determined by $^{11}$C-donepezil PET, led to a paradigm shift regarding our understanding of the pathophysiology of LBD and established the definition of the body-first versus brain-first LBD subtypes (*7,8*).

## CONCLUSIONS AND FUTURE DIRECTIONS

The possibility of obtaining in vivo information about the integrity of cholinergic transmission by means of PET imaging is of major interest in studying neurodegenerative disorders. This option refers to all the different compartments of this complex neurotransmitter system.

The development and successful clinical translation of $^{18}$F-FEOBV was a breakthrough for PET imaging of VAChT binding in the human brain. Recently, the number of $^{18}$F-FEOBV PET studies on AD and LBD has rapidly increased. The study findings are exciting, provide novel information on VAChT pathophysiology, and may lead to novel paradigms for cholinergic drug therapy in LBD.

Several α4β2 nAChR–targeting tracers have been developed, with the recent-generation tracers $^{18}$F-AZAN, $^{18}$F-XTRA, $^{18}$F-nifene, (−)-$^{18}$F-flubatine, and (+)-$^{18}$F-flubatine possessing favorable imaging characteristics. The highest potential for PET imaging of α4β2 nAChRs seems to be in monitoring disease progression and the respective therapies.

Only recently has it become possible to image α7 nAChR availability in the human brain in vivo by PET using $^{18}$F-ASEM or $^{11}$C-MeQAA. α7 nAChRs have a complex behavior and represent an interesting diagnostic and therapeutic target in neurodegenerative disorders because the brain availability of α7 nAChRs in these disorders is a function of disease stage as well as degree of neurodegeneration and neuroinflammation. Of special note for AD imaging, β-amyloid interferes with α7 nAChRs in a concentration-dependent manner. As such, α7 nAChR PET imaging is seen as the most promising for disease staging, progression estimation, and drug testing in neurodegenerative disorders.

The development of selective mAChR PET ligands is important but difficult. There are promising findings from first-in-humans PET applications using the M1 mAChR–selective ligand $^{11}$C-LSN3172176 and the M4 mAChR–selective ligand $^{11}$C-MK-6884. The M2 mAChR–selective ligand $^{18}$F-FP-TZTP is established. First-in-humans application of the nonselective mAChR PET ligand 4-$^{18}$F-fluorodexetimide showed promising results.

PET imaging of AChE activity has a long history. $^{11}$C-PMP or $^{11}$C-MP4A PET ligands were extensively used to assess lower cortical AChE availability in dementia associated with neurodegenerative diseases such as AD and LBD. More recently, novel findings in LBD (PD, PDD, and DLB) showed the relationship between lower cortical and subcortical cholinergic (AChE) binding and noncognitive dysfunctions such as balance and gait, wake/sleep cycle, olfaction, and mood in LBD. AChE inhibitors are one of the only two approved drug groups to treat AD, PDD, and DLB.

Higher AChE and VAChT binding in LRRK2 mutation carriers of manifest and premanifest PD and early PD may be a result of compensation or inflammation. The use of novel network analyses of cholinergic receptors in AD and LBD enables us to understand

the cholinergic modulatory contributions to large-scale network functions. The findings of cholinergic PET in the body, such as the gut, in early or prodromal PD contributed to a paradigm shift in our understanding of the pathophysiology of LBD and established the concept of a body-first and brain-first subtype of LBD.

Taken together, molecular imaging of different compartments of cholinergic neurotransmission is of great interest in different neurodegenerative disorders. For many aspects of cholinergic transmission, suitable tracers are available, with more to come. They will broaden our research application portfolio and potentially gain relevance in clinical care, such as by promoting the use of personalized medicine to guide cholinergic treatment decisions.

## DISCLOSURE

No potential conflict of interest relevant to this article was reported.

## REFERENCES


1. Mufson EJ, Ginsberg SD, Ikonomovic MD, DeKosky ST. Human cholinergic basal forebrain: chemoanatomy and neurologic dysfunction. *J Chem Neuroanat.* 2003;26:233–242.
2. Fisher SK, Wonnacott S. Acetylcholine. In: Brady ST, Siegel GJ, Albers RW, Price DL, eds. *Basic Neurochemistry.* 8th ed. Academic Press; 2012:258–282.
3. Hampel H, Mesulam M-M, Cuello AC, et al. The cholinergic system in the pathophysiology and treatment of Alzheimer's disease. *Brain.* 2018;141:1917–1933.
4. Bohnen NI, Albin RL. The cholinergic system and Parkinson disease. *Behav Brain Res.* 2011;221:564–573.
5. Bartus RT, Dean RL III, Beer B, Lippa AS. The cholinergic hypothesis of geriatric memory dysfunction. *Science.* 1982;217:408–414.
6. Christensen H, Maltby N, Jorm AF, Creasey H, Broe GA. Cholinergic 'blockade' as a model of the cognitive deficits in Alzheimer's disease. *Brain.* 1992;115: 1681–1699.
7. Fedorova TD, Seidelin LB, Knudsen K, et al. Decreased intestinal acetylcholinesterase in early Parkinson disease: an $^{11}$C-donepezil PET study. *Neurology.* 2017; 88:775–781.
8. Borghammer P, Horsager J, Andersen K, et al. Neuropathological evidence of body-first vs. brain-first Lewy body disease. *Neurobiol Dis.* 2021;161:105557.
9. Wenzel B, Deuther-Conrad W, Scheunemann M, Brust P. Radioligand development for PET imaging of the vesicular acetylcholine transporter (VAChT) in the brain. In: Dierckx RA, Otte A, de Vries EF, van Waarde A, Lammertsma AA, eds. *PET and SPECT of Neurobiological Systems.* Springer International Publishing; 2021:1061–1090.
10. Jung YW, Frey KA, Mulholland GK, et al. Vesamicol receptor mapping of brain cholinergic neurons with radioiodine-labeled positional isomers of benzovesamicol. *J Med Chem.* 1996;39:3331–3342.
11. Kuhl DE, Koeppe RA, Fessler JA, et al. In vivo mapping of cholinergic neurons in the human brain using SPECT and IBVM. *J Nucl Med.* 1994;35:405–410.
12. Mulholland GK, Wieland DM, Kilbourn MR, et al. [$^{18}$F]fluoroethoxy-benzovesamicol, a PET radiotracer for the vesicular acetylcholine transporter and cholinergic synapses. *Synapse.* 1998;30:263–274.
13. Kilbourn MR, Hockley B, Lee L, et al. Positron emission tomography imaging of (2R,3R)-5-[($^{18}$)F]fluoroethoxybenzovesamicol in rat and monkey brain: a radioligand for the vesicular acetylcholine transporter. *Nucl Med Biol.* 2009;36:489–493.
14. Parent MJ, Bedard MA, Aliaga A, et al. Cholinergic depletion in Alzheimer's disease shown by [$^{18}$F]FEOBV autoradiography. *Int J Mol Imaging.* 2013;2013: 205045.
15. Petrou M, Frey KA, Kilbourn MR, et al. In vivo imaging of human cholinergic nerve terminals with (−)-5-$^{18}$F-fluoroethoxybenzovesamicol: biodistribution, dosimetry, and tracer kinetic analyses. *J Nucl Med.* 2014;55:396–404.
16. Albin RL, Bohnen NI, Muller MLTM, et al. Regional vesicular acetylcholine transporter distribution in human brain: a [$^{18}$F]fluoroethoxybenzovesamicol positron emission tomography study. *J Comp Neurol.* 2018;526:2884–2897.
17. Aghourian M, Legault-Denis C, Soucy JP, et al. Quantification of brain cholinergic denervation in Alzheimer's disease using PET imaging with [$^{18}$F]-FEOBV. *Mol Psychiatry.* 2017;22:1531–1538.
18. Nejad-Davarani S, Koeppe RA, Albin RL, Frey KA, Müller MLTM, Bohnen NI. Quantification of brain cholinergic denervation in dementia with Lewy bodies using PET imaging with [$^{18}$F]-FEOBV. *Mol Psychiatry.* 2019;24:322–327.
19. Jin H, Yue X, Liu H, et al. Kinetic modeling of [$^{18}$F]VAT, a novel radioligand for positron emission tomography imaging vesicular acetylcholine transporter in nonhuman primate brain. *J Neurochem.* 2018;144:791–804.
20. Liang Q, Joshi S, Liu H, et al. In vitro characterization of [$^{3}$H]VAT in cells, animal and human brain tissues for vesicular acetylcholine transporter. *Eur J Pharmacol.* 2021;911:174556.
21. Kuhl DE, Minoshima S, Fessler JA, et al. In vivo mapping of cholinergic terminals in normal aging, Alzheimer's disease, and Parkinson's disease. *Ann Neurol.* 1996;40:399–410.
22. Liu AK, Chang RC, Pearce RK, Gentleman SM. Nucleus basalis of Meynert revisited: anatomy, history and differential involvement in Alzheimer's and Parkinson's disease. *Acta Neuropathol (Berl).* 2015;129:527–540.
23. Mazère J, Lamare F, Allard M, Fernandez P, Mayo W. $^{123}$I-iodobenzovesamicol SPECT imaging of cholinergic systems in dementia with Lewy bodies. *J Nucl Med.* 2017;58:123–128.
24. Bohnen NI, Kanel P, Zhou Z, et al. Cholinergic system changes of falls and freezing of gait in Parkinson's disease. *Ann Neurol.* 2019;85:538–549.
25. van der Zee S, Müller MLTM, Kanel P, van Laar T, Bohnen NI. Cholinergic denervation patterns across cognitive domains in Parkinson's disease. *Mov Disord.* 2021;36:642–650.
26. Sanchez-Catasus CA, Bohnen NI, Yeh FC, D'Cruz N, Kanel P, Müller MLTM. Dopaminergic nigrostriatal connectivity in early Parkinson disease: in vivo neuroimaging study of $^{11}$C-DTBZ PET combined with correlational tractography. *J Nucl Med.* 2021;62:545–552.
27. Legault-Denis C, Aghourian M, Soucy JP, et al. Normal cognition in Parkinson's disease may involve hippocampal cholinergic compensation: an exploratory PET imaging study with [$^{18}$F]-FEOBV. *Parkinsonism Relat Disord.* 2021;91:162–166.
28. Jørgensen NP, Alstrup AK, Mortensen FV, et al. Cholinergic PET imaging in infections and inflammation using $^{11}$C-donepezil and $^{18}$F-FEOBV. *Eur J Nucl Med Mol Imaging.* 2017;44:449–458.
29. Gotti C, Moretti M, Gaimarri A, Zanardi A, Clementi F, Zoli M. Heterogeneity and complexity of native brain nicotinic receptors. *Biochem Pharmacol.* 2007;74: 1102–1111.
30. Court JA, Martin-Ruiz C, Graham A, Perry E. Nicotinic receptors in human brain: topography and pathology. *J Chem Neuroanat.* 2000;20:281–298.
31. Paterson D, Nordberg A. Neuronal nicotinic receptors in the human brain. *Prog Neurobiol.* 2000;61:75–111.
32. Shimohama S, Taniguchi T, Fujiwara M, Kameyama M. Changes in nicotinic and muscarinic cholinergic receptors in Alzheimer-type dementia. *J Neurochem.* 1986;46:288–293.
33. Laikowski MM, Reisdorfer F, Moura S. NAChR $\alpha4\beta2$ subtype and their relation with nicotine addiction, cognition, depression and hyperactivity disorder. *Curr Med Chem.* 2019;26:3792–3811.
34. Flynn DD, Mash DC. Characterization of L-[$^{3}$H]nicotine binding in human cerebral cortex: comparison between Alzheimer's disease and the normal. *J Neurochem.* 1986;47:1948–1954.
35. Nordberg A, Winblad B. Reduced number of [$^{3}$H]nicotine and [$^{3}$H]acetylcholine binding sites in the frontal cortex of Alzheimer brains. *Neurosci Lett.* 1986;72: 115–119.
36. Perry E, Martin-Ruiz C, Lee M, et al. Nicotinic receptor subtypes in human brain ageing, Alzheimer and Lewy body diseases. *Eur J Pharmacol.* 2000;393: 215–222.
37. Perry EK, Morris CM, Court JA, et al. Alteration in nicotine binding sites in Parkinson's disease, Lewy body dementia and Alzheimer's disease: possible index of early neuropathology. *Neuroscience.* 1995;64:385–395.
38. Pimlott SL, Piggott M, Owens J, et al. Nicotinic acetylcholine receptor distribution in Alzheimer's disease, dementia with Lewy bodies, Parkinson's disease, and vascular dementia: in vitro binding study using 5-[$^{125}$I]-a-85380. *Neuropsychopharmacology.* 2004;29:108–116.
39. Schmaljohann J, Gündisch D, Minnerop M, et al. In vitro evaluation of nicotinic acetylcholine receptors with 2-[$^{18}$F]F-A85380 in Parkinson's disease. *Nucl Med Biol.* 2006;33:305–309.
40. Sihver W, Gillberg PG, Svensson AL, Nordberg A. Autoradiographic comparison of [$^{3}$H](−)nicotine, [$^{3}$H]cytisine and [$^{3}$H]epibatidine binding in relation to vesicular acetylcholine transport sites in the temporal cortex in Alzheimer's disease. *Neuroscience.* 1999;94:685–696.
41. Whitehouse PJ, Martino AM, Antuono PG, et al. Nicotinic acetylcholine binding sites in Alzheimer's disease. *Brain Res.* 1986;371:146–151.
42. Lao PJ, Betthauser TJ, Tudorascu DL, et al. [$^{18}$F]nifene test-retest reproducibility in first-in-human imaging of $\alpha4\beta2$* nicotinic acetylcholine receptors. *Synapse.* 2017;71:10.1002/syn.21981.
43. Wong DF, Kuwabara H, Kim J, et al. PET imaging of high-affinity $\alpha4\beta2$ nicotinic acetylcholine receptors in humans with $^{18}$F-AZAN, a radioligand with optimal brain kinetics. *J Nucl Med.* 2013;54:1308–1314.

44. Sabri O, Becker GA, Meyer PM, et al. First-in-human PET quantification study of cerebral $\alpha4\beta2$* nicotinic acetylcholine receptors using the novel specific radioligand (−)-[$^{18}$F]flubatine. *Neuroimage.* 2015;118:199–208.
45. Sabri O, Meyer PM, Gräf S, et al. Cognitive correlates of $\alpha4\beta2$ nicotinic acetylcholine receptors in mild Alzheimer's dementia. *Brain.* 2018;141:1840–1854.
46. Coughlin JM, Slania S, Du Y, et al. $^{18}$F-XTRA PET for enhanced imaging of the extrathalamic $\alpha4\beta2$ nicotinic acetylcholine receptor. *J Nucl Med.* 2018;59:1603–1608.
47. Tiepolt S, Becker G-A, Wilke S, et al. (+)-[$^{18}$F]flubatine as a novel $\alpha4\beta2$ nicotinic acetylcholine receptor PET ligand: results of the first-in-human brain imaging application in patients with $\beta$-amyloid PET-confirmed Alzheimer's disease and healthy controls. *Eur J Nucl Med Mol Imaging.* 2021;48:731–746.
48. Mukhin AG, Kimes AS, Chefer SI, et al. Greater nicotinic acetylcholine receptor density in smokers than in nonsmokers: a PET study with 2-$^{18}$F-FA-85380. *J Nucl Med.* 2008;49:1628–1635.
49. Brody AL, Mandelkern MA, London ED, et al. Cigarette smoking saturates brain alpha 4 beta 2 nicotinic acetylcholine receptors. *Arch Gen Psychiatry.* 2006;63:907–915.
50. Bhatt S, Hillmer AT, Nabulsi N, et al. Evaluation of (−)-[$^{18}$F]flubatine-specific binding: implications for reference region approaches. *Synapse.* 2018;72:10.1002/syn.22016.
51. Sabri O, Kendziorra K, Wolf H, Gertz HJ, Brust P. Acetylcholine receptors in dementia and mild cognitive impairment. *Eur J Nucl Med Mol Imaging.* 2008;35(suppl 1)S30–S45.
52. Kendziorra K, Wolf H, Meyer PM, et al. Decreased cerebral $\alpha4\beta2$* nicotinic acetylcholine receptor availability in patients with mild cognitive impairment and Alzheimer's disease assessed with positron emission tomography. *Eur J Nucl Med Mol Imaging.* 2011;38:515–525.
53. Okada H, Ouchi Y, Ogawa M, et al. Alterations in $\alpha4\beta2$ nicotinic receptors in cognitive decline in Alzheimer's aetiopathology. *Brain.* 2013;136:3004–3017.
54. Sultzer DL, Melrose RJ, Riskin-Jones H, et al. Cholinergic receptor binding in Alzheimer disease and healthy aging: assessment in vivo with positron emission tomography imaging. *Am J Geriatr Psychiatry.* 2017;25:342–353.
55. Fujita M, Ichise M, Zoghbi SS, et al. Widespread decrease of nicotinic acetylcholine receptors in Parkinson's disease. *Ann Neurol.* 2006;59:174–177.
56. O'Brien JT, Colloby SJ, Pakrasi S, et al. Nicotinic $\alpha4\beta2$ receptor binding in dementia with Lewy bodies using $^{123}$I-5IA-85380 SPECT demonstrates a link between occipital changes and visual hallucinations. *Neuroimage.* 2008;40:1056–1063.
57. Kas A, Bottlaender M, Gallezot JD, et al. Decrease of nicotinic receptors in the nigrostriatal system in Parkinson's disease. *J Cereb Blood Flow Metab.* 2009;29:1601–1608.
58. Meyer PM, Strecker K, Kendziorra K, et al. Reduced $\alpha4\beta2$*-nicotinic acetylcholine receptor binding and its relationship to mild cognitive and depressive symptoms in Parkinson disease. *Arch Gen Psychiatry.* 2009;66:866–877.
59. Lorenz R, Samnick S, Dillmann U, et al. Nicotinic $\alpha4\beta2$ acetylcholine receptors and cognitive function in Parkinson's disease. *Acta Neurol Scand.* 2014;130:164–171.
60. Isaias IU, Spiegel J, Brumberg J, et al. Nicotinic acetylcholine receptor density in cognitively intact subjects at an early stage of Parkinson's disease. *Front Aging Neurosci.* 2014;6:213.
61. Breese CR, Adams C, Logel J, et al. Comparison of the regional expression of nicotinic acetylcholine receptor $\alpha7$ mRNA and [$^{125}$I]-alpha-bungarotoxin binding in human postmortem brain. *J Comp Neurol.* 1997;387:385–398.
62. Wang H, Yu M, Ochani M, et al. Nicotinic acetylcholine receptor $\alpha7$ subunit is an essential regulator of inflammation. *Nature.* 2003;421:384–388.
63. Dajas-Bailador FA, Mogg AJ, Wonnacott S. Intracellular Ca2+ signals evoked by stimulation of nicotinic acetylcholine receptors in SH-SY5Y cells: contribution of voltage-operated Ca2+ channels and Ca2+ stores. *J Neurochem.* 2002;81:606–614.
64. Wu J, Ishikawa M, Zhang J, Hashimoto K. Brain imaging of nicotinic receptors in Alzheimer's disease. *Int J Alzheimers Dis.* 2010;2010:548913.
65. Ikonomovic MD, Wecker L, Abrahamson EE, et al. Cortical $\alpha7$ nicotinic acetylcholine receptor and $\beta$-amyloid levels in early Alzheimer disease. *Arch Neurol.* 2009;66:646–651.
66. Wang HY, Lee DH, D'Andrea MR, Peterson PA, Shank RP, Reitz AB. $\beta$-amyloid(1-42) binds to $\alpha7$ nicotinic acetylcholine receptor with high affinity: implications for Alzheimer's disease pathology. *J Biol Chem.* 2000;275:5626–5632.
67. O'Neill MJ, Murray TK, Lakics V, Visanji NP, Duty S. The role of neuronal nicotinic acetylcholine receptors in acute and chronic neurodegeneration. *Curr Drug Targets CNS Neurol Disord.* 2002;1:399–411.
68. Dziewczapolski G, Glogowski CM, Masliah E, Heinemann SF. Deletion of the $\alpha7$ nicotinic acetylcholine receptor gene improves cognitive deficits and synaptic pathology in a mouse model of Alzheimer's disease. *J Neurosci.* 2009;29:8805–8815.
69. Toyohara J, Sakata M, Wu J, et al. Preclinical and the first clinical studies on [$^{11}$C]CHIBA-1001 for mapping $\alpha7$ nicotinic receptors by positron emission tomography. *Ann Nucl Med.* 2009;23:301–309.
70. Ishikawa M, Sakata M, Toyohara J, et al. Occupancy of $\alpha7$ nicotinic acetylcholine receptors in the brain by tropisetron: a positron emission tomography study using $^{11}$C-CHIBA-1001 in healthy human subjects. *Clin Psychopharmacol Neurosci.* 2011;9:111–116.
71. Brust P, Deuther-Conrad W, Donat C, et al. Preclinical and clinical aspects of nicotinic acetylcholine receptor imaging. In: Dierckx RA, Otte A, de Vries EF, van Waarde A, Lammertsma AA, eds. *PET and SPECT of Neurobiological Systems.* Springer International Publishing; 2021:593–660.
72. Brust P, Peters D, Deuther-Conrad W. Development of radioligands for the imaging of $\alpha7$ nicotinic acetylcholine receptors with positron emission tomography. *Curr Drug Targets.* 2012;13:594–601.
73. Coughlin JM, Du Y, Rosenthal HB, et al. The distribution of the $\alpha7$ nicotinic acetylcholine receptor in healthy aging: an in vivo positron emission tomography study with [$^{18}$F]ASEM. *Neuroimage.* 2018;165:118–124.
74. Ogawa M, Tsukada H, Hatano K, Ouchi Y, Saji H, Magata Y. Central in vivo nicotinic acetylcholine receptor imaging agents for positron emission tomography (PET) and single photon emission computed tomography (SPECT). *Biol Pharm Bull.* 2009;32:337–340 .
75. Ogawa M, Nishiyama S, Tsukada H, et al. Synthesis and evaluation of new imaging agent for central nicotinic acetylcholine receptor $\alpha7$ subtype. *Nucl Med Biol.* 2010;37:347–355.
76. Nakaizumi K, Ouchi Y, Terada T, et al. In vivo depiction of $\alpha7$ nicotinic receptor loss for cognitive decline in Alzheimer's disease. *J Alzheimers Dis.* 2018;61:1355–1365.
77. Coughlin JM, Rubin LH, Du Y, et al. High availability of the $\alpha7$-nicotinic acetylcholine receptor in brains of individuals with mild cognitive impairment: a pilot study using $^{18}$F-ASEM PET. *J Nucl Med.* 2020;61:423–426.
78. Thomsen M, Sørensen G, Dencker D. Physiological roles of CNS muscarinic receptors gained from knockout mice. *Neuropharmacology.* 2018;136:411–420.
79. Eckelman WC. Imaging of muscarinic receptors in the central nervous system. *Curr Pharm Des.* 2006;12:3901–3913.
80. Assous M. Striatal cholinergic transmission: focus on nicotinic receptors' influence in striatal circuits. *Eur J Neurosci.* 2021;53:2421–2442.
81. Lebois EP, Thorn C, Edgerton JR, Popiolek M, Xi S. Muscarinic receptor subtype distribution in the central nervous system and relevance to aging and Alzheimer's disease. *Neuropharmacology.* 2018;136:362–373.
82. Flynn DD, Ferrari-DiLeo G, Mash DC, Levey AI. Differential regulation of molecular subtypes of muscarinic receptors in Alzheimer's disease. *J Neurochem.* 1995;64:1888–1891.
83. Tsang SWY, Lai MKP, Kirvell S, et al. Impaired coupling of muscarinic M1 receptors to G-proteins in the neocortex is associated with severity of dementia in Alzheimer's disease. *Neurobiol Aging.* 2006;27:1216–1223.
84. Yi JH, Whitcomb DJ, Park SJ, et al. M1 muscarinic acetylcholine receptor dysfunction in moderate Alzheimer's disease pathology. *Brain Commun.* 2020;2:fcaa058.
85. Brugnoli A, Pisanò CA, Morari M. Striatal and nigral muscarinic type 1 and type 4 receptors modulate levodopa-induced dyskinesia and striato-nigral pathway activation in 6-hydroxydopamine hemilesioned rats. *Neurobiol Dis.* 2020;144:105044.
86. Ztaou S, Maurice N, Camon J, et al. Involvement of striatal cholinergic interneurons and M1 and M4 muscarinic receptors in motor symptoms of Parkinson's disease. *J Neurosci.* 2016;36:9161–9172.
87. Araujo DM, Lapchak PA, Robitaille Y, Gauthier S, Quirion R. Differential alteration of various cholinergic markers in cortical and subcortical regions of human brain in Alzheimer's disease. *J Neurochem.* 1988;50:1914–1923.
88. Mash DC, Flynn DD, Potter LT. Loss of M2 muscarine receptors in the cerebral cortex in Alzheimer's disease and experimental cholinergic denervation. *Science.* 1985;228:1115–1117.
89. Moran SP, Maksymetz J, Conn PJ. Targeting muscarinic acetylcholine receptors for the treatment of psychiatric and neurological disorders. *Trends Pharmacol Sci.* 2019;40:1006–1020.
90. McOmish C, Pavey G, McLean C, Horne M, Dean B, Scarr E. Muscarinic receptor binding changes in postmortem Parkinson's disease. *J Neural Transm.* 2017;124:227–236.
91. Ozenil M, Aronow J, Millard M, et al. Update on PET tracer development for muscarinic acetylcholine receptors. *Pharmaceuticals (Basel).* 2021;14:530.
92. Naganawa M, Nabulsi N, Henry S, et al. First-in-human assessment of $^{11}$C-LSN3172176, an M1 muscarinic acetylcholine receptor PET radiotracer. *J Nucl Med.* 2021;62:553–560.
93. Cannon DM, Carson RE, Nugent AC, et al. Reduced muscarinic type 2 receptor binding in subjects with bipolar disorder. *Arch Gen Psychiatry.* 2006;63:741–747.

94. Ravasi L, Tokugawa J, Nakayama T, et al. Imaging of the muscarinic acetylcholine neuroreceptor in rats with the M2 selective agonist [$^{18}$F]FP-TZTP. *Nucl Med Biol.* 2012;39:45–55.
95. Ichise M, Cohen RM, Carson RE. Noninvasive estimation of normalized distribution volume: application to the muscarinic-2 ligand [$^{18}$F]FP-TZTP. *J Cereb Blood Flow Metab.* 2008;28:420–430.
96. Tong L, Li W, Lo MM, et al. Discovery of [$^{11}$C]MK-6884: a positron emission tomography (PET) imaging agent for the study of M4 muscarinic receptor positive allosteric modulators (PAMs) in neurodegenerative diseases. *J Med Chem.* 2020;63:2411–2425.
97. Li W, Wang Y, Lohith TG, et al. The PET tracer [$^{11}$C]MK-6884 quantifies M4 muscarinic receptor in rhesus monkeys and patients with Alzheimer's disease. *Sci Transl Med.* 2022;14:eabg3684.
98. Rowe CC, Krishnadas N, Ackermann U, et al. PET imaging of brain muscarinic receptors with $^{18}$F-fluorobenzyl-dexetimide: a first in human study. *Psychiatry Res Neuroimaging.* 2021;316:111354.
99. Colloby SJ, Nathan PJ, McKeith IG, Bakker G, O'Brien JT, Taylor JP. Cholinergic muscarinic $M_1$/$M_4$ receptor networks in dementia with Lewy bodies. *Brain Commun.* 2020;2:fcaa098.
100. Colloby SJ, McKeith IG, Wyper DJ, O'Brien JT, Taylor JP. Regional covariance of muscarinic acetylcholine receptors in Alzheimer's disease using (R, R) [$^{123}$I]-QNB SPECT. *J Neurol.* 2015;262:2144–2153.
101. Atack JR, Perry EK, Bonham JR, Candy JM, Perry RH. Molecular forms of acetylcholinesterase and butyrylcholinesterase in the aged human central nervous system. *J Neurochem.* 1986;47:263–277.
102. Bohnen NI, Frey KA. Imaging of cholinergic and monoaminergic neurochemical changes in neurodegenerative disorders. *Mol Imaging Biol.* 2007;9:243–257.
103. Shinotoh H, Hirano S, Shimada H. PET imaging of acetylcholinesterase. In: Dierckx RA, Otte A, de Vries EF, van Waarde A, Lammertsma AA, eds. *PET and SPECT of Neurobiological Systems.* Springer International Publishing; 2020:193–220.
104. Mesulam MM, Geula C. Overlap between acetylcholinesterase-rich and choline acetyltransferase-positive (cholinergic) axons in human cerebral cortex. *Brain Res.* 1992;577:112–120.
105. Irie T, Fukushi K, Akimoto Y, Tamagami H, Nozaki T. Design and evaluation of radioactive acetylcholine analogs for mapping brain acetylcholinesterase (AchE) in vivo. *Nucl Med Biol.* 1994;21:801–808.
106. Irie T, Fukushi K, Namba H, et al. Brain acetylcholinesterase activity: validation of a PET tracer in a rat model of Alzheimer's disease. *J Nucl Med.* 1996;37:649–655.
107. Namba H, Iyo M, Shinotoh H, Nagatsuka S, Fukushi K, Irie T. Preserved acetylcholinesterase activity in aged cerebral cortex. *Lancet.* 1998;351:881–882.
108. Kuhl DE, Koeppe RA, Minoshima S, et al. In vivo mapping of cerebral acetylcholinesterase activity in aging and Alzheimer's disease. *Neurology.* 1999;52:691–699.
109. Bohnen NI, Kanel P, Müller MLTM. Molecular imaging of the cholinergic system in Parkinson's disease. *Int Rev Neurobiol.* 2018;141:211–250.
110. Pasquini J, Brooks DJ, Pavese N. The cholinergic brain in Parkinson's disease. *Mov Disord Clin Pract (Hoboken).* 2021;8:1012–1026.
111. Iyo M, Namba H, Fukushi K, et al. Measurement of acetylcholinesterase by positron emission tomography in the brains of healthy controls and patients with Alzheimer's disease. *Lancet.* 1997;349:1805–1809.
112. Shinotoh H, Namba H, Fukushi K, et al. Progressive loss of cortical acetylcholinesterase activity in association with cognitive decline in Alzheimer's disease: a positron emission tomography study. *Ann Neurol.* 2000;48:194–200.
113. Rinne JO, Kaasinen V, Järvenpää T, et al. Brain acetylcholinesterase activity in mild cognitive impairment and early Alzheimer's disease. *J Neurol Neurosurg Psychiatry.* 2003;74:113–115.
114. Bohnen NI, Kaufer DI, Hendrickson R, et al. Cognitive correlates of alterations in acetylcholinesterase in Alzheimer's disease. *Neurosci Lett.* 2005;380:127–132.
115. Kuhl DE, Minoshima S, Frey KA, Foster NL, Kilbourn MR, Koeppe RA. Limited donepezil inhibition of acetylcholinesterase measured with positron emission tomography in living Alzheimer cerebral cortex. *Ann Neurol.* 2000;48:391–395.
116. Richter N, Beckers N, Onur OA, et al. Effect of cholinergic treatment depends on cholinergic integrity in early Alzheimer's disease. *Brain.* 2018;141:903–915.
117. Gilman S, Koeppe RA, Nan B, et al. Cerebral cortical and subcortical cholinergic deficits in parkinsonian syndromes. *Neurology.* 2010;74:1416–1423.
118. Bohnen NI, Kaufer DI, Ivanco LS, et al. Cortical cholinergic function is more severely affected in parkinsonian dementia than in Alzheimer disease: an in vivo positron emission tomographic study. *Arch Neurol.* 2003;60:1745–1748.
119. Bohnen NI, Kaufer DI, Hendrickson R, et al. Cognitive correlates of cortical cholinergic denervation in Parkinson's disease and parkinsonian dementia. *J Neurol.* 2006;253:242–247.
120. Liu SY, Wile DJ, Fu JF, et al. The effect of LRRK2 mutations on the cholinergic system in manifest and premanifest stages of Parkinson's disease: a cross-sectional PET study. *Lancet Neurol.* 2018;17:309–316.

# Imaging Neuroinflammation in Neurodegenerative Disorders

Joseph C. Masdeu[1], Belen Pascual[1], and Masahiro Fujita[1,2]

*[1]Nantz National Alzheimer Center, Stanley H. Appel Department of Neurology, Houston Methodist Neurological Institute, Houston Methodist Research Institute, Weill Cornell Medicine, Houston, Texas; and [2]PET Core, Houston Methodist Research Institute, Weill Cornell Medicine, Houston, Texas*

Neuroinflammation plays a major role in the etiopathology of neurodegenerative diseases, including Alzheimer and Parkinson diseases, frontotemporal lobar degeneration, and amyotrophic lateral sclerosis. In vivo monitoring of neuroinflammation using PET is critical to understand this process, and data are accumulating in this regard, thus a review is useful. From PubMed, we retrieved publications using any of the available PET tracers to image neuroinflammation in humans as well as selected articles dealing with experimental animal models or the chemistry of currently used or potential radiotracers. We reviewed 280 articles. The most common PET neuroinflammation target, translocator protein (TSPO), has limitations, lacking cellular specificity and the ability to separate neuroprotective from neurotoxic inflammation. However, TSPO PET is useful to define the amount and location of inflammation in the brain of people with neurodegenerative disorders. We describe the characteristics of TSPO and other potential PET neuroinflammation targets and PET tracers available or in development. Despite target and tracer limitations, in recent years there has been a sharp increase in the number of reports of neuroinflammation PET in humans. The most studied has been Alzheimer disease, in which neuroinflammation seems initially neuroprotective and neurotoxic later in the progression of the disease. We describe the findings in all the major neurodegenerative disorders. Neuroinflammation PET is an indispensable tool to understand the process of neurodegeneration, particularly in humans, as well as to validate target engagement in therapeutic clinical trials.

**Key Words:** molecular imaging; neurology; PET; Alzheimer's disease; neurodegeneration; neuroinflammation; positron emission tomography; TSPO

**J Nucl Med 2022; 63:45S–52S**
DOI: 10.2967/jnumed.121.263200

Neuroinflammation is being increasingly recognized as a key component of the etiopathology of neurodegenerative diseases, spanning from Alzheimer disease (AD) through Parkinson disease (PD), frontotemporal lobar degeneration (FTD) and amyotrophic lateral sclerosis (ALS) (*1,2*). However, while PET biomarkers for some of these disorders, such as β-amyloid and tau tracers for AD, are widely used in both clinical and research work, the use of neuroinflammation tracers remains restricted to a small number of research centers. This limited use can be explained by the lack of cellular specificity of the currently used neuroinflammation target, the translocator protein 18 kDa (TSPO); its ubiquity in the brain, which precludes uptake quantification by comparing a brain region harboring the target with a region devoid of it (*3*); and the low affinity of the original neuroinflammation PET tracers. However, tracer development, improved quantification (*3,4*), and the increasing awareness of the importance of neuroinflammation in neurodegenerative disorders have resulted in a sharp increase in the number of publications. For instance, on clinical AD, 4 times as many articles were published between 2021 (the date of this review) and 2013 than between 2013 and 1995 (the date of the first publication). We hope that this review will encourage additional work in this important field. After a description of the characteristics of available PET tracers and their application to the study of various neurodegenerative disorders, we discuss the characteristics and applicability of potentially new PET inflammation biomarkers.

## TSPO PET: CURRENT TARGET TO IMAGE NEUROINFLAMMATION

### What Is TSPO?

TSPO is an ion-channel-type receptor located on the outer membrane of mitochondria. Initially reported as transporting cholesterol, porphyrin, and $Ca^{2+}$ (*5*), its function is still under investigation and likely involved in steroidogenesis, apoptosis, mitochondrial respiration, and processing reactive oxygen species (*6*). TSPO is not selectively expressed by microglia but also by astrocytes, vascular endothelial cells, some neurons, immune cells, and some tumor cells. Thus, frequent statements in papers that TSPO PET measured an increase in "activated" microglia oversimplify the matter (*7*). Furthermore, some (*8,9*), but not all (*10,11*), postmortem studies of AD brains have failed to find significant increases in TSPO, fueling skepticism on the use of TSPO PET to image neuroinflammation in neurodegenerative disorders. But even the negative studies, which contained small samples, showed in some patients much higher TSPO levels in areas typically affected in AD, such as the frontal lobe, than in the cerebellum, little involved in this disorder (*8*). In other diseases as well, TSPO is increased specifically in areas characteristically affected by the pathology, such as the motor cortex in ALS (*12*). Thus, despite its limitations, TSPO PET is useful to measure neuroinflammation in neurodegeneration.

### PET Ligands to Image TSPO

Since the 1980s initial PET studies on neuroinflammation used $^{11}$C-PK11195. However, later, $^{11}$C-PK11195 was found to have low specific binding (*13,14*). Around 2000, a new series of TSPO ligands with different chemical structures was published (*15*), and subsequently an original chemical, $^{11}$C-DAA1106, and analogs such as $^{11}$C-PBR28 have been used in PET studies (*16,17*). PET ligands with different structure have also been developed including $^{11}$C-DPA-713 (*18*). $^{18}$F-GE180, useful for rodent studies, does not penetrate the intact blood–brain barrier in humans (*19*), with $K_1$ (rate constant for

Received Jan. 15, 2022; revision accepted May. 3, 2022.
For correspondence or reprints, contact Joseph C. Masdeu (jcmasdeu@houstonmethodist.org).

transfer from arterial plasma to tissue, according to Innis et al. (*20*)) of only 0.01 mL/g/min (*21*). $^{18}$F-GE180 is thus questionable for human studies of neuroinflammation. Radioligands developed after PK11195 are called second-generation PET TSPO ligands. Animal PET studies showed that most of the second-generation ligands have much greater specific binding to TSPO than PK11195 (*13*).

A limitation of nearly all second-generation TSPO ligands is that binding is affected by the single nucleotide polymorphism (SNP) rs6971 (*22*). Depending on the SNP they carry, subjects can be high-, mixed-, or low-affinity binders. In low-affinity binders, the low signal precludes useful PET using most ligands. The effect of the SNP needs to be included in the analysis of PET data. Therefore, a potential improvement over the second-generation ligands is to minimize the influence of the SNP.

To select a PET ligand to study changes in TSPO, several factors need to be considered including the equilibrium ratio of specific-to-nondisplaceable binding, $BP_{ND}$; influences of radiometabolites in the quantification; and feasibility to measure binding in low-affinity binders. Greater $BP_{ND}$ provides PET signals more sensitive to the changes in specific binding. $BP_{ND}$ is typically measured in animals by comparing scans under baseline and near complete binding blockade. However, because both in vitro and PET studies show large species differences in the density of TSPO (*23–25*) it is necessary to measure $BP_{ND}$ of each ligand in humans. The Lassen plot allows measurement of $BP_{ND}$ with only partial blockade of the binding, which is unlikely to cause pharmacologic effects (*26*). Thus, this method has been used in humans for 4 $^{11}$C-labeled TSPO ligands: $^{11}$C-*R*-PK11195, $^{11}$C-PBR28, $^{11}$C-DPA-713, and $^{11}$C-ER176 (*14*). Feasibility of measuring TSPO in low-affinity binders and possible influences of radiometabolites have also been investigated for these 4 ligands (*14*). On the basis of these most comprehensive investigations in humans so far, $^{11}$C-ER176 is the current choice to study TSPO. $^{11}$C-ER176 has an adequate $BP_{ND}$ even in low-affinity binders and shows the least influence from radiometabolites.

In neurodegeneration, the permeability of the blood–brain barrier may be altered (*27*). In theory, because greater permeability increases the movement of chemical compounds both in ($K_1$) and out ($k_2$) of the brain, changes in permeability are not expected to influence equilibrium parameters such as $BP_{ND}$ and total distribution volume ($V_T$).

## NEUROINFLAMMATION PET IN NEURODEGENERATIVE DISORDERS

### Alzheimer Disease (AD)

The discovery of AD risk genes involved in inflammation signaling (*28*) has emphasized the critical role of neuroinflammation for the onset and progression of AD. In AD transgenic mouse models, innate immune microglia are initial responders to neuronal release of amyloid-β (Aβ), activating microglial pattern recognition toll-like receptors, and intracellular NLRP3 inflammasomes, thereby inducing tau hyperphosphorylation and aggregation (*1*). Subsequent release of truncated phosphorylated tau also enhances immune cell activation, promoting the release of inflammatory mediators and a self-propagating cascade of synaptic dysfunction, neuronal injury, and cell death (*1*). Current understanding of the role of inflammation in AD stems largely from work with rodents. However, interspecies differences with humans may be large, as shown, for instance, by profiling microglial RNA from frozen AD and control brains (*29*). In human brain, the proportion of morphologically activated microglia in cortical tissue is associated with β-amyloid, tau-related neuropathology, and the rate of cognitive decline (*30*). However, neuroinflammation may be neuroprotective or harmful in neurodegeneration (*31*). It is possible that the predominant role of inflammation may shift at various stages of AD, being neuroprotective at earlier stages and neurotoxic at advanced stages, but this is yet to be proven in human AD. TSPO PET provides a tool to characterize brain inflammation at the various stages of human AD (Fig. 1). A preclinical stage, when the person is still cognitively unimpaired, but brain β-amyloid is already high, may be most amenable to therapy but has been least studied by PET. As the disease worsens, the patient has mild cognitive impairment, already with some degree of memory or language impairment, but not enough to interfere seriously with activities of daily living as it is in the next stage, clinical AD. Clinical AD, still not severe enough to render the patient uncooperative for brain PET, is the stage at which most early TSPO PET studies were performed and will be described first below. Although single photon emission tomography has been used to image TSPO in AD, most groups have used PET. The 2 tracers most often used have been $^{11}$C-PK11195, in 28 publications, and $^{11}$C-PBR28, in 16 publications. The first article (*32*) using $^{11}$C-PK11195 in AD was published in 1995 and the first ones (*33,34*) using $^{11}$C-PBR28, in 2013. Several studies have used an arterial input function (Supplemental Table 1; supplemental materials are available at http://jnm.snmjournals.org), but in AD the cerebellum is spared until the disease is very advanced and may serve as a pseudoreference region, that is, a region with TSPO receptors but no change in patients (*4*).

*TSPO PET at the Clinical Alzheimer Disease (AD) Stage.* At the clinical AD stage, most studies have detected significant neuroinflammation. Brain regions most often affected have been the medial temporal region, including the entorhinal cortex; temporoparietal association cortex, including precuneus; and cingulate cortex (*35–37*). The localization of inflammation matched the clinical syndrome (*37*) and correlated negatively with metabolism measured with $^{18}$F-FDG PET (*35–37*). Furthermore, the degree of TSPO uptake correlated with worse cognition (*33,38,39*), better than the degree of amyloid deposition and, together with the degree of tau deposition, predicted the degree of cognitive worsening over 3 y (*40*). Inflammation correlated with white matter changes (*41*) and impaired large-scale functional connectivity on MRI (*42*).

*TSPO PET at the Mild Cognitive Impairment (MCI) Stage.* Abnormal TSPO density (*43*) has not been found as consistently in MCI as in AD, with some studies reporting no difference with controls (*33*). Most cross-sectional studies reported greater neuroinflammation in the AD than in the MCI stage (*36,44*), although greater inflammation at the MCI stage has also been reported (*45*). To this variability may contribute the behavior of neuroinflammation at the MCI stage. A biphasic inflammation peak has been postulated by following MCI patients longitudinally with repeated TSPO PET over 2 y. Some patients with greater initial inflammation had decreased inflammation in the second scan, although their β-amyloid levels continued to rise (*31,46*). This observation supported the notion that initial inflammation may be neuroprotective (*31*), a concept supported by slower decline in patients with more initial inflammation at the MCI stage (*47*) and the inverse correlation between inflammation and neurofilament light levels (*48*). As at the AD stage, in MCI a negative correlation has been found between regional inflammation and metabolism (*49*). The relation of TSPO density to a marker of neurodegeneration, cortical atrophy on MRI, is complex. At the AD and MCI stages, inflammation was associated with decreased cortical thickness in the neocortex but

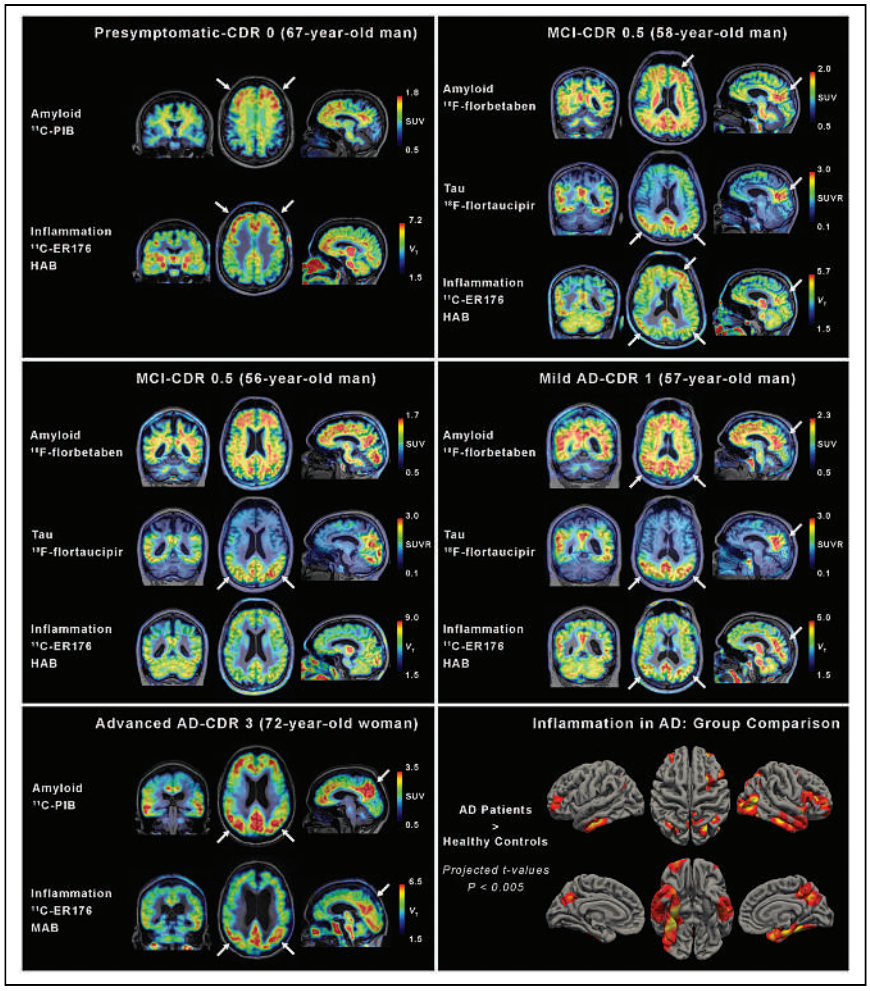


**FIGURE 1.** Translocator protein 18 kDa (TSPO) PET in AD. Inflammation imaging at presymptomatic, MCI, and dementia stages of AD process. In each subject, multimodal imaging is shown, to illustrate spatial correlation of inflammation, in bottom row of every individual scan, with amyloid and tau imaging. CDR = clinical dementia rating scale; HAB = TSPO-high-affinity binder subject; MAB = TSPO-mixed-affinity binder subject; SUVR = standardized uptake value ratio; $V_T$ = volume of distribution.

not in the hippocampus (*50*). However, at the early MCI stage, inflammation was associated with increased gray matter volume, including in the hippocampus (*51*).

*TSPO PET at the Presymptomatic Stage.* A few studies at the presymptomatic stage, defined by normal cognition but abnormal amyloid brain deposition, have reported variable findings. Although an association of inflammation with amyloid deposition, but not with tau, has been reported in presymptomatic individuals (*52*), a closer correlation of inflammation with amyloid has been reported at the stage when amyloid PET is still negative, rather than when it becomes positive, although then the absolute level of inflammation is higher (*53*). This intriguing finding suggests that inflammation may be a very early factor in the neurodegenerative cascade (*44*), just as shown in experimental animal models.

*TSPO PET in Normal Aging.* Initial PET studies, when amyloid imaging was not consistently performed, found increased TSPO binding in subcortical structures and, particularly, in the thalamus of cognitively unimpaired older people (*54,55*). This aging effect may interfere with the interpretation of studies in diseases that affect the basal ganglia, such as corticobasal degeneration or progressive supranuclear palsy unless controls are closely matched by age. Increased inflammation with aging has also been reported in cortical regions (*44,52*).

*TSPO Versus β-Amyloid and Tau Brain Density.* To ensure that the cognitive impairment is due to AD, most groups are currently reporting the β-amyloid and tau status of the subjects studied. Thus, the relation of neuroinflammation to the proteins characteristic of AD is being clarified (Fig. 1). The scant studies at the presymptomatic stage are discussed in the previous section. At the MCI and AD stages, the degree and location of neuroinflammation are correlated with both amyloid and tau deposition but reported r values oscillate around 0.35 for both associations (*44*), reflecting in part that amyloid and tau deposition are only partially colocalized (*45*). Inflammation may correlate more closely with amyloid at the MCI stage and with tau at the AD stage (*45,46*).

### Dementia with Lewy-Bodies (DLB)

DLB is characterized clinically by progressive cognitive impairment with fluctuating cognition; visual hallucinations; REM sleep behavior disorder, which may precede cognitive decline; and one or more cardinal features of parkinsonism (*56*). Pathologically, the protein α-synuclein is present in intraneuronal Lewy bodies and neurites spread throughout the cortex, hippocampus, and amygdala (*57*). About 50% of DLB patients have associated AD pathology (*58*). This association is more frequent with advancing age and confers a worse prognosis (*58*). Several studies have reported increased neuroinflammation (*59,60*) and a negative correlation between inflammation and metabolism (*35,61*). A positive correlation with tau has also been reported (*62*). Individuals with glucocerebrosidase mutations are predisposed to DLB (*63*). They have been reported to have increased neuroinflammation (*64*).

### Parkinson Disease (PD)

Clinically, PD presents with bradykinesia, rigidity, and resting tremor. Pathologically, while there are neuronal loss and Lewy bodies in the substantia nigra, these changes are not widespread in the cortex, hippocampus, and amygdala, as they are in DLB. PET TSPO findings have not been uniform. Increased inflammation in the midbrain or other regions of the brain has been found in some studies (*61,65*) but not in others (*66,67*). In a large study, it was reported that multiple-system atrophy, which presents with parkinsonian clinical findings, was associated with increased brain $^{11}$C-PBR28 uptake, which PD is not, thus allowing for a ready differentiation of either disease (*66*).

### Frontotemporal Dementia (FTD)

This heterogeneous group of diseases, known also as frontotemporal lobar degeneration, encompasses disorders that begin with behavioral, language, or motor impairment and are associated with

tau or TDP-43 deposition in the brain. Neuroinflammation plays a major role in FTD (*2*) and it has been shown to be increased in the likely location of pathology (*68–70*), which differs among FTD variants. Thus, inflammation is greatest in the frontal and temporal poles in behavioral variant, premotor cortex in nonfluent primary progressive aphasia, in superomedial convexity in corticobasal degeneration, and temporal lobe in semantic dementia (Fig. 2). Although in semantic dementia the damage begins and is greatest in the temporal tip, inflammation is greatest at the periphery of the affected region, suggesting a major role for inflammation in damage propagation (Fig. 2) (*71*). In progressive supranuclear palsy, greater neuroinflammation may predict faster worsening (*72*).

### Amyotrophic Lateral Sclerosis (ALS)

Inflammation has been found in the paracentral cortex, which is most affected in ALS (*73*). Although an abnormal signal was detected with the TSPO tracers $^{11}$C-PBR28 and $^{18}$F-DPA714 (*12*), in a small study no signal was detected in ALS using the purine receptor P2 × 7 tracer $^{11}$C-JNJ54173717 (*74*).

### Other Neurodegenerative Disorders

*Huntington's Chorea.* Genetic testing allows for the determination of the carrier state at the presymptomatic stage of the fully penetrant autosomal dominantly inherited disorder. Some (*75*) but not others (*76*) have found increased neuroinflammation in subjects at risk, whereas there is consensus on the presence of neuroinflammation in symptomatic patients (*76,77*).

*Nieman–Pick Disease.* In adult Nieman–Pick disease, neuroinflammation was increased in the white matter and correlated with decreased fractional anisotropy (*78*).

*Chronic Traumatic Encephalopathy.* Chronic traumatic encephalopathy may be considered to have a neurodegenerative component, as have many other diseases, such as multiple sclerosis. Although these disorders are not covered in this review, some of the studies of neuroinflammation in chronic traumatic encephalopathy are listed in Supplemental Table 1.

## LIMITATIONS OF TSPO PET

As a marker of neuroinflammation, TSPO has 2 major limitations: it is not specific for activated microglia and does not differentiate between microglia that protect or harm neurons.

### No Selectivity to Cell Type

Although activated microglia are often considered as the main neuroinflammatory cell, astrocytes play critical roles in neuroinflammation. Both microglia and astrocytes respond to Aβ plaques but the response is different, possibly because microglia respond to the chemotactic effects of Aβ whereas astrocytes respond to neuritic damage (*79*). Astrocytes are heavily involved in the clearance of Aβ (*80*). However, close interactions between these 2 types of glia may be linked to neurodegenerative pathology. Activated microglia induce neurotoxic reactive astrocytes (*81*). The interaction of the microglial receptor TREM2 with lipoparticles is integral for the transfer of cholesterol from astrocytes to microglia (*82*), and mutations in *TREM2* increase AD risk (*83*). All these rich interactions are not identifiable by TSPO PET, which provides a snapshot of the regional density in the brain of both microglia and astrocytes.

### No Differentiation Between Beneficial and Detrimental Effects of Inflammation

Neuroinflammation has both protective and damaging effects. Although activation of microglia at early stages facilitates phagocytosis of Aβ plaques and maintains neuronal survival, chronic inflammation becomes skewed toward a proinflammatory pattern, which might be neurotoxic (*84*). Ongoing inflammation may also facilitate phosphorylation and truncation of tau, causing further damage to neurons (*85*). TSPO PET studies in both humans (reviewed in the section "TSPO PET at the Mild Cognitive Impairment [MCI] Stage") and mice suggest that TSPO presents 2 peaks in the AD process: an earlier peak, associated with neuroprotection, and a later peak as the disease worsens, associated with neurotoxicity (*31,86,87*). The 2 facets of inflammation indicate that simple suppression of inflammation may not help AD. Therefore, novel therapies are being developed to shift microglia from neurotoxic to neuroprotective (*88*).

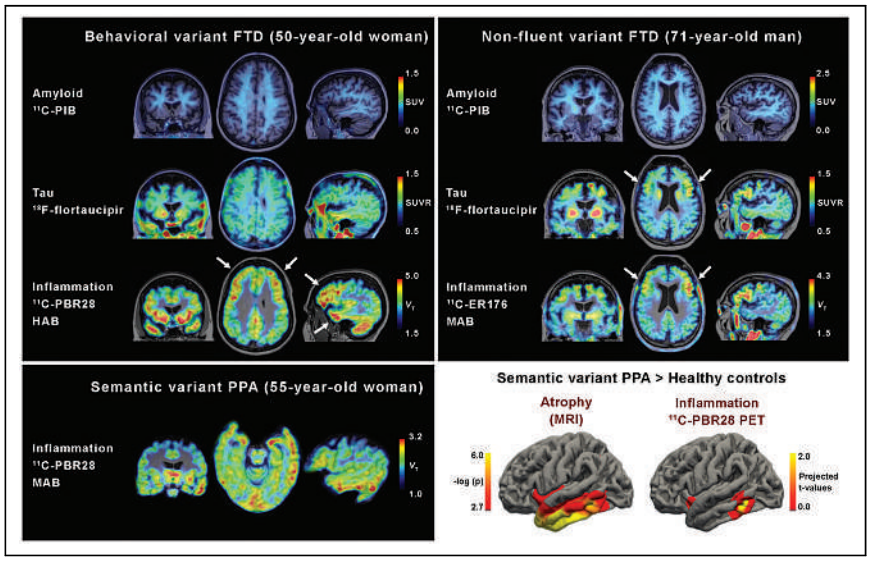


**FIGURE 2.** TSPO PET in FTD. Inflammation imaging in behavioral variant of FTD and in the nonfluent and semantic variants of primary progressive aphasia (PPA), also categorized as FTD. Amyloid PET was negative in all subjects. In semantic variant PPA, peak of inflammation is at periphery of most affected area, which has atrophy on MRI. HAB = TSPO-high-affinity binder subject; MAB = TSPO-mixed-affinity binder subject; SUVR = standardized uptake value ratio; $V_T$ = volume of distribution. (Lower 2 panels are adapted with permission of (*71*)).

## NEW INFLAMMATION IMAGING TARGETS TO OVERCOME THE LIMITATIONS OF TSPO PET

To overcome these limitations, new and improved imaging markers are being investigated.

### Cell-Type Selective Imaging

Colony-stimulating factor 1 receptor (CSF1R) is predominantly expressed by microglia and macrophages and plays a key role in differentiation and survival of immune cells (*89*). Inhibitors of CSF1R

decrease microglia and prevent loss of neurons and memory (*90*). A novel ligand, $^{11}$C-CPPC, successfully detected an increase in CSF1R in rodent and nonhuman primate after bacterial lipopolysaccharide was administered (*91*), but it had off-target and low specific binding (*92*). Another ligand, $^{11}$C-GW2580, detected increased microglia in a rodent model of neuroinflammation with greater sensitivity than $^{11}$C-CPPC (*93*).

Monoamine oxidase-B (MAO-B) is a potential PET marker of astrocytes. MAO-B is highly expressed by astrocytes and serotonin (5-HT)-releasing neurons but not by microglia (*94*). MAO-B is upregulated in reactive astrocytes (*95*) and correlates with glial fibrillary acidic protein (*96*). To image MAO-B, L-$^{11}$C-deprenyl has been used since the 1980s (*97*). The irreversible nature of tracer uptake makes the PET measurement more sensitive to blood flow than to the enzyme activity, especially in areas with high MAO-B activity (*98*). To cope with this limitation, a deuterium-substituted PET tracer, L-$^{11}$C-deprenyl-$D_2$, was developed (*97*). Still, the specific-to-nondisplaceable ratio of L-$^{11}$C-deprenyl is only 1.5 in humans (*99*). Semiquantitative analyses in healthy humans indicated that a new ligand to image MAO-B, $^{18}$F-SMBT-1 (*100*), has a $BP_{ND}$ of approximately 6, which is about 4 times greater than that of L-$^{11}$C-deprenyl (*101*).

### Differentiating Beneficial and Detrimental Effects of Neuroinflammation

Because TSPO PET imaging does not differentiate between beneficial and detrimental effects of neuroinflammation, better PET markers are needed to monitor novel immunomodulatory therapies. For this purpose, potential markers are two adenosine diphosphate (ADP) / adenosine triphosphate (ATP) receptors with markedly different functions, $P2X_7$ and $P2Y_{12}$. Both $P2X_7$ and $P2Y_{12}$ are highly expressed by microglia. $P2X_7$ has proinflammatory functions. Increased ATP and ADP in the extracellular space activates $P2X_7$ and leads to proinflammatory cytokines (*102*). On the contrary, in basic studies, $P2Y_{12}$ is used as a marker of homeostatic microglia and may protect neurons by regulating somatic microglia-neuron junctions (*103*). Postmortem studies on AD showed increased $P2X_7$ (*104,105*) and decreased $P2Y_{12}$ (*106*), consistent with greater detrimental than neuroprotective effects of neuroinflammation in moderate-advanced stages of AD. To image $P2X_7$, $^{18}$F-JNJ-64413739 (*107*) and $^{11}$C-JNJ54173717 (*108*) have been successfully used in humans. PET ligands to image $P2Y_{12}$ are still under development.

## OTHER PET MARKERS TO STUDY NEUROINFLAMMATION

In the following, we list a few additional markers of neuroinflammation, for which PET scans have detected specific binding.

### Type 2 Cannabinoid Receptor (CB2)

CB2 is involved in immunomodulatory functions and expressed by microglia, astrocytes, and neurons (*109*). Activation of CB2 shows protective effects against Aβ (*110*). Several PET ligands are being developed to image CB2 (*111*). Among these, the most tested is $^{11}$C-NE40, which has been used to compare healthy controls and AD patients and showed a decrease in AD (*112*). Because type 1 cannabinoid receptor (CB1) is highly and widely expressed in brain, high selectivity against CB1 is required to interpret CB2 PET results.

### Mitochondrial Function and Reactive Oxygen Species

Because mitochondrial dysfunction has been reported in neurodegenerative disorders such as AD and PD and linked to neuroinflammation (*113*), there have been attempts to image mitochondrial activity. The most explored imaging target is mitochondrial complex 1 (MC1) imaged with $^{18}$F-BCPP-EF (*114*). MC1 is the first enzyme complex in the electron transfer chain, having a critical role in oxidative phosphorylation in mitochondria. AD patients had reduced $^{18}$F-BCPP-EF binding in the medial temporal cortex, which negatively correlated with tau (*113*). Recent attempts to image reactive oxygen species detected an increase induced by the local injection of bacterial lipopolysaccharide (*115*).

### Phosphodiesterase Type 4B (PDE4B)

Cyclic nucleotide phosphodiesterases are enzymes that hydrolyze the second messengers, cyclic adenosine monophosphate (cAMP) and cyclic guanosine monophosphate. Among 11 families of PDE, phosphodiesterase type 4, expressed by neurons and immune cells, is one of the main enzymes hydrolyzing cAMP. Among the 4 subtypes, A, B, C, and D, subtype B (PDE4B) is involved in microglial functions in neuroinflammation (*116*). Proinflammatory cytokines such as IL-1β and TNF-α increase PDE4B. A PET ligand, $^{18}$F-PF-06445974, has been developed to selectively image PDE4B (*117*).

## LINKAGE BETWEEN PERIPHERAL AND CENTRAL INFLAMMATION

In addition to inflammation within the brain, inflammation in peripheral tissue and organs and interactions between peripheral and central inflammation are increasingly being recognized as important in pathogenesis. A pathogen of periodontitis was found in the brain of AD patients (*118*), and Aβ protects against microbial infection (*119*). Gut bacteria are involved in the production of α-synuclein, which accumulates in PD and DLB brain. Newly developed total body scanners allow for the gathering of full dynamic data in both brain and peripheral tissues and organs and open new opportunities to explore interactions between peripheral and central inflammation. In the brain, the choroid plexus is the major component of the blood–cerebrospinal fluid barrier, which may be a major player to connect peripheral and central inflammation (*120*). The function of the choroid plexus in neuroinflammation and neurodegeneration can be studied by brain imaging.

## DISCLOSURE

Joseph Masdeu is a consultant and received research funding from Eli Lilly, parent co. of Avid Radiopharmaceuticals, manufacturer of $^{18}$F-flortaucipir. No other potential conflict of interest relevant to this article was reported.

## REFERENCES

1. Ising C, Venegas C, Zhang S, et al. NLRP3 inflammasome activation drives tau pathology. *Nature.* 2019;575:669–673.
2. Bright F, Werry EL, Dobson-Stone C, et al. Neuroinflammation in frontotemporal dementia. *Nat Rev Neurol.* 2019;15:540–555.
3. Guo Q, Owen DR, Rabiner EA, Turkheimer FE, Gunn RN. A graphical method to compare the in vivo binding potential of PET radioligands in the absence of a reference region: application to [$^{11}$C]PBR28 and [$^{118}$F]PBR111 for TSPO imaging. *J Cereb Blood Flow Metab.* 2014;34:1162–1168.
4. Zanotti-Fregonara P, Kreisl WC, Innis RB, Lyoo CH. Automatic extraction of a reference region for the noninvasive quantification of translocator protein in brain using $^{11}$C-PBR28. *J Nucl Med.* 2019;60:978–984.

5. Papadopoulos V, Baraldi M, Guilarte TR, et al. Translocator protein (18kDa): new nomenclature for the peripheral-type benzodiazepine receptor based on its structure and molecular function. *Trends Pharmacol Sci.* 2006;27:402–409.
6. Notter T, Coughlin JM, Gschwind T, et al. Translational evaluation of translocator protein as a marker of neuroinflammation in schizophrenia. *Mol Psychiatry.* 2018; 23:323–334.
7. Notter T, Schalbetter SM, Clifton NE, et al. Neuronal activity increases translocator protein (TSPO) levels. *Mol Psychiatry.* 2021;26:2025–2037.
8. Gui Y, Marks JD, Das S, Hyman BT, Serrano-Pozo A. Characterization of the 18 kDa translocator protein (TSPO) expression in post-mortem normal and Alzheimer's disease brains. *Brain Pathol.* 2020;30:151–164.
9. Xu J, Sun J, Perrin RJ, et al. Translocator protein in late stage Alzheimer's disease and Dementia with Lewy bodies brains. *Ann Clin Transl Neurol.* 2019;6: 1423–1434.
10. Metaxas A, Thygesen C, Briting SRR, Landau AM, Darvesh S, Finsen B. Increased inflammation and unchanged density of synaptic vesicle glycoprotein 2A (SV2A) in the postmortem frontal cortex of Alzheimer's Disease patients. *Front Cell Neurosci.* 2019;13:538.
11. Ni R, Röjdner J, Voytenko L, et al. In vitro characterization of the regional binding distribution of amyloid PET tracer florbetaben and the glia tracers deprenyl and PK11195 in autopsy Alzheimer's brain tissue. *J Alzheimers Dis.* 2021;80: 1723–1737.
12. Van Weehaeghe D, Babu S, De Vocht J, et al. Moving toward multicenter therapeutic trials in amyotrophic lateral sclerosis: feasibility of data pooling using different translocator protein PET radioligands. *J Nucl Med.* 2020;61: 1621–1627.
13. Kreisl WC, Fujita M, Fujimura Y, et al. Comparison of [$^{11}$C]-(*R*)-PK 11195 and [$^{11}$C]PBR28, two radioligands for translocator protein (18 kDa) in human and monkey: Implications for positron emission tomographic imaging of this inflammation biomarker. *Neuroimage.* 2010;49:2924–2932.
14. Fujita M, Kobayashi M, Ikawa M, et al. Comparison of four $^{11}$C-labeled PET ligands to quantify translocator protein 18 kDa (TSPO) in human brain: (R)-PK11195, PBR28, DPA-713, and ER176-based on recent publications that measured specific-to-non-displaceable ratios. *EJNMMI Res.* 2017;7:84.
15. Okuyama S, Chaki S, Yoshikawa R, et al. Neuropharmacological profile of peripheral benzodiazepine receptor agonists, DAA1097 and DAA1106. *Life Sci.* 1999;64:1455–1464.
16. Zhang MR, Kida T, Noguchi J, et al. [$^{11}$C]DAA1106: radiosynthesis and in vivo binding to peripheral benzodiazepine receptors in mouse brain. *Nucl Med Biol.* 2003;30:513–519.
17. Briard E, Zoghbi SS, Imaizumi M, et al. Synthesis and evaluation in monkey of two sensitive $^{11}$C-labeled aryloxyanilide ligands for imaging brain peripheral benzodiazepine receptors in vivo. *J Med Chem.* 2008;51:17–30.
18. James ML, Fulton RR, Henderson DJ, et al. Synthesis and in vivo evaluation of a novel peripheral benzodiazepine receptor PET radioligand. *Bioorg Med Chem.* 2005;13:6188–6194.
19. Zanotti-Fregonara P, Pascual B, Rizzo G, et al. Head-to-head comparison of $^{11}$C-PBR28 and $^{18}$F-GE180 for quantification of the translocator protein in the human brain. *J Nucl Med.* 2018;59:1260–1266.
20. Innis RB, Cunningham VJ, Delforge J, et al. Consensus nomenclature for in vivo imaging of reversibly binding radioligands. *J Cereb Blood Flow Metab.* 2007;27: 1533–1539.
21. Feeney C, Scott G, Raffel J, et al. Kinetic analysis of the translocator protein positron emission tomography ligand [$^{18}$F]GE-180 in the human brain. *Eur J Nucl Med Mol Imaging.* 2016;43:2201–2210.
22. Owen DR, Yeo AJ, Gunn RN, et al. An 18-kDa translocator protein (TSPO) polymorphism explains differences in binding affinity of the PET radioligand PBR28. *J Cereb Blood Flow Metab.* 2012;32:1–5.
23. Cymerman U, Pazos A, Palacios JM. Evidence for species differences in 'peripheral' benzodiazepine receptors: an autoradiographic study. *Neurosci Lett.* 1986;66:153–158.
24. Imaizumi M, Briard E, Zoghbi SS, et al. Brain and whole-body imaging in nonhuman primates of [$^{11}$C]PBR28, a promising PET radioligand for peripheral benzodiazepine receptors. *Neuroimage.* 2008;39:1289–1298.
25. Fujita M, Imaizumi M, Zoghbi SS, et al. Kinetic analysis in healthy humans of a novel positron emission tomography radioligand to image the peripheral benzodiazepine receptor, a potential biomarker for inflammation. *Neuroimage.* 2008;40: 43–52.
26. Cunningham VJ, Rabiner EA, Slifstein M, Laruelle M, Gunn RN. Measuring drug occupancy in the absence of a reference region: the Lassen plot re-visited. *J Cereb Blood Flow Metab.* 2010;30:46–50.
27. Montagne A, Nation DA, Sagare AP, et al. APOE4 leads to blood-brain barrier dysfunction predicting cognitive decline. *Nature.* 2020;581:71–76.
28. Schwartzentruber J, Cooper S, Liu JZ, et al. Genome-wide meta-analysis, fine-mapping and integrative prioritization implicate new Alzheimer's disease risk genes. *Nat Genet.* 2021;53:392–402.
29. Srinivasan K, Friedman BA, Etxeberria A, et al. Alzheimer's patient microglia exhibit enhanced aging and unique transcriptional activation. *Cell Rep.* 2020;31: 107843.
30. Felsky D, Roostaei T, Nho K, et al. Neuropathological correlates and genetic architecture of microglial activation in elderly human brain. *Nat Commun.* 2019; 10:409.
31. Fan Z, Brooks DJ, Okello A, Edison P. An early and late peak in microglial activation in Alzheimer's disease trajectory. *Brain.* 2017;140:792–803.
32. Groom GN, Junck L, Foster NL, Frey KA, Kuhl DE. PET of peripheral benzodiazepine binding sites in the microgliosis of Alzheimer's disease. *J Nucl Med.* 1995;36:2207–2210.
33. Kreisl WC, Lyoo CH, McGwier M, et al; Biomarkers Consortium PET Radioligand Project Team. In vivo radioligand binding to translocator protein correlates with severity of Alzheimer's disease. *Brain.* 2013;136:2228–2238.
34. Kim S, Nho K, Risacher SL, et al. PARP1 gene variation and microglial activity on [$^{11}$C]PBR28 PET in older adults at risk for Alzheimer's disease. *Multimodal Brain Image Anal.* 2013;8159:150–158.
35. Fan Z, Aman Y, Ahmed I, et al. Influence of microglial activation on neuronal function in Alzheimer's and Parkinson's disease dementia. *Alzheimers Dement.* 2015;11:608–21.e7.
36. Kreisl WC, Lyoo CH, Liow JS, et al. $^{11}$C-PBR28 binding to translocator protein increases with progression of Alzheimer's disease. *Neurobiol Aging.* 2016;44: 53–61.
37. Tondo G, Iaccarino L, Caminiti SP, et al. The combined effects of microglia activation and brain glucose hypometabolism in early-onset Alzheimer's disease. *Alzheimers Res Ther.* 2020;12:50.
38. Lindgren N, Tuisku J, Vuoksimaa E, et al. Association of neuroinflammation with episodic memory: a [$^{11}$C]PBR28 PET study in cognitively discordant twin pairs. *Brain Commun.* 2020;2:fcaa024.
39. Passamonti L, Rodríguez PV, Hong YT, et al. [$^{11}$C]PK11195 binding in Alzheimer disease and progressive supranuclear palsy. *Neurology.* 2018;90:e1989–e1996.
40. Malpetti M, Kievit RA, Passamonti L, et al. Microglial activation and tau burden predict cognitive decline in Alzheimer's disease. *Brain.* 2020;143:1588–1602.
41. Low A, Mak E, Malpetti M, et al. In vivo neuroinflammation and cerebral small vessel disease in mild cognitive impairment and Alzheimer's disease. *J Neurol Neurosurg Psychiatry.* 2020;92:45–52.
42. Passamonti L, Tsvetanov KA, Jones PS, et al. Neuroinflammation and functional connectivity in Alzheimer's disease: interactive influences on cognitive performance. *J Neurosci.* 2019;39:7218–7226.
43. Fan Z, Dani M, Femminella GD, et al. Parametric mapping using spectral analysis for $^{11}$C-PBR28 PET reveals neuroinflammation in mild cognitive impairment subjects. *Eur J Nucl Med Mol Imaging.* 2018;45:1432–1441.
44. Pascoal TA, Benedet AL, Ashton NJ, et al. Microglial activation and tau propagate jointly across Braak stages. *Nat Med.* 2021;27:1592–1599.
45. Dani M, Wood M, Mizoguchi R, et al. Microglial activation correlates in vivo with both tau and amyloid in Alzheimer's disease. *Brain.* 2018;141: 2740–2754.
46. Ismail R, Parbo P, Madsen LS, et al. The relationships between neuroinflammation, beta-amyloid and tau deposition in Alzheimer's disease: a longitudinal PET study. *J Neuroinflammation.* 2020;17:151.
47. Hamelin L, Lagarde J, Dorothée G, et al. Distinct dynamic profiles of microglial activation are associated with progression of Alzheimer's disease. *Brain.* 2018; 141:1855–1870.
48. Parbo P, Madsen LS, Ismail R, et al. Low plasma neurofilament light levels associated with raised cortical microglial activation suggest inflammation acts to protect prodromal Alzheimer's disease. *Alzheimers Res Ther.* 2020;12:3.
49. Tondo G, Boccalini C, Caminiti SP, et al. Brain metabolism and microglia activation in mild cognitive impairment: A combined [$^{18}$F]FDG and [$^{11}$C]-(R)-PK11195 PET study. *J Alzheimers Dis.* 2021;80:433–445.
50. Nicastro N, Malpetti M, Mak E, et al. Gray matter changes related to microglial activation in Alzheimer's disease. *Neurobiol Aging.* 2020;94:236–242.
51. Femminella GD, Dani M, Wood M, et al. Microglial activation in early Alzheimer trajectory is associated with higher gray matter volume. *Neurology.* 2019;92: e1331–e1343.
52. Zou J, Tao S, Johnson A, et al. Microglial activation, but not tau pathology, is independently associated with amyloid positivity and memory impairment. *Neurobiol Aging.* 2020;85:11–21.
53. Toppala S, Ekblad LL, Tuisku J, et al. Association of early beta-amyloid accumulation and neuroinflammation measured with [$^{11}$C]PBR28 in elderly individuals without dementia. *Neurology.* 2021;96:e1608–e1619.

54. Kumar A, Muzik O, Shandal V, Chugani D, Chakraborty P, Chugani HT. Evaluation of age-related changes in translocator protein (TSPO) in human brain using $^{11}$C-[R]-PK11195 PET. *J Neuroinflammation.* 2012;9:232.
55. Schuitemaker A, van der Doef TF, Boellaard R, et al. Microglial activation in healthy aging. *Neurobiol Aging.* 2012;33:1067–1072.
56. McKeith IG, Boeve BF, Dickson DW, et al. Diagnosis and management of dementia with Lewy bodies: fourth consensus report of the DLB Consortium. *Neurology.* 2017;89:88–100.
57. Dickson DW. Dementia with Lewy bodies: neuropathology. *J Geriatr Psychiatry Neurol.* 2002;15:210–216.
58. Irwin DJ, Grossman M, Weintraub D, et al. Neuropathological and genetic correlates of survival and dementia onset in synucleinopathies: a retrospective analysis. *Lancet Neurol.* 2017;16:55–65.
59. Iannaccone S, Cerami C, Alessio M, et al. In vivo microglia activation in very early dementia with Lewy bodies, comparison with Parkinson's disease. *Parkinsonism Relat Disord.* 2013;19:47–52.
60. Surendranathan A, Su L, Mak E, et al. Early microglial activation and peripheral inflammation in dementia with Lewy bodies. *Brain.* 2018;141:3415–3427.
61. Edison P, Ahmed I, Fan Z, et al. Microglia, amyloid, and glucose metabolism in Parkinson's disease with and without dementia. *Neuropsychopharmacology.* 2013;38:938–949.
62. Mak E, Nicastro N, Malpetti M, et al. Imaging tau burden in dementia with Lewy bodies using [$^{18}$F]-AV1451 positron emission tomography. *Neurobiol Aging.* 2021;101:172–180.
63. Goker-Alpan O, Masdeu JC, Kohn PD, et al. The neurobiology of glucocerebrosidase-associated parkinsonism: a positron emission tomography study of dopamine synthesis and regional cerebral blood flow. *Brain.* 2012;135:2440–2448.
64. Mullin S, Stokholm MG, Hughes D, et al. Brain microglial activation increased in glucocerebrosidase (GBA) mutation carriers without Parkinson's disease. *Mov Disord.* 2021;36:774–779.
65. Lavisse S, Goutal S, Wimberley C, et al. Increased microglial activation in patients with Parkinson disease using [$^{18}$F]-DPA714 TSPO PET imaging. *Parkinsonism Relat Disord.* 2021;82:29–36.
66. Jucaite A, Cselenyi Z, Kreisl WC, et al. Glia imaging differentiates multiple system atrophy from Parkinson's disease: a positron emission tomography study with [$^{11}$C]PBR28 and machine learning analysis. *Mov Disord.* 2022;37:119–129.
67. Varnäs K, Cselényi Z, Jucaite A, et al. PET imaging of [$^{11}$C]PBR28 in Parkinson's disease patients does not indicate increased binding to TSPO despite reduced dopamine transporter binding. *Eur J Nucl Med Mol Imaging.* 2019;46:367–375.
68. Bevan-Jones WR, Cope TE, Jones PS, et al. Neuroinflammation and protein aggregation co-localize across the frontotemporal dementia spectrum. *Brain.* 2020;143:1010–1026.
69. Malpetti M, Rittman T, Jones PS, et al. In vivo PET imaging of neuroinflammation in familial frontotemporal dementia. *J Neurol Neurosurg Psychiatry.* 2021;92:319–322.
70. Zhang J. Mapping neuroinflammation in frontotemporal dementia with molecular PET imaging. *J Neuroinflammation.* 2015;12:108.
71. Pascual B, Funk Q, Zanotti-Fregonara P, et al. Neuroinflammation is highest in areas of disease progression in semantic dementia. *Brain.* 2021;144:1565–1575.
72. Malpetti M, Passamonti L, Jones PS, et al. Neuroinflammation predicts disease progression in progressive supranuclear palsy. *J Neurol Neurosurg Psychiatry.* 2021;92:769–775.
73. Alshikho MJ, Zürcher NR, Loggia ML, et al. Integrated magnetic resonance imaging and [$^{11}$C]-PBR28 positron emission tomographic imaging in amyotrophic lateral sclerosis. *Ann Neurol.* 2018;83:1186–1197.
74. Van Weehaeghe D, Van Schoor E, De Vocht J, et al. TSPO versus P2X7 as a target for neuroinflammation: An in vitro and in vivo study. *J Nucl Med.* 2020;61:604–607.
75. Politis M, Lahiri N, Niccolini F, et al. Increased central microglial activation associated with peripheral cytokine levels in premanifest Huntington's disease gene carriers. *Neurobiol Dis.* 2015;83:115–121.
76. Rocha NP, Charron O, Latham LB, et al. Microglia activation in basal ganglia is a late event in Huntington disease pathophysiology. *Neurol Neuroimmunol Neuroinflamm.* 2021;8:e984.
77. Lois C, González I, Izquierdo-García D, et al. Neuroinflammation in Huntington's disease: new insights with $^{11}$C-PBR28 PET/MRI. *ACS Chem Neurosci.* 2018;9:2563–2571.
78. Walterfang M, Di Biase MA, Cropley VL, et al. Imaging of neuroinflammation in adult Niemann-Pick type C disease: a cross-sectional study. *Neurology.* 2020;94:e1716–e1725.
79. Serrano-Pozo A, Muzikansky A, Gómez-Isla T, et al. Differential relationships of reactive astrocytes and microglia to fibrillar amyloid deposits in Alzheimer disease. *J Neuropathol Exp Neurol.* 2013;72:462–471.
80. Iliff JJ, Wang M, Liao Y, et al. A paravascular pathway facilitates CSF flow through the brain parenchyma and the clearance of interstitial solutes, including amyloid β. *Sci Transl Med.* 2012;4:147ra111.
81. Liddelow SA, Guttenplan KA, Clarke LE, et al. Neurotoxic reactive astrocytes are induced by activated microglia. *Nature.* 2017;541:481–487.
82. Bohlen CJ, Bennett FC, Tucker AF, Collins HY, Mulinyawe SB, Barres BA. Diverse requirements for microglial survival, specification, and function revealed by defined-medium cultures. *Neuron.* 2017;94:759–773.e8.
83. Jonsson T, Stefansson H, Steinberg S, et al. Variant of TREM2 associated with the risk of Alzheimer's disease. *N Engl J Med.* 2013;368:107–116.
84. Del-Aguila JL, Li Z, Dube U, et al. A single-nuclei RNA sequencing study of Mendelian and sporadic AD in the human brain. *Alzheimers Res Ther.* 2019;11:71.
85. Lee DC, Rizer J, Selenica ML, et al. LPS- induced inflammation exacerbates phospho-tau pathology in rTg4510 mice. *J Neuroinflammation.* 2010;7:56.
86. Hamelin L, Lagarde J, Dorothée G, et al; Clinical IMABio3 team. Early and protective microglial activation in Alzheimer's disease: a prospective study using $^{18}$F-DPA-714 PET imaging. *Brain.* 2016;139:1252–1264.
87. Focke C, Blume T, Zott B, et al. Early and longitudinal microglial activation but not amyloid accumulation predicts cognitive outcome in PS2APP mice. *J Nucl Med.* 2019;60:548–554.
88. Cummings J, Lee G, Ritter A, Sabbagh M, Zhong K. Alzheimer's disease drug development pipeline: 2020. *Alzheimers Dement (N Y).* 2020;6:e12050.
89. Elmore MR, Najafi AR, Koike MA, et al. Colony-stimulating factor 1 receptor signaling is necessary for microglia viability, unmasking a microglia progenitor cell in the adult brain. *Neuron.* 2014;82:380–397.
90. Han J, Chitu V, Stanley ER, Wszolek ZK, Karrenbauer VD, Harris RA. Inhibition of colony stimulating factor-1 receptor (CSF-1R) as a potential therapeutic strategy for neurodegenerative diseases: opportunities and challenges. *Cell Mol Life Sci.* 2022;79:219.
91. Horti AG, Naik R, Foss CA, et al. PET imaging of microglia by targeting macrophage colony-stimulating factor 1 receptor (CSF1R). *Proc Natl Acad Sci USA.* 2019;116:1686–1691.
92. Knight AC, Varlow C, Zi T, et al. In vitro evaluation of [$^{3}$H]CPPC as a tool radioligand for CSF-1R. *ACS Chem Neurosci.* 2021;12:998–1006.
93. Zhou X, Ji B, Seki C, et al. PET imaging of colony-stimulating factor 1 receptor: a head-to-head comparison of a novel radioligand, $^{11}$C-GW2580, and $^{11}$C-CPPC, in mouse models of acute and chronic neuroinflammation and a rhesus monkey. *J Cereb Blood Flow Metab.* 2021;41:2410–2422.
94. Saura J, Kettler R, Da Prada M, Richards JG. Quantitative enzyme radioautography with $^{3}$H-Ro 41-1049 and $^{3}$H-Ro 19-6327 in vitro: localization and abundance of MAO-A and MAO-B in rat CNS, peripheral organs, and human brain. *J Neurosci.* 1992;12:1977–1999.
95. Ekblom J, Jossan SS, Bergström M, Oreland L, Walum E, Aquilonius SM. Monoamine oxidase-B in astrocytes. *Glia.* 1993;8:122–132.
96. Gulyás B, Pavlova E, Kása P, et al. Activated MAO-B in the brain of Alzheimer patients, demonstrated by [$^{11}$C]-L-deprenyl using whole hemisphere autoradiography. *Neurochem Int.* 2011;58:60–68.
97. Fowler JS, Wolf AP, MacGregor RR, et al. Mechanistic positron emission tomography studies: demonstration of a deuterium isotope effect in the monoamine oxidase-catalyzed binding of [$^{11}$C]L-deprenyl in living baboon brain. *J Neurochem.* 1988;51:1524–1534.
98. Lammertsma AA, Bench CJ, Price GW, et al. Measurement of cerebral monoamine oxidase B activity using L-[$^{11}$C]deprenyl and dynamic positron emission tomography. *J Cereb Blood Flow Metab.* 1991;11:545–556.
99. Freedman NM, Mishani E, Krausz Y, et al. In vivo measurement of brain monoamine oxidase B occupancy by rasagiline, using $^{11}$C-l-deprenyl and PET. *J Nucl Med.* 2005;46:1618–1624.
100. Harada R, Hayakawa Y, Ezura M, et al. $^{18}$F-SMBT-1: a selective and reversible PET tracer for monoamine oxidase-B imaging. *J Nucl Med.* 2021;62:253–258.
101. Villemagne VL, Harada R, Dore V, et al. First-in-human evaluation of $^{18}$F-SMBT-1, a novel $^{18}$F-labeled MAO-B PET tracer for imaging reactive astrogliosis. *J Nucl Med*. January 27, 2022 [Epub ahead of print].
102. Bhattacharya A, Biber K. The microglial ATP-gated ion channel P2X7 as a CNS drug target. *Glia.* 2016;64:1772–1787.
103. Cserép C, Pósfai B, Lénárt N, et al. Microglia monitor and protect neuronal function through specialized somatic purinergic junctions. *Science.* 2020;367:528–537.
104. Martin E, Amar M, Dalle C, et al. New role of P2X7 receptor in an Alzheimer's disease mouse model. *Mol Psychiatry.* 2019;24:108–125.
105. McLarnon JG, Ryu JK, Walker DG, Choi HB. Upregulated expression of purinergic P2X(7) receptor in Alzheimer disease and amyloid-beta peptide-treated microglia and in peptide-injected rat hippocampus. *J Neuropathol Exp Neurol.* 2006;65:1090–1097.

106. Mildner A, Huang H, Radke J, Stenzel W, Priller J. $P2Y_{12}$ receptor is expressed on human microglia under physiological conditions throughout development and is sensitive to neuroinflammatory diseases. *Glia.* 2017;65:375–387.
107. Koole M, Schmidt ME, Hijzen A, et al. $^{18}$F-JNJ-64413739, a novel PET ligand for the P2X7 ion channel: radiation dosimetry, kinetic modeling, test-retest variability, and occupancy of the P2X7 antagonist JNJ-54175446. *J Nucl Med.* 2019; 60:683–690.
108. Van Weehaeghe D, Koole M, Schmidt ME, et al. [$^{11}$C]JNJ54173717, a novel P2X7 receptor radioligand as marker for neuroinflammation: human biodistribution, dosimetry, brain kinetic modelling and quantification of brain P2X7 receptors in patients with Parkinson's disease and healthy volunteers. *Eur J Nucl Med Mol Imaging.* 2019;46:2051–2064.
109. Bisogno T, Oddi S, Piccoli A, Fazio D, Maccarrone M. Type-2 cannabinoid receptors in neurodegeneration. *Pharmacol Res.* 2016;111:721–730.
110. Janefjord E, Mååg JL, Harvey BS, Smid SD. Cannabinoid effects on β amyloid fibril and aggregate formation, neuronal and microglial-activated neurotoxicity in vitro. *Cell Mol Neurobiol.* 2014;34:31–42.
111. Ni R, Mu L, Ametamey S. Positron emission tomography of type 2 cannabinoid receptors for detecting inflammation in the central nervous system. *Acta Pharmacol Sin.* 2019;40:351–357.
112. Ahmad R, Postnov A, Bormans G, Versijpt J, Vandenbulcke M, Van Laere K. Decreased in vivo availability of the cannabinoid type 2 receptor in Alzheimer's disease. *Eur J Nucl Med Mol Imaging.* 2016;43:2219–2227.
113. Terada T, Therriault J, Kang MSP, et al. Mitochondrial complex I abnormalities is associated with tau and clinical symptoms in mild Alzheimer's disease. *Mol Neurodegener.* 2021;16:28.
114. Fukumoto D, Nishiyama S, Harada N, Yamamoto S, Tsukada H. Detection of ischemic neuronal damage with [$^{118}$F]BMS-747158-02, a mitochondrial complex-1 positron emission tomography ligand: small animal PET study in rat brain. *Synapse.* 2012;66:909–917.
115. Hou C, Hsieh CJ, Li S, et al. Development of a positron emission tomography radiotracer for imaging elevated levels of superoxide in neuroinflammation. *ACS Chem Neurosci.* 2018;9:578–586.
116. Pearse DD, Hughes ZA. PDE4B as a microglia target to reduce neuroinflammation. *Glia.* 2016;64:1698–1709.
117. Zhang L, Chen L, Beck EM, et al. The discovery of a novel phosphodiesterase (PDE) 4B-preferring radioligand for positron emission tomography (PET) imaging. *J Med Chem.* 2017;60:8538–8551.
118. Dominy SS, Lynch C, Ermini F, et al. *Porphyromonas gingivalis* in Alzheimer's disease brains: Evidence for disease causation and treatment with small-molecule inhibitors. *Sci Adv.* 2019;5:eaau3333.
119. Kumar DK, Choi SH, Washicosky KJ, et al. Amyloid-β peptide protects against microbial infection in mouse and worm models of Alzheimer's disease. *Sci Transl Med.* 2016;8:340ra72.
120. Carloni S, Bertocchi A, Mancinelli S, et al. Identification of a choroid plexus vascular barrier closing during intestinal inflammation. *Science.* 2021;374:439–448.

# Cyclooxygenases as Potential PET Imaging Biomarkers to Explore Neuroinflammation in Dementia

Bruny V. Kenou*, Lester S. Manly*, Sara B. Rubovits*, Somachukwu A. Umeozulu*, Maia G. Van Buskirk*, Andrea S. Zhang*, Victor W. Pike, Paolo Zanotti-Fregonara, Ioline D. Henter, and Robert B. Innis

*Molecular Imaging Branch, National Institute of Mental Health, National Institutes of Health, Bethesda, Maryland*

The most frequently studied target of neuroinflammation using PET is 18-kDa translocator protein, but its limitations have spurred the molecular imaging community to find more promising targets. This article reviews the development of PET radioligands for cyclooxygenase (COX) subtypes 1 and 2, enzymes that catalyze the production of inflammatory prostanoids in the periphery and brain. Although both isozymes produce the same precursor compound, prostaglandin $H_2$, they have distinct functions based on their differential cellular localization in the periphery and brain. For example, COX-1 is located primarily in microglia, a resident inflammatory cell in the brain whose role in producing inflammatory cytokines is well documented. In contrast, COX-2 is located primarily in neurons and can be markedly upregulated by inflammatory and excitatory stimuli, but its functions are poorly understood. This article reviews these 2 isozymes as biomarkers of neuroinflammation, as well as the radioligands that have recently been developed to image them in animals and humans. To place this work into context, the properties of COX-1 and COX-2 are compared with 18-kDa translocator protein, with special consideration of their application in Alzheimer disease as a representative neurodegenerative disorder.

**Key Words**: PET; COX-1; COX-2; biomarkers; neuroinflammation

**J Nucl Med 2022; 63:53S–59S**
DOI: 10.2967/jnumed.121.263199

PET is a powerful clinical and research tool with adequate sensitivity to measure specific proteins at low density in vivo (*1*). Some of these proteins can be used in clinical trials as biomarkers to stratify patients and facilitate therapeutic drug development. Pharmacokinetic biomarkers can be used to determine whether the therapeutic agent reaches its target by measuring target engagement or receptor occupancy. In addition, dynamic biomarkers can confirm the expected pharmacological action, which is distinct from clinical efficacy. For example, a dynamic biomarker of anti-inflammatory action could demonstrate that the drug had the expected pharmacological action shortly after administration, even though weeks or years may be required to show clinical efficacy.

Neuroinflammation is a significant contributor to the pathophysiology of several neurologic and psychiatric disorders, including Alzheimer disease (AD), multiple sclerosis, Huntington disease, and possibly major depressive disorder (*1,2*). The 18-kDa translocator protein (TSPO) has been extensively studied as a PET biomarker of neuroinflammation, and AD has been the most-studied disease (*1,2*). Although PET imaging of TSPO in AD has been shown to successfully reflect disease state and disease severity, it has several limitations as a biomarker of neuroinflammation, including its nonspecific localization in microglia, astrocytes, and vascular endothelium (*1*).

In the search for more useful targets of neuroinflammation, several new radioligands have been developed that target the cyclooxygenase (COX) system. Two isoforms of COX, subtypes 1 and 2 (*2*), catalyze the rate-limiting step in the production of proinflammatory mediators, which makes these enzymes potentially useful biomarkers of neuroinflammation. This article will review the development of PET radioligands selective for COX-1 and COX-2 as well as the potential utility of these 2 targets, in comparison to TSPO, as biomarkers of neuroinflammation in AD.

## COX-1 AND COX-2: BACKGROUND

Given that both COX-1 and COX-2 convert arachidonic acid to prostaglandin $H_2$ (Fig. 1), they might be expected to have the same functions. However, the specificities of their function derive from the varying cellular locations of COX-1 and COX-2 (*3*). For example, platelets contain enzymes that convert prostaglandin $H_2$ to thromboxane $A_2$, which promotes platelet aggregation and clotting. Vascular endothelium contains enzymes that convert prostaglandin $H_2$ to prostaglandin $I_2$, which inhibits platelet aggregation and clotting. In addition, platelets contain primarily COX-1, whereas vascular endothelium contains primarily COX-2. Thus, a nonselective COX inhibitor will have not only different actions but opposing actions (e.g., inhibiting clotting in platelets but promoting clotting in the vascular endothelium). The differential effects of the COX isozymes have been revealed by studying selective, or at least preferential, inhibitors. For example, the preferential COX-1 inhibitor aspirin is commonly used to decrease clotting in patients at risk for or with a history of heart attack and stroke. Conversely, selective COX-2 inhibitors such as rofecoxib (Vioxx [Tremeau Pharmaceuticals, Inc.], effective as an antiinflammatory drug) increase clotting to the point that this agent was removed from use because it increased the risk of heart attacks (*4*). Thus, the differential effects of COX-1 and COX-2 derive from different cellular localizations and can be responsible for both therapeutic efficacy and unwanted side effects.

### Cellular Location and Inducibility

Given the importance of cellular location for pharmacological effects, the issue of where COX-1 and COX-2 are located in the brain is critical. Although reports vary, COX-1 appears to be

Received Oct. 18, 2021; revision accepted Jan. 12, 2022.
For correspondence or reprints, contact Robert B. Innis (robert.innis@mail.nih.gov).
*Contributed equally to this work.

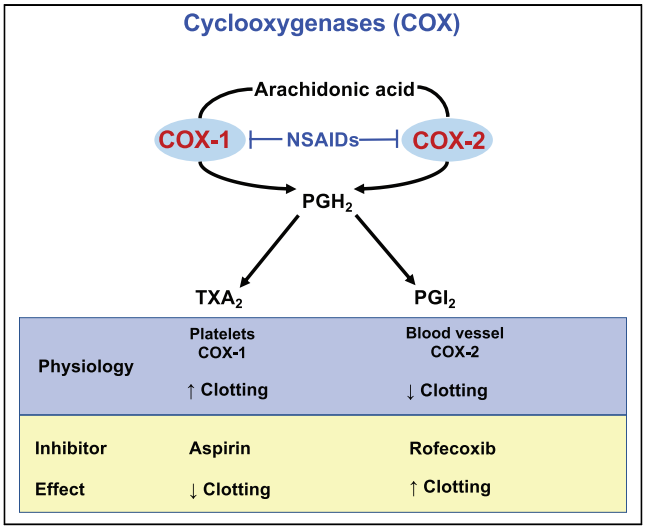


**FIGURE 1.** Distinct functions of COX-1 and COX-2 derive from their cellular location. Both COX-1 and COX-2 convert arachidonic acid into prostaglandin $H_2$ ($PGH_2$), which is later enzymatically converted into several bioactive prostanoids with different and sometimes opposing functions. The specific prostanoid depends on the enzymes in a given cell. Platelets contain primarily COX-1 and produce thromboxane $A_2$ ($TXA_2$), which promotes clotting. Vascular endothelium primarily contains COX-2 and produces prostaglandin $I_2$ ($PGI_2$), which inhibits clotting. Nonsteroidal antiinflammatory drugs (NSAIDs) inhibit COX isomers, either nonselectively (e.g., naproxen) or selectively (e.g., aspirin for COX-1 and rofecoxib for COX-2). Thus, the pharmacological effect of inhibiting COX-1 is to inhibit clotting and that of inhibiting COX-2 is to promote clotting.

located primarily in microglia and COX-2 in neurons (Table 1) (*5–7*). This differential cellular localization is found both in animals after an inflammatory challenge and in humans with neurologic conditions, including AD.

The functional differences between COX-1 and COX-2 derive not only from their varying cellular localizations but also from a differential response to inflammatory stimuli between the periphery and the brain. In the periphery, COX-1 is generally regarded as a constitutive enzyme and not upregulated by inflammation. In contrast, COX-2 can be quickly upregulated severalfold, and the increase can be blocked or reversed (*8*).

In the brain, the response of the COX isoforms is less conclusive and may be species-dependent. Four studies using microglia cultured from mice reported that COX-1 was upregulated on exposure to stimulants such as lipopolysaccharide and β-amyloid (*9*). In contrast, a study using cultured human microglia found no upregulation (*5*). Additional studies may help resolve the extent to which this differential effect is species-dependent.

In contrast to COX-1, the response of COX-2 to inflammatory stimuli in the brain has been more consistently reported as an elevation (*5,10*). In fact, COX-2 reacts like an immediate early gene and is rapidly upregulated in neurons after activation. For example, COX-2—but not COX-1—was found to be elevated in monkeys 1 d after intracerebral injection of lipopolysaccharide, and a postmortem analysis showed that most COX-2 transcript was in neurons (*6*). Although not an inflammatory stimulus, electroconvulsive seizures markedly and rapidly (within 1 h) increased COX-2 in rat neurons (*11*); prednisone blocked the increase in COX-2, suggesting that this upregulation is likely related to inflammatory pathways.

### Postmortem Studies in AD Brain

Immunohistochemical staining in the brains of individuals with AD found that COX-1 was present in microglia and was especially elevated surrounding amyloid plaques (Table 1) (*7*). However, the increased density of COX-1 surrounding amyloid plaques may simply reflect an increased number of microglia rather than an increased amount of COX-1 in individual microglia. A follow-up study using a large postmortem dataset found that the proportion of activated microglia strongly correlated with β-amyloid load, tau-related neuropathology, and rate of cognitive decline (*12*).

In postmortem brain studies, COX-2 was present predominantly in the neurons of individuals with AD compared with control tissue (*5,7*). Though clearly needed, quantitative measures of COX-2 in postmortem AD are likely to be confounded by the rapid turnover or degradation of this enzyme in healthy states and during the postmortem interval. For instance, the half-life of COX-2 messenger RNA in postmortem human brain is estimated to be less than 3.5 h (*13*), and the half-life of the protein in vivo varies from 2 to 7 h (*14*).

### Microglia as Brain's Macrophages

Microglia—which both release cytokines and phagocytose foreign protein and cellular debris—are often described as the resident macrophages of the brain. However, the 2 cells have different embryonic lineages: microglia derive from the embryonic yolk sac, whereas most monocytes and macrophages derive from fetal liver or bone marrow (*15*). Both activated microglia and macrophages (i.e., the activated form of bone marrow monocytes) are virtually identical on histologic examination and can be distinguished only

**TABLE 1**
Properties of 3 Biomarkers of Neuroinflammation

| Property | COX-1 | COX-2 | TSPO |
|---|---|---|---|
| Primary cell | Microglia | Neurons | Microglia, astroglia, vessels |
| Constitutive? | Yes | Yes | Yes |
| Induced?* | Species-dependent† | Yes | Uncertain‡ |
| Remains elevated? | Days | Hours | Weeks/mo |
| AD brain | Microglia around amyloid plaques | Elevated in neurons, especially early disease | Microglia, astrocytes, vessels |

*Defined as increased expression of protein per cell on exposure to inflammatory stimuli.
†Three positive reports in mouse microglia (*9*), and 1 negative report in human microglia (*5*).
‡May also be species-dependent (*63*).

by nonoverlapping transcriptomic or proteomic profiles (*15*). Because microglia express high concentrations of COX-1, COX-1 inhibitors may have antiinflammatory effects in the brain, analogous to the effects of COX-2 inhibitors in macrophages. In fact, evidence suggests that COX-1 inhibition may have antiinflammatory and beneficial effects in animal models, including the reduction of amyloid pathology and improved memory in a mouse model of AD (*16*).

## PET IMAGING OF COX-1

Few radioligands have succeeded in imaging COX-1. Many early candidates were unsuccessful for various reasons, including poor entry into brain, high nonspecific binding, and inadequate affinity. The nonsteroidal antiinflammatory drug and COX-1 inhibitor ketoprofen has low brain uptake because of the extensive deprotonation of its carboxyl group at physiologic pH. Nonetheless, $^{11}$C-ketoprofen-methyl ester (Supplemental Table 1; supplemental materials are available at http://jnm.snmjournals.org) enters brain and is rapidly hydrolyzed to $^{11}$C-ketoprofen for binding to COX-1. Whereas studies with this prodrug radioligand showed uptake in inflamed rat brain regions, COX-1–specific binding could not be verified in blocking studies. Therefore, it remained unclear whether radioactivity in brain was due mainly to binding of $^{11}$C-ketoprofen to COX-1 or to the inability of $^{11}$C-ketoprofen to leave brain because of its negative charge (*17*).

Despite this uncertainty, $^{11}$C-ketoprofen-methyl ester was studied in healthy human volunteers, individuals with mild cognitive impairment, and individuals with AD (*18*). No differences in washout of radioactivity from brain were observed among these 3 groups. These results might reflect insufficient COX-1 expression, insufficient binding of $^{11}$C-ketoprofen to COX-1, or inability of the radioligand or its radiometabolites to leave the brain. In our opinion, these results are also uninterpretable given that radioactivity reflects both the prodrug ($^{11}$C-ketoprofen-methyl ester) and the product of hydrolysis (i.e., $^{11}$C-ketoprofen) trapped in the brain. $^{11}$C-ketoprofen-methyl ester underscores that prodrug-type radioligands are usually difficult to quantify because PET cannot distinguish the prodrug from its radiometabolites. $^{18}$F-FDG provides a notable contrast. Its ability to quantify the rate of glucose metabolism is based on the irreversible trapping of its radiometabolite in brain. Such is not the case for reversibly binding radioligands, for which both uptake and washout of the active component must be measured.

The direct-acting radioligand $^{11}$C-1,5-bis(4-methoxyphenyl)-3-(2,2,2-trifluoroethoxy)-1H-1,2,4-triazole ($^{11}$C-PS13) was developed to overcome the issues associated with prodrugs (*19*). $^{11}$C-PS13 was found to be potent (half-maximal inhibitory concentration, ~1 nM) and selective (>1,000 fold) for COX-1 compared with COX-2 (*20*). High affinities—particularly those in the nanomolar or subnanomolar range—are desired because they increase specific binding to the target of interest. In contrast, nonspecific binding is determined by lipophilicity, as measured by the experimental distribution coefficient, logD. LogD values of 2.0–3.5 indicate moderate lipophilicity and are optimal for brain entry. Ligands with values that are too low risk not crossing the blood–brain barrier, whereas those with values that are too high may have high nonspecific binding to brain tissue and plasma proteins (*21,22*). Despite its very high logD of 4.26, $^{11}$C-PS13 crossed the blood–brain barrier and bound to COX-1. $^{18}$F-PS13 has also been prepared, thus providing another avenue to synthesize the radiotracer and extend its use, given the longer half-life associated with $^{18}$F (*23*).

Both animal and human studies indicate that $^{11}$C-PS13 is promising for the in vivo imaging of COX-1. In whole-body scans of rhesus monkeys, $^{11}$C-PS13 showed significant uptake in organs where COX-1 was expected, including the gastrointestinal tract, spleen, kidneys, and brain, indicating appropriate distribution (Fig. 2) (*24*). This uptake was blocked after administration of ketoprofen, a COX-1–specific inhibitor, but not celecoxib, a preferential COX-2 inhibitor, indicating good in vivo pharmacological specificity (*24*). Whole-body scans in healthy human volunteers found $^{11}$C-PS13 uptake in most major organs and subsequent blockade by ketoprofen but not celecoxib, reproducing the appropriate distribution and pharmacological specificity seen in animals (*25*). Furthermore, in the brains of healthy human volunteers, $^{11}$C-PS13 uptake was highest in the hippocampus, occipital cortex, and pericentral cortex (Fig. 3) (*19*). This distribution appears to be appropriate given the significant correlation with COX-1 gene transcript levels, as obtained from the Allen Human Brain Atlas (*24*). $^{11}$C-PS13 also demonstrated good absolute test–retest variability (range, 6.0%–8.5%) and reliability (intraclass correlation coefficient range, 0.74–0.87), with no radiometabolite accumulation and excellent time stability (*19*).

## PET IMAGING OF COX-2

Numerous radioligands have been tested to image COX-2, but most have either failed or not progressed to human studies. Extensive reviews detail the synthesis, in vitro results, and in vivo results for these radioligands (*26,27*). Arachidonic acid is the substrate for both COX-1 and COX-2 (Fig. 1), and $^{11}$C-arachidonic acid is the only radiotracer mentioned in these reviews that has moved to human studies (*28,29*). Both these early radioligands and more recently developed ones (*30–35*) were primarily unsuccessful because of high nonspecific binding. However, in some cases, radiodefluorination (*36,37*), rapid metabolism (*36*), and poor brain entry (*38–40*) were also reasons for failure. A few radioligands appeared successful in small animals, but no ensuing human studies were published (Supplemental Table 1) (*41–43*).

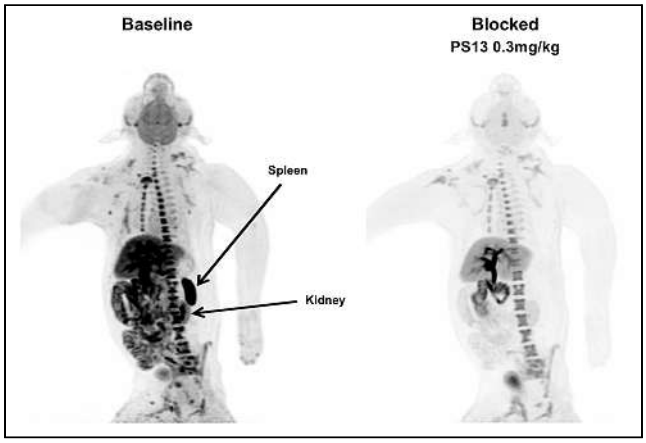


**FIGURE 2.** Imaging of COX-1 with $^{11}$C-PS13 in monkey at baseline and after blocking with nonradioactive PS13, which is highly selective for COX-1. High specific binding (i.e., blockable) was shown in brain (percentage blockade, 35%), spleen (86%), gastrointestinal tract (61%), and kidney (~75%). (Reprinted from (*24*).)

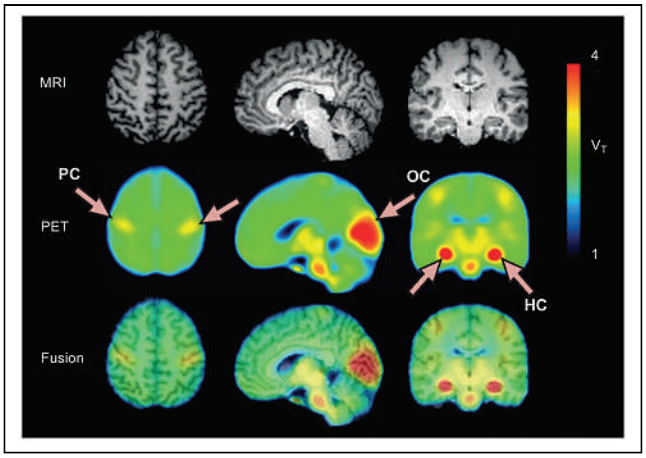


**FIGURE 3.** Distribution of COX-1 in healthy human brain. After $^{11}$C-PS13 injection, enzyme density was calculated on the pixel level as distribution volume ($V_T$). The MRI is from a representative participant, and PET images of COX-1 are an average from 10 participants. Notable $^{11}$C-PS13 binding (arrows) was detected in hippocampus (HC), occipital cortex (OC), and pericentral cortex (PC). The third row shows images fused from MRI and PET scans. (Reprinted from (*19*).)

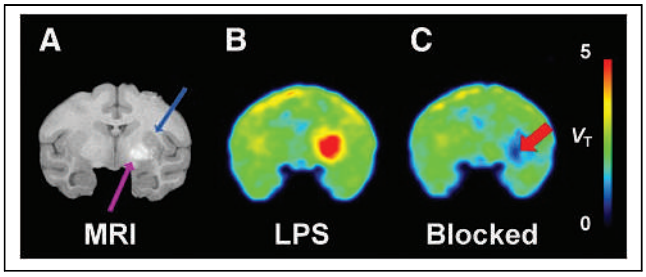


**FIGURE 4.** COX-2 was increased after a lesion in the brain of a rhesus macaque was found. The inflammatory agent lipopolysaccharide (LPS) was injected into the right putamen and initially caused edema and, later, a hemorrhage. (A) The coronal T2-weighted magnetic resonance image (MRI) scan of a rhesus macaque showing poorly visualized edema (blue arrow) and hematoma (purple arrow) around the injection site. (B) The PET image after $^{11}$C-MC1 injection showed markedly elevated COX-2, especially overlying the hematoma. (C) The COX-2 selective compound MC1 (1 mg/kg intravenously) blocked uptake in the lesion area, confirming the existence of both specific (i.e., blockable) and non-specific (i.e., residual) binding of the radioligand. (Adapted from (*6*).)

Other radioligands are still being investigated and have not yet moved to in vitro or in vivo studies (*44–46*).

Currently, 3 radioligands exist to image COX-2, but only one—$^{11}$C-6-methoxy-2-(4-(methylsulfonyl)phenyl)-*N*-(thiophen-2-ylmethyl)pyrimidin-4-amine ($^{11}$C-MC1)—has moved on to human studies. $^{11}$C-celecoxib and $^{11}$C-3-(4-methylsulfonylphenyl)-4-phenyl-5-trifluoromethyl isoxazole ($^{11}$C-TMI) (Supplemental Table 1) have been studied in baboons and have been shown to penetrate the blood–brain barrier, accumulate in brain, and gradually wash out (*47*). Both $^{11}$C-celecoxib and $^{11}$C-TMI produced a heterogeneous distribution in the brain that aligned with known COX-2 distribution (*48,49*). $^{11}$C-celecoxib also had uptake in organs known to express COX-2. However, no animal models of inflammation and no human studies have yet been published for either $^{11}$C-celecoxib or $^{11}$C-TMI.

$^{11}$C-MC1 is the most recently developed radioligand with the potential to image COX-2 in human neuroinflammation. On the basis of a 2-(4-methylsulfonylphenyl)pyrimidine scaffold, $^{11}$C-MC1 was found to be potent (half-maximal inhibitory concentration, ~1 nM) and selective (>1,000 fold) for COX-2 over COX-1. $^{11}$C-MC1, which has a slightly high logD of 3.74, crossed the blood–brain barrier and bound to COX-2 (*20,50*). $^{11}$C-MC1 lacked the sensitivity needed to measure low baseline concentrations of COX-2 in the brains of healthy rhesus macaques (*24*). In addition, the radioligand had minimal specific uptake in major organs except the ovaries and possibly the kidneys, both of which have high COX-2 expression (*24*). $^{11}$C-MC1 uptake in the ovaries was blocked by inhibitors of COX-2 but not COX-1, thereby affirming its pharmacological specificity.

Because COX-2 can be rapidly upregulated by inflammation, Shrestha et al. (*6*) subsequently tested whether $^{11}$C-MC1 could image upregulated COX-2 in monkey brain after intracerebral injection of the inflammagen lipopolysaccharide. In this PET study, 2 monkeys received a single lipopolysaccharide injection, and 2 monkeys received a second lipopolysaccharide injection. COX-2 binding of $^{11}$C-MC1 increased after 1 and 2 lipopolysaccharide injections, and postmortem brain analysis at the gene transcript or protein level confirmed these in vivo PET results (*6*). Interestingly, the monkeys that received 2 lipopolysaccharide injections developed delayed intracerebral hemorrhages after the first lipopolysaccharide injection, and the increased uptake of $^{11}$C-MC1 overlaid the hemorrhage rather than the injection site (Fig. 4). Thus, the increased uptake of $^{11}$C-MC1 likely resulted from a delayed effect associated with the first lipopolysaccharide injection rather than an acute effect associated with the second lipopolysaccharide injection.

Building on this work, another study evaluated the ability of $^{11}$C-MC1 to measure COX-2 concentrations in humans when concentrations were adequately elevated by peripheral inflammation. This first-in-human study (*6*) examined 2 individuals with rheumatoid arthritis (RA) and 2 healthy volunteers who were imaged with both $^{11}$C-MC1 and the TSPO radioligand $^{11}$C-ER176. Patients with RA were chosen because COX-2 is known to be upregulated in the affected joints of RA patients and because COX-2 gene expression is known to be upregulated in synoviocytes (*51*) and macrophages (*52*) in response to cytokine triggers. In individuals with RA, the symptomatic joints had increased $^{11}$C-MC1 and $^{11}$C-ER176 uptake, but $^{11}$C-ER176 also showed uptake in asymptomatic joints (Fig. 5), reflecting past evidence of inflammation. $^{11}$C-MC1 uptake was partially blocked by 400 mg of the preferential COX-2 inhibitor celecoxib (*6*), confirming that $^{11}$C-MC1 can be used to image elevated COX-2 levels in humans. Higher oral doses of celecoxib would likely have caused complete blockade in the symptomatic joints because higher intravenous doses of celecoxib or more potent inhibitors completely blocked elevated COX-2 in monkey brain (*6*).

A preliminary study then explored whether $^{11}$C-MC1 could measure COX-2 in 10 healthy human brains. In 9 of the 10 healthy participants, $^{11}$C-MC1 detected specific binding in brain that could be displaced by 600 mg of celecoxib, and the binding distribution correlated with that of the gene transcript in the Allen Brain Atlas (*53*). On the basis of the Lassen plot, celecoxib occupied 72% of available COX-2 in the brain, but this specific binding was only about 20% of total uptake. This finding suggests that $^{11}$C-MC1 has adequate sensitivity to measure low-density COX-2 in healthy human brain. However, because of the low specific binding in the normal brain, additional studies of individuals with neuroinflammatory disorders—who presumably would have higher densities of COX-2—are needed.

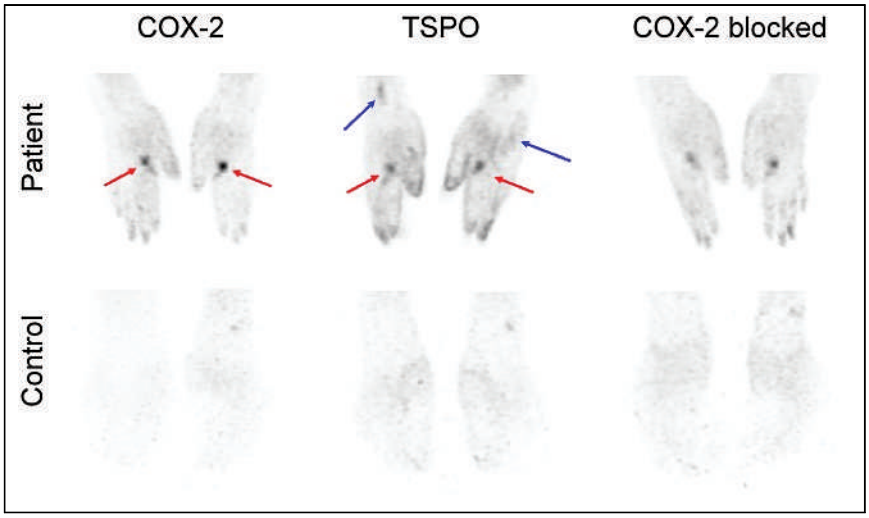


**FIGURE 5.** PET images of COX-2 and TSPO in a patient with RA and a healthy volunteer. The red arrows indicate symptomatic joints, and the blue arrows indicate asymptomatic joints. Increased COX-2 in the hands reflected currently symptomatic joints, whereas increased TSPO binding reflected both currently symptomatic and previously symptomatic joints. Celecoxib (400 mg orally) blocked only ~25% of the $^{11}$C-MC1 uptake in the joints of the patient, confirming uptake selectivity for COX-2 compared to COX-1. Animal studies suggest that higher doses of celecoxib are required for complete blockade. Adapted from (*6*).

## POTENTIAL USE OF COX-1 AND COX-2 AS BIOMARKERS

The most extensively studied biomarker of neuroinflammation in neurologic (*1*) and psychiatric (*2*) disorders has, to date, been TSPO. Thus, the potential use of COX-1 and COX-2 as biomarkers of neuroinflammation in AD and other neuropsychiatric disorders will inevitably be compared with the success and limitations of TSPO (Tables 1 and 2). As background, TSPO is concentrated in microglia and astrocytes that have been activated by various inflammatory stimuli (Table 1). AD, which generates a significant inflammatory response in the brain, is the disorder most frequently studied with TSPO radioligands. One large metaanalysis of 28 studies comprising 755 individuals (318 healthy volunteers, 168 individuals with mild cognitive impairment, and 269 with AD) found that elevated TSPO was a biomarker of disease state and disease severity (*54*), and another study found that TSPO was a biomarker of disease progression (*55*). Although these findings seem quite promising, TSPO has at least 3 clear limitations: it is not specific to a single cell type, it remains elevated for long periods, and the TSPO gene has a codominantly expressed polymorphism that affects the binding affinity of all known PET radioligands. In this context, COX imaging of neuroinflammation would have several advantages.

First, TSPO is not specific to a single cell type but, rather, is present in microglia, astroglia, and vascular endothelium. In contrast, COX-1 is located almost exclusively in microglia. Specifically, COX-1 is elevated surrounding amyloid plaques, and the elevation may reflect the induction of the amount of COX-1 in microglia. Most researchers and pharmaceutical companies are interested in biomarkers selective to microglia because that is the current target for several neuroinflammatory therapies.

Second, pharmaceutical companies seek a dynamic biomarker of pharmacological effects, and TSPO is unlikely to fulfill that role. With regard to AD drugs in particular, a novel antiinflammatory drug would require months to years to show a beneficial effect on cognition. Such long studies would benefit from identifying a biomarker—preferably in the brain but possibly in plasma—that could confirm antiinflammatory activity while assessing therapeutic efficacy. In this context, TSPO is unlikely to fulfill the role of a dynamic biomarker because TSPO levels remain elevated long after inflammation has resolved, limiting its utility as a biomarker of active inflammation (*1,2*); ultimately, however, it may prove to be a good reflection of the cumulative effects of neuroinflammation over time (*2*). In contrast, because COX-2 is rapidly upregulated and degraded, it could potentially be used as a biomarker of active neuroinflammation. In the aforementioned study of RA patients imaged for COX-2 and TSPO, COX-2 was elevated only in symptomatic joints, whereas TSPO was elevated in both symptomatic and asymptomatic joints (*6*). If replicated, these results suggest that COX-2 may be useful as a dynamic biomarker of current inflammation and be decreased by some antiinflammatory medications.

Third, the TSPO gene has a codominantly expressed polymorphism that affects the binding affinity of all known PET radioligands (*1*); thus, TSPO studies must correct or control for this polymorphism in all participants. Although no polymorphism is currently known to affect radioligand binding to COX-1 and COX-2, future studies should be alert to this possibility. Indeed,

**TABLE 2**
Potential Role of 3 Proteins as Biomarkers of Neuroinflammation in AD*

| Biomarker | COX-1 | COX-2 | TSPO |
|---|---|---|---|
| Disease state | Yes, numerous microglia | Visual increase in neurons, no quantitation | Yes |
| Disease severity | ? | ? | Yes |
| Disease progression | ? | ? | Possibly |
| Dynamic, reflecting pharmacological action | ? | Periphery, yes; brain, possibly | Unlikely: remains elevated for long time |

*Because COXs have not yet been imaged in AD, their biomarker potential is estimated from postmortem studies. The utility of TSPO is based on numerous PET studies.

both COX-1 and COX-2 genes have several encoding polymorphisms (*56*) that may contribute to functional differences (*57,58*). For instance, COX-1 polymorphisms may modulate the response of platelets to aspirin (*59,60*), and COX-2 polymorphisms may be associated with interindividual variability in gene expression and response to COX-2 inhibitors (*61,62*).

## CONCLUSION

Neuropathological studies in AD show elevated COX-1 in microglia surrounding amyloid plaques as well as elevated COX-2 in neurons. Although these results are based largely on the semiquantitative method of immunohistochemistry, both isozymes may be biomarkers of disease state—that is, the presence of neuroinflammation. Steroids block or reverse the elevation of COX-2 in peripheral inflammation and in neurons after electroconvulsive shock. Thus, in addition to being a biomarker of disease state, COX-2 may also be a dynamic biomarker of pharmacological action (i.e., of antiinflammatory action).

Recently developed radioligands show promise in animal models and healthy humans to selectively image both COX-1 and COX-2. $^{11}$C-PS13 can quantify the distribution of COX-1 in the periphery and brain and is pharmacologically specific, based on blockade in humans by COX-1 versus COX-2 preferential inhibitors. $^{11}$C-MC1 can quantify COX-2 upregulation in monkey brain after lipopolysaccharide injection and has the sensitivity to measure the low density of this target in healthy human brain. In our opinion, both radioligands are well suited to study as biomarkers of disease state or as dynamic biomarkers of pharmacological action in neurodegenerative diseases such as AD.

## DISCLOSURE

This study was funded by the Intramural Research Program of the National Institute of Mental Health, National Institutes of Health (ZIAMH002795, ZIAMH002852, and ZIAMH002793). No other potential conflict of interest relevant to this article was reported.

## ACKNOWLEDGMENT

We thank Paul Parcon, MD, for helpful insights on the use of nonsteroidal antiinflammatory drugs in AD.

## REFERENCES

1. Kreisl WC, Kim M-J, Coughlin JM, Henter ID, Owen DR, Innis RB. PET imaging of neuroinflammation in neurological disorders. *Lancet Neurol.* 2020;19:940–950.
2. Meyer JH, Cervenka S, Kim M-J, Kreisl WC, Henter ID, Innis RB. Neuroinflammation in psychiatric disorders: PET imaging and promising new targets. *Lancet Psychiatry.* 2020;7:1064–1074.
3. Schrör K. Aspirin and platelets: the antiplatelet action of aspirin and its role in thrombosis treatment and prophylaxis. *Semin Thromb Hemost.* 1997;23:349–356.
4. Yu Y, Ricciotti E, Scalia R, et al. Vascular COX-2 modulates blood pressure and thrombosis in mice. *Sci Transl Med.* 2012;4:132ra54.
5. Hoozemans JJ, Rozemuller AJ, Janssen I, De Groot CJ, Veerhuis R, Eikelenboom P. Cyclooxygenase expression in microglia and neurons in Alzheimer's disease and control brain. *Acta Neuropathol (Berl).* 2001;101:2–8.
6. Shrestha S, Kim MJ, Eldridge M, et al. PET measurement of cyclooxygenase-2 using a novel radioligand: upregulation in primate neuroinflammation and first-in-human study. *J Neuroinflammation.* 2020;17:140.
7. Yasojima K, Schwab C, McGeer EG, McGeer PL. Distribution of cyclooxygenase-1 and cyclooxygenase-2 mRNAs and proteins in human brain and peripheral organs. *Brain Res.* 1999;830:226–236.
8. Murakami M, Kudo I. Recent advances in molecular biology and physiology of the prostaglandin E2-biosynthetic pathway. *Prog Lipid Res.* 2004;43:3–35.
9. Ghazanfari N, van Waarde A, Dierckx RAJO, Doorduin J, de Vries EFJ. Is cyclooxygenase-1 involved in neuroinflammation? *J Neurosci Res.* 2021;99:2976–2998.
10. Fiebich BL, Mueksch B, Boehringer M, Hüll M. Interleukin-1beta induces cyclooxygenase-2 and prostaglandin $E_2$ synthesis in human neuroblastoma cells: involvement of p38 mitogen-activated protein kinase and nuclear factor-kappaB. *J Neurochem.* 2000;75:2020–2028.
11. Yamagata K, Andreasson KI, Kaufmann WE, Barnes CA, Worley PF. Expression of a mitogen-inducible cyclooxygenase in brain neurons: regulation by synaptic activity and glucocorticoids. *Neuron.* 1993;11:371–386.
12. Felsky D, Roostaei T, Nho K, et al. Neuropathological correlates and genetic architecture of microglial activation in elderly human brain. *Nat Commun.* 2019;10:409.
13. Lukiw WJ, Bazan NG. Cyclooxygenase 2 RNA message abundance, stability, and hypervariability in sporadic Alzheimer neocortex. *J Neurosci Res.* 1997;50:937–945.
14. Kang Y-J, Mbonye UR, DeLong CJ, Wada M, Smith WL. Regulation of intracellular cyclooxygenase levels by gene transcription and protein degradation. *Prog Lipid Res.* 2007;46:108–125.
15. Li Q, Barres BA. Microglia and macrophages in brain homeostasis and disease. *Nat Rev Immunol.* 2018;18:225–242.
16. Choi S-H, Aid S, Caracciolo L, et al. Cyclooxygenase-1 inhibition reduces amyloid pathology and improves memory deficits in a mouse model of Alzheimer's disease. *J Neurochem.* 2013;124:59–68.
17. Takashima-Hirano M, Shukuri M, Takashima T, et al. General method for the $^{11}$C-labeling of 2-arylpropionic acids and their esters: construction of a PET tracer library for a study of biological events involved in COXs expression. *Chemistry.* 2010;16:4250–4258.
18. Ohnishi A, Senda M, Yamane T, et al. Exploratory human PET study of the effectiveness of $^{11}$C-ketoprofen methyl ester, a potential biomarker of neuroinflammatory processes in Alzheimer's disease. *Nucl Med Biol.* 2016;43:438–444.
19. Kim M-J, Lee JH, Juarez Anaya F, et al. First-in-human evaluation of [$^{11}$C]PS13, a novel PET radioligand, to quantify cyclooxygenase-1 in the brain. *Eur J Nucl Med Mol Imaging.* 2020;47:3143–3151.
20. Singh P, Shrestha S, Cortes-Salva MY, et al. 3-substituted 1,5-diaryl-1*H*-1,2,4-triazoles as prospective PET radioligands for imaging brain COX-1 in monkey. Part 1: synthesis and pharmacology. *ACS Chem Neurosci.* 2018;9:2610–2619.
21. Pike VW. PET radiotracers: crossing the blood-brain barrier and surviving metabolism. *Trends Pharmacol Sci.* 2009;30:431–440.
22. Pike VW. Considerations in the development of reversibly binding PET radioligands for brain imaging. *Curr Med Chem.* 2016;23:1818–1869.
23. Taddei C, Morse CL, Kim M-J, et al. Synthesis of [$^{18}$F]PS13 and evaluation as a PET radioligand for cyclooxygenase-1 in monkey. *ACS Chem Neurosci.* 2021;12:517–530.
24. Kim MJ, Shrestha SS, Cortes M, et al. Evaluation of two potent and selective PET radioligands to image COX-1 and COX-2 in rhesus monkeys. *J Nucl Med.* 2018;59:1907–1912.
25. Manly L, Kim M-J, Montero Santamaria J, et al. Aspirin blockade of COX-1 in human organs is reduced by plasma as shown by PET imaging and blood assays with $^{11}$C-PS13 [abstract]. *J Nucl Med.* 2021;62(suppl 1):115.
26. Laube M, Kniess T, Pietzsch J. Radiolabeled COX-2 inhibitors for non-invasive visualization of COX-2 expression and activity: a critical update. *Molecules.* 2013;18:6311–6355.
27. Pacelli A, Greenman J, Cawthorne C, Smith G. Imaging COX-2 expression in cancer using PET/SPECT radioligands: current status and future directions. *J Labelled Comp Radiopharm.* 2014;57:317–322.
28. Giovacchini G, Chang MC, Channing MA, et al. Brain incorporation of [$^{11}$C]arachidonic acid in young healthy humans measured with positron emission tomography. *J Cereb Blood Flow Metab.* 2002;22:1453–1462.
29. Rapoport SI. In vivo approaches to quantifying and imaging brain arachidonic and docosahexaenoic acid metabolism. *J Pediatr.* 2003;143(suppl):S26–S34.
30. Nolting DD, Nickels M, Tantawy MN, et al. Convergent synthesis and evaluation of $^{18}$F-labeled azulenic COX2 probes for cancer imaging. *Front Oncol.* 2013;2:207.
31. Lebedev A, Jiao J, Lee J, et al. Radiochemistry on electrodes: synthesis of an $^{18}$F-labelled and in vivo stable COX-2 inhibitor. *PLoS One.* 2017;12:e0176606.
32. Chang CW, Yeh CN, Chung YH, et al. Synthesis and evaluation of ortho-[$^{18}$F] fluorocelecoxib for COX-2 cholangiocarcinoma imaging. *Drug Des Devel Ther.* 2018;12:1467–1478.
33. Prabhakaran J, Underwood M, Zanderigo F, et al. Radiosynthesis and in vivo evaluation of [$^{11}$C]MOV as a PET imaging agent for COX-2. *Bioorg Med Chem Lett.* 2018;28:2432–2435.
34. Carpinelli A, Rainone P, Belloli S, et al. Radiosynthesis and preclinical evaluation of $^{11}$C-VA426, a cyclooxygenase-2 selective ligand. *Contrast Media Mol Imaging.* 2019;2019:5823261.
35. Elie J, Vercouillie J, Arlicot N, et al. Design of selective COX-2 inhibitors in the (aza)indazole series: chemistry, in vitro studies, radiochemistry and evaluations in rats of a [$^{18}$F] PET tracer. *J Enzyme Inhib Med Chem.* 2019;34:1–7.

36. Prabhakaran J, Underwood MD, Parsey RV, et al. Synthesis and in vivo evaluation of [$^{18}$F]-4-[5-(4-methylphenyl)-3-(trifluoromethyl)-$^{1}$H-pyrazol-1-yl]benzenesulfonamide as a PET imaging probe for COX-2 expression. *Bioorg Med Chem.* 2007; 15:1802–1807.
37. Toyokuni T, Kumar JS, Walsh JC, et al. Synthesis of 4-(5-[$^{18}$F]fluoromethyl-3-phenylisoxazol-4-yl)benzenesulfonamide, a new [$^{18}$F]fluorinated analogue of valdecoxib, as a potential radiotracer for imaging cyclooxygenase-2 with positron emission tomography. *Bioorg Med Chem Lett.* 2005;15:4699–4702.
38. Fujisaki Y, Kawamura K, Wang WF, et al. Radiosynthesis and in vivo evaluation of $^{11}$C-labeled 1,5-diarylpyrazole derivatives for mapping cyclooxygenases. *Ann Nucl Med.* 2005;19:617–625.
39. Tanaka M, Fujisaki Y, Kawamura K, et al. Radiosynthesis and evaluation of $^{11}$C-labeled diaryl-substituted imidazole and indole derivatives for mapping cyclooxygenase-2. *Biol Pharm Bull.* 2006;29:2087–2094.
40. Yamamoto Y, Toyohara J, Ishiwata K, et al. $^{11}$C-labeled analogs of indomethacin esters and amides for brain cyclooxygenase-2 imaging: radiosynthesis, in vitro evaluation and in vivo characteristics in mice. *Chem Pharm Bull (Tokyo)*. 2011;59: 938–946.
41. Uddin MJ, Crews BC, Ghebreselasie K, et al. Fluorinated COX-2 inhibitors as agents in PET imaging of inflammation and cancer. *Cancer Prev Res (Phila).* 2011;4:1536–1545.
42. Litchfield M, Wuest M, Glubrecht D, Wuest F. Radiosynthesis and biological evaluation of [($^{18}$)F]triacoxib: a new radiotracer for PET imaging of COX-2. *Mol Pharm.* 2020;17:251–261.
43. Tietz O, Wuest M, Marshall A, et al. PET imaging of cyclooxygenase-2 (COX-2) in a pre-clinical colorectal cancer model. *EJNMMI Res.* 2016;6:37.
44. Tian H, Lee Z. Synthesis of $^{18}$F-labelled cyclooxygenase-2 (COX-2) inhibitor as a potential PET imaging agent. *J Labelled Comp Radiopharm.* 2006;49:583–593.
45. Majo VJ, Prabhakaran J, Simpson NR, Van Heertum RL, Mann JJ, Kumar JSD. A general method for the synthesis of aryl [$^{11}$C]methylsulfones: potential PET probes for imaging cyclooxygenase-2 expression. *Bioorg Med Chem Lett.* 2005;15: 4268–4271.
46. Wüst FR, Höhne A, Metz P. Synthesis of $^{18}$F-labelled cyclooxygenase-2 (COX-2) inhibitors via Stille reaction with 4-[$^{18}$F]fluoroiodobenzene as radiotracers for positron emission tomography (PET). *Org Biomol Chem.* 2005;3:503–507.
47. Kumar JSD, Zanderigo F, Prabhakaran J, Rubin-Falcone H, Parsey RV, Mann JJ. In vivo evaluation of [$^{11}$C]TMI, a COX-2 selective PET tracer, in baboons. *Bioorg Med Chem Lett.* 2018;28:3592–3595.
48. Kaufmann WE, Andreasson KI, Isakson PC, Worley PF. Cyclooxygenases and the central nervous system. *Prostaglandins.* 1997;54:601–624.
49. Breder CD, Dewitt D, Kraig RP. Characterization of inducible cyclooxygenase in rat brain. *J Comp Neurol.* 1995;355:296–315.
50. Cortes-Salva MY, Shrestha S, Singh P, et al. 2-(4-methylsulfonylphenyl)pyrimidines as prospective radioligands for imaging cyclooxygenase-2 with PET-synthesis, triage, and radiolabeling. *Molecules.* 2018;23:2850.
51. Crofford LJ. The role of COX-2 in rheumatoid arthritis synovial tissues [abstract]. *Arthritis Res.* 2000;1(suppl 1):S30.
52. Simon LS. Role and regulation of cyclooxygenase-2 during inflammation. *Am J Med.* 1999;106(suppl):37S–42S.
53. Yan X, Zhang A, Zoghbi S, et al. $^{11}$C-MC1 has adequate sensitivity to measure low density cyclooxygenase 2 (COX-2) in healthy human brain [abstract]. *J Nucl Med.* 2021;62(suppl 1):103.
54. Bradburn S, Murgatroyd C, Ray N. Neuroinflammation in mild cognitive impairment and Alzheimer's disease: a meta-analysis. *Ageing Res Rev.* 2019;50:1–8.
55. Kreisl WC, Lyoo CH, Liow JS, et al. $^{11}$C-PBR28 binding to translocator protein increases with progression of Alzheimer's disease. *Neurobiol Aging.* 2016;44:53–61.
56. Ulrich CM, Bigler J, Potter JD. Non-steroidal anti-inflammatory drugs for cancer prevention: promise, perils and pharmacogenetics. *Nat Rev Cancer.* 2006;6:130–140.
57. Lee CR, Bottone FG, Krahn JM, et al. Identification and functional characterization of polymorphisms in human cyclooxygenase-1 (PTGS1). *Pharmacogenet Genomics.* 2007;17:145–160.
58. Bruno A, Tacconelli S, Patrignani P. Variability in the response to non-steroidal anti-inflammatory drugs: mechanisms and perspectives. *Basic Clin Pharmacol Toxicol.* 2014;114:56–63.
59. Halushka MK, Walker LP, Halushka PV. Genetic variation in cyclooxygenase 1: effects on response to aspirin. *Clin Pharmacol Ther.* 2003;73:122–130.
60. Maree AO, Curtin RJ, Chubb A, et al. Cyclooxygenase-1 haplotype modulates platelet response to aspirin. *J Thromb Haemost.* 2005;3:2340–2345.
61. Fries S, Grosser T, Price TS, et al. Marked interindividual variability in the response to selective inhibitors of cyclooxygenase-2. *Gastroenterology.* 2006;130:55–64.
62. Lee Y-S, Kim H, Wu T-X, Wang X-M, Dionne RA. Genetically mediated interindividual variation in analgesic responses to cyclooxygenase inhibitory drugs. *Clin Pharmacol Ther.* 2006;79:407–418.
63. Owen DR, Narayan N, Wells L, et al. Pro-inflammatory activation of primary microglia and macrophages increases 18 kDa translocator protein expression in rodents but not humans. *J Cereb Blood Flow Metab.* 2017;37:2679–2690.

# Imaging of Synaptic Density in Neurodegenerative Disorders

Richard E. Carson[1,2], Mika Naganawa[1], Takuya Toyonaga[1], Sheida Koohsari[1], Yanghong Yang[1], Ming-Kai Chen[1], David Matuskey[1,3,4], and Sjoerd J. Finnema[5]

[1]*Department of Radiology and Biomedical Imaging, Yale Positron Emission Tomography Center, Yale University, New Haven, Connecticut;* [2]*Department of Biomedical Engineering, Yale University, New Haven, Connecticut;* [3]*Department of Psychiatry, Yale School of Medicine, New Haven, Connecticut;* [4]*Department of Neurology, Yale School of Medicine, New Haven, Connecticut; and* [5]*Neuroscience Discovery Research, Translational Imaging, AbbVie, North Chicago, Illinois*

PET technology has produced many radiopharmaceuticals that target specific brain proteins and other measures of brain function. Recently, a new approach has emerged to image synaptic density by targeting the synaptic vesicle protein 2A (SV2A), an integral glycoprotein in the membrane of synaptic vesicles and widely distributed throughout the brain. Multiple SV2A ligands have been developed and translated to human use. The most successful of these to date is $^{11}$C-UCB-J, because of its high uptake, moderate metabolism, and effective quantification with a 1-tissue-compartment model. Further, since SV2A is the target of the antiepileptic drug levetiracetam, human blocking studies have characterized specific binding and potential reference regions. Regional brain SV2A levels were shown to correlate with those of synaptophysin, another commonly used marker of synaptic density, providing the basis for SV2A PET imaging to have broad utility across neuropathologic diseases. In this review, we highlight the development of SV2A tracers and the evaluation of quantification methods, including compartment modeling and simple tissue ratios. Mouse and rat models of neurodegenerative diseases have been studied with small-animal PET, providing validation by comparison to direct tissue measures. Next, we review human PET imaging results in multiple neurodegenerative disorders. Studies on Parkinson disease and Alzheimer disease have progressed most rapidly at multiple centers, with generally consistent results of patterns of SV2A or synaptic loss. In Alzheimer disease, the synaptic loss patterns differ from those of amyloid, tau, and $^{18}$F-FDG, although intertracer and interregional correlations have been found. Smaller studies have been reported in other disorders, including Lewy body dementia, frontotemporal dementia, Huntington disease, progressive supranuclear palsy, and corticobasal degeneration. In conclusion, PET imaging of SV2A has rapidly developed, and qualified radioligands are available. PET studies on humans indicate that SV2A loss might be specific to disease-associated brain regions and consistent with synaptic density loss. The recent availability of new $^{18}$F tracers, $^{18}$F-SynVesT-1 and $^{18}$F-SynVesT-2, will substantially broaden the application of SV2A PET. Future studies are needed in larger patient cohorts to establish the clinical value of SV2A PET and its potential for diagnosis and progression monitoring of neurodegenerative diseases, as well as efficacy assessment of disease-modifying therapies.

**Key Words:** PET; synaptic vesicle glycoprotein 2A; synaptic density; SV2A; neurodegeneration

**J Nucl Med 2022; 63:60S–67S**
DOI: 10.2967/jnumed.121.263201

The great strength of PET imaging is its ability to quantify specific physiologic functions and to measure unique elements of the brain, including receptors, transporters, and enzymes. In the area of neurodegeneration, this has yielded a plethora of novel radiopharmaceuticals to target protein aggregates such as β-amyloid (Aβ) and tau, and the search continues for useful tracers for other targets such as α-synuclein. The recent advent of PET synaptic imaging by targeting the synaptic vesicle protein 2A (SV2A) has opened many novel avenues of investigation into neurodegenerative disorders. The general utility of this marker in a wide range of disorders makes it uniquely suited to human studies, including disease diagnosis and differentiation and treatment monitoring. In many cases, the pairing of SV2A PET with a second PET study using a radioligand with a greater disease-specific focus provides unique multimodal information on brain pathophysiology. Here, we review the SV2A target protein, the development and quantification of SV2A PET tracers, synaptic imaging studies on animal models, and clinical studies on Parkinson disease (PD), dementia with Lewy bodies (DLB), Alzheimer disease (AD), frontotemporal dementia (FTD), Huntington disease (HD), progressive supranuclear palsy (PSP), and corticobasal degeneration (CBD). Rodent studies are summarized in Table 1, and human studies are listed in Table 2.

## SV2

SV2 is a glycoprotein (*1*) located on secretory vesicles of neurons and endocrine cells (*2,3*). SV2 is critical for synaptic function and is involved in vesicle trafficking and exocytosis (*4*), although investigations continue into its exact functions (*5,6*). SV2 has 3 isoforms (*7,8*) with different distributions in the brain. SV2A is ubiquitously expressed in virtually all synapses, SV2B is more restricted (*7–9*), and SV2C was observed in only a few rat brain areas (*8*). Among glutamatergic and γ-aminobutyric acid–ergic neurons, SV2A is thought to be located in both classes, whereas SV2B might be more restricted to the former and SV2C to the latter (*6*).

In 2004, Lynch et al. demonstrated that SV2A is the target of the antiepileptic drug levetiracetam (*10,11*). This led the pharmaceutical company UCB to identify a novel generation of antiepileptic drugs with increased SV2A affinity and antiseizure potency, ultimately resulting in the development of brivaracetam (*12,13*).

## DEVELOPMENT OF SV2A PET RADIOLIGANDS

The first attempt to develop a SV2A PET radioligand was $^{11}$C-levetiracetam (*14*), but this tracer did not progress, probably because of its low binding affinity to SV2A ($K_i$ = 1.74 μM) (*15*). Subsequently, high-affinity SV2A-specific ligands were synthesized

Received Dec. 23, 2021; revision accepted Feb. 10, 2022.
For correspondence or reprints, contact Richard E. Carson (richard.carson@yale.edu).

**TABLE 1**
Literature with $^{11}$C-UCB-J PET in Animal Models of Neurodegenerative Disorders

| Species | Model | Procedures or genotypes | Subjects | Outcome measure | Decrease | Reference |
|---|---|---|---|---|---|---|
| Mouse | AD | APP/PS1 | 9 | SUVR | 26% (hippocampus) | (*48*) |
| Rat | PD lesion | 6-OHDA (20 μg) local injection in striatum | 3 | SUV | 6% (striatum) | (*51*) |
| Rat | HD lesion | QA (20 μg) local injection in striatum | 4 | $V_T$ | 39% (striatum) | (*51*) |
| Rat | HD lesion | QA (40 μg) local injection in striatum | 4 | $V_T$ | 55% (striatum) | (*51*) |
| Mouse | PD | Heterozygous Thy1-αSyn mouse model line 61 | 10 | AUCR | 12% (hippocampus) | (*49*) |
| Mouse | AD | ArcSwe transgenic mouse model | 11 | AUCR | — | (*49*) |
| Mouse | HD | Heterozygous Q175DN knock-in mouse model | 19 | $V_T$ (IDIF) | 20% (striatum) | (*50*) |
| Rat | PD | 6-OHDA local injection in medial forebrain bundle and rostral SN | 4 | $V_T$ (IDIF | 9% (striatum) | (*52*) |

APP/PS1 = Swedish (APP KM670/671NL) and PSEN1-L166P mutations; 6-OHDA = 6-hydroxydopamine; QA = quinolinic acid; AUCR = area under curve ratio; ArcSwe = arctic (APP E693G) and Swedish (APP KM670/671NL) mutations; IDIF = image-derived input function. Listing is in chronologic order.

and evaluated (*16,17*). Three of the SV2A ligands were radiolabeled as $^{11}$C-UCB-A (4-(3,5-Difluorophenyl)-1-((1-methyl-1H-imidazol-5-yl)methyl)pyrrolidin-2-one) (*18*), $^{18}$F-UCB-H (1-((3-Fluoropyridin-4-yl)methyl)-4-(3,4,5-trifluorophenyl)pyrrolidin-2-one) (*19–22*), and $^{11}$C-UCB-J ((*R*)-1-((3-($^{11}$C-methyl-$^{11}$C)pyridin-4-yl)methyl)-4-(3,4,5-trifluorophenyl)pyrrolidin-2-one) (*23*), and all were evaluated in nonhuman primates. Of these, $^{11}$C-UCB-J possessed the most suitable pharmacokinetics, that is, rapid and high brain uptake, reversible binding kinetics, and relatively low nonspecific binding in white matter (*23*). $^{11}$C-UCB-A showed slower brain penetration in nonhuman primate brains, making quantitative analysis more challenging. Furthermore, $^{18}$F-UCB-H showed relatively low specific binding in the nonhuman primate brain, probably because of lower binding affinity (negative log of half-maximal inhibitory concentration, $p$IC$_{50}$, 7.8 for UCB-H, vs. 8.2 for UCB-J) (*16,23*).

Subsequent SV2A human imaging data were highly consistent with preclinical data; that is, $^{11}$C-UCB-J has ideal imaging characteristics (*24*), with $^{11}$C-UCB-A possessing slow binding kinetics (*25*) and $^{18}$F-UCB-H having low specific binding in the brain (*26*).

On the basis of the initial success of $^{11}$C-UCB-J, $^{18}$F-labeled SV2A radioligands with similar chemical backbones became of interest, as the half-life of $^{11}$C (20.4 min) limits its broad applicability. Initial work focused on $^{18}$F-UCB-J, which provided nonhuman primate data similar to that of $^{11}$C-UCB-J (*27*); however, the radiosynthetic process was unsuitable for routine production. The subsequent focus was on mono- and difluorinated UCB-J analogs, that is, $^{18}$F-SynVesT-1 ((*R*)-4-(3-Fluoro-5-(fluoro-$^{18}$F)phenyl)-1-((3-methylpyridin-4-yl)methyl)pyrrolidin-2-one ($^{18}$F-SDM-8, $^{18}$F-MNI-1126) (*28,29*) and $^{18}$F-SynVesT-2 ((*R*)-4-(3-([$^{18}$F]Fluoro)phenyl)-1-((3-methylpyridin-4-yl)methyl)pyrrolidin-2-one ($^{18}$F-SDM-2) (*30*). In humans, $^{18}$F-SynVesT-1 displayed outstanding characteristics, that is, very high brain uptake, fast and reversible kinetics, excellent test–retest reproducibility, and binding specificity to SV2A (*31,32*). Compared with $^{11}$C-UCB-J, $^{18}$F-SynVesT-1 displayed higher binding potential ($BP_{ND}$). Recent human scans with $^{18}$F-SynVesT-2 showed a slightly lower $BP_{ND}$ but with faster kinetics. The availability of these $^{18}$F-labeled SV2A PET radioligands provides the opportunity for multicenter clinical studies of various neurodegenerative disorders.

## SV2A AS A BIOMARKER OF SYNAPTIC DENSITY

Synaptic vesicle proteins, such as SV2A, have previously been established as histologic markers of synaptic density (*33–35*) because of their localization to synaptic boutons. SV2A is a promising biomarker of synaptic density as it is ubiquitously and homogeneously present in synaptic vesicles (*7*), with a low variation in copy number per vesicle (*36*). To examine whether SV2A PET provides an index of synaptic density, a baboon underwent an $^{11}$C-UCB-J scan, followed by postmortem brain tissue studies. The PET-measured $^{11}$C-UCB-J distribution volume ($V_T$) correlated well with the regional SV2A distribution measured by a homogenate binding assay and Western blotting. Importantly, there was also a good correlation between SV2A and the gold standard synaptic density marker synaptophysin in Western blot and confocal microscopy experiments; that is, SV2A can be used as an alternative to synaptophysin for quantification of synapse density (*24*). Analogous biochemical studies with resected human tissue after epilepsy surgery also show promising results. Additional studies with postmortem human tissue are required to further validate SV2A as a biomarker of synaptic density.

## QUANTIFICATION OF SV2A PET RADIOLIGANDS

Modeling studies of SV2A PET in humans revealed that the best models to quantify $V_T$ values are the 1-tissue-compartment model (1TC) for $^{11}$C-UCB-J (*37–39*), $^{18}$F-SynVesT-1 (*32*), and $^{18}$F-SynVesT-2 and Logan graphical analysis for $^{18}$F-UCB-H (*26*). Excellent test–retest reproducibility and low-noise $V_T$ images can be obtained with the 1TC model for $^{11}$C-UCB-J (*37*) and $^{18}$F-SynVesT-1 (*31,32*). Activation studies in humans showed that $V_T$ was unaffected by visual stimulation, whereas $K_1$, the tracer influx constant, increased in the visual cortex (*40*).

For quantification of specific binding, a reference tissue is required, and the centrum semiovale (CS) has been proposed on the basis of in vitro biochemical data (*24*), showing negligible specific binding. However, there was a small displacement of $^{11}$C-UCB-J in the CS with levetiracetam and brivaracetam (*24,41*), consistent with autoradiography data (*42*), and the CS $V_T$ overestimates the gray matter

**TABLE 2**
Literature with SV2A PET in Human Studies of Neurodegenerative Disorders

| Population | Subjects | Tracer | Outcome measure | Major finding | Reference |
|---|---|---|---|---|---|
| PD and CN | 12 PD | $^{11}$C-UCB-J | $BP_{ND}$ | ≤45% lower binding in PD; largest in SN (45%), with multiple cortical areas included | (*56*) |
| PD (early drug-naïve) and CN | 12 PD | $^{11}$C-UCB-J | $V_T$ | Lower binding in PD ranged from 15% (caudate) to 8% in multiple areas; SN was 7% | (*57*) |
| PD and CN | 30 PD | $^{11}$C-UCB-J | $BP_{ND}$ | Lower binding in PD from 15%; largest in SN | (*58*) |
| PD and CN | 21 PD | $^{11}$C-UCB-J | SUVR-1 | Lower binding in PD in SN | (*60*) |
| DLB/PDD and CN | 13 DLB/PDD | $^{11}$C-UCB-J | SUVR-1 | Lower binding in DLB/PDD in multiple areas | (*60*) |
| AD and CN | 10 AD/MCI | $^{11}$C-UCB-J | $BP_{ND}$ | 41% lower binding in hippocampus of AD | (*69*) |
| AD and CN | 24 AD/MCI | $^{18}$F-UCB-H | $V_T$ | Lower binding in hippocampus (31%), cortex (11%–18%), and thalamus (16%) of AD | (*71*) |
| AD and CN | 34 AD/MCI | $^{11}$C-UCB-J | $DVR_{Cb}$ | Extensive cortical and subcortical reductions of $DVR_{Cb}$ in AD | (*72*) |
| AD and CN | 12 AD | $^{18}$F-UCB-H | $V_T$ | 33% decrease in right hippocampus in AD (trend level) | (*82*) |
| AD and CN | 38 AD/MCI | $^{11}$C-UCB-J<br>$^{11}$C-PiB | $DVR_{Cb}$ | Inverse association between global amyloid deposition and hippocampal SV2A binding in participants with aMCI but not mild dementia | (*74*) |
| AD and CN | 10 MCI | $^{11}$C-UCB-J<br>$^{18}$F-MK-6240 | SUVR | Higher $^{18}$F-MK-6240 binding inversely related to lower $^{11}$C-UCB-J binding in medial temporal lobe | (*75*) |
| AD and CN | 7 AD | $^{11}$C-UCB-J<br>$^{18}$F-flortaucipir | $BP_{ND}$ | Higher regional $^{18}$F-flortaucipir uptake with lower $^{11}$C-UCB-J uptake | (*76*) |
| AD and CN | 10 AD/MCI | $^{11}$C-UCB-J<br>$^{18}$F-flortaucipir | $DVR_{Cb}$ | Entorhinal cortical tau inversely associated with hippocampal synaptic density | (*77*) |
| AD and CN | 14 AD/MCI | $^{11}$C-UCB-J<br>$^{18}$F-FDG | $DVR_{Cb}$ | Similar reduction of $^{11}$C-UCB-J and $^{18}$F-FDG in medial temporal lobe of AD, but smaller reduction of $^{11}$C-UCB-J in neocortex than $^{18}$F-FDG | (*78*) |
| bvFTD and CN | 1 bvFTD | $^{11}$C-UCB-J | $BP_{ND}$ | Lower binding in frontotemporal and subcortical regions | (*81*) |
| Presymptomatic C9orf72 mutation carriers and CN | 3 carriers | $^{11}$C-UCB-J | $BP_{ND}$ | Decrease in thalamus in carriers | (*81*) |
| bvFTD and CN | 12 bvFTD | $^{18}$F-UCB-H | $V_T$ | 41% decrease in right parahippocampal area in bvFTD (trend level) | (*82*) |
| HD (premanifest and early stage) and CN | 18 HD | $^{11}$C-UCB-J | $BP_{ND}$ | Lower binding in putamen (−19%), caudate (−16%) in premanifest; putamen (−33%), caudate (−31%), whole gray matter (−12%) in early stage | (*85*) |
| PSP and CN | 14 PSP | $^{11}$C-UCB-J | $BP_{ND}$ | ≤50% lower binding in cortical and subcortical areas | (*89*) |
| CBD and CN | 15 CBD | $^{11}$C-UCB-J | $BP_{ND}$ | ≤50% lower binding in cortical and subcortical areas | (*89*) |

PDD = PD dementia; MCI = mild cognitive impairment; $DVR_{Cb}$ = $V_T$ ratio (cerebellum reference); PiB = Pittsburgh compound B; aMCI = amnestic MCI; bvFTD = behavioral-variant FTD. Listing is in chronologic order per disorder.

nondisplaceable $V_T$ ($V_{ND}$) (*38,43*). Nevertheless, CS $V_T$ significantly correlates with gray matter $V_{ND}$, suggesting that it remains a useful proxy reference region (*43*). However, for disorders with white matter pathology, $V_T$ (*44*) or $V_T$ normalized by plasma protein binding ($f_p$) (*45*) is a useful outcome measure.

To avoid arterial sampling, there are 2 analysis approaches: using a reference tissue model or using the SUV ratio (SUVR). Since 1TC is the optimal model for $^{11}$C-UCB-J, SRTM and SRTM2 were suitable. However, estimating $k_2'$, the efflux rate from the CS, is challenging for $^{11}$C-UCB-J. For scanning time, SRTM2 was shown to work well, with an acquisition of about 90 min (*46*). For shorter scans, SRTM2 had poorer performance, and the variance of $k_2'$ estimates increased. When the 1TC $k_2$ value of CS is similar between cognitively normal (CN) subjects and patients, SRTM2 with a population average $k_2'$ is a promising method to generate $BP_{ND}$ images, although this approach requires validation in each population.

After bolus injection, the tissue-to-plasma ratio (i.e., the apparent $V_T$) continued to increase through a 2-h scan and overestimated the 1TC $V_T$ (*47*). However, the overestimation in gray matter and CS tended to cancel out while computing the SUVR (ratio of target tissue to CS). Although the SUVRs also increased monotonically, a good match between SUVR-1 and 1TC $BP_{ND}$ was observed at 60–90 min after injection regardless of subject conditions (*38,45,46*). Similar results have been found for $^{18}$F-SynVesT-1 (*32*), which should allow the use of SUVR.

## PRECLINICAL SV2A PET

Several preclinical SV2A studies were conducted on animal models of neurodegenerative diseases. A transgenic AD mouse model (APP/PS1) was scanned with $^{11}$C-UCB-J and showed significantly lower SUVR in the hippocampus than did the wild type. In addition, after 1 mo of treatment with saracatinib, a Fyn kinase inhibitor, a significant SUVR increase in the hippocampus was found (*48*). Other SV2A PET studies have shown significant SV2A tracer binding decreases in mouse models, such as heterozygous Thy1-αSyn for PD (*49*) and heterozygous Q175DN knock-in for HD (*50*). In the PD model, a 12% decline was seen in the hippocampus using an area under the curve ratio between hippocampus and blood as the outcome measure (*49*). The HD mouse model showed a 20% lower $V_T$ in the striatum as estimated using an image-derived input function (*50*).

In rats, striatal lesion models with 6-hydroxydopamine for PD and quinolinic acid for HD showed significant striatal decreases in $^{11}$C-UCB-J binding (*51*). With 6-hydroxydopamine injected in the medial forebrain bundle and substantia nigra (SN), ipsilateral striatal reductions were found, demonstrating network effects within the brain circuits (*52*). These preclinical results support the use of SV2A PET to assess disease-specific synaptic deficits and the possibility of monitoring treatment effects. These rodent studies are summarized in Table 1.

## PD AND DLB

Studies of PD have demonstrated the involvement of several neurotransmitter systems beyond dopamine and the importance of using new tools and biomarkers to investigate this condition (*53,54*). Growing evidence has drawn attention to the significance of exploring synaptic changes in this condition (*55*).

Matuskey et al. conducted the first in vivo investigation of SV2A/synaptic density in 12 subjects with mild bilateral PD and 12 matched CN subjects using $^{11}$C-UCB-J. A lower $BP_{ND}$ was found in PD, with between-group differences in subcortical regions including the SN (−45%), red nucleus (−31%), and locus coeruleus (−17%). Interestingly, lower synaptic density was also observed in cortical areas, including the posterior cingulate cortex (−15%), parahippocampal gyrus (−12%), orbitofrontal cortex (−11%), and ventromedial prefrontal cortex (−11%) (*56*).

In a related study, Wilson et al. compared SV2A PET in 12 drug-naïve early PD patients and 16 CN subjects. Similarly, the PD group had a significantly lower $^{11}$C-UCB-J $V_T$ in the striatum, thalamus, brain stem, dorsal raphe, and cortical regions. Differences in this cohort were less pronounced in the SN (−7%). This study also investigated the correlation between clinical symptoms and $V_T$ values, revealing a negative correlation between synaptic density in the brain stem and clinical rating scores. Furthermore, 8 PD patients underwent a longitudinal $^{11}$C-UCB-J PET scan at a 1-y interval with no significant changes detected (*57*).

In a third study, Delva et al. used $^{11}$C-UCB-J, comparing 30 patients with PD and 20 CN subjects (*58*) and reported significantly lower $BP_{ND}$ in the SN (−15%). They also reported lower $BP_{ND}$ in dorsal striatum (−7%), caudate (−6%), and putamen (−6%) in the PD group. No correlation between $BP_{ND}$ values and clinical symptoms was found.

DLB is closely related to PD with 4 major characteristics: parkinsonism, visual hallucinations, cognitive fluctuations, and rapid-eye-movement sleep behavior disorder (*59*). Andersen et al. used $^{11}$C-UCB-J to compare synaptic density in 21 nondemented PD subjects, 13 patients with PD dementia or DLB, and 15 age-matched CN subjects using SUVR-1 as the outcome, with cerebellar white matter as a reference region (*60*). The nondemented PD group showed lower values only in the SN compared with CN subjects. The brain changes in the DLB/PD dementia group were more extensive, with significantly lower SUVR-1 values in the SN, occipital cortices, parietal cortices, primary sensorimotor cortex, middle frontal gyrus, and orbitofrontal cortex.

These preliminary investigations with $^{11}$C-UCB-J have shown its ability to assess PD changes and the potential to add to the understanding of its pathophysiology and potentially improving diagnosis of conditions such as PD and DLB. Further studies with larger samples are currently ongoing to reach that goal.

## AD

From a diagnostic perspective, AD is increasingly viewed along a continuum from preclinical AD to mild cognitive impairment and to AD dementia. The clinical dementia stage of AD is coupled to a distinct pathology with formation of plaques composed of Aβ, neurofibrillary tangles, and synaptic density loss (*61*). Synapses are crucial for cognitive function, and synaptic density loss is a robust and consistent pathology in AD (*62*). Cognitive impairment in AD is closely associated with synaptic density loss (*63*). Synaptic density damage is observed in the earliest stages of clinical AD with loss of synapses and several presynaptic proteins (*64*). Thus, the ability to assess synaptic density in vivo can be extremely valuable in studies of AD and in monitoring efficacy of potential therapies.

PET imaging is heavily used in AD studies to measure glucose metabolism (i.e., $^{18}$F-FDG), β-amyloid plaques, and neurofibrillary tangles under the amyloid-tau-neurodegeneration (AT(N)) framework (*65*). $^{18}$F-FDG PET is widely used to differentiate AD

from FTD and to track disease progression by measuring neuronal activity (*66*). However, $^{18}$F-FDG is not a direct biomarker of synaptic density and is affected by stimulation, medication, and blood glucose level (*67,68*). SV2A PET can provide a direct indicator of synaptic density in AD.

In the first SV2A PET AD study with $^{11}$C-UCB-J, 10 AD (all Aβ+) and 11 CN subjects were compared (*69*). Reduced hippocampal binding was hypothesized on the basis of early degeneration of entorhinal cortical cell projections to the hippocampus via the perforant pathway (*70*) and postmortem studies (*64*). $BP_{ND}$ using CS as the reference region (*43*) was lower by 41% in the hippocampus of AD patients than in CN subjects and was larger than the volume loss (22%) measured by MRI (*69*). Statistically significant correlations were found between hippocampus $BP_{ND}$ and cognitive tests, including an episodic memory score and the clinical dementia rating sum of boxes (*69*). Bastin et al. used $^{18}$F-UCB-H in 24 patients with mild cognitive impairment or AD (all Aβ+) and 19 CN subjects (*71*), and $V_T$ was lower in the hippocampus (31%), cortical regions (11%–18%), and thalamus (16%). Hippocampal binding was directly related to patients' cognitive decline and unawareness of memory problems.

In a subsequent $^{11}$C-UCB-J study in a larger cohort of early AD patients ($n = 34$) and CN subjects ($n = 19$), more extensive cortical and subcortical reductions in SV2A binding were seen, which were more widespread than reductions in gray matter volume (*72*). Here, the outcome measure was $V_T$ ratio with cerebellum as an alternative reference region, which provided a more robust signal than the small CS region. These findings better reflect the pathologic findings of reduced cortical synaptic density in AD postmortem studies (*73*).

The pattern of relationships between SV2A PET for synaptic density with amyloid (*74*), tau (*75–77*), and $^{18}$F-FDG (*78*) have been investigated in AD. We measured $^{11}$C-UCB-J $V_T$ ratio and $^{11}$C-PiB for Aβ deposition and observed a significant inverse association between global Aβ deposition and hippocampal SV2A binding in participants with mild cognitive impairment but not mild dementia (*74*). A paradoxic positive association between hippocampal Aβ and SV2A binding was found (*74*), suggesting that fibrillar Aβ is still accumulating in the early stages of disease before plateauing at later stages (*74*).

A study of 10 patients with mild cognitive impairment and 10 CN subjects found an inverse association between tau deposition ($^{18}$F-MK-6240) and $^{11}$C-UCB-J within the medial temporal lobe (*75*). Decreased performance on cognitive tests was associated with both increased tau and decreased SV2A binding in the hippocampus, although in a multivariate analysis only tau binding was significantly related to cognitive performance (*75*). Similarly, higher regional $^{18}$F-flortaucipir uptake was reported with lower $^{11}$C-UCB-J uptake across the subjects in a cohort study of 7 AD patients (*76*). Both higher $^{18}$F-flortaucipir and lower $^{11}$C-UCB-J uptake were associated with altered synaptic function by magnetoencephalography spectral measures (*76*). A third correlation study between $^{11}$C-UCB-J and $^{18}$F-flortaucipir in 10 AD patients and 10 CN participants showed that entorhinal cortical tau was inversely associated with hippocampal synaptic density, reflecting synaptic failure due to tau pathology in entorhinal cortical neurons projecting to the hippocampus (*77*).

A study comparing $^{11}$C-UCB-J and $^{18}$F-FDG in 14 AD patients and 11 CN participants found that these measures showed a similar magnitude of reduction in the medial temporal lobe of AD patients (*78*). However, the reduction of $^{11}$C-UCB-J in the neocortex was smaller than that of $^{18}$F-FDG. The highest intertracer correlations were found in the medial temporal cortex. Interestingly, there was a similar pattern of $^{11}$C-UCB-J delivery and perfusion (e.g., $K_1$) and $^{18}$F-FDG uptake (e.g., Patlak $K_i$). Thus, measures of synaptic loss and perfusion or metabolism that can be obtained with a single dynamic $^{11}$C-UCB-J scan provide complementary information on the pathophysiology of AD (*78*).

### FTD

FTD is commonly misdiagnosed as AD or other neuropsychiatric disorders because of its 2 major patterns: gradual or progressive changes in behavior or language impairments. The affected population is usually younger than AD patients (35–75 y), and 20%–40% of patients have a family history of FTD (*79*). Previous studies have provided evidence of synaptic dysfunction and loss in FTD (*80*). Malpetti et al. assessed in vivo synaptic density in 3 presymptomatic C9orf72 mutation carriers, 1 symptomatic patient with the behavioral variant (bvFTD), and 19 healthy controls (*81*). In the presymptomatic group, they reported a prominent decline in thalamic $^{11}$C-UCB-J binding, with a minor reduction in the cortex. The patient with bvFTD demonstrated extensive synaptic loss in the frontotemporal regions. Salmon et al. assessed use of $^{18}$F-UCB-H PET in 12 patients with probable bvFTD compared with 12 CN subjects and 12 AD patients and reported decreased binding in the right anterior parahippocampal gyrus in bvFTD (*82*). Anosognosia correlated with synaptic density in the caudate nucleus and the anteromedial prefrontal cortex. Ongoing studies in bvFTD are being conducted to further characterize this disorder.

### HD

HD is an autosomal dominant disease caused by an expanded CAG triplet in the Huntington chromosome. Clinical characterizations of HD are progressive movement disorders (including chorea), cognitive deficits (culminating in dementia), and psychiatric symptoms (e.g., depression) (*83*). The pathogenesis of HD is not clear, but studies have found synaptic and neuronal dysfunction and death in the cortex and striatum in HD patients (*84*). Lower SV2A levels (~25%) were observed in the cortical area in HD gene carriers than in controls by $^{3}$H-UCB-J autoradiography and SV2A immunofluorescence in human brain tissue (*50*). Recently, an in vivo human PET study found a significant loss of SV2A in multiple regions including the putamen (−28%), caudate (−25%), and whole gray matter (−9%) in the HD group ($n = 11$) compared with the CN group ($n = 15$), with similar findings in the premanifest HD mutation carrier group ($n = 7$) (*85*). Striatal $^{11}$C-UCB-J binding correlated positively with clinical measures in motor and cognitive domains (*85*).

### PSP AND CBD

PSP and CBD are both neurodegenerative primary tauopathies and have similarities in clinical symptoms (e.g., motor, behavioral, and cognitive abnormalities) (*86*) but are considered different disorders because different tau strains and brain regions are affected (*87*). Previous work has suggested that oligomeric tau leads to synaptic loss (*88*), which may play an essential role in PSP and CBD. Recently, Holland et al. found widespread (≤50%) cortical and subcortical reductions in $^{11}$C-UCB-J binding in both PSP ($n = 14$) and CBD ($n = 15$) compared with controls (*89*), consistent with postmortem data (*88*). They also reported a negative

correlation between global $^{11}$C-UCB-J binding and the PSP and CBD rating scales and a positive correlation with the revised Addenbrooke Cognitive Examination (*89*).

## FUTURE CONSIDERATIONS

In summary, PET imaging of SV2A provides a direct measure of synaptic vesicles and is a proxy for synaptic density. High-quality PET radioligands labeled with $^{11}$C and $^{18}$F have been developed and validated for application in human studies. The potentially general utility of synaptic imaging has prompted wide initial application of these tools. Here we have focused on SV2A PET in studies of neurodegenerative disorders, both preclinically (Table 1) and clinically (Table 2). In general, these PET studies indicate SV2A loss to be specific to disease-associated brain regions and consistent with synaptic density loss. Although the loss of synaptic density may not be specific to neurodegeneration, the regional pattern of synaptic loss could potentially provide insights for differentiating various types of dementia.

In addition, clinical studies have been performed in epilepsy (*90*), schizophrenia (*91,92*), depression (*44*), posttraumatic stress disorder (*44*), stroke (*93*), cocaine-use disorder (*45*), and cannabis-use disorder (*94*), as well as in normal aging (*95*). The utility of SV2A as a general marker of synaptic density is promising and warrants formal validation by comparison of in vivo SV2A PET signal to postmortem evaluation of SV2A and synapse levels in the human brain. Further studies also warrant use of $^{18}$F-labeled radioligands in larger patient cohorts to establish the potential clinical applications of SV2A PET imaging, including the early detection of synaptic density loss, differential diagnosis among different types of dementia, and the monitoring of disease progression. SV2A PET could also be used as an outcome measure for trials of disease-modifying therapies, particularly those that target the preservation and restoration of synapses. Overall, SV2A PET is an exciting new tool in the nuclear medicine arsenal and holds great promise as a novel in vivo biomarker for dementia and neurodegeneration.

## DISCLOSURE

The radioligand $^{18}$F-SynVesT-1 is contained in the international patent application PCT/US2018/018388, "Radiolabeled Pharmaceuticals and Methods of Making and Using Same," filed on February 15, 2018, and Richard Carson is listed as an inventor. Sjoerd Finnema is a full-time employee of Abbvie. No other potential conflict of interest relevant to this article was reported.

## REFERENCES


1. Bajjalieh SM, Peterson K, Shinghal R, Scheller RH. SV2, a brain synaptic vesicle protein homologous to bacterial transporters. *Science.* 1992;257:1271–1273.
2. Buckley K, Kelly RB. Identification of a transmembrane glycoprotein specific for secretory vesicles of neural and endocrine cells. *J Cell Biol.* 1985;100:1284–1294.
3. Floor E, Feist BE. Most synaptic vesicles isolated from rat brain carry three membrane proteins, SV2, synaptophysin, and p65. *J Neurochem.* 1989;52:1433–1437.
4. Nowack A, Yao J, Custer KL, Bajjalieh SM. SV2 regulates neurotransmitter release via multiple mechanisms. *Am J Physiol Cell Physiol.* 2010;299:C960–C967.
5. Mendoza-Torreblanca JG, Vanoye-Carlo A, Phillips-Farfan BV, Carmona-Aparicio L, Gomez-Lira G. Synaptic vesicle protein 2A: basic facts and role in synaptic function. *Eur J Neurosci.* 2013;38:3529–3539.
6. Bartholome O, Van den Ackerveken P, Sanchez Gil J, et al. Puzzling out synaptic vesicle 2 family members functions. *Front Mol Neurosci.* 2017;10:148.
7. Bajjalieh SM, Frantz GD, Weimann JM, McConnell SK, Scheller RH. Differential expression of synaptic vesicle protein 2 (SV2) isoforms. *J Neurosci.* 1994;14:5223–5235.
8. Janz R, Sudhof TC. SV2C is a synaptic vesicle protein with an unusually restricted localization: anatomy of a synaptic vesicle protein family. *Neuroscience.* 1999;94:1279–1290.
9. Bajjalieh SM, Peterson K, Linial M, Scheller RH. Brain contains two forms of synaptic vesicle protein 2. *Proc Natl Acad Sci USA.* 1993;90:2150–2154.
10. Lynch BA, Lambeng N, Nocka K, et al. The synaptic vesicle protein SV2A is the binding site for the antiepileptic drug levetiracetam. *Proc Natl Acad Sci USA.* 2004;101:9861–9866.
11. Gillard M, Chatelain P, Fuks B. Binding characteristics of levetiracetam to synaptic vesicle protein 2A (SV2A) in human brain and in CHO cells expressing the human recombinant protein. *Eur J Pharmacol.* 2006;536:102–108.
12. Gillard M, Fuks B, Leclercq K, Matagne A. Binding characteristics of brivaracetam, a selective, high affinity SV2A ligand in rat, mouse and human brain: relationship to anti-convulsant properties. *Eur J Pharmacol.* 2011;664:36–44.
13. Klein P, Diaz A, Gasalla T, Whitesides J. A review of the pharmacology and clinical efficacy of brivaracetam. *Clin Pharmacol.* 2018;10:1–22.
14. Cai H, Mangner TJ, Muzik O, Wang M-W, Chugani DC, Chugani HT. Radiosynthesis of $^{11}$C-levetiracetam: a potential marker for PET imaging of SV2A expression. *ACS Med Chem Lett.* 2014;5:1152–1155.
15. Danish A, Namasivayam V, Schiedel AC, Muller CE. Interaction of approved drugs with synaptic vesicle protein 2A. *Arch Pharm (Weinheim).* 2017;350:1700003.
16. Mercier J, Archen L, Bollu V, et al. Discovery of heterocyclic nonacetamide synaptic vesicle protein 2A (SV2A) ligands with single-digit nanomolar potency: opening avenues towards the first SV2A positron emission tomography (PET) ligands. *ChemMedChem.* 2014;9:693–698.
17. Mercier J, Provins L, Valade A. Discovery and development of SV2A PET tracers: potential for imaging synaptic density and clinical applications. *Drug Discov Today Technol.* 2017;25:45–52.
18. Estrada S, Lubberink M, Thibblin A, et al. [$^{11}$C]UCB-A, a novel PET tracer for synaptic vesicle protein 2 A. *Nucl Med Biol.* 2016;43:325–332.
19. Warnock GI, Aerts J, Bahri MA, et al. Evaluation of $^{18}$F-UCB-H as a novel PET tracer for synaptic vesicle protein 2A in the brain. *J Nucl Med.* 2014;55:1336–1341.
20. Becker G, Warnier C, Serrano ME, et al. Pharmacokinetic characterization of [$^{18}$F]UCB-H PET radiopharmaceutical in the rat brain. *Mol Pharm.* 2017;14:2719–2725.
21. Warnier C, Lemaire C, Becker G, et al. Enabling efficient positron emission tomography (PET) imaging of synaptic vesicle glycoprotein 2A (SV2A) with a robust and one-step radiosynthesis of a highly potent $^{18}$F-labeled ligand ([$^{18}$F]UCB-H). *J Med Chem.* 2016;59:8955–8966.
22. Bretin F, Warnock G, Bahri MA, et al. Preclinical radiation dosimetry for the novel SV2A radiotracer [$^{18}$F]UCB-H. *EJNMMI Res.* 2013;3:35.
23. Nabulsi NB, Mercier J, Holden D, et al. Synthesis and preclinical evaluation of $^{11}$C-UCB-J as a PET tracer for imaging the synaptic vesicle glycoprotein 2A in the brain. *J Nucl Med.* 2016;57:777–784.
24. Finnema SJ, Nabulsi NB, Eid T, et al. Imaging synaptic density in the living human brain. *Sci Transl Med.* 2016;8:348ra96.
25. Lubberink M, Appel L, Daging J, et al. Tracer kinetic analysis of the SV2A ligand $^{11}$C-UCBA as a PET marker for synaptic density in humans [abstract]. *J Nucl Med.* 2017;58(suppl):631.
26. Bahri MA, Plenevaux A, Aerts J, et al. Measuring brain synaptic vesicle protein 2A with positron emission tomography and [$^{18}$F]UCB-H. *Alzheimers Dement (N Y).* 2017;3:481–486.
27. Li S, Cai Z, Zhang W, et al. Synthesis and in vivo evaluation of [$^{18}$F]UCB-J for PET imaging of synaptic vesicle glycoprotein 2A (SV2A). *Eur J Nucl Med Mol Imaging.* 2019;46:1952–1965.
28. Li S, Cai Z, Wu X, et al. Synthesis and in vivo evaluation of a novel PET radiotracer for imaging of synaptic vesicle glycoprotein 2A (SV2A) in nonhuman primates. *ACS Chem Neurosci.* 2019;10:1544–1554.
29. Constantinescu CC, Tresse C, Zheng M, et al. Development and in vivo preclinical imaging of fluorine-18-labeled synaptic vesicle protein 2A (SV2A) PET tracers. *Mol Imaging Biol.* 2019;21:509–518.
30. Cai Z, Li S, Zhang W, et al. Synthesis and preclinical evaluation of an $^{18}$F-labeled synaptic vesicle glycoprotein 2A PET imaging probe: [$^{18}$F]SynVesT-2. *ACS Chem Neurosci.* 2020;11:592–603.
31. Li S, Naganawa M, Pracitto R, et al. Assessment of test-retest reproducibility of [$^{18}$F]SynVesT-1, a novel radiotracer for PET imaging of synaptic vesicle glycoprotein 2A. *Eur J Nucl Med Mol Imaging.* 2021;48:1327–1338.

32. Naganawa M, Li S, Nabulsi N, et al. First-in-human evaluation of $^{18}$F-SynVesT-1, a radioligand for PET imaging of synaptic vesicle glycoprotein 2A. *J Nucl Med.* 2021;62:561–567.
33. De Camilli P, Harris SM Jr, Huttner WB, Greengard P, Synapsin I (protein I), a nerve terminal-specific phosphoprotein. II. Its specific association with synaptic vesicles demonstrated by immunocytochemistry in agarose-embedded synaptosomes. *J Cell Biol.* 1983;96:1355–1373.
34. Goelz SE, Nestler EJ, Chehrazi B, Greengard P. Distribution of protein I in mammalian brain as determined by a detergent-based radioimmunoassay. *Proc Natl Acad Sci USA.* 1981;78:2130–2134.
35. Masliah E, Terry RD, Alford M, DeTeresa R. Quantitative immunohistochemistry of synaptophysin in human neocortex: an alternative method to estimate density of presynaptic terminals in paraffin sections. *J Histochem Cytochem.* 1990;38:837–844.
36. Mutch SA, Kensel-Hammes P, Gadd JC, et al. Protein quantification at the single vesicle level reveals that a subset of synaptic vesicle proteins are trafficked with high precision. *J Neurosci.* 2011;31:1461–1470.
37. Finnema SJ, Nabulsi NB, Mercier J, et al. Kinetic evaluation and test-retest reproducibility of [$^{11}$C]UCB-J, a novel radioligand for positron emission tomography imaging of synaptic vesicle glycoprotein 2A in humans. *J Cereb Blood Flow Metab.* 2018;38:2041–2052.
38. Koole M, van Aalst J, Devrome M, et al. Quantifying SV2A density and drug occupancy in the human brain using [$^{11}$C]UCB-J PET imaging and subcortical white matter as reference tissue. *Eur J Nucl Med Mol Imaging.* 2019; 46:396–406.
39. Mansur A, Rabiner EA, Comley RA, et al. Characterization of 3 PET tracers for quantification of mitochondrial and synaptic function in healthy human brain: $^{18}$F-BCPP-EF, $^{11}$C-SA-4503, and $^{11}$C-UCB-J. *J Nucl Med.* 2020;61:96–103.
40. Smart K, Liu H, Matuskey D, et al. Binding of the synaptic vesicle radiotracer [$^{11}$C]UCB-J is unchanged during functional brain activation using a visual stimulation task. *J Cereb Blood Flow Metab.* 2021;41:1067–1079.
41. Finnema SJ, Rossano S, Naganawa M, et al. A single-center, open-label positron emission tomography study to evaluate brivaracetam and levetiracetam synaptic vesicle glycoprotein 2A binding in healthy volunteers. *Epilepsia.* 2019;60:958–967.
42. Varnäs K, Stepanov V, Halldin C. Autoradiographic mapping of synaptic vesicle glycoprotein 2A in non-human primate and human brain. *Synapse.* 2020;74:e22157.
43. Rossano S, Toyonaga T, Finnema SJ, et al. Assessment of a white matter reference region for $^{11}$C-UCB-J PET quantification. *J Cereb Blood Flow Metab.* 2020;40: 1890–1901.
44. Holmes SE, Scheinost D, Finnema SJ, et al. Lower synaptic density is associated with depression severity and network alterations. *Nat Commun.* 2019;10:1529.
45. Angarita GA, Worhunsky PD, Naganawa M, et al. Lower prefrontal cortical synaptic vesicle binding in cocaine use disorder: an exploratory $^{11}$C-UCB-J positron emission tomography study in humans. *Addict Biol.* December 1, 2021 [Epub ahead of print].
46. Mertens N, Maguire RP, Serdons K, et al. Validation of parametric methods for [$^{11}$C]UCB-J PET imaging using subcortical white matter as reference tissue. *Mol Imaging Biol.* 2020;22:444–452.
47. Naganawa M, Gallezot JD, Finnema SJ, et al. Simplified quantification of $^{11}$C-UCB-J PET evaluated in a large human cohort. *J Nucl Med.* 2021;62:418–421.
48. Toyonaga T, Smith LM, Finnema SJ, et al. In vivo synaptic density imaging with $^{11}$C-UCB-J detects treatment effects of saracatinib in a mouse model of Alzheimer disease. *J Nucl Med.* 2019;60:1780–1786.
49. Xiong M, Roshanbin S, Rokka J, et al. In vivo imaging of synaptic density with [$^{11}$C]UCB-J PET in two mouse models of neurodegenerative disease. *Neuroimage.* 2021;239:118302.
50. Bertoglio D, Verhaeghe J, Wyffels L, et al. Synaptic vesicle glycoprotein 2A is affected in the CNS of Huntington's disease mice and post-mortem human HD brain. *J Nucl Med.* September 16, 2021[Epub ahead of print].
51. Thomsen MB, Jacobsen J, Lillethorup TP, et al. In vivo imaging of synaptic SV2A protein density in healthy and striatal-lesioned rats with [$^{11}$C]UCB-J PET. *J Cereb Blood Flow Metab.* 2021;41:819–830.
52. Raval NR, Gudmundsen F, Juhl M, et al. Synaptic density and neuronal metabolic function measured by positron emission tomography in the unilateral 6-OHDA rat model of Parkinson's disease. *Front Synaptic Neurosci.* 2021;13: 715811.
53. Picconi B, Piccoli G, Calabresi P. Synaptic dysfunction in Parkinson's disease. *Adv Exp Med Biol.* 2012;970:553–572.
54. Jellinger KA. Neuropathology of sporadic Parkinson's disease: evaluation and changes of concepts. *Mov Disord.* 2012;27:8–30.
55. Villalba RM, Smith Y. Differential striatal spine pathology in Parkinson's disease and cocaine addiction: a key role of dopamine? *Neuroscience.* 2013;251: 2–20.
56. Matuskey D, Tinaz S, Wilcox KC, et al. Synaptic changes in Parkinson disease assessed with in vivo imaging. *Ann Neurol.* 2020;87:329–338.
57. Wilson H, Pagano G, de Natale ER, et al. Mitochondrial complex 1, sigma 1, and synaptic vesicle 2A in early drug-naive Parkinson's disease. *Mov Disord.* 2020;35: 1416–1427.
58. Delva A, Van Weehaeghe D, Koole M, Van Laere K, Vandenberghe W. Loss of presynaptic terminal integrity in the substantia nigra in early Parkinson's disease. *Mov Disord.* 2020;35:1977–1986.
59. McKeith IG, Boeve BF, Dickson DW, et al. Diagnosis and management of dementia with Lewy bodies: fourth consensus report of the DLB consortium. *Neurology.* 2017;89:88–100.
60. Andersen KB, Hansen AK, Damholdt MF, et al. Reduced synaptic density in patients with Lewy body dementia: An [$^{11}$C]UCB-J PET imaging study. *Mov Disord.* 2021;36:2057–2065.
61. Overk CR, Masliah E. Pathogenesis of synaptic degeneration in Alzheimer's disease and Lewy body disease. *Biochem Pharmacol.* 2014;88:508–516.
62. Selkoe DJ. Alzheimer's disease is a synaptic failure. *Science.* 2002;298: 789–791.
63. DeKosky ST, Scheff SW. Synapse loss in frontal cortex biopsies in Alzheimer's disease: correlation with cognitive severity. *Ann Neurol.* 1990;27: 457–464.
64. Robinson JL, Molina-Porcel L, Corrada MM, et al. Perforant path synaptic loss correlates with cognitive impairment and Alzheimer's disease in the oldest-old. *Brain.* 2014;137:2578–2587.
65. Jack CR Jr, Bennett DA, Blennow K, et al. NIA-AA Research Framework: toward a biological definition of Alzheimer's disease. *Alzheimers Dement.* 2018;14:535–562.
66. Landau SM, Harvey D, Madison CM, et al. Associations between cognitive, functional, and FDG-PET measures of decline in AD and MCI. *Neurobiol Aging.* 2011; 32:1207–1218.
67. Ishibashi K, Onishi A, Fujiwara Y, Ishiwata K, Ishii K. Relationship between Alzheimer disease-like pattern of $^{18}$F-FDG and fasting plasma glucose levels in cognitively normal volunteers. *J Nucl Med.* 2015;56:229–233.
68. Burns CM, Chen K, Kaszniak AW, et al. Higher serum glucose levels are associated with cerebral hypometabolism in Alzheimer regions. *Neurology.* 2013;80: 1557–1564.
69. Chen MK, Mecca AP, Naganawa M, et al. Assessing synaptic density in Alzheimer disease with synaptic vesicle glycoprotein 2A positron emission tomographic imaging. *JAMA Neurol.* 2018;75:1215–1224.
70. Braak H, Thal DR, Ghebremedhin E, Del Tredici K. Stages of the pathologic process in Alzheimer disease: age categories from 1 to 100 years. *J Neuropathol Exp Neurol.* 2011;70:960–969.
71. Bastin C, Bahri MA, Meyer F, et al. In vivo imaging of synaptic loss in Alzheimer's disease with [$^{18}$F]UCB-H positron emission tomography. *Eur J Nucl Med Mol Imaging.* 2020;47:390–402.
72. Mecca AP, Chen MK, O'Dell RS, et al. In vivo measurement of widespread synaptic loss in Alzheimer's disease with SV2A PET. *Alzheimers Dement.* 2020;16:974–982.
73. de Wilde MC, Overk CR, Sijben JW, Masliah E. Meta-analysis of synaptic pathology in Alzheimer's disease reveals selective molecular vesicular machinery vulnerability. *Alzheimers Dement.* 2016;12:633–644.
74. O'Dell RS, Mecca AP, Chen MK, et al. Association of Aβ deposition and regional synaptic density in early Alzheimer's disease: a PET imaging study with [$^{11}$C]UCB-J. *Alzheimers Res Ther.* 2021;13:11.
75. Vanhaute H, Ceccarini J, Michiels L, et al. In vivo synaptic density loss is related to tau deposition in amnestic mild cognitive impairment. *Neurology.* 2020;95: e545–e553.
76. Coomans EM, Schoonhoven DN, Tuncel H, et al. In vivo tau pathology is associated with synaptic loss and altered synaptic function. *Alzheimers Res Ther.* 2021; 13:35.
77. Mecca AP, Chen M-K, O'Dell RS, et al. Association of entorhinal cortical tau deposition and hippocampal synaptic density in older individuals with normal cognition and early Alzheimer's disease. *Neurobiol Aging.* 2022; 111:44–53.
78. Chen MK, Mecca AP, Naganawa M, et al. Comparison of [$^{11}$C]UCB-J and [$^{18}$F]FDG PET in Alzheimer's disease: a tracer kinetic modeling study. *J Cereb Blood Flow Metab.* 2021:271678X211004312.
79. McKhann GM, Albert MS, Grossman M, Miller B, Dickson D, Trojanowski JQ. Clinical and pathological diagnosis of frontotemporal dementia: report of the Work Group on Frontotemporal Dementia and Pick's Disease. *Arch Neurol.* 2001;58: 1803–1809.
80. Marttinen M, Kurkinen KM, Soininen H, Haapasalo A, Hiltunen M. Synaptic dysfunction and septin protein family members in neurodegenerative diseases. *Mol Neurodegener.* 2015;10:16.

81. Malpetti M, Holland N, Jones PS, et al. Synaptic density in carriers of C9orf72 mutations: a [$^{11}$C]UCB-J PET study. *Ann Clin Transl Neurol.* 2021; 8:1515–1523.
82. Salmon E, Bahri MA, Plenevaux A, et al. In vivo exploration of synaptic projections in frontotemporal dementia. *Sci Rep.* 2021;11:16092.
83. Nithianantharajah J, Hannan AJ. Dysregulation of synaptic proteins, dendritic spine abnormalities and pathological plasticity of synapses as experience-dependent mediators of cognitive and psychiatric symptoms in Huntington's disease. *Neuroscience.* 2013;251:66–74.
84. Fourie C, Kim E, Waldvogel H, et al. Differential changes in postsynaptic density proteins in postmortem Huntington's disease and Parkinson's disease human brains. *J Neurodegener Dis.* 2014;2014:938530.
85. Delva A, Michiels L, Koole M, Van Laere K, Vandenberghe W. Synaptic damage and its clinical correlates in people with early Huntington disease: a PET study. *Neurology.* 2022;98:e83–e94.
86. Burrell JR, Hodges JR, Rowe JB. Cognition in corticobasal syndrome and progressive supranuclear palsy: a review. *Mov Disord.* 2014;29:684–693.
87. Sanders DW, Kaufman SK, DeVos SL, et al. Distinct tau prion strains propagate in cells and mice and define different tauopathies. *Neuron.* 2014;82:1271–1288.
88. Bigio EH, Vono MB, Satumtira S, et al. Cortical synapse loss in progressive supranuclear palsy. *J Neuropathol Exp Neurol.* 2001;60:403–410.
89. Holland N, Jones PS, Savulich G, et al. Synaptic loss in primary tauopathies revealed by [$^{11}$C]UCB-J positron emission tomography. *Mov Disord.* 2020;35: 1834–1842.
90. Finnema SJ, Toyonaga T, Detyniecki K, et al. Reduced synaptic vesicle protein 2A binding in temporal lobe epilepsy: A [$^{11}$C]UCB-J positron emission tomography study. *Epilepsia.* 2020;61:2183–2193.
91. Onwordi EC, Whitehurst T, Mansur A, et al. The relationship between synaptic density marker SV2A, glutamate and N-acetyl aspartate levels in healthy volunteers and schizophrenia: a multimodal PET and magnetic resonance spectroscopy brain imaging study. *Transl Psychiatry.* 2021;11:393.
92. Radhakrishnan R, Skosnik PD, Ranganathan M, et al. In vivo evidence of lower synaptic vesicle density in schizophrenia. *Mol Psychiatry.* June 16, 2021 [Epub ahead of print].
93. Michiels L, Mertens N, Thijs L, et al. Changes in synaptic density in the subacute phase after ischemic stroke: A $^{11}$C-UCB-J PET/MR study. *J Cereb Blood Flow Metab.* 2021:271678X211047759.
94. D'Souza DC, Radhakrishnan R, Naganawa M, et al. Preliminary in vivo evidence of lower hippocampal synaptic density in cannabis use disorder. *Mol Psychiatry.* 2021;26:3192–3200.
95. Michiels L, Delva A, van Aalst J, et al. Synaptic density in healthy human aging is not influenced by age or sex: a $^{11}$C-UCB-J PET study. *Neuroimage.* 2021;232:117877.

# Future Directions in Molecular Imaging of Neurodegenerative Disorders

Henryk Barthel[1], Victor L. Villemagne[2], and Alexander Drzezga[3]

[1]*Department of Nuclear Medicine, University Medical Center, University of Leipzig, Leipzig, Germany;* [2]*Department of Psychiatry, University of Pittsburgh, Pittsburgh, Pennsylvania; and* [3]*Department of Nuclear Medicine, Faculty of Medicine and University Hospital Cologne, University of Cologne, German Center for Neurodegenerative Diseases, Bonn, Germany, and Institute of Neuroscience and Medicine, Molecular Organization of the Brain, Forschungszentrum Jülich, Jülich, Germany*

The improvement of existing techniques and the development of new molecular imaging methods are an exciting and rapidly developing field in clinical care and research of neurodegenerative disorders. In the clinic, molecular imaging has the potential to improve early and differential diagnosis and to stratify and monitor therapy in these disorders. Meanwhile, in research, these techniques improve our understanding of the underlying pathophysiology and pathobiochemistry of these disorders and allow for drug testing. This article is an overview on our perspective on future developments in neurodegeneration tracers and the associated imaging technologies. For example, we predict that the current portfolio of β-amyloid and tau aggregate tracers will be improved and supplemented by tracers allowing imaging of other protein aggregation pathologies, such as α-synuclein and transactive response DNA binding protein 43 kDa. Future developments will likely also be observed in imaging neurotransmitter systems. This refers to both offering imaging to a broader population in cases involving the dopaminergic, cholinergic, and serotonergic systems and making possible the imaging of systems not yet explored, such as the glutamate and opioid systems. Tracers will be complemented by improved tracers of neuroinflammation and synaptic density. Technologywise, the use of hybrid PET/MRI, dedicated brain PET, and total-body PET scanners, as well as advanced image acquisition and processing protocols, will open doors toward broader and more efficient clinical use and novel research applications. Molecular imaging has the potential of becoming a standard and essential clinical and research tool to diagnose and study neurodegenerative disorders and to guide treatments. On that road, we will need to redefine the role of molecular imaging in relation to that of emerging blood-based biomarkers. Taken together, the unique features of molecular imaging—that is, the potential to provide direct noninvasive information on the presence, extent, localization, and quantity of molecular pathologic processes in the living body—together with the predicted novel tracer and imaging technology developments, provide optimism about a bright future for this approach to improved care and research on neurodegenerative disorders.

**Key Words**: molecular imaging; neurodegeneration; PET; FDG; dopamine

**J Nucl Med 2022; 63:68S–74S**
DOI: 10.2967/jnumed.121.263202

With the growing elderly population and the consequently increased prevalence of neurodegenerative conditions, there is a public health need to identify individuals at risk of developing syndromes associated with these diseases. Alzheimer disease (AD) and Parkinson diseases are the most prevalent neurodegenerative conditions in the elderly. Furthermore, better understanding of the interaction of the known pathomechanisms involved in neurodegeneration is required, as well as better insight into additionally contributing factors, yet insufficiently understood.

Molecular imaging biomarkers today allow identification and quantification of the degree and extent of several of the known underlying pathologic traits in these conditions, permitting better characterization of disease and a more precise approach to the identification of risk factors. These can have independent or combined—synergistic, potentiating, or antagonistic—effects on the specific phenotype.

Molecular imaging markers of pathology, such as β-amyloid and tau imaging, and markers of neurodegeneration, such as brain glucose hypometabolism, have already been incorporated into new diagnostic criteria. Furthermore, molecular imaging studies have proven that the development of the underlying pathologic traits, such Aβ deposition in AD or loss of nigrostriatal terminals in Parkinson disease, is a long and protracted process that precedes the clinical phenotype for decades.

In AD, the introduction of biomarker-based approaches for the identification of brain pathology has informed new strategies for the design of clinical trials aimed at preventing or delaying the onset of cognitive impairment and dementia. The implementation of these biomarkers has shown that defining disease purely on the basis of the clinical syndromal appearance will not be sufficient to select suitable patients for therapies (i.e., exhibiting the therapy target or neuropathology). The implementation of multimodal imaging may also be the most reliable way to allow early initiation of therapy in patients at risk before development of extended irreversible neuronal injury. These imaging biomarkers may therefore play an increasingly important role in patient selection and monitoring of novel therapy approaches.

Many of the great advances and developments in the field of molecular imaging in neurodegeneration are covered in greater detail in the other articles of this supplement issue. In this article, we give a general outlook on the needs and further developments in the field.

## DEVELOPING NEW TRACERS FOR PROTEIN AGGREGATION PATHOLOGY IMAGING IN NEURODEGENERATIVE DISORDERS

Most neurodegenerative disorders are histopathologically characterized by the presence of certain protein aggregates. These

Received Jan. 31, 2022; revision accepted Apr. 19, 2022.
For correspondence or reprints, contact Henryk Barthel (henryk.barthel@medizin.uni-leipzig.de).

include β-amyloid, tau, α-synuclein, transactive response DNA binding protein 43 kDa (TDP-43), and other aggregates.

The detection of these pathologic protein accumulations in certain brain areas by postmortem histopathology has been considered the gold standard to diagnose these disorders. The successful introduction of radiotracers to image β-amyloid and tau pathology in vivo has shifted the time point of accurate diagnosis from postmortem to antemortem, and even possibly to prodromal disease stages, and allows assessment of changes over time. This is important because accurate in vivo diagnosis can impact individual patient management.

The current state of already-established PET tracers to image brain β-amyloid and tau pathology is discussed in separate contributions to this supplement. However, further developments in the field of tracers for protein aggregation pathologies are highly relevant in several respects. In specific neurodegenerative diseases, more than one proteinopathy is often present, as in AD, in which β-amyloid and tau proteins are found. Conversely, specific protein pathologies are often found in different neurodegenerative diseases, such as tau, which is present not only in AD but also in certain forms of frontotemporal dementia, movement disorders such as corticobasal degeneration or progressive supranuclear palsy, and primary age-related tauopathy. Although the aggregates found in these tauopathies are based on the same protein, they differ in brain location, affected cell type, and structure. Whereas in AD, for instance, predominantly intraneuronal tau aggregates in the form of paired helical filaments are found, in other tauopathies, such as corticobasal degeneration or progressive supranuclear palsy, aggregates of straight filaments are observed more frequently, located also in glial cells (*1*). These facts explain the need for tracers with high affinity for specific tau accumulation forms. Some of the second-generation tau PET tracers have been studied (discussed in another article in this supplement), but the development of tauopathy-selective compounds may be worthwhile. With regard to β-amyloid tracers, this development might also refer to different amyloid pathologies such as vascular β-amyloid to diagnose cerebral amyloid angiopathy, or β-amyloid oligomers in AD to place PET imaging closer to the neurodegenerative process.

Regarding β-amyloid imaging, there is also the question of whether we will see SPECT tracers emerge. In principle, a relevant place for such tracers as an addition to the established PET tracers is anticipated because the prevalence of AD is growing, the hope for the emergence of more disease-modifying drugs is high, and the target density in the affected brain is high enough to allow visualization by SPECT. To explore this intriguing concept, different groups have performed intensive work over the last few years (*2–6*) but without a major breakthrough so far, although preclinical data were promising. This current lack of success seems to be related mainly to insufficient signal-to-noise ratios in the human brain and high blood flow effects on target retention. It will be fascinating to observe whether optimized β-amyloid SPECT tracer candidates, eventually developed by novel drug development technologies, will be more successful.

Apart from these efforts to extend the tracer portfolio to image β-amyloid and tau, there are increasing efforts to develop PET tracers for other protein aggregates. These include tracers to image α-synuclein aggregates, which represent the histopathologic hallmark of Parkinson disease, Lewy body dementia, and multisystem atrophy. If successful, PET tracers selective for α-synuclein would significantly extend the concept of in vivo histopathology-based diagnosis to many new patients. The current state of development in this field was recently reviewed in an elegant manner by Korat et al. (*7*). The development of α-synuclein tracers faces 3 challenges. First, the target density is low compared with that of β-amyloid and tau aggregates or some enzymes such as monoamine oxidases. Second, avoidance of cross-selectivity is complicated, because to date, the tracers are aimed at binding β-sheets, the same secondary structure as found in β-amyloid and tau aggregates. Third, there is a lack of knowledge on the full crystal structure of the target, but progress with cryogenic electron microscopy might facilitate tracer development (*8*). As a consequence, α-synuclein tracers need to have exceptionally high binding affinity and selectivity. As Korat et al. noted, molecule candidates of 37 different chemical classes have so far been developed up to different stages (Fig. 1). According to Korat et al., only 2 of them, namely the diphenylpyrazole derivative $^{11}$C-MODAG-001 (*9*) and the quinolinyl analogs of $^{125}$I-TZ6184 (*10*) show sufficient target affinity, and 4 of them present with sufficient binding selectivity over β-amyloid and tau. To our knowledge, none of the tracers tested so far in humans by academic or commercial researchers was successful. The breakthrough may also be hindered by a lack of reliability and reproducibility of the available evaluation assays. There is, however, hope that advanced development strategies such as high-throughput screening, computational modeling, or antibody engineering might be more promising (*7*).

With regard to TDP-43 (a histopathologic hallmark of amyotrophic lateral sclerosis, some forms of frontotemporal dementia, and limbic-predominant age-related TDP-43 encephalopathy), no suitable PET tracers are yet available. It will, thus, also be fascinating to observe whether TDP-43 or other neurodegeneration pathology tracer candidates emerge.

## EXTENDING THE ROLE OF IMAGING NEUROTRANSMITTER SYSTEMS IN NEURODEGENERATIVE DISORDERS

In neurodegenerative disorders, the degenerative process may affect all kinds of brain tissue components. Thus, many neurotransmitter systems can be altered in these diseases. Further, specific

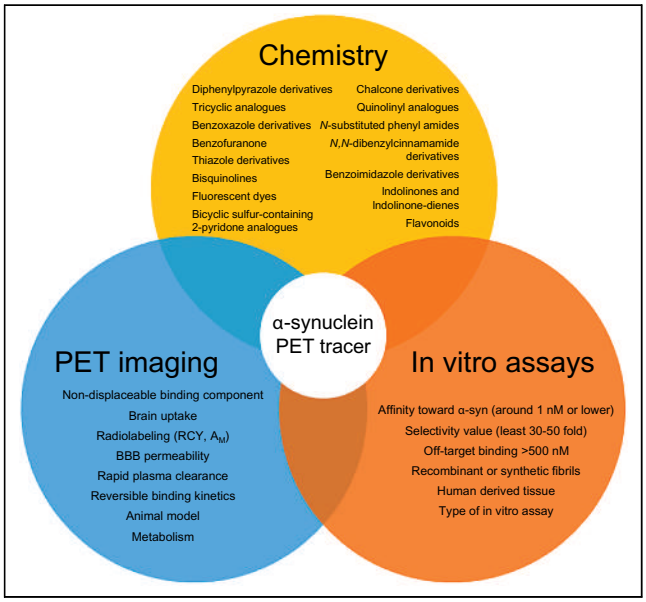


**FIGURE 1.** Overview on current state of candidate classes tested for their potential to provide viable α-synuclein PET tracers, together with recommended in vitro/PET imaging testing strategy. $A_M$ = molar activity; BBB = blood–brain barrier; RCY = radiochemical yield. (Reprinted from (*7*).)

neurotransmitter deficits can drive the clinical phenotype or represent main symptomatic treatment targets, such as the dopaminergic deficit in Parkinson disease (*11*) and, at least in part, the cholinergic deficit in AD (*12*). Other neurotransmitter disbalances seem to be responsible for comorbidity, such as serotonergic imbalance causing depressive symptoms (*13*) in several neurodegenerative diseases. PET and SPECT are the only imaging techniques capable of in vivo tracking of the state of these neurotransmitter systems and of respective drug effects. These imaging techniques play a significant role, both for clinical routine and for research—for example, to investigate the involvement of different neuroreceptor or transmitter systems in neurodegenerative disorders and to potentially develop new treatments. Imaging of the cholinergic and serotonergic systems may improve patient selection for and monitoring of specific symptomatic treatments and, in combination with pathologic imaging markers, measurement of potential multilevel drug effects.

Because of their exceptional role in neurodegenerative diseases, molecular imaging techniques assessing the dopaminergic and cholinergic systems in the brain are discussed in separate contributions to this supplement. Could imaging of other neurotransmitter systems find greater application in neurodegenerative diseases? One definitive candidate is the serotonergic system. Several PET tracers are available to image different aspects of this system (*14*). Of major interest is the serotonin transporter, a monoamine transporter that carries serotonin back from the synaptic cleft to the presynaptic neuron. Serotonin reuptake inhibitors, drugs that ameliorate depressive symptoms via increasing the concentration of serotonin in the synaptic cleft, target this structure. Future strategies for wider imaging use in the clinic as a means of personalized medicine might individually determine the presence and degree of a serotonergic deficit to guide decisions on whether serotonergic drugs will be considered in subsequent individual treatment decisions (Fig. 2).

Another neurotransmitter system that recently emerged as an attractive PET imaging target is the $\sigma_1$ receptor system. $\sigma_1$ receptors, formerly grouped with other opioid receptors, are membrane proteins at the endoplasmic reticulum that modulate calcium signaling. They seem to be involved in regulating metabolic cell stress in neurodegenerative diseases. Several PET tracers to image $\sigma_1$ receptors are now available (*15*). As a striking example of how to use them in research, the United Kingdom–based multipartner MIND-MAPS initiative is applying the $\sigma_1$ receptor tracer $^{11}$C-SA-4503 in combination with tracers of mitochondrial complex 1 and synaptic vesicle 2A to monitor the multiparametric progress of neurodegeneration across different disorders (*16*). The first published results of this initiative were encouraging (*17*). Another recently applied approach—this one using $^{18}$F-fluspidine—is to investigate the state of $\sigma_1$ receptors by PET imaging as a potential drug target to treat Huntington disease (*18*). It will also be interesting to observe whether and to what extent PET techniques or tracers targeting other neurotransmitter systems, such as tracers that bind to metabotropic glutamate subtype 5 receptors (*19*) that modulate synaptic transmission and can be compromised by, for instance, β-amyloid oligomers in AD, will find broader research or even some clinical applications. At least for the latter, the fate of such tracers will certainly also depend on the progress made in specific drug developments.

Regarding dopaminergic-system tracers currently in clinical use, the most widely applied is the SPECT tracer $^{123}$I-FP-CIT (*20*). This tracer binds to presynaptic dopamine transporters, thus providing a valuable surrogate readout for the integrity of the nigrostriatal pathway or dopamine-producing neurons in patients with Parkinsonian syndrome or suspected Lewy body dementia. It will be interesting to observe whether this SPECT imaging predominance for this application will change. There are, as an example, tracers available to image dopamine transporters and vesicular monoamine transporters by PET. The use of PET instead of SPECT as the image acquisition technique would have the advantage of providing a higher spatial resolution, quantitative data and the new option of combining molecular with structural imaging by hybrid PET/MRI systems. $^{18}$F-FE-PE21, $^{18}$F-FP-CIT, and $^{18}$F-AV-133 are examples of promising tracers in this regard (Fig. 3) (*21–23*).

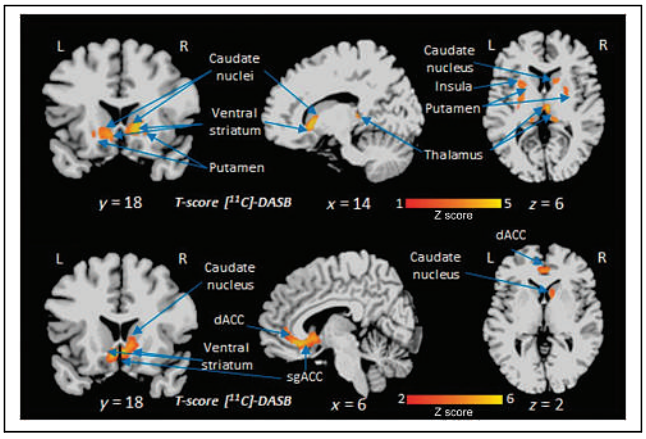


**FIGURE 2.** Voxelwise comparison of $^{11}$C-labeled 3-amino-4-(2-dimethylaminomethyl-phenylsulfanyl)-benzonitrile ($^{11}$C-DASB) serotonin transporter PET data of patients with de novo Parkinson disease depending on level of apathy. Clusters of reduced serotonin transporter availability (orange) in several deeper brain areas of apathetic PD patients as compared with healthy controls (top row) and nonapathetic PD patients (bottom row). dACC = dorsal anterior cingulate cortex; sgACC = subgenual anterior cingulate cortex. (Reprinted with permission of (*44*).)

## APPLYING NEW TECHNOLOGIES FOR MOLECULAR IMAGING OF NEURODEGENERATIVE DISORDERS

The application of new image acquisition and processing technology is anticipated to improve and broaden the application of molecular imaging in neurodegenerative disorders as well. The following developments are predicted to provide the most significant impact on future neurodegeneration imaging.

### PET/MRI

Hybrid PET/MRI technology allows the simultaneous evaluation of molecular and structural or functional changes in the living body. It is considered the tool of choice for brain imaging research. In clinical practice, a breakthrough application has not yet emerged, probably because of the relatively high purchasing and running costs of the scanners and the limited reimbursement options. Clinically, in suspected neurodegenerative diseases, MRI represents the first-line imaging technique, performed mainly to exclude other diseases such as vascular disorders, inflammation, trauma, or tumor. Diagnostic algorithms are available advocating the subsequent use of specific molecular imaging techniques depending on the diagnostic question, such as in dementia workup (*24*). However, PET or SPECT imaging is currently performed on only a subset of patients. This limited use might change; for example, the demand for β-amyloid imaging in AD may increase

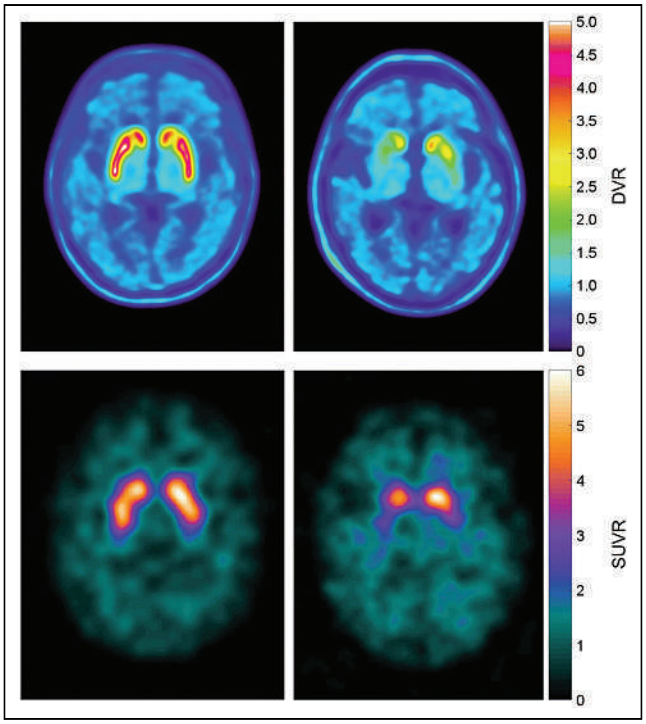


**FIGURE 3.** Intraindividual comparison between dopamine transporter imaging by $^{18}$F-FE-PE2I PET (top row) and $^{123}$I-FP-CIT SPECT (bottom row) in healthy control (left) and patient with Parkinson disease (right). DVR = distribution value ratio; SUVR = SUV ratio. (Reprinted from (*21*).)

in conjunction with broader availability of antiamyloid drugs. These drugs have relevant side effects, and PET/MRI might be the most expedient way not only to confirm the presence and engagement of the target (*25,26*) but also to provide structural information before and throughout therapy (*27*). In particular, regular monitoring for amyloid-related imaging abnormalities (*28*) by MRI is mandatory for these novel therapies. There is also potential to improve the quality of brain PET data with the support of simultaneously acquired MRI data, such as through MRI-supported PET reconstruction, PET tracer input-function generation, movement correction, partial-volume-effect correction, and PET tracer uptake quantification (Fig. 4) (*25*).

### Dedicated Brain PET Scanners

The idea of developing dedicated brain PET scanners follows the desire to allow access of a wider population to PET imaging as the social burden of neurodegenerative diseases increases and effective disease-modifying drugs emerge. Several academic and commercial groups are developing such systems (*29*). The initial clinical applications for this technology will likely use $^{18}$F-FDG but will rapidly extend to the use of amyloid and tau tracers.

### Total-Body and Large-Field-of-View PET Scanners

With the recent emergence of total-body and large-field-of-view PET scanners (*30*), there is a chance to simplify and improve studying the pharmacokinetics, pharmacodynamics, and dosimetry of new PET tracers (Fig. 5). What is more exciting is that it will also be possible to study, for the first time, the integrity of neurohumoral communication systems in the body, such as that of the gut–brain and heart–brain axes, as well as drug effects on these systems simultaneously for the entire body.

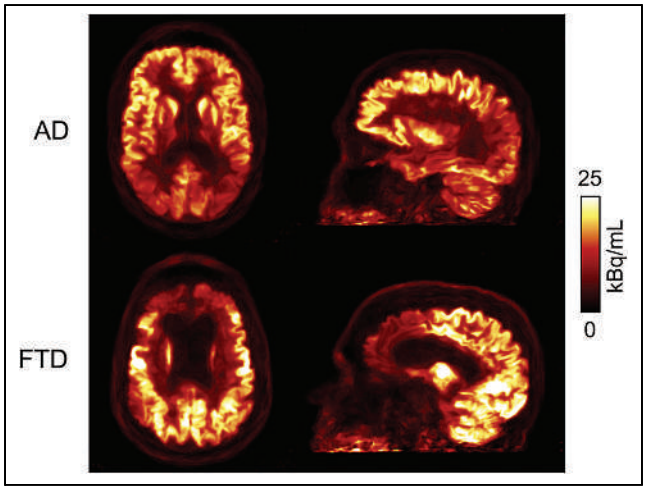


**FIGURE 4.** $^{18}$F-FDG glucose utilization PET images as obtained by hybrid PET/MRI and optimized by MRI-assisted attenuation correction, reconstruction, and movement correction in AD patient and frontotemporal dementia patient. (Reprinted from (*34*).)

### Advanced Image Acquisition and Processing Protocols

Molecular brain imaging may also benefit from advanced image acquisition protocols. In particular, early perfusion-phase acquisitions with different tracers for amyloid and tau PET have provided results consistent with $^{18}$F-FDG PET, allowing dual information to be obtained from a single imaging session (*31–33*). In addition to this multipurpose function, such protocols would also allow correction of the specific (late-phase) image information for perfusion effects. This ability may allow reliable, perfusion-independent protein pathology quantification, potentially of great importance for therapy response monitoring. In addition to benefiting from new imaging protocols, molecular imaging of the brain may also strongly benefit from new data-processing techniques, particularly using artificial intelligence. These techniques may allow improved

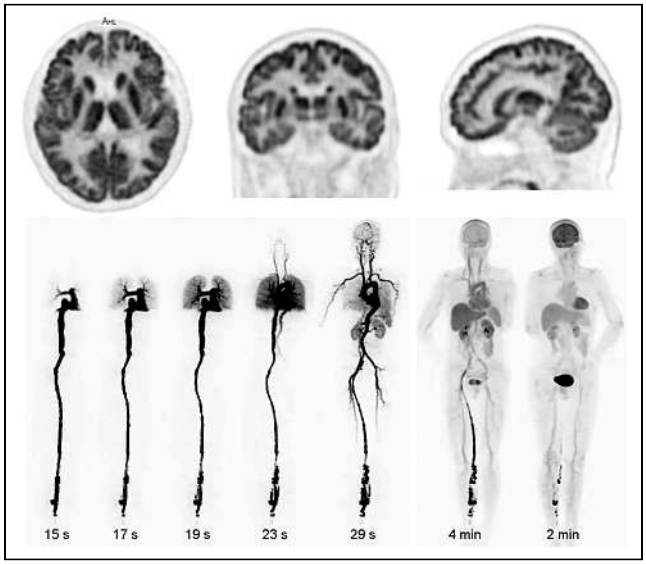


**FIGURE 5.** $^{18}$F-FDG glucose utilization PET images of brain (top row) and dynamically of whole body in healthy volunteers at different time points 0–60 min after tracer administration, with scan durations provided (bottom row). Data were acquired within first-in-humans study of EXPLORER total-body scanner. (Reprinted from (*30*).)

image reconstruction of scans with low activity (*34*), calculation of attenuation even without requiring a CT scan (*35*), and improved automated image analysis. One example of the latter is extraction of information on multiple pathologies from a single tracer, thus enabling amyloid, tau, and neurodegeneration classification in a single session, as suggested for tau PET (*36*). Artificial intelligence may open many further unforeseeable opportunities.

All these technologic developments also might reduce radiation exposure, scanning time, and tracer dose by improving system sensitivity (total-body systems), preventing the need for a CT acquisition (hybrid PET/MRI), allowing for single-tracer multipurpose protocols, or improving image reconstruction (artificial intelligence). These advantages might increase acceptance of the imaging tests, reduce costs, allow imaging of less compliant or more radiation-sensitive subjects, allow for larger series of repeated imaging, and allow application of multiple tracers.

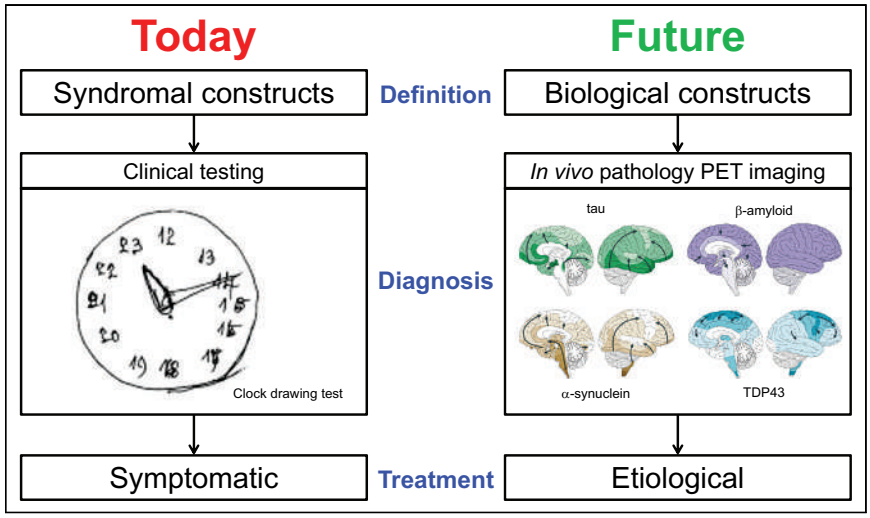


**FIGURE 6.** Schematic presentation of expected paradigm shift in how neurodegenerative diseases will be defined, diagnosed, and treated in future, together with role of PET imaging. (Reprinted from (*45*) and with permission of (*46*).)

## WHAT WILL THE FUTURE BRING FOR MOLECULAR IMAGING OF NEURODEGENERATIVE DISORDERS? AN OPTIMISTIC LOOK INTO THE GLASS BALL

### Molecular Imaging Will Become the Standard for Diagnosis of Neurodegenerative Diseases

In most centers, PET imaging of patients with suspected neurodegenerative disorders is currently used only as a diagnostic adjunct in uncertain cases. Diagnosis in these patients is based mainly on clinical testing for the presence of certain symptoms, whereas CT or MRI is used to exclude other disorders.

Through the years, this approach to defining neurodegenerative diseases as a syndromal construct, and consequently to diagnosing them on the basis of a certain clinical phenotype, has not led to a breakthrough in curative or disease-modifying treatment. AD was the first neurodegenerative disorder for which a new diagnostic concept was developed. Jack et al. proposed defining AD via biomarker testing for amyloid, tau, and neurodegeneration (*37*). This concept is already extensively used in research and for drug testing. With the approval of aducanumab by the Food and Drug Administration, we now have a β-amyloid–reducing drug approved to treat AD (*38*). Other anti–β-amyloid drugs and drugs effectively removing or preventing the formation of tau, α-synuclein, and other pathologic aggregates will hopefully follow. The concept of defining neurodegenerative diseases as a syndromal construct will potentially continue to change toward a definition of neurodegenerative diseases as a biologic construct. New etiologic treatment approaches will require a biomarker-based diagnosis. In this paradigm shift, PET imaging will potentially play a decisive role (Fig. 6).

### Molecular Imaging Will Become the Decisive Imaging Test for Experimental and Clinical Drug Application

Already, $^{18}$F-FDG, amyloid, tau, dopaminergic-system, and other neurotransmission tracers are being used for drug evaluation in neurodegenerative disorders (*27*). This portfolio will be reinforced by tracers to image different aspects of neuroinflammation and synaptic density, for which the current state of knowledge is summarized in separate reviews in this supplement.

For example, there is increasing understanding that removing pathologic proteins might produce a better clinical outcome if the drug is administered earlier. The concept is being explored of applying these drugs in prodromal or even asymptomatic subjects to prevent clinical manifestation of the disease, with the ongoing A4 trial in AD being one example (*39*). In such subjects, because clinical testing or structural imaging does not allow validation of the treatment rationale, molecular imaging will potentially gain more relevance for this purpose. Further, longitudinal molecular imaging is the ideal tool to assess regional treatment effects directly within the brain. Future scenarios are imaginable in which serial imaging allows individual tailoring of treatment intensity and duration, another perfect example of personalized medicine. Because PET is the only technique that can measure the regional distribution and density of the imaging target in an absolute quantitative manner, efforts to standardize quantitative PET readouts across different tracers for the same target and across centers will potentially gain more relevance, such as the centiloid concept in amyloid imaging (*40*).

Use of β-amyloid PET in aducanumab prescription is a subject of controversy, which recently culminated in a limited-coverage decision by the Centers for Medicare and Medicaid Services (*41*). β-amyloid PET was used in the drug development program, first, to stratify patients at baseline according to the presence of the drug target and, second, to serve as a secondary outcome measure. Amyloid PET imaging should be considered mandatory for selecting patients for therapy with this drug. Interestingly, however, the authors of recently published appropriate-use criteria for aducanumab treatment suggested that patients may also be included on the basis of cerebrospinal fluid (CSF) analysis, although conceding that patients positive on CSF testing but negative on β-amyloid PET should not be treated and that patients with inconclusive CSF results should undergo amyloid PET (*42*). Because CSF sampling was not validated as an entry test for aducanumab treatment, and specifically given the potentially avoidable side effects and costs in cases of false-positive CSF tests, caution should be used when considering this suggestion. Because of the controversies about the efficacy of anti-amyloid therapy at the

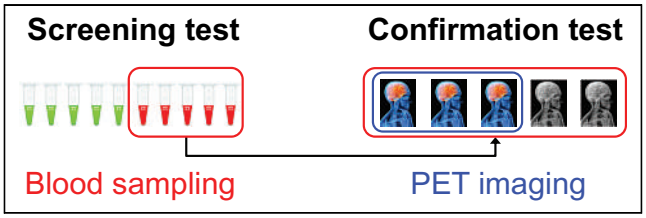


**FIGURE 7.** Schematic presentation of future scenario in diagnosis of neurodegenerative disease based on pathology biomarkers. Subjects at risk or even all subjects will be screened by blood test for β-amyloid, tau, α-synuclein, TDP-43, and others. This screening test will be optimized for sensitivity, that is, tolerating certain number of false-positives. Positives based on blood test will then undergo respective (or multiple) brain PET scans as confirmation testing. This confirmation testing will be optimized for specificity. It will establish or exclude diagnosis, as well as presence of dedicated drug targets, and will serve as baseline test for subsequent therapy monitoring in cases of disease-modifying drug prescription.

dementia stage, it also appears advisable to perform amyloid PET follow-up examinations to validate and quantify therapy effects, which CSF sampling is not capable of doing (*38*).

### Molecular Imaging Will Redefine Its General Role with Regard to Fluid Biomarkers to Diagnose Neurodegeneration

β-amyloid and tau PET imaging are competing with CSF sampling when it comes to clinical routine binary classification of suspected AD patients. It is interesting that there has also been relevant progress in potentially substituting CSF testing for AD biomarkers by less invasive blood sampling (*43*). This progress raises the question of what specific value PET imaging will have. The answer potentially depends on what kind of PET readout is obtained and for which purpose the diagnostic test is performed. In stages of clinically manifest dementia, blood sampling may provide a similar answer on whether β-amyloid pathology is present. However, in prodromal disease stages, which probably last for decades, β-amyloid PET may allow assessment not only of the presence but also the stage and location of the pathology and therapeutic target—an assessment that does not seem feasible by CSF or blood tests. The situation may again be different for tau imaging, for which different tauopathies are diagnosed and differentiated via evaluation of the regional PET signal, a property that fluid biomarkers cannot provide. An alternative prediction combines relatively inexpensive screening of at-risk subjects with blood biomarker testing, followed by diagnostic confirmation through PET imaging to provide a rationale for drug treatment and a baseline for subsequent drug monitoring (a property that, again, fluid biomarkers have not been shown capable of providing; Fig. 7). Besides this use, PET imaging of β-amyloid and tau will certainly still play a decisive role in testing during the early development phase of drugs because of its unique ability to provide absolute quantitative data on the density of treatment targets in the brain. PET imaging will also serve as the gold standard in vivo test against which novel fluid biomarkers are validated.

## SUMMARY AND CONCLUSION

Motivated by the ongoing paradigm shift in defining and diagnosing neurodegenerative diseases through the underlying pathology, and by new hope for a breakthrough in disease-modifying drugs, there is great enthusiasm about advancing this facet of the field of molecular imaging. It is predicted that techniques will be improved, be made more broadly available, be supplemented by new tracers targeting aspects of neurodegeneration not previously trackable in vivo, and be enhanced by new approaches to acquiring, processing, and analyzing images.

There is still a considerable gap between the unique possibilities of in vivo characterization of neurodegenerative diseases and the frequency with which these modern molecular imaging methods are applied. Although some imaging biomarkers, such as $^{18}$F-FDG, dopaminergic, or β-amyloid tracers, have been available for a quite some time and their value is well established, their broader integration into clinical neurologic routine has not yet been achieved. This shortfall is seriously discrepant with, for instance, the extent to which PET imaging has been integrated into the oncologic standard of care. Thus, the results of prospective, outcome-oriented multicenter trials such as IDEAS (https://www.ideas-study.org/) and AMYPAD (https://amypad.eu/) need to be translated into reimbursement decisions. Also, for the recently Food and Drug Administration–approved tau tracer $^{18}$F-flortaucipir, application has been restricted mainly to drug testing trials, with only limited use for diagnostic assessment, internationally. Systematic integration of these tools into clinical practice appears overdue.

In addition to improved implementation of existing tools into the clinical praxis, molecular imaging bears great potential to extend our view outside the beaten track to other factors involved in neurodegeneration, such as different protein aggregates, synaptic loss, inflammation, and various neurotransmitter dysbalances. Finally, molecular imaging in neurodegeneration may benefit from developments in imaging instrumentation and data processing, such as hybrid PET/MRI and artificial intelligence. We believe that colleagues in neuronuclear medicine would be well advised to take advantage of these innovations. Also, the obvious advantages of imaging tools over other biomarkers of neurodegeneration—that is, the provision of direct information on the presence, extent, localization, and quantity of neuropathology—justify mandatory use of these tools in selecting patients and monitoring their response to modern causal therapy. Finally, advances in tracers and imaging technology may even allow clinical protocols with multiple time points and multiple tracers. The nuclear imaging community should intensify efforts to implement such personalized protocols.

Because of space restrictions, this overview cannot address all questions and future challenges in greater detail. One question is, What are the limitations of the biomarkers mentioned, and how do these limitations impact diagnostic value? For example, in emerging tau tracers, the selectivity and degree of binding translate to differences in the effect on differential diagnosis and on detection of changes on longitudinal imaging. Another question is, To what degree is the possibility of new biomarkers to image neurodegenerative diseases counterbalanced by practical problems such as access to instrumentation and tracers, imaging capacity, equity and cost-effectiveness? Regional differences in these features only add to the complexity. As a third question to consider, Are the thoroughness of neurodegeneration biomarker development and the speed of clinical translation always adequate? Similar questions can be asked about drug development. Academia should abstain from pressure related to nonacademic factors and adhere to the concept of evidence-based science. All open questions such as these are significant and deserve careful consideration.

The future of molecular imaging of neurodegenerative diseases is bright. More work is required, but developments in this exciting field will expand use both clinically and in research, to the betterment of our patient care.

## DISCLOSURE

Henryk Barthel received speaker honoraria from Novartis/AAA and reader honoraria from Life Molecular Imaging. Victor Villemagne received consulting fees from Eli Lilly, Life Molecular Imaging, Hospicom, and IXICO and speaker honoraria from ACE Barcelona and IXICO. Alexander Drzezga received research support from Siemens Healthineers, Life Molecular Imaging, GE Healthcare, AVID Radiopharmaceuticals, and SOFIE; received speaker/advisory board honoraria from Siemens Healthineers, Sanofi, GE Healthcare, Biogen, Novo Nordisk, and Invicro; owns stocks from Siemens Healthineers and Lantheus Holding; and holds a pending patent for $^{18}$F-PSMA7. No other potential conflict of interest relevant to this article was reported.

## REFERENCES


1. Villemagne VL, Fodero-Tavoletti MT, Masters CL, Rowe CC. Tau imaging: early progress and future directions. *Lancet Neurol.* 2015;14:114–124.
2. Valotassiou V, Archimandritis S, Sifakis N, Papatriantafyllou J, Georgoulias P. Alzheimer's disease: SPECT and PET tracers for beta-amyloid imaging. *Curr Alzheimer Res.* 2010;7:477–486.
3. Chen CJ, Bando K, Ashino H, et al. Synthesis and biological evaluation of novel radioiodinated imidazopyridine derivatives for amyloid-β imaging in Alzheimer's disease. *Bioorg Med Chem.* 2014;22:4189–4197.
4. Maya Y, Okumura Y, Kobayashi R, et al. Preclinical properties and human in vivo assessment of $^{123}$I-ABC577 as a novel SPECT agent for imaging amyloid-β. *Brain.* 2016;139:193–203.
5. Watanabe H. Development of SPECT probes for in vivo imaging of β-amyloid and tau aggregates in the Alzheimer's disease brain [in Japanese]. *Yakugaku Zasshi.* 2017;137:1361–1365.
6. Gustavsson T, Syvänen S, O'Callaghan P, Sehlin D. SPECT imaging of distribution and retention of a brain-penetrating bispecific amyloid-β antibody in a mouse model of Alzheimer's disease. *Transl Neurodegener.* 2020;9:37.
7. Korat Š, Bidesi NSR, Bonanno F, et al. Alpha-synuclein PET tracer development: an overview about current efforts. *Pharmaceuticals (Basel).* 2021;14:847.
8. Guerrero-Ferreira R, Taylor NM, Mona D, et al. Cryo-EM structure of alpha-synuclein fibrils. *eLife.* 2018;7:e36402.
9. Kuebler L, Buss S, Leonov A, et al. [$^{11}$C]MODAG-001: towards a PET tracer targeting α-synuclein aggregates. *Eur J Nucl Med Mol Imaging.* 2021;48:1759–1772.
10. Yue X, Dhavale DD, Li J, et al. Design, synthesis, and in vitro evaluation of quinolinyl analogues for α-synuclein aggregation. *Bioorg Med Chem Lett.* 2018;28:1011–1019.
11. Bloem BR, Okun MS, Klein C. Parkinson's disease. *Lancet.* 2021;397:2284–2303.
12. Francis PT, Palmer AM, Snape M, Wilcock GK. The cholinergic hypothesis of Alzheimer's disease: a review of progress. *J Neurol Neurosurg Psychiatry.* 1999;66:137–147.
13. Chakraborty S, Lennon JC, Malkaram SA, Zeng Y, Fisher DW, Dong H. Serotonergic system, cognition, and BPSD in Alzheimer's disease. *Neurosci Lett.* 2019;704:36–44.
14. Saulin A, Savli M, Lanzenberger R. Serotonin and molecular neuroimaging in humans using PET. *Amino Acids.* 2012;42:2039–2057.
15. Agha H, McCurdy CR. *In vitro* and *in vivo* sigma 1 receptor imaging studies in different disease states. *RSC Med Chem.* 2020;12:154–177.
16. Mind maps. Invicro website. https://lp.invicro.com/mind-maps. Accessed May 2, 2022.
17. Wilson H, Pagano G, de Natale ER, et al. Mitochondrial complex 1, sigma 1, and synaptic vesicle 2A in early drug-naive Parkinson's disease. *Mov Disord.* 2020;35:1416–1427.
18. Grachev ID, Meyer PM, Becker GA, et al. Sigma-1 and dopamine D2/D3 receptor occupancy of pridopidine in healthy volunteers and patients with Huntington disease: a [$^{18}$F] fluspidine and [$^{18}$F] fallypride PET study. *Eur J Nucl Med Mol Imaging.* 2021;48:1103–1115.
19. Mecca AP, McDonald JW, Michalak HR, et al. PET imaging of mGluR5 in Alzheimer's disease. *Alzheimers Res Ther.* 2020;12:15.
20. Morbelli S, Esposito G, Arbizu J, et al. EANM practice guideline/SNMMI procedure standard for dopaminergic imaging in Parkinsonian syndromes 1.0. *Eur J Nucl Med Mol Imaging.* 2020;47:1885–1912.
21. Jakobson Mo S, Axelsson J, Jonasson L, et al. Dopamine transporter imaging with [$^{18}$F]FE-PE2I PET and [$^{123}$I]FP-CIT SPECT: a clinical comparison. *EJNMMI Res.* 2018;8:100.
22. Kazumata K, Dhawan V, Chaly T, et al. Dopamine transporter imaging with fluorine-18-FPCIT and PET. *J Nucl Med.* 1998;39:1521–1530.
23. Villemagne VL, Okamura N, Pejoska S, et al. Differential diagnosis in Alzheimer's disease and dementia with Lewy bodies via VMAT2 and amyloid imaging. *Neurodegener Dis.* 2012;10:161–165.
24. Chételat G, Arbizu J, Barthel H, et al. Amyloid-PET and $^{18}$F-FDG-PET in the diagnostic investigation of Alzheimer's disease and other dementias. *Lancet Neurol.* 2020;19:951–962.
25. Drzezga A, Barthel H, Minoshima S, Sabri O. Potential clinical applications of PET/MR imaging in neurodegenerative diseases. *J Nucl Med.* 2014;55(suppl 2):47S–55S.
26. Schütz L, Lobsien D, Fritzsch D, et al. Feasibility and acceptance of simultaneous amyloid PET/MRI. *Eur J Nucl Med Mol Imaging.* 2016;43:2236–2243.
27. Barthel H, Seibyl J, Sabri O. The role of positron emission tomography imaging in understanding Alzheimer's disease. *Expert Rev Neurother.* 2015;15:395–406.
28. Sperling RA, Jack CR Jr, Black SE, et al. Amyloid-related imaging abnormalities in amyloid-modifying therapeutic trials: recommendations from the Alzheimer's Association Research Roundtable Workgroup. *Alzheimers Dement.* 2011;7:367–385.
29. Catana C. Development of dedicated brain PET imaging devices: recent advances and future perspectives. *J Nucl Med.* 2019;60:1044–1052.
30. Badawi RD, Shi H, Hu P, et al. First human imaging studies with the EXPLORER total-body PET scanner. *J Nucl Med.* 2019;60:299–303.
31. Florek L, Tiepolt S, Schroeter ML, et al. Dual time-point [$^{18}$F]florbetaben PET delivers dual biomarker information in mild cognitive impairment and Alzheimer's disease. *J Alzheimers Dis.* 2018;66:1105–1116.
32. Hammes J, Leuwer I, Bischof GN, Drzezga A, van Eimeren T. Multimodal correlation of dynamic [$^{18}$F]-AV-1451 perfusion PET and neuronal hypometabolism in [$^{18}$F]-FDG PET. *Eur J Nucl Med Mol Imaging.* 2017;44:2249–2256.
33. Beyer L, Nitschmann A, Barthel H, et al. Early-phase [$^{18}$F]PI-2620 tau-PET imaging as a surrogate marker of neuronal injury. *Eur J Nucl Med Mol Imaging.* 2020;47:2911–2922.
34. Chen KT, Salcedo S, Gong K, et al. An efficient approach to perform MR-assisted PET data optimization in simultaneous PET/MR neuroimaging studies. *J Nucl Med.* 2018;60:272–278.
35. Schramm G, Holler M, Rezaei A, et al. Evaluation of parallel level sets and Bowsher's method as segmentation-free anatomical priors for time-of-flight PET reconstruction. *IEEE Trans Med Imaging.* 2018;37:590–603.
36. Hammes J, Bischof GN, Bohn KP, et al. One-stop shop: $^{18}$F-flortaucipir PET differentiates amyloid-positive and -negative forms of neurodegenerative diseases. *J Nucl Med.* 2021;62:240–246.
37. Jack CR Jr, Bennett DA, Blennow K, et al. NIA-AA Research Framework: Toward a biological definition of Alzheimer's disease. *Alzheimers Dement.* 2018;14:535–562.
38. Garibotto V, Albert NL, Barthel H, et al; EANM Neuroimaging Committee. The approval of a disease-modifying treatment for Alzheimer's disease: impact and consequences for the nuclear medicine community. *Eur J Nucl Med Mol Imaging.* 2021;48:3033–3036.
39. Welcome to the A4 study. The A4 Study website. https://a4study.org/. Accessed May 2, 2022.
40. Klunk WE, Koeppe RA, Price JC, et al. The Centiloid Project: standardizing quantitative amyloid plaque estimation by PET. *Alzheimers Dement.* 2015;11:1–15.e1–4.
41. Imaging advocate concerned after CMS grants limited coverage of controversial Alzheimer's drug, related PET scans. Radiology Business website. https://www.radiologybusiness.com/topics/policy/imaging-aduhelm-alzheimers-cms-medicare-pet-scan-snmmi. Published January 12, 2022. Accessed April 28, 2022.
42. Cummings J, Aisen P, Apostolova LG, Atri A, Salloway S, Weiner M. Aducanumab: appropriate use recommendations. *J Prev Alzheimers Dis.* 2021;8:398–410.
43. Leuzy A, Cullen NC, Mattsson-Carlgren N, Hansson O. Current advances in plasma and cerebrospinal fluid biomarkers in Alzheimer's disease. *Curr Opin Neurol.* 2021;34:266–274.
44. Maillet A, Krack P, Lhommée E, et al. The prominent role of serotonergic degeneration in apathy, anxiety and depression in de novo Parkinson's disease. *Brain.* 2016;139:2486–2502.
45. Weber WA, Czernin J, Anderson CJ, et al. The future of nuclear medicine, molecular imaging, and theranostics. *J Nucl Med.* 2020;61(suppl 2):263S–272S.
46. Brettschneider J, Del Tredici K, Lee VM, Trojanowski JQ. Spreading of pathology in neurodegenerative diseases: a focus on human studies. *Nat Rev Neurosci.* 2015;16:109–120.

# Advancement drives us. Purpose compels us.

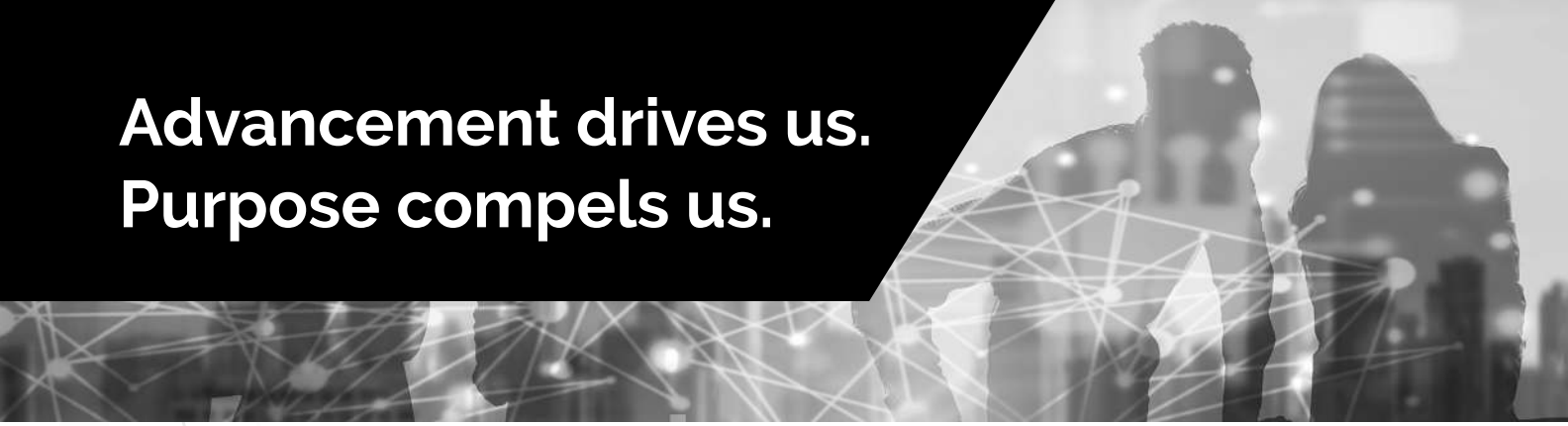

## Theranostic Pipeline

We have taken bold steps to advance the development of next generation theranostic agents.

## Contract Manufacturing

We offer a range of PET radiopharmaceuticals to meet your clinical needs through our network and new Theranostics Center of Excellence.

## PET Education

We have created a multi-faceted approach designed to strengthen the quality of PET programs and maximize productivity.

## Our Network

We are committed to the on-time delivery of high-quality radiopharmaceuticals to meet our clients need in diagnosing and treating critical illnesses every day.

SOFIE
From start to clinic

To learn more, visit sofie.com

The SNMMI and the editors of *The Journal of Nuclear Medicine* gratefully acknowledge the following companies for their generous support of this supplement:

## Gold Sponsor

SIEMENS Healthineers

## Silver Sponsors

Biogen

Eisai

Lilly

## Bronze Sponsors

SOFIE
From start to clinic